



---

# Understanding Ovarian Cancer and Chemoresistance through Chromosome Spatial Organisation and Nuclear Motors

---

by

**Aakila Sammy**

A thesis submitted for the degree of  
**Doctor of Philosophy**  
College of Health, Medicine and Life Sciences  
Brunel University London  
August 2020

# DECLARATION

I hereby declare that this submission is my work, except where otherwise stated, and has not been presented for any other degree.

*Aakila Sammy*

# ACKNOWLEDGEMENTS

First and foremost, many thanks to my supervisor, Professor Joanna Bridger, for the opportunity, respected knowledge, the appropriate amount of support, guidance, and timely encouragement throughout this journey.

I also appreciate my academic support, for the daunting meetings that invaluable contributed to the construction of this project; Dr Gudrun Stenbeck, Dr Rhona Anderson, Dr David Tree, Dr Concetta Bubici and Dr Paola Vagnarelli for helping me visualise westerns using her Li-Cor system. I am also grateful to Dr Emmanuel Karteris and his team for providing me with ovarian cancer cell lines, support with western blots and most importantly, cupcakes.

Sometimes I found myself between a rock and a hard place, and this is where casual conversations amongst my office besties Juhi, Ruchira and Saqlain lead to breakthroughs, along with the laughs and drama. To the rest of my office mates, thank you for the maintenance of a weird vibe and banter. Which brings me to thanking the Bridger lab alumni and senior members; Dr Marianne Henry, Dr Daniel Horton and Mr Kumars Riyahi for the knowledge and techniques they passed on to me.

I would also like to thank my friends and family here and back in Trinidad, for holidays that recharged me during this venture. My nieces (Hibba, Zaara, Aalayna, Faaria and Nura), who

demand I mention them by name (a compromise against full names). A special thank you to my dad Robert, for funding this research despite the challenges we faced together and those that he sheltered me from. Cheers to my brother Aakil, for the cheeky financial support that allowed me to enjoy life as well.

I am also appreciative to my husband Matthew O'Neill who not only provided a wonderful life here but has been my biggest cheerleader (pom-poms and all), picked up slack when hours in the lab got long, constantly provided tea, cakes and laughs while writing, and most importantly helped fix the mess I made with my headers and footers.

And to my dear baby girl Summer, I forgive you for the massive kick that jolted me during a 96-well plating session (I had to start again), because you kept me company during many lone working hours and through no intention of yours, I challenged my self-limiting belief of being a PhD momma.

Finally, the entirety of this acknowledgement would not be possible without God.

**Dedicated to:**

---

To SHALEZA HOSEIN-SAMMY (1965-2017),

*my dearest mom, a victim of ovarian cancer.*

&

To AZZA SAMMY,

*because a loving and caring sister is the next best thing to*

*a mom.*

---

# TABLE OF CONTENTS

- DECLARATION .....2**
- ACKNOWLEDGEMENTS.....3**
- TABLE OF CONTENTS .....5**
- LIST OF FIGURES.....9**
- LIST OF TABLES.....12**
- ABBREVIATIONS .....14**
- ABSTRACT .....18**
- CHAPTER 1 GENERAL INTRODUCTION .....20**
  - 1.1 OVARIAN CANCER (OC) ..... 20**
    - 1.1.1 Reasons for Concern .....20
    - 1.1.2 The Disease.....22
    - 1.1.3 OC Oncogenes and Tumour Suppressor Genes .....26
    - 1.1.4 Genes .....28
    - 1.1.5 Current Surveillance .....30
    - 1.1.6 Current Treatment .....32
    - 1.1.7 Drug Resistance .....36
    - 1.1.8 Summary .....38
  - 1.2 THE NUCLEUS..... 40**

---

1.2.1	Genome Organisation – The Right Place at the Right Time.....	41
1.2.2	Lamins.....	56
1.2.3	Emerin.....	61
1.2.4	Nuclear Myosins.....	63
1.2.5	Nuclear Actin.....	71
1.2.6	Hypothetical Motor Complex:.....	73
1.2.7	Outlook.....	74
 <b>CHAPTER 2 CHROMOSOME SPATIAL ORGANISATION AND NUCLEAR MOTORS IN OC....</b>		<b>75</b>
<b>2.1</b>	<b>INTRODUCTION.....</b>	<b>75</b>
2.1.1	Spatial Chromosomal Organisation in Cancer.....	76
2.1.2	NM cancer-specificity.....	77
2.1.3	Lamins.....	78
2.1.4	Why these chromosomes?.....	78
2.1.5	Outlook.....	80
<b>2.2</b>	<b>METHODS.....</b>	<b>82</b>
2.2.1	Cell Culture.....	82
2.2.2	Fluorescence <i>in-situ</i> Hybridisation (FISH).....	86
2.2.3	Indirect Immunofluorescence.....	91
2.2.4	Western Blot Assay.....	93
<b>2.3</b>	<b>RESULTS.....</b>	<b>95</b>
2.3.1	Spatial Chromosomal Organisation in OC:.....	95
2.3.2	Nuclear Myosin Presence and Distribution in OC:.....	100
<b>2.4</b>	<b>DISCUSSION.....</b>	<b>106</b>
2.4.5	Chromosomes.....	106
2.4.6	Nuclear Lamins.....	110
2.4.7	Nuclear Myosins.....	116
2.4.8	Conclusion.....	119
 <b>CHAPTER 3 RESTORING CHROMOSOME SPATIAL POSITIONING IN OC CELLS VIA RNAI</b>		
<b>OF NUCLEAR MYOSINS 1 AND 6.....</b>		<b>121</b>
<b>3.1</b>	<b>INTRODUCTION.....</b>	<b>121</b>
3.1.1	RNA interference (RNAi) of NM1 and NM6 in Cancer.....	122
3.1.2	Outlook.....	124
<b>3.2</b>	<b>METHODS.....</b>	<b>125</b>

---

---

3.2.1	RNA interference .....	125
3.2.2	Cell Culture – refer to section 2.2.1 .....	126
3.2.3	FISH – refer to section 2.2.2.....	126
3.2.4	Indirect IF – refer to section 2.2.3.....	126
3.2.5	WB – refer to section 2.2.4.....	126
<b>3.3</b>	<b>RESULTS .....</b>	<b>127</b>
3.3.1	Knockdown of NM1 and NM6 in 4 OC Cell Lines: .....	127
3.3.2	Spatial Chromosome Organisation Post-NM1 and -NM6 Knockdown: .....	132
<b>3.4</b>	<b>DISCUSSION .....</b>	<b>142</b>
3.4.1	Disruption of the tumorigenic superfamily stoichiometry of NM1/NM6 .....	143
3.4.2	One size does not fit all.....	145
3.4.3	Conclusion.....	146
<b>CHAPTER 4 UNDERSTANDING CHEMORESISTANCE AND RE-SENSITISATION IN OC ...</b>		<b>147</b>
<b>4.1</b>	<b>INTRODUCTION.....</b>	<b>147</b>
4.1.1	Modelling a Lab-Grade Platinum-Resistant Cell Line .....	148
4.1.2	Understanding Drug Resistance by Spatial Chromosome Organisation.....	149
4.1.3	Re-sensitisation using siRNA .....	149
4.1.4	Outlook.....	150
<b>4.2</b>	<b>METHODS.....</b>	<b>151</b>
4.2.1	Sulforhodamine B (SRB) Calibration for use in Cytotoxicity Assays .....	151
4.2.2	50% Growth Inhibitory Concentration (IC <sub>50</sub> ) Assay .....	152
4.2.3	Chemoresistance induction .....	152
4.2.4	Cytotoxic Assay .....	152
4.2.5	Cell Culture – refer to section 2.2.1 .....	153
4.2.6	FISH – refer to section 2.2.2.....	153
4.2.7	Indirect IF – refer to section 2.2.3.....	153
4.2.8	WB – refer to section 2.2.4.....	153
4.2.9	RNAi – refer to section 3.2.1.....	153
<b>4.3</b>	<b>RESULTS .....</b>	<b>154</b>
4.3.1	Creation of a Platinum-Resistant MDAH-2774, MDAH-2774 <sub>CR</sub> : .....	154
4.3.2	NMI and NM6 Distribution and Quantity of newly created Platinum-Resistant MDAH-2774CR: .....	158
4.3.3	Investigating Re-Sensitisation of MDAH-2774CR through Combination Treatments of siRNA and Cisplatin: .....	161
4.3.4	The Role of Spatial Chromosomal Organisation in Platinum-Resistance and Re-Sensitisation:.....	163
<b>4.4</b>	<b>DISCUSSION .....</b>	<b>167</b>
4.4.1	NM1/NM6 Role in Acquiring Chemoresistance.....	167

---

4.4.2 Synergy .....	168
4.4.3 Chemoresistance and Spatial Chromosomal Organisation .....	168
4.4.4 Conclusion.....	169
<b>CHAPTER 5 GENERAL DISCUSSION .....</b>	<b>171</b>
<b>6 REFERENCES .....</b>	<b>179</b>
<b>7 APPENDIX .....</b>	<b>194</b>



# LIST OF FIGURES

## Chapter 1

Figure 1. 1 Average 5-Year Survival Rate Amongst Male and Female Reproductive Cancers: .....	21
Figure 1. 2 Stages of OC: .....	23
Figure 1. 3 Three Categories of OC Origin:.....	24
Figure 1. 4 The Compromising Anatomical Location of the Ovaries:.....	25
Figure 1. 5 eOC Subtypes, Mutations and Platinum Sensitivity: .....	26
Figure 1. 6 Historical View of Chemotherapy Usage for OC: .....	33
Figure 1. 7 Causes and Characteristics of Drug resistance: .....	37
Figure 1. 8 Summary of the Treatment Guidelines in OC (advanced): .....	39
Figure 1. 9 Phase Separation in the Eukaryotic Cell: .....	42
Figure 1. 10 Human Genome Organisation within the 3D Nucleus:.....	43
Figure 1. 11 A Schematic Representation of Radial Positioning within the Nucleus: .....	44
Figure 1. 12 Chromosomal Translocations: .....	46
Figure 1. 13 Chromosome Out-Looping: .....	51
Figure 1. 14 Topologically Associated Domains (TADs): .....	53
Figure 1. 15 Summary of Sub-LADs Hierarchy: .....	55
Figure 1. 16 The Major Forms of Lamins (in somatic cells of human, mice and most other vertebrates):.....	56
Figure 1. 17 Continuity from the Cytoskeleton to the Nucleoskeleton: .....	57
Figure 1. 20 Schematic Representation of Unconventional Myosins Fulfilling Multiple Roles in Vital Cellular Processes: .....	64
Figure 1. 21 Simplified Structure of NM1 and NM6:.....	68
Figure 1. 22 Anchoring/transport of RNA polymerase II by Nuclear myosin: .....	69
Figure 1. 23 Possible Arrangement of the Hypothetical Motor Complex:.....	73

## Chapter 2

Figure 2. 1 Karyotype Background .....	83
Figure 2. 2 Erosion Analysis Representation: .....	89

---

Figure 2. 3 Erosion Analysis Sample Output: .....	90
Figure 2. 4 Chromosome Spatial Positioning: .....	96
Figure 2. 5 Image Analysis: Chromosome Spatial Positioning: .....	98
Figure 2. 6 NM1 and NM6 Distribution Patterns Images: .....	100
Figure 2. 7 NM1 Distribution Patterns Score: .....	101
Figure 2. 8 NM6 Distribution Patterns Score: .....	102
Figure 2. 9 NM1 and NM6 Levels (Li-Cor Images): .....	104
Figure 2. 10 NM1 and NM6 Band Intensities: .....	104
Figure 2. 11 'Chromosome Stretching' in HOSEpi: .....	110
Figure 2. 12 B-type Lamin Distribution Patterns: .....	112
Figure 2. 13 A-type Lamin Distribution Patterns: .....	112
Figure 2. 14 Lamin A/C and B <sub>1</sub> levels: .....	113
Figure 2. 15 Lamin Distribution in Breast Cancer: .....	114
Figure 2. 16 Failed Compensation/Feedback Mechanism (Hypothetical Schematic): .....	118

### Chapter 3

Figure 3. 1 NM1 and NM6 Levels Pre- and Post-knockdown of NM1 and NM6 in Cell Lines SKOV-3, PEO-1 and MDAH-2774: .....	128
Figure 3. 2 NM1 Band Intensities: .....	129
Figure 3. 3 NM6 Band Intensities: .....	129
Figure 3. 4 NM1 and NM6 Positively and Negatively Stained Nuclei: .....	130
Figure 3. 5 NM1 Levels Pre- and Post-Knockdown of NM1 in Cell Lines SKOV-3, PEO-1, PEO-4 and MDAH-2774 as Estimated by Indirect-IF: .....	131
Figure 3. 6 NM1 Levels Pre and Post Knockdown of NM1 in Cell Lines SKOV-3, PEO-1, PEO-4 and MDAH-2774 as Estimated by Indirect-IF: .....	131
Figure 3. 7 Post-NM1 Knockdown Chromosome Spatial Positioning Images: .....	132
Figure 3. 8 Post-NM6 Knockdown Chromosome Spatial Positioning Images: .....	133
Figure 3. 9 Image Analysis Chromosome Spatial Positioning Post-NM1 Knockdown: .....	134
Figure 3. 10 Image Analysis Chromosome Spatial Positioning Post-NM6 Knockdown: .....	135
Figure 3. 11 Heat-Map of Post-Knockdowns Effect Using <i>p</i> -values Against HOSEpi: .....	137
Figure 3. 12 Spatial Gap Influence: .....	141
Figure 3. 13 NM1 and NM6 Levels Before and After Knockdown: .....	144

### Chapter 4

Figure 4. 1 SRB Calibration: .....	155
Figure 4. 2 Seeding Density Determination for Cytotoxic Assay: .....	156
Figure 4. 3 IC <sub>50</sub> for MDAH-2774 and PEO-1: .....	157
Figure 4. 4 NM1 and NM6 Distribution Patterns Score: .....	158
Figure 4. 5 NM1 and NM6 Distribution Patterns Images: .....	159

Figure 4. 6 NM1 and NM6 Levels: ..... 160

Figure 4. 7 NM1 and NM6 Band Intensities: ..... 160

Figure 4. 8 MDAH-2774<sub>CR</sub> NM1 and NM6 levels: ..... 161

Figure 4. 9 Cisplatin Cytotoxic Assay:..... 162

Figure 4. 10 Chromosome Spatial Positioning Images: MDAH-2774<sub>CR</sub> Pre- and Post-NM1 Knockdown ..... 163

Figure 4. 11 Graphical Representation: MDAH-2774<sub>CR</sub> Image Analysis Chromosome Spatial Positioning Pre- and Post-NM1 Knockdown:..... 164

Figure 4. 12 Post-Knockdown Effect by *p*-values Against HOSEpi: ..... 166

## Chapter 5

Figure 5. 1 NM16, NM18 $\beta$  and NM5 $\beta$  Patterns Images: ..... 175

Figure 5. 2 Summary of the CT Re-Positionings from Healthy to Cancer to NM Knockdown and Chemoresistance: ..... 177

# LIST OF TABLES

## Chapter 1

Table 1. 1 Signs and Symptoms of OC: .....	22
Table 1. 2 Brief Background of the Notable Chemotherapeutic Drugs Approved Use in OC Therapy: .....	34
Table 1. 3 Levels of A-type and B-type Lamins in Cancer: .....	59
Table 1. 4 Summary of Nuclear Myosins and their Genes .....	66

## Chapter 2

Table 2. 1 Ovarian Cell Lines Summary: .....	83
Table 2. 2 The DOP-PCR Reagents: .....	86
Table 2. 3 DOP-PCR Cycle Conditions: .....	86
Table 2. 4 Antibody List: .....	91
Table 2. 5 Li-Cor Antibody List: .....	94
Table 2. 6 <i>p</i> -values against HOSEpi: .....	99
Table 2. 7 <i>p</i> -values for Cell Lines SKOV-3, PEO-1, PEO-4 And MDAH-2774 Compared Against Each Other: .....	109
Table 2. 8 <i>p</i> -values for Cell Lines SKOV-3, PEO-1, PEO-4 and MDAH-2774 Compared Against HOSEpi (IF): .....	116
Table 2. 9 NM1 and NM6 % Elevation: .....	117

## Chapter 3

Table 3. 1 <i>p</i> -values Post-NM1 and NM6 Knockdown Against HOSEpi: .....	136
Table 3. 2 Summary of <i>p</i> -values Post-Knockdown Cancer Cells vs Control Cell: .....	138
Table 3. 3 Spatial Gap: values CT Position Post-Knockdown Against its Pre-Knockdown CT Position: .....	139

**Chapter 4**

Table 4. 1  $p$ -values for MDAH-2774<sub>CR</sub> and Post-NM1 Knockdown Against HOSEpi:..... 165

Table 4. 2  $p$ -values of MDAH-2774<sub>CR</sub> Pre- and Post-NM1 Knockdown Against HOSEpi: ..... 165

# ABBREVIATIONS

<b>2D</b>	2-Dimensional
<b>3D</b>	3-Dimensional
<b>ACS</b>	American Cancer Society
<b>ADP</b>	Adenosine Diphosphate
<b>ATCC</b>	American Type Culture Collection
<b>ATP</b>	Adenosine Triphosphate
<b>BAF</b>	Barrier-to-Autointegration Factor
<b>BSA</b>	Bovine Serum Albumin
<b>CA-125</b>	Cancer Antigen 125
<b>CaM</b>	Calmodulin
<b>CIN</b>	Chromosome INstability
<b>CR</b>	Cisplatin Resistance
<b>CRISPR</b>	Clustered Regularly Interspaced Short Palindromic Repeats
<b>CRUK</b>	Cancer Research, UK
<b>CT</b>	Chromosome Territory
<b>CTCs</b>	Circulating Tumor Cell
<b>Cy3</b>	Cyanine3
<b>DAPI</b>	4,6-Diamidino-2-Phenylindole
<b>DDR</b>	DNA Damage Repair
<b>DMSO</b>	Dimethyl Sulfoxide

<b>DNA</b>	Deoxyribonucleic Acid
<b>DOP</b>	Degenerated Oligonucleotide-Primed
<b>EDMD</b>	Emery-Dreifuss Muscular Dystrophy
<b>EDTA</b>	Ethylenediaminetetraacetic Acid
<b>eOC</b>	epithelial Ovarian Cancer
<b>FCS</b>	Fetal Calf Serum
<b>FIGO</b>	International Federation of Gynecology and Obstetrics
<b>FISH</b>	Fluorescence <i>in-situ</i> Hybridisation
<b>GAPDH</b>	Glyceraldehyde 3-Phosphate Dehydrogenase
<b>GI</b>	Gastrointestinal
<b>GTP</b>	Guanosine-5'-Triphosphate
<b>HE-4</b>	Human Epididymal Secretory Protein E4
<b>HGPS</b>	Hutchinson-Gilford Progeria Syndrome
<b>Hi-C</b>	High-Throughput Chromosome Conformation Capture
<b>HPV</b>	Human Papillomavirus
<b>HRT</b>	Hormone Replacement Therapy
<b>hTERT</b>	Human Telomerase Reverse Transcriptase
<b>IC50</b>	Inhibitory Concentration 50%
<b>ICD</b>	Inter-Chromosome Domain
<b>IF</b>	Immunofluorescence
<b>iLAD</b>	Internal LAD
<b>IQ</b>	Isoleucine–Glutamine
<b>LAD</b>	Lamin-Associated Domain
<b>LAP</b>	Lamin-Associated Protein
<b>LINC</b>	Linker of Nucleoskeleton and Cytoskeleton
<b>MAC</b>	Macintosh Apple Computer
<b>MAPK</b>	Mitogen-Activated Protein Kinase
<b>MDR</b>	Multi-Drug Resistance
<b>MHC class II</b>	Human Major Histocompatibility Complex II
<b>MS</b>	Microsoft

<b>mTOR</b>	Mammalian Target of Rapamycin
<b>NAD</b>	Nucleoli-Associated Domain
<b>NCI</b>	National Cancer Institute
<b>NE</b>	Nuclear Envelope
<b>NET</b>	Nuclear Envelope Transmembrane
<b>NICE</b>	National Institute for Health and Care Excellence
<b>NL</b>	Nuclear Lamina
<b>NLS</b>	Nuclear Localisation Sequence
<b>NM</b>	Nuclear Myosins
<b>NOCC</b>	National Ovarian Cancer Coalition
<b>OC</b>	Ovarian Cancer
<b>PAD</b>	Pericentric Heterochromatin-Associated Domain
<b>PAGE</b>	Polyacrylamide Gel Electrophoresis
<b>PBS</b>	Phosphate-Buffered Saline
<b>PCOS</b>	Polycystic Ovary Syndrome
<b>PCR</b>	Polymerase Chain Reaction
<b>PHE</b>	Public Health England
<b>RNA</b>	Ribonucleic Acid
<b>RNAi</b>	RNA Interference
<b>rpm</b>	Revolutions per Minute
<b>RPMI</b>	Roswell Park Memorial Institute
<b>SDS</b>	Sodium Dodecyl Sulphate
<b>SEM</b>	Standard Error of Mean
<b>siRNA</b>	Small Interfering RNA
<b>SRB</b>	Sulforhodamine B
<b>SSC</b>	Sodium Saline Citrate
<b>TAD</b>	Topologically Associating Domain
<b>TBS</b>	Tris-Buffered Saline
<b>TCA</b>	Tricarboxylic Acid Cycle
<b>TSG</b>	Tumour Suppressor Gene



## Abbreviations

---

<b>UTP</b>	Uridine-5'-Triphosphate
<b>UV</b>	Ultraviolet
<b>VEGF</b>	Vascular Endothelial Growth Factor
<b>WB</b>	Western Blot
<b>WOCC</b>	World Ovarian Cancer Coalition
<b>XCI</b>	X Chromosome Inactivation

# ABSTRACT

20% of patients diagnosed with ovarian cancer (OC) cannot receive treatment at all due to the severity of the disease when discovered. The 80% of patients that receive treatment, as much as, 90% relapse in less than six months and, by the end of two years fail to respond to treatment as a result of multi-drug resistance. As genetic studies fail to provide a complete picture in the biology of disease, epigenetics including spatial and radial organisation of the genome has become a well-established that provides a greater understanding beyond the sequence. Chromosomes are non-randomly organised within interphase nuclei, which can vary slightly from cell type to cell type, their proliferation and disease status. The functional organisation within interphase nuclei is kept in place and regulated by a plethora of structural and mechanical proteins such as lamins and nuclear myosins (NMs), and along with many other proteins are known together as the nucleoskeleton. Irregularities in these proteins have been implicated in many diseases, including metastatic cancers and their chemoresistant counterparts. NM1 role in spatial chromosome organisation has been established, and with the emergence of NM6 role in nuclear organisation, both their overexpression in OC and involvement transcription presents them as an attractive co-study.

This research investigates the disease-related chromosome territory (CT) positionings of OC through four key chromosomes in a panel of OC cells; SKOV-3 PEO-1 PEO-4 MDAH-2774, in addition to a control control cell line HOSEpi. Internally located CT were observed for chromosomes 1, 13 and 17

and a peripheral localisation was observed chromosome X. Chromosomes were subsequently assessed for location post-NM1/6 knockdown revealing that chromosome territories relocalised closer to the localisations of the control cell line, and following the acquisition of platinum-resistance of MDAH-2774, all four chromosomes predominated centrally in nuclei. The analysis also revealed that chromosome X might play a more fundamental role in ovarian tissue and cancer than previously thought and the initial aim of its use as a control was challenged. Distribution discrepancies in the OC cells were found in the nuclear lamins and myosins with further investigations revealing significant elevations of NM1 and NM6. The elevations also displayed a different stoichiometry ratio in the platinum-resistant cell line PEO-4 which led to the creation of a novel lab-grade platinum-resistant cell line MDAH-2774<sub>CR</sub> from the naïve line MDAH-2774 to investigate further resistant-specific NM1/NM6 stoichiometry and spatial CT organisation in OC. Moreover, combination assays with MDAH-2774<sub>CR</sub> and NM1 knockdown resulted in cell death that surpassed its sensitive counterpart, that has future clinical potential to treat chemoresistant OC.

In this research, we aim to broaden the comprehension of the many mechanisms involved in the development and progression of an aggressive cancer. The analysis of the CT positioning of 4 out of 23 chromosomes was able to reveal characteristics within OC nuclei at key milestones of the disease, making this level of investigation, and information, important in understanding OC and its successful treatment.

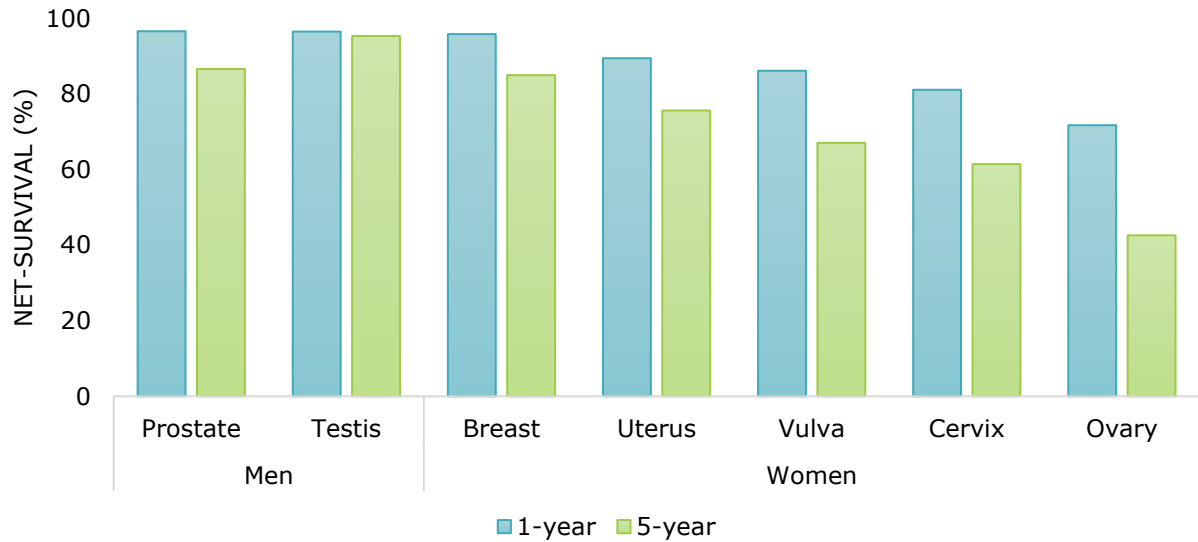
# CHAPTER 1

## GENERAL INTRODUCTION

### 1.1 OVARIAN CANCER (OC)

#### 1.1.1 Reasons for Concern

Globally, when compared to other female gynaecological cancers (breast, endometrial and cervical), ovarian cancer (OC) has the lowest **five**-year survival rate due to its high metastatic potential, late diagnosis and multi-drug resistance (figure [1.1](#)). In women, it is the **fourth** most common cancer, the **second** most common gynaecological cancer and is the **number one** cause of death for female cancers, claiming 140,000 lives globally in 2012, that was due to late diagnosis at an advanced stage (III and IV), with a sizeable metastatic tumour present in the abdomen (Dakubo, 2017). In the UK (2002-06), the five-year survival for stage I, II, III and IV were 90%, 43%, 19% and 4% respectively signifying that even though 10% of women diagnosed at stage I, they still do not survive beyond five-years (Cancer Research, UK). A significant number of women respond well to initial treatment, however, those with advance stages relapse within 18 months, and those who retained sensitivity are re-treated until restricted by chemoresistance. Even more alarming is that 20% of women diagnosed with OC cannot receive any treatment at all due to the severity of the disease when it is discovered (Target Ovarian Cancer, UK).



- adapted from Public Health England, 2018.

**Figure 1. 1 Average Five-Year Survival Rate Amongst Male and Female Reproductive Cancers:**

Age: 15 to 99 years. Diagnosed between 2013 and 2017 then followed up to 2018 in England. OC has the lowest survival rate.

Despite the late-stage diagnosis; improved cytoreductive surgery and chemotherapy have been able to increase the five-year survival rate from 37% in the 1970s to 46% in 1999-2005 (Dakubo, 2017). Expertise in imaging, histopathology, surgery, chemotherapy, and palliation are all required for optimum outcomes. Histopathology, however, determines the specifics of the latter procedures as it distinguishes between different sub-types that harbour genetic mutations with the potential to predict the efficacy of tailored treatments. In 2012, the worldwide incidence rate of OC was 239,000 and mortality rate at 152,000 with a projected increase by 2035 of 55% and 67% respectively (The World Ovarian Cancer Coalition, 2018). OC is ranked fifth in the UK and US, and seventh worldwide of all lethal female cancers and though the incidence rates vary among geographic region and ethnicities, the goal of earlier detection and novel drug targets remains the same across all borders, and the continued progress of developing new treatments can improve the outlook (National Cancer Institute, US and CRUK).

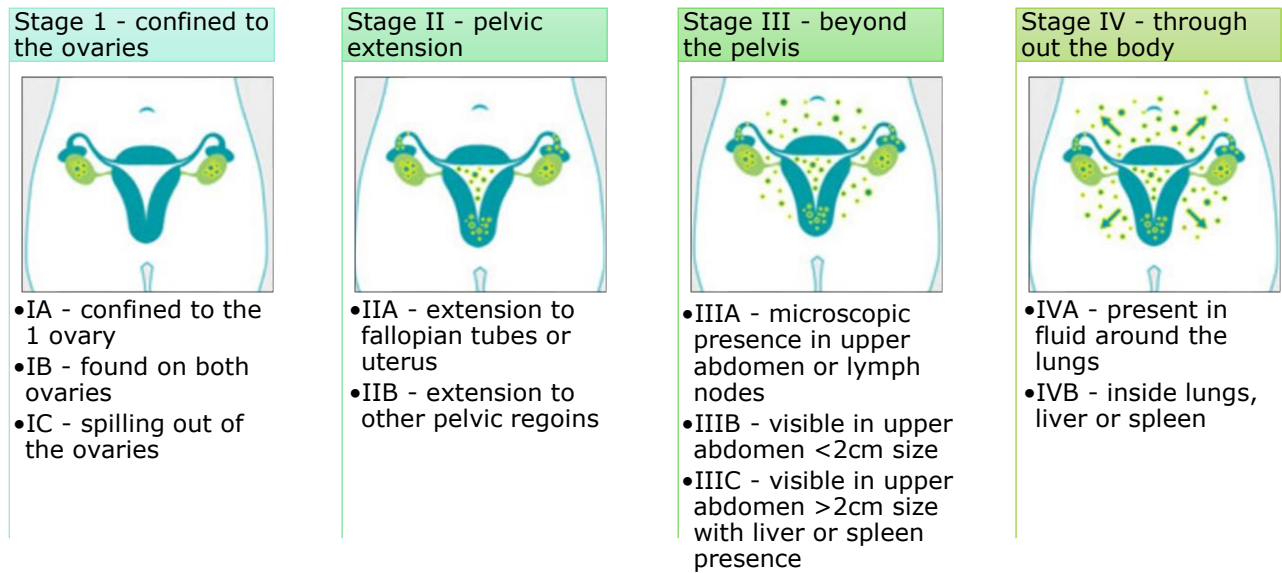
### 1.1.2 The Disease

Often termed the 'silent killer' or 'the whispering disease,' as its lethality surfaces at the advanced stage when diagnosed due to the lack of recognisable and absolute symptoms in earlier stages (figure [1.1](#) and [1.2](#)). In the UK the lifetime risk is 1 in 60, with the median age of 58 years (randomised trials), the median age of diagnosis is 63 years in the overall population and for those genetically predisposed a median age of 53 years (Mavaddat *et al.*, 2013). For these reasons, it is one of the deadliest cancers to affect women.

#### Table 1. 1 Signs and Symptoms of OC:

According to the 2015 National Institute for Health and Care Excellence (NICE) guidelines for suspected recognition and referral.

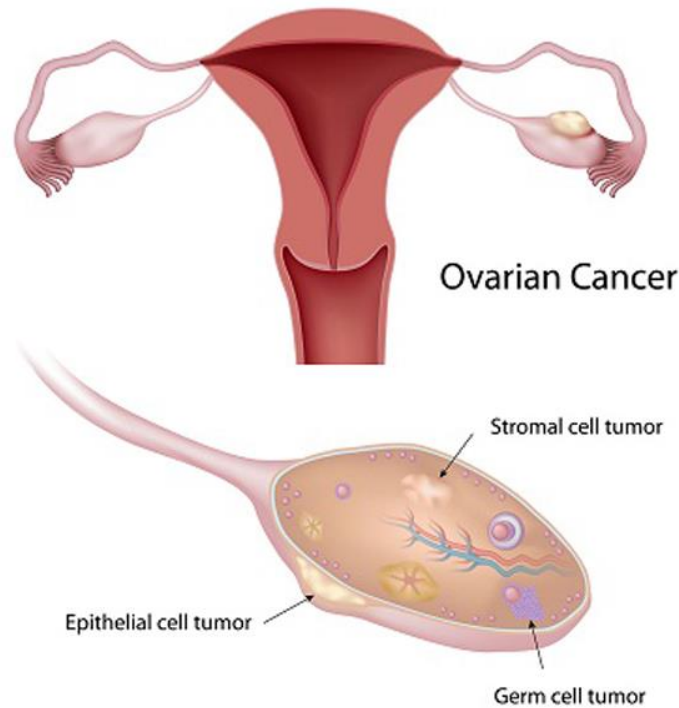
Abdominal distension/bloating
Loss of appetite +/- early satiety
Pelvic/abdominal pain
Increased urinary urgency/frequency
Unexplained weight loss/fatigue
Unexplained changes in bowel habits
New IBS symptoms in over 50s
Ascites/pelvic/abdominal mass on examination



- adapted from the International Federation of Gynecology and Obstetrics (FIGO) staging system and National Ovarian Cancer Coalition (NOCC)

**Figure 1. 2 FIGO and NOCC Stages of OC**

Depending on their originator cell, there are three types of OC: Epithelial (85-90%), Stromal (~10%) and germ (1-2%). The research for this PhD focuses on epithelial OC than the rare germ and stromal tumours (figure 1.3).



<http://www.dovemed.com/diseases-conditions/mucinous-adenocarcinoma-ovary>

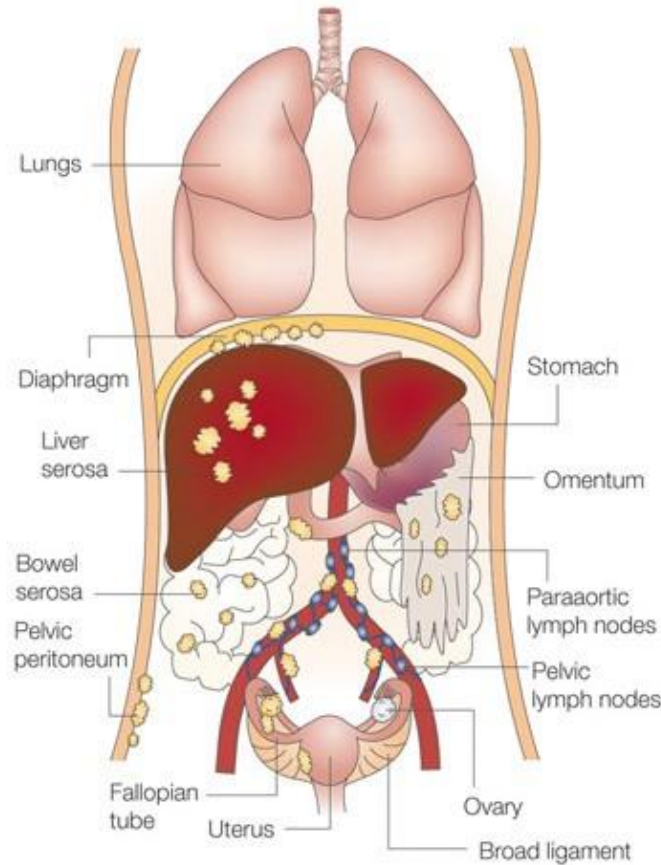
**Figure 1. 3 Three Categories of OC Origin:**

Surface epithelium, germ cell and stromal, which closely resembles epithelial in terms of morphology, symptoms, spread and treatment (reviewed in Jayson *et al.*, 2014).

---

The insidious nature of OC as compared to tumours of other organs, stems from its location, as it directly extends to major neighbouring organs which are aided by the peritoneal cavity that facilitates the transport of exfoliated tumour cells (figure 1.4). This intricate and diffused environment makes chemotherapy more feasible than surgery unless it is of a low grade and organ-confined nature (reviewed in Naora and Montell, 2005). Dissemination also takes a route through the lymphatic system (pelvic and para-aortic lymph node) than the more common vascular system (reviewed in Naora and Montell, 2005).





-Naora and Montell, 2005

**Figure 1. 4 The Compromising Anatomical Location of the Ovaries:**

In the peritoneal cavity, the ovarian tumour is compressing against multiple organs; tumour cells detach, overcome anoikis and settle onto the other organs (Naora and Montell, 2005).

During ovulation, the rupture and release of egg produces a local inflammatory microenvironment and explains why increased ovulation is associated with increased OC risk (Yang-Hartwich *et al.*, 2015). Epidemiological findings stated that the risk of OC is reduced by states of anovulation such as pregnancy, oral contraceptives, and tubal ligation (reviewed in Jayson *et al.*, 2014). In contrast, states of supraphysiological ovarian stimulation such as fertility treatments and hormone replacement therapy (HRT) during menopause have been implicated in increasing its risk in both breast and OCs (reviewed in Jayson *et al.*, 2014). Endometriosis, polycystic ovary syndrome

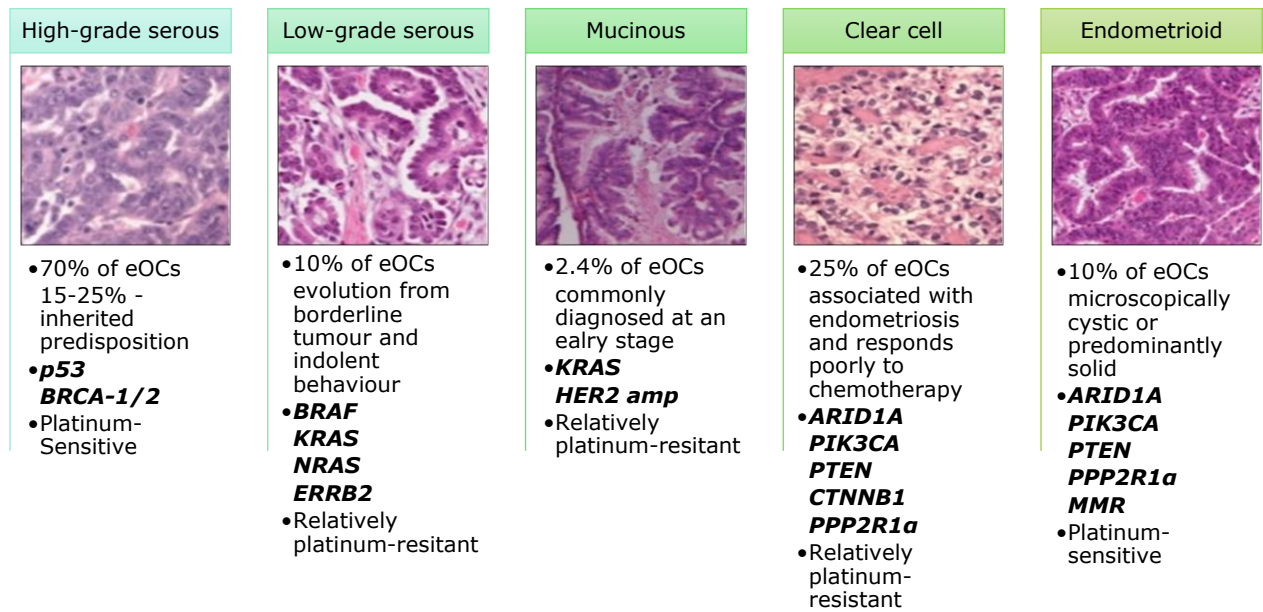
(PCOS), human papillomavirus (HPV), perineal talc and smoking have all been found associated with the disease (reviewed in Jayson *et al.*, 2014).

### **1.1.3 OC Oncogenes and Tumour Suppressor Genes**

Cell division and differentiation are regulated by a family of growth factors (cytokines) and are carefully balanced by another family of apoptotic regulators. When the balance is disturbed, the result is cancer where cells start dividing uncontrollably or damaged cells circumventing apoptosis. The disturbance of this balance begins at the genetic level, and the accumulation of molecular genetic alterations gives critical roles to several oncogenes and tumour suppressor genes (TSG).

Oncogenes first start as a proto-oncogene, and alteration of a single allele is sufficient to activate its oncogenic form; whereas TSGs requires the activation of both alleles to remove its negative control on cell growth. Oncogenes are activated predominantly through mutations, translocations, and amplification, whereas TSGs can be activated by mutation, deletion, or chromosome loss. Oncogene mutations produce a faulty form of the regulatory protein, enhancing its role in the cell cycle whereby TSG mutations rid the regulatory protein restraints on cell division.

In OC, the primary oncogenes comprise of *HER2/ERBB2/neu*, *c-myc*, *K-ras/Braf* and *PIK3CA* (Aunoble *et al.*, 2000 and Shayesteh *et al.*, 1999) and the primary TSGs include *p53*, *BRCA1/2*, *PTEN* and *ARID1A* (Aunoble *et al.*, 2000; Takeda *et al.*, 2016; Tamwar, 2013). OC description and diagnosis are extensive and everchanging as Shih and Kurman, 2004 proposed a classification of epithelial OC (eOC) tumours in type I: low grade with *BRAF*, *KRAS*, and *PTEN* mutations and type II: high-grade with *p53*, *BRCA1*, and *BRCA2* mutations, however, together with this, figure [1.5](#) highlights the mainstream model.



- adapted from Banerjee and Kaye, 2013 and Lheureux, Braunstein and Oza, 2019.

**Figure 1. 5 eOC Subtypes Summary (FIGO classification):**

The 5 subtypes of eOC showing their morphology, prevalence, characteristic genetic markers, and platinum sensitivity.

### 1.1.4 Genes

My PhD research examined the location of chromosomes that contain genes *p53* and *BRCA 1/2* found in high-grade tumours, *HER2* in low-grade and mucinous and the particularly interesting *ARID1A* for its additional role in spatially partitioning chromosomes (Wu *et al.*, 2019). There is much cross-talk between these genes and their pathways, that is often a result of mutations leading to carcinogenesis; however, cases, where carcinogenesis takes place without an evident mutation, cause and effect is not as clear cut which requires investigations beyond the sequence.

#### 1.1.4.1 *ARID1A*

*ARID1A* protein is a multi-kinase inhibitor encoded by the *ARID1A* gene on **chromosome 1** (Takeda *et al.*, 2016). It is a member of the BAF sub-complex of the SWI/SNF chromatin remodelling complex that has critical roles in the cell cycle, apoptosis, differentiation, gene stability and DNA repair where its knockdown reveals increased cellular proliferation (Hoffman and Liebermann, 2008; Takeda *et al.*, 2016; Reyes-Gonzales *et al.*, 2015). There is a high frequency of *ARID1A* mutations in OC; 30-61% depending on the severity, type, and origin, whereas 86-100% of OC cases have *ARID1A* protein deficiency (Hoffman and Liebermann, 2008; Takeda *et al.*, 2016).

#### 1.1.4.2 *BRCA1 and BRCA2*

The five times increased prevalence of *BRCA* mutations in the Ashkenazi Jewish population has greatly increased their risk for breast and OC compared to the general population (Simchoni *et al.*, 2006). *BRCA* proteins are localised in nuclei and produced abundantly in the thymus and testis with lower levels in the breast and ovaries. They are associated with breast and OC that is known to affect women through hereditary means. 5-10% of OC stems from the hereditary disposition of *BRCA1* and *BRCA2* genes located on **chromosomes 17** and **13**, respectively (Aunoble *et al.*, 2000). Though less affected, men can also inherit the mutation as illustrated by CRUK, where for every

143rd female, one male is diagnosed with breast cancer. The risk of OC associated with *BRCA2* is considerably lower at 30% than *BRCA1* with 50% and women with either germline mutation have a 40-60% lifetime risk; however, the *BRCA* gene test can make patients aware of their pre-disposition and following options such as routine check-ups, hysterectomy, and mastectomy (Prat *et al.*, 2005; Aunoble *et al.*, 2000; Jayson *et al.*, 2014). *BRCA1* is a 220 kDa protein, and *BRCA2* is a 400kDa protein that works in genome protection, each at different stages (Roy, Chun and Powell, 2012).

#### **1.1.4.3 p53**

*p53* mutation is the most common genetic alteration in OC found on **chromosome 17**. Almost universal, a mutation is found in over 79% of OCs, 75% of all cancers and many chemoresistant tumours are also positive for *p53* alteration (Aunoble *et al.*, 2000; Jayson *et al.*, 2014; Carrillo *et al.*, 2015). The gene encodes for a 53kDa protein performing roles in arresting cell cycle and inducing programmed cell death (Aunoble *et al.*, 2000; Lakin and Jackson, 1999).

#### **1.1.4.4 HER2-(*neu*, *ErbB2*, and *p185*)**

First identified by a group of scientists in the 1980s, *HER2* is located on **chromosome 17** and in OC, its overexpression reduces the survival of the patient as compared to one with a regular expression (Iqbal and Iqbal, 2014). Although generally essential in cell growth, a mutated *HER2* protein plays a crucial role in approximately 30% of OCs also extending to breast and cervical cancer (reviewed in Aunoble *et al.*, 2000). The transmembrane protein has a tyrosine kinase activity belonging to a family of epidermal growth factor receptors (Aunoble *et al.*, 2000). In cancer, both oncogenic mutation and overexpression lead to independent and constant cell cycle activation.

### **1.1.5 Current Surveillance**

OC usually presents itself with 3-4 months of abdominal pain or enlargement often mistaken for irritable bowel syndrome such that NICE has recommended women experiencing these symptoms get serum cancer antigen 125 (CA-125) as a supplementary screen (reviewed in Jayson *et al.*, 2014). If CA-125 shows no elevation, screening then proceeds to a pelvic exam, transvaginal/abdominal ultrasonography, and laparoscopy (Coticchia, Yang and Moses, 2008; reviewed in Jayson *et al.*, 2014). There are no single reliable early screening or predictive markers for OC; however, there are screening algorithms that combine biomarkers on premenopausal and postmenopausal women over 40 years for OC risk (WOCC, 2018). The two main clinical biomarkers are CA-125 which has a relatively higher sensitivity and HE-4 that has a relatively higher specificity (WOCC, 2018).

#### **1.1.5.1 1981 - Serum CA-125**

CA-125 is the most routine non-invasive biomarker preoperatively used to predict malignancy potential in diagnostic, prognostic and monitoring purposes. This mucin-like transmembrane glycoprotein shows a strong correlation connecting its rise and fall with disease progression and regression, respectively (reviewed in Boivin *et al.*, 2009). Approximately 80% of women diagnosed at late-stage OC show elevated CA-125 serum levels, which highlights that roughly 20% of people with late-stage cancer do not express CA-125 (Coticchia, Yang and Moses, 2008; WOCC, 2018). Furthermore, only 50% of early-stage OC show elevated CA-125 expression. CA-125 also lacks specificity and sensitivity since it is also expressed amid benign non-gynaecologic circumstances. Additionally, women can have elevated CA-125 levels and be considered low risk if it remains unchanged for years (WOCC, 2018). Interestingly, CA-125 over-expression has been recently found to protect cells against the effects of genotoxic drugs, thus reducing cancer cells sensitivity to chemotherapy (Boivin *et al.*, 2009).

### **1.1.5.2 1991 - Serum HE4**

Human epididymal secretory protein E4 (HE-4) was first identified in 1991 then later in 1999 in OC cells, this glycoprotein is involved in tumour progression extending to the breast, lungs, kidneys, bladder, GI tract and endometrium (WOCC, 2018). However, the highest HE-4 levels are expressed in ovarian and endometrial cancers. HE-4 is also expressed in healthy tissues that include the breast, colon, respiratory tract, distal renal tubules, genital tract, epididymis, vas deferens, salivary glands and fallopian tubes with the highest in the trachea and salivary glands (WOCC, 2018). It is important to note that 32% of the cells that do not express CA-125 express HE-4, and 50% of the patients that do not express serum CA-125 have elevated HE-4 (WOCC, 2018).

### **1.1.5.3 The Newcomers**

Both CA-125 and HE-4 have the potential as screening, diagnostic, prognostic, monitoring and predictive markers, especially when combined in algorithms that can also determine risk and discriminate between benign and malignant tumours (WOCC, 2018). Currently, more than thirty potential biomarkers in serum are being evaluated with, and without CA-125, since by itself, CA-125 is insufficient as a screening biomarker (Coticchia, Yang and Moses, 2008). Other biomarking methods include screening circulating tumour cells, stem cells and circulating tumour DNA in addition to genome, transcriptome, microRNA, and proteasome profiling. The OncoOVARIAN Dx test by Bioprognos combines six serum tumour markers for early statistical probability (non-definitive) that exceeds all current tests including individual biomarkers, algorithms, and its predecessor OVA1 by Vermillion that is based on five serum biomarkers (Bioprognos, 2020).

### **1.1.6 Current Treatment**

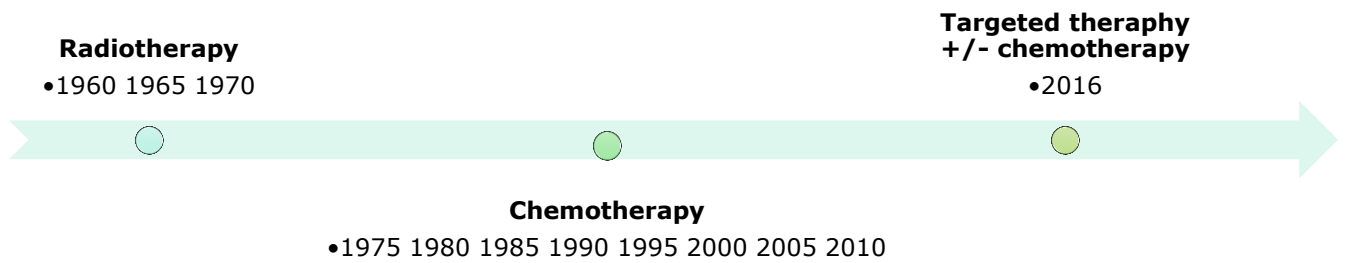
Largely unchanged for the last 40 years, the standard first-line care involves a combination of de-bulking surgery, platinum-based drugs and/or Taxol-based drugs (depends on the patient's tolerance). Chemotherapy is administered before surgery, shrinking the tumour for effective cytoreduction or after to remove remnants post-surgery.

#### **1.1.6.1 Surgery**

Surgery entails preoperative imaging and discussion followed by removal of the entire womb, ovaries, fallopian tube, omentum (the thin fold of abdominal fatty tissue containing lymph and vasculature tissue) and tumour de-bulking to remove as much tumour tissue as possible, provide a histopathological diagnosis and stage the disease (Jayson *et al.*, 2014). Conservative surgery options are considered for fertile women in early stages wanting to maintain their fertility. The field of surgery has had its improvements with multidisciplinary surgical teams and improved imaging however in cases where disease spread is extensive, beyond the abdominal cavity patients are switched to chemotherapy only or offered preoperative chemotherapy before de-bulking (Jayson *et al.*, 2014).



### 1.1.6.2 Chemotherapy



- adapted from Roche, 2017

**Figure 1. 6 Historical View of Chemotherapy Usage for OC**

Chemotherapeutics can be used in mono-, combination or as adjuvant therapy which is often preferred for its synergistic effects; mono-therapy is favoured in cases where side effects of the combination are too severe, maintenance therapy is used in remission to prevent relapse, especially in cases of hereditary predispositions (table 1.2) (Palmer and Sorger, 2017). Targeted therapies have become highly successful as they are incredibly selective for characteristics specific to cancer cells, thus reducing/eliminating effects on the healthy cells (Palmer and Sorger, 2017). Radiotherapy, on the other hand, is no longer accepted as standard practice since other contents of the abdominal cavity can suffer (figure 1.6) (Einhorn *et al.*, 1999).

**Table 1. 2 Brief Background of the Notable Chemotherapeutic Drugs Approved Use in OC Therapy:**

An overview of the mechanisms, drawbacks and how they are circumvented in the management of OC.

Drug	Description	Mechanism	Drawbacks	Alternatives	Reference
<b>TARGET: Nucleic Acids</b>					
<b>1844</b> <b>Platins /</b> <b>Platinols -</b> <b>Cisplatin,</b> <b>Carboplatin</b>	Cisplatin accidentally discovered in the 1970s and its safer analogue carboplatin in the 1980s have been successful anticancer drugs for decades.	Its alkylating property damages mitotic DNA via aquation that then crosslinks preferably with the guanine base, rendering the DNA beyond repair, committing the cell to apoptosis.	Chemoresistance	Alternative mono- or combination therapy	Kelland, 2007
<b>1960s</b> <b>Anthracyclines</b>	It is ranked one of the most effective mono-therapy chemotherapeutic agents ever developed.	Derived from the bacteria <i>Streptomyces</i> , anthracycline localises in the nucleus, intercalates with DNA and RNA to stop transcription and replication.	Cardiotoxic side effects	Cardio-protectant drugs, longer infusion rates or most commonly formulated with a polyethylene glycol conjugated (PEGylated) liposome that enhances its circulation increase tumour cell specificity and lowers its toxicity profile.	Minotti <i>et al.</i> , 2004
<b>TARGET: Cell Cycle</b>					
<b>1978</b> <b>Taxanes -</b> <b>Paclitaxel</b> <b>(Taxol®),</b> <b>Docetaxel</b> <b>(Taxotere®)</b>	Originating from the well-publicised pacific yew plant, approved for use in OC in 1992	Tubular-targeting drug that inhibits microtubule segregation, promoting its polymerisation, thus preventing cell cycle events such as spindle assembly and chromosome segregation. The cell averts cell division or undergoes apoptosis.	Dose-limiting toxicity	Due to its toxicity, it is usually used post-platinum-resistance as a second-line of treatment or first-line with steroids.	Weaver, 2014
<b>1990s</b> <b>Gemcitabine</b>	Gemcitabine is commonly used for platinum-sensitive recurrent OC, and less so in platinum-resistant disease.	It primarily blocks G1/S progression at the S-phase as cell growth is also inhibited through minor mechanisms as the gemcitabine metabolites affect other regulatory processes.	Mono-therapy has the lowest response rate when compared to combination therapy with cisplatin, oxaliplatin, PEGylated liposomal doxorubicin and topotecan	Its rare property of 'self-potential' makes gemcitabine attractive, especially in platinum resistance disease.	Matsuo <i>et al.</i> , 2010 Grisham <i>et al.</i> , 2013 Plunkett <i>et al.</i> , 1995

TARGET: Survival Pathways					
<p><b>1997</b> <b>Bevacizumab</b></p>	<p>Bevacizumab is a humanised monoclonal antibody with mouse origin</p>	<p>Inhibits Vascular endothelial growth factor (VEGF) that promotes the growth of blood vessels in response to hypoxia, thus reducing tumour activity by altering its vascular nature.</p>	<p>Adverse effects such as hypertension and gastrointestinal perforation were noticed</p>	<p>Side effects need to be considered when treating cancer of this nature</p>	<p>Ellis, 2006 Perren <i>et al.</i>, 2011</p>
<p><b>1997</b> <b>PARP inhibitors</b></p>	<p>Poly-ADP ribose polymerase (PARP) inhibitors capitalise on the difference between healthy and cancer cells.</p>	<p>Healthy cells have many compensatory pathways to deal with DNA damage; however, as tumours become increasingly mutagenic their pathways streamline leaving them with fewer repair pathways than the healthy cells, sometimes only one compensatory pathway is left. Many times, this compensatory pathway involves PARP, a DNA damage sensor for both DSB and SSB repair pathways, and a PARP inhibitor can completely cut the tumour of its survival.</p>		<p>PARP mono-therapy is used in BRCA deficient cells, where it was found 90% more effective than in wild-type cells in addition to being 3X more potent than cisplatin. In combination therapy, PARP inhibitors render the cell unable to repair damage after cytotoxic effects.</p>	<p>Brown <i>et al.</i>, 2017 Kelley <i>et al.</i>, 2014 Weil and Chen, 2011</p>

### **1.1.7 Drug Resistance**

While chemotherapy is highly effective, especially in earlier stages, OC can be oftentimes diagnosed too late. In less than six months, 80 - 90% of patients relapse and by the end of two years, they fail to respond to any available chemotherapy, where this resultant chemoresistance can be due to a plethora of factors (figure [1.7](#)) (Norouzi-Barough *et al.*, 2017). Recurrence typically diagnosed via a CA-125 test or computed tomography (CT-) scan receives second-line chemotherapy and are also considered for surgery if beneficial (Jayson *et al.*, 2014).

The interest in 'platins' has slowed down; however, it has resurged amid the increase of drug resistance. The platinum-resistant disease has the potential of 15% response within six months of platinum treatment, partial sensitivity after 6-12 months of being platinum-free with increasing sensitivity in reoccurrence after 12 months (Jayson *et al.*, 2014). Following further rounds of alternative drugs, surgical de-bulking and relapses, the patient is left with an inoperable metastatic disease with multi-drug resistance (MDR). Post-acquisition of MDR, the patient is switched from curative to palliative care where a series of non-specific/sub-standard chemotherapeutics, hormone therapy and pain relievers are used to ensure comfort over cure (Palaia *et al.*, 2019).

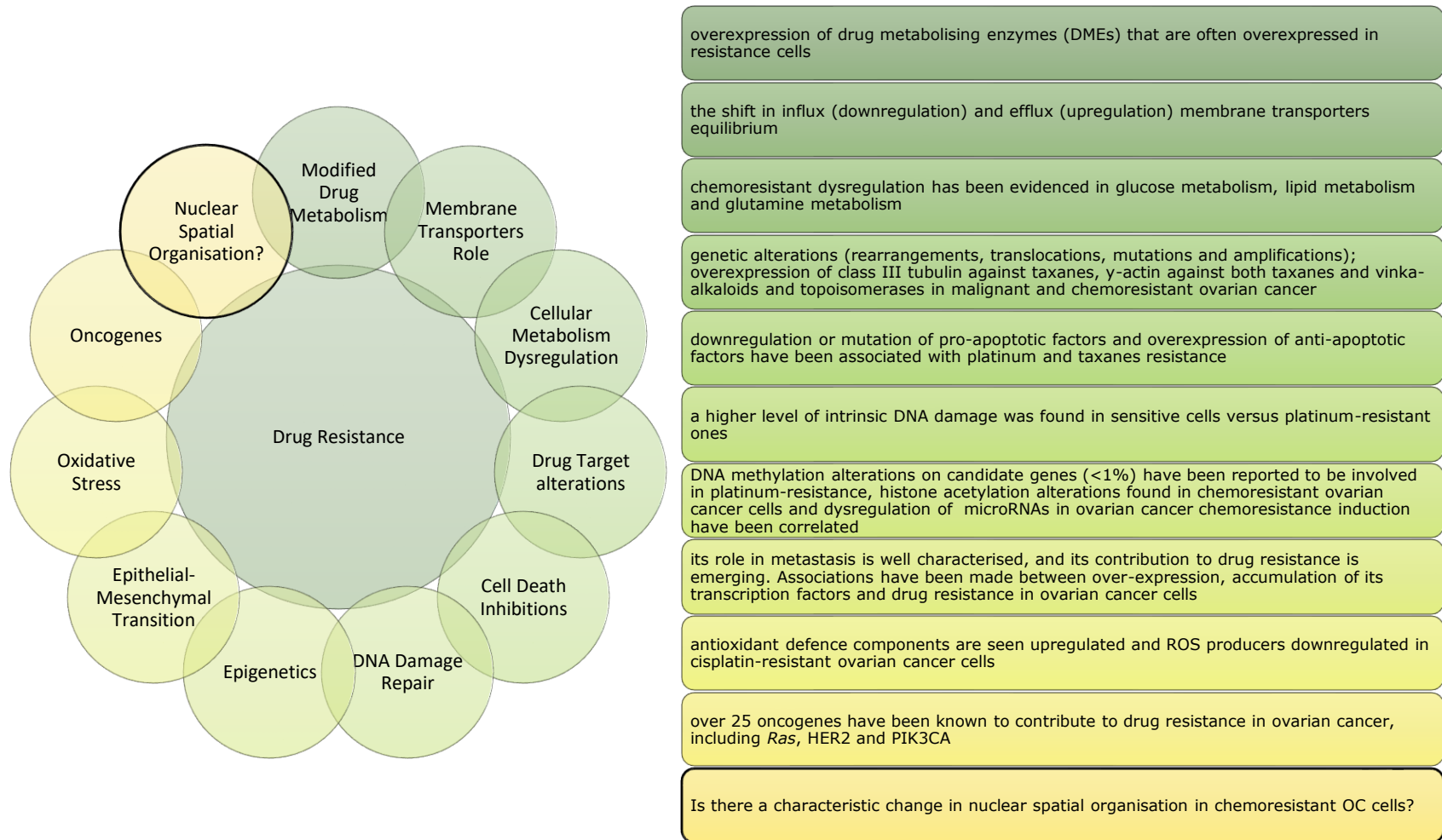


**Figure 1. 7 Causes and Characteristics of Drug resistance:**

The plethora of factors or a combination of adaptive dysregulations continues to be a challenge in combating drug-resistance.

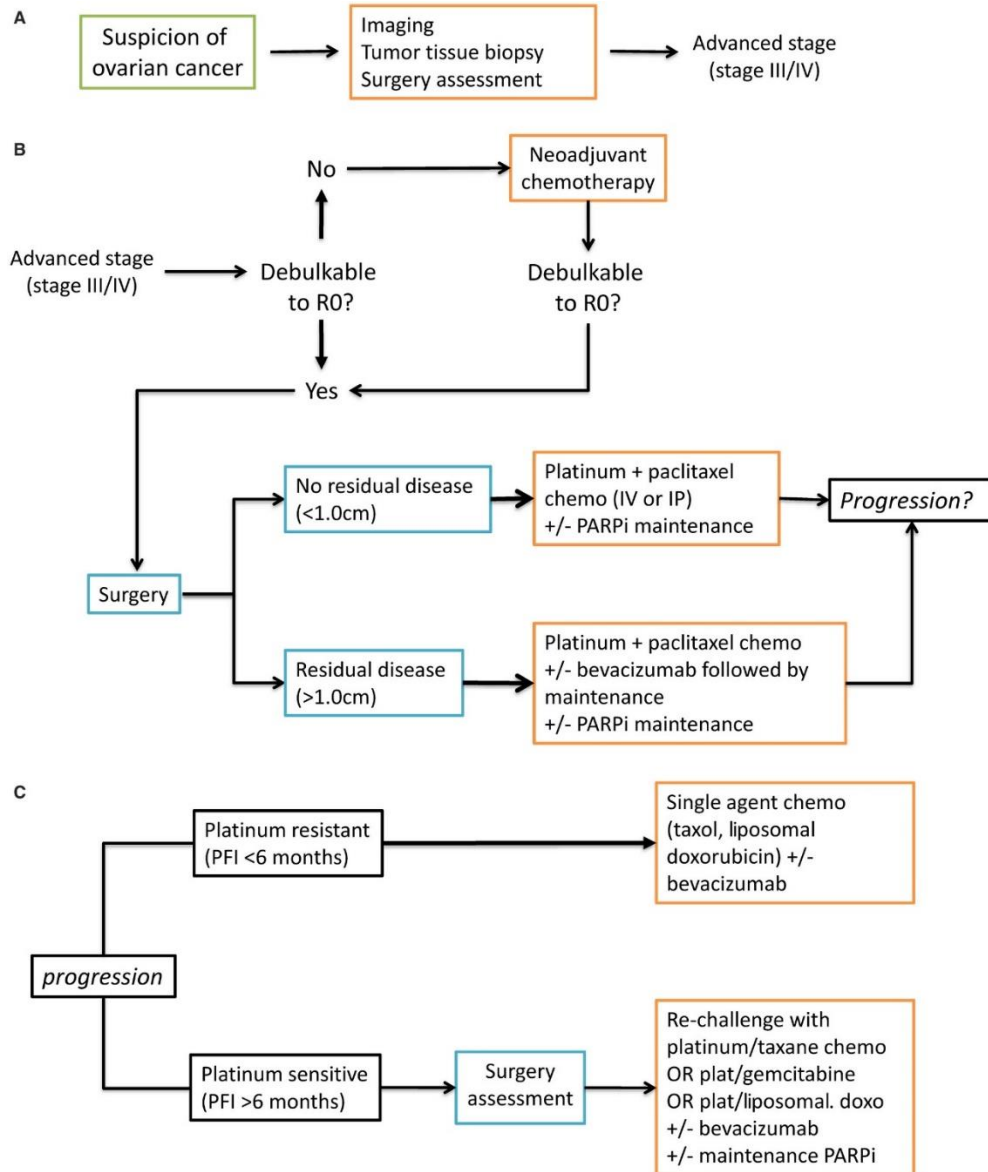
- adapted from in Norouzi-Barough et al., 2017.

**5.1.1.1 Resistance principle**

Under the 'resistance principle', the tumour cells undergo selective pressure through chemo-drugs and adapt through the acquisition of new traits that resembles that of the healthy cell, thus evading treatment like non-tumorigenic cells (Rosa *et al.*, 2014; Bell & Gilan, 2020). The new traits can be auto-acquired or from healthy cells that they used as a template (Rosa *et al.*, 2014). This includes reverse mutations such as in BRCA1/2 mutations, the reappearance of healthy copies of chromosomes as seen in the PEO1/PEO4 eOC cell lines and an increase genomic stability since proliferation rate is slowed due to the re-activation of pathways such as DDR, MAPK and mTOR, both previously interrupted in the sensitive cancer versions (Swisher *et al.*, 2008; Cooke *et al.*, 2010; Kozar *et al.*, 2019). Chemotherapy relies on rapidly dividing cells; therefore, our thinking of tackling chemoresistant cells needs to change as they may not be as rapidly dividing in the same way.

**1.1.8 Summary**

OC is a daunting reality, and the timespan between diagnosis to a chemoresistant disease is short, thus equal attention is needed on both earlier diagnosis and chemoresistance. There is still a long way to go for reliable early-stage / predictive biomarker and curative adjuvant options in chemoresistance, but information on the molecular mechanisms is growing rapidly; however, offering a better outlook on the disease.



-image source: Lheureux, Braunstein and Oza, 2019

**Figure 1. 8 Summary of the Treatment Guidelines in OC (advanced):**

**A.** Diagnosis, **B.** frontline management, and **C.** treatment upon recurrence.

+/- indicates with/without; chemo -chemotherapy; doxo -doxorubicin; IP -intraperitoneal; IV -intravenous; PARPi -PARP-inhibitor; PFI -platinum-free interval; plat -platinum; R0 -reduction of tumour bulk with 0 residual disease.

## 1.2 THE NUCLEUS

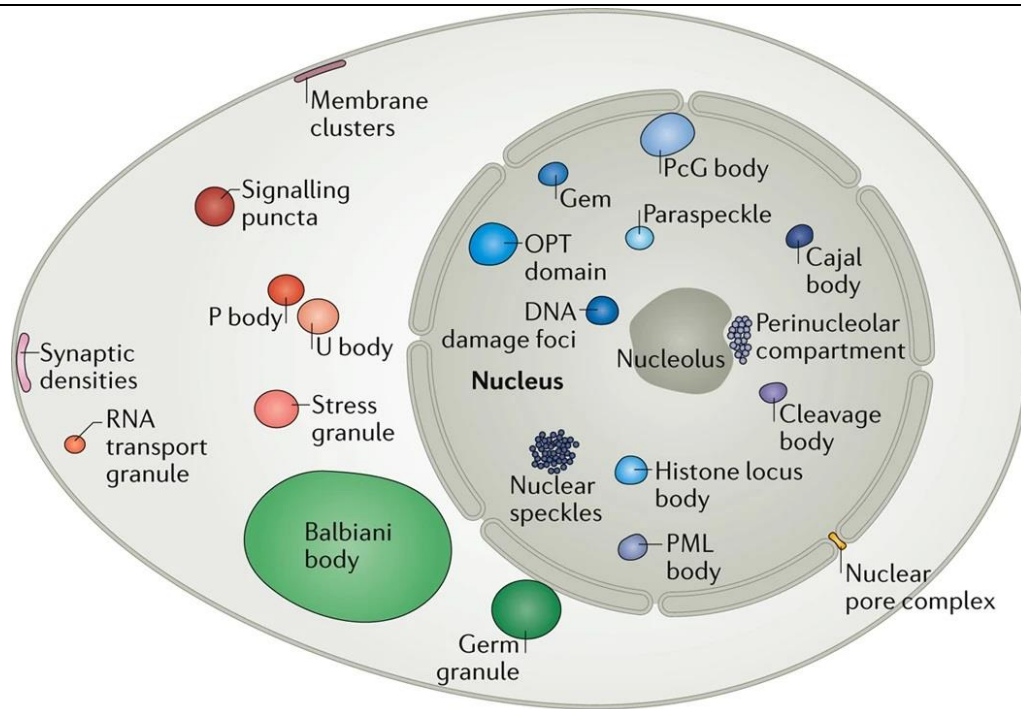
Cells and tissues are routinely used as diagnostic tools, however in the 1930s-40s, as technology improved studies started looking towards the nucleus. During these decades, **George Papanicolaou**, developed a stain, known as the 'Pap test' that studied the structure of the cytoplasm and the nucleus, differentiating and diagnosing pre-malignant stages cervical cancer which led to its decrease from the leading cause to the eighth cause of cancer-related death amongst women (Zink *et al.*, 2004). Nuclear morphological features such as shape, size and nucleus-cytoplasmic ratio has potent disease diagnostic and prognostic potential that also translates to OC cells as they can be distinguished by their large nucleus; and it was not until recently that nuclear architecture could be studied on a molecular level (Sengupta *et al.*, 2020). The first and largest organelle discovered within the cell was the nucleus in the 17th century, a recognised site of numerous functions; preservation, storage, processing, and duplication of information encoded on DNA made possible by a tightly controlled high-level spatial architecture (Crosetto and Bienko, 2020).

There is a growing wealth of information that supports the non-random three-dimensional (3D) arrangement of the genome as a determining factor in transcription which has not been limited to mammalian cells as a similar organisation was found in yeast (Zink *et al.*, 2004; Lanctôt *et al.*, 2007; Zaidi *et al.*, 2007; Akhtar and Gasser, 2007; Gorkin, Leung and Ren, 2014). Transcription and transcription factors, determine if, when and what extent a gene is expressed or not, thus, any perturbations (genetic or epigenetic) set off a chain reaction to the disease. Most carcinogenic pathways are not fully understood; as cancer was thought to be driven primarily by sequence mutations; nevertheless, it is now widely acknowledged that the contribution to carcinogenesis goes beyond the sequence (Crosetto and Bienko, 2020).



### **1.2.1 Genome Organisation – The Right Place at the Right Time**

Within recent years, the high degree of nuclear organisation research directed the recognition of chromatin and sub-nuclear components such as the nuclear envelope (NE), nuclear matrix, nuclear bodies, and the nucleoli that ensures the efficient functioning and cross-talk of processes; where disruptions to the components led to nucleopathies and cancer (van Driel, Humbel and de Jong, 1991, Strouboulis and Wolffe, 1996, Foster and Bridger, 2005). This also revealed chromosome territories (CTs) where chromosomes are packaged into a spatially limited volume and, at the sub-chromosomal level, organisation comprises of the metaphase chromosomes, A/B compartments (as identified by high-throughput chromosome conformation capture (Hi-C)), small domains such as lamin-associated domains (LADs), larger domains such as topologically associating domains (TADs) and long-range chromatin looping (Lieberman-Aiden *et al.*, 2009; Dixon *et al.*, 2012; Rao *et al.*, 2014). The organisation of membrane-less bodies and domains spontaneously arise as outlined by the recent emergence of the phase separation principle (figure [1.9](#)) (Banani *et al.*, 2017; Shin and Brangwynne, 2017). This would explain why bodies such as the nucleoli and nuclear speckles remain distinct from nucleoplasm without a membraned divider (Dundr, 2012). These bodies collectively recognised as 'biomolecular condensates' contain macroscopic properties that govern specific molecular interactions resulting in behaviour similar to that of liquid droplets and by extension may play a role in compartmentalising chromosomes into territories or sub-compartments in the nucleus (reviewed in Adriaens *et al.*, 2018).



- image Source: Banani et al., 2017

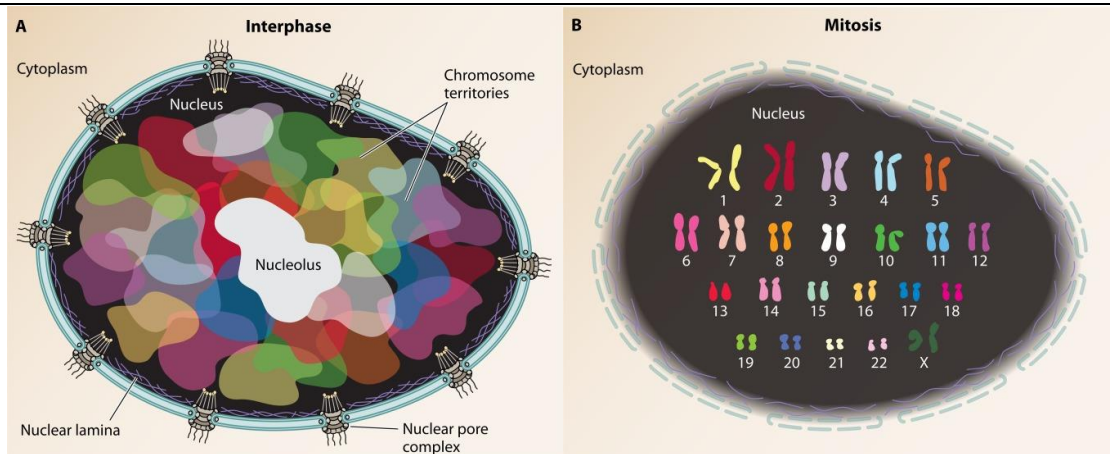
### Figure 1. 9 Phase Separation in the Eukaryotic Cell:

Schematic of the numerous biomolecular condensates in the membranes, cytoplasm and nucleus of eukaryotic cells. Some compartments are cell-type specific, such as Balbiani bodies and germ granules in germ cells, and RNA transport granules and synaptic densities in neuronal cell types.

Phase separation does not account for the location or relocation of a body or domain, and while it is a relatively new, more multidisciplinary high-throughput work on its dynamics is required. Aside from the genome being organised in an energetically stable emulsion of concentrated condensates, phase separation still poses many questions such as what determines the sites of the condensates, time of assembly or disassembly, how does it affect the genome, and its contribution to disease progression and cancer?

### 1.2.1.1 Chromosome Territory History

Up until the 19th century, it was believed that chromosomes were temporary structures that formed at the start of mitosis and subsequently dissolved in the daughter nuclei like soup. Turning into the 20th century, Carl Rabl, 1885 hypothesised that chromosomes are organised into territories while still maintaining their genetic and structural integrity throughout the cell cycle and Theodor Boveri, 1909 coined the term 'chromosome territories' (figure 1.10) (Cremer *et al.*, 1993). They further stated that the territories also do not mix; however, the idea was abandoned up until five decades ago when Cremer *et al.*, 1976 applied laser-UV-micro-irradiation (257nm) on the interphase nuclei Chinese hamster cells, qualitatively confirming territorial organisation postulated by Rabl and Boveri. Thomas and Christoph Cremer used radiography to track radioactively labelled nucleotides incorporating into the location of DNA, damaged by the laser beam, which showed very few adjacent chromosomes affected following the next metaphase cycle. Finally, in 1999, Croft *et al.* demonstrated the radial organisation of human chromosomes 18 and 19 in the nucleus relative to the periphery and centre.



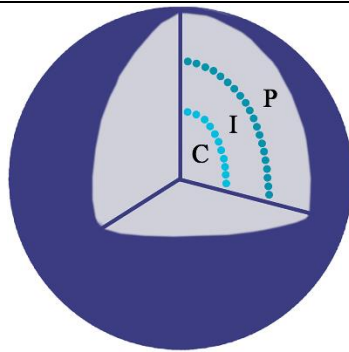
- image source: Fraser *et al.*, 2015.

**Figure 1. 10 Human Genome Organisation within the 3D Nucleus:**

**A.** CTs during interphase; nuclear pore complexes perforate the NE, and the nuclear lamina shown as a filamentous mesh inside the NE and the nucleolus in white. **B.** Female karyotype in mitotic cells.

### 1.2.1.2 Radial Position

From 1985 onwards, quantitative progress was made with fluorescence *in-situ* hybridisation (FISH), and three-dimensional microscopy, which further found that CTs are not randomly positioned but are situated in preferred radial positions relative to the **nuclear periphery** emphasising the significance of functional compartmentalisation (figure 1.11) (Bridger and Bickmore, 1998; Croft *et al.*, 1999; Cremer *et al.*, 1993).



- image source: Orsztynowicz *et al.*, 2017.

#### Figure 1. 11 A Schematic Representation of Radial Positioning within the Nucleus:

FISH probe signal is positioned radially from nuclear border to the nuclear centre divided three locations C - central, I - intermediate and P - peripheral as evaluated distance.

In the mammalian cell, compartmentalisation begins with chromatin of two types; tightly packed heterochromatin, that is intensely stained with a predominance at the nuclear lamina (NL) and euchromatin which is 1.4x less condensed in the nuclear interior (Fedorova and Zink, 2008). This has led to the notion that the nuclear periphery is transcriptionally repressive and the nuclear interior is transcriptionally permissive, however more recent findings suggest that this compartmentalisation is not exclusive and that there are other determinants of radial chromatin positioning (Kupper *et al.*, 2007; Kumaran and Spector, 2008; Finlan *et al.*, 2008).

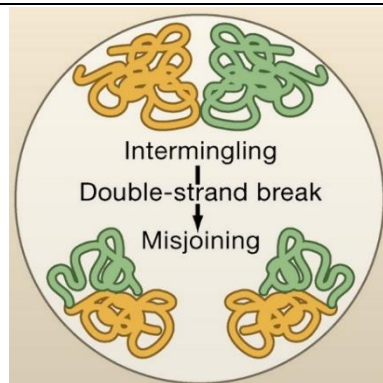
There are many studies of the altered radial organisation of chromosomes in cancer, for example, Cremer *et al.*, 2003 reported that while cancer cell lines showed positioning according to gene

density, up to 31% had inverted positions for chromosome 18 and 19 and Murata *et al.*, 2007 reported a similar inversion in a third of papillary thyroid carcinoma cells. Furthermore, activated oncogenes were observed to be preferentially located in the nuclear interior in some cancers, while others appeared at the periphery (Harnicarova *et al.*, 2006; Bartova *et al.*, 2000/2005; Wiech *et al.*, 2009; Meaburn and Misteli., 2008). In Meaburn and Misteli, 2008 extensive study in breast cancer, identified genes with altered positions that repositioned during early tumorigenesis, however, many of which showed no correlation with the change in transcription. Aberrant radial positioning of the genome remains unclear.

### **1.2.1.3 Karyotype and translocations**

Radial positioning is evolutionarily conserved for over 300million years irrespective of highly divergent karyotypes (Tanabe *et al.*, 2002). In humans, chromosome positioning appears stable with aneuploidy, as the regulating, positioning mechanism stays the same even though the chromosome numbers change (Bridger, 2000; Boyle *et al.*, 2001; Tanabe *et al.*, 2002). This can be observed when chromosome 18 and 19 maintained their positions as diploids and triploids (including cancer) in addition to chromosome X being maintained at the periphery despite increased ploidy (Croft *et al.*, 1999; Boyle *et al.*, 2001; Cremer *et al.*, 2003. For these reasons, the karyotype of these cell lines (figure [2.1](#)) would not be considered a primary factor.

Differences in chromosomes position for translocated derivatives are specific to the chromosomes involved, but in several human tumours, no shift in chromosome territory has been observed (Cremer *et al.*, 2003). In the lymphocyte nuclei, chromosome 18 (periphery) and 19 (interior) are located separately, where the derivative t(18;19) did not significantly relocate however the translocated material of chromosome 19 oriented towards the centre where it typically locates (Croft *et al.*, 1999). On the other hand, chromosome organisation in terms of proximity can, in turn, influence the frequency of translocations resulting in novel fusion transcripts inducing carcinogenesis (figure 1.12) (Lever and Sheer, 2010).



- image source: Misteli, 2007.

### Figure 1. 12 Chromosomal Translocations:

Physical chromosome proximity contributes to the probability of translocations. Following the malfunctioning of DSB repair and apoptosis evasion, parallel double-strand breaks illegitimately join possibly creating rearrangements with a selective growth advantage (reviewed in Lever and Sheer, 2010).

Chromosomal rearrangements can lead to aberrant gene expressions that are essential in carcinogenesis, as the resultant gene fusions can produce oncogenic activity (duplications and amplifications) or remove tumour suppressing activity (deletions) (Mitelman *et al.*, 2007). In cancer, the formation of translocations can be explained by two models; the 'breakage-first' model DSBs move then recombine or the 'contact-first' model DSBs recombination arise from already proximally positioned chromosomes (Soutoglou and Misteli., 2007; Misteli and Soutoglou., 2009). Translocation recombination events of proximally close chromosomes are proposed to take place at

the boundary of the chromosome territory (CT) since transcriptionally active loci are located at the boundary it increases the tendency for translocation also supporting correlations of transcriptional activity and recurrent translocations (reviewed in Lever and Sheer, 2010).

#### **1.2.1.4 Gene Density vs Chromosome Size**

CT organisation builds that gene-rich regions of the genome are positioned at the interior and gene-poor chromosomes peripherally (Croft *et al.*, 1999 and Bridger *et al.*, 2000). In the rod cells of nocturnal mammals, this is observed where the active gene-rich chromosomes hold a perinuclear location and the inactive genes towards the nuclear centre, possibly accounting for an evolutionary adaptation to low-intensity light vision (Solovei *et al.*, 2009). Pigs also showed gene-rich regions; murine fibroblasts have gene-rich and -poor regions internally and peripherally respectively; the primate homologues of chromosome 18 (gene-poor) and 19 (gene-rich) in chickens showed periphery and central locations respectively; however, there was also a tendency for larger chromosomes to occupy peripheral locations highlighting that gene density is not the sole determinant of chromosome positioning (Habermann *et al.*, 2001; Federico *et al.*, 2004; Mayer *et al.*, 2005; Tanabe *et al.*, 2005).

Gene-density organisation correlated with round nuclei as in lymphocytes, and, when the nucleus shape was oval or ellipsoid as in fibroblasts, a size-dependent organisation predominates; however, this was primarily under quiescence or early S-phase in fibroblast as gene-density was observed outside these phases (Bridger *et al.*, 2000; Cremer and Cremer, 2001; Croft *et al.*, 1999; Sun, Shen and Yokota, 2000; Boyle *et al.* 2001; Bolzer *et al.*, 2005; Meaburn *et al.*, 2007). In lymphocytes and fibroblasts, chromosome 18 is at the periphery, and chromosome 19 is at the nuclear interior; furthermore, it was also observed in fibroblasts when chromosome 18 and 19 were both centrally located; chromosome 19 would locate more internally due to having double the number of genes than chromosome 18 (Croft *et al.*, 1999; Bolzer *et al.*, 2005; Sun, Shen and Yokota, 2000). In

addition, Sun, Shen and Yokota, 2000 outlined that smaller chromosomes like 19 and 21 are centrally located in fibroblasts cells while Bickmore, 2013 showed gene-rich chromosome 22 as the most centrally located chromosome, supporting both the size and gene density factor. The influence of gene density or chromosome size is not absolute, but one can take precedence over the other.



### 1.2.1.5 Activity

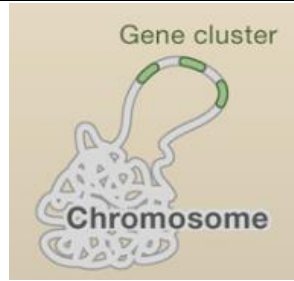
Location is also determined by activity and expression where chromosomes are functionally compartmentalised for two main regulatory processes; activation (compartment A) and silencing (compartment B), and for the same reasons, they are re-organised within the nucleus (Lieberman-Aiden *et al.*, 2009; Simonis *et al.*, 2006). The distinct location and relocation of chromosomes are influenced by transcriptional activity within the nuclei (Finlan *et al.*, 2008; Fritz *et al.*, 2016).

The nuclear interior is correlated with activity, and the nuclear periphery is often implicated as the silencing regions; however, being positioned at the nuclear periphery does not render a gene inactive nor inaccessible, as some expression does take place at the periphery in mammalian cells and yeast while some active genes are found at the nuclear pores, in other words, peripheral location does not mean peripheral repression (Brickner and Walter *et al.*, 2004; Casolari *et al.*, 2004; Cabal *et al.*, 2006; Taddei *et al.*, 2006; Takizawa *et al.*, 2008). Whole chromosome re-positioning has been observed in erythroid differentiation, adipogenesis, T-cell differentiation, porcine spermatogenesis, post hormonal stimulus, and serum stimulation that was further shown to take place within 15 minutes (reviewed in Bartova and Kozubek, 2006; Mehta *et al.*, 2010). Though the mechanisms are not clear, genes have also been evidenced in the same manner; the non-random spatial positioning of active genes in the interior and inactive genes towards the periphery has been observed for *IGH* and *CD4*, vice versa for *CD8* and *RB1* that does not move regardless of activity (Skok *et al.*, 2001; Bartova *et al.*, 2002; Mahy, Perry and Bickmore, 2002; Kosak *et al.*, 2002; Roix *et al.*, 2003; Kim *et al.*, 2004; Scheuermann *et al.*, 2004; Takizawa *et al.*, 2008).

### 1.2.1.6 *Out-looping*

Within CTs, genes cluster for transcription efficiency, where gene-rich clusters orient towards the interior and gene-poor clusters orient towards the periphery (Shopland *et al.*, 2006). Within the X CT, the rim is lined with gene-rich regions, and the non-coding regions are internalised, regardless of activity (Clemson *et al.*, 2006). Some genes such as *c-MYC*, *PAX6* and *TTN* do not significantly alter their location within their chromosomal territory and on the other extreme are genes or gene clusters that extend out (generally towards the interior) and intermingle with the territory of another (Volpi *et al.*, 2000; Mahy, Perry and Bickmore, 2002; Williams *et al.*, 2002; Bartova *et al.*, 2002; Ragozczy *et al.*, 2003; Galiová, Bártoová and Kozubek, 2004; Scheuermann *et al.*, 2004; Chambeyron *et al.*, 2005; Branco and Pombo, 2006).

The 'neighbourhood effect' highlights that nearby changes in expression sometimes drive re-positioning events where genes are simply a passenger of adjacent genes (preferentially clusters). The extreme case of loop expulsion over several micrometres encompassing active multigene clusters from their CT is prominently exemplified in murine and human cells; when actively transcribing, the human major histocompatibility complex II (MHC class II) locus extends out of chromosome 6, however, does so preferentially towards chromosome 1, 2, and 9 but not chromosome 8 territory (figure [1.13](#)) (Volpi *et al.*, 2000; Branco and Pombo, 2006). Later observations include clusters containing *FLNA* on chromosome X, genes on chromosome 11, epidermal differentiation complex genes,  $\beta$ -globin-like genes, mouse *Hox* cluster, genes inducing porcine stem cell differentiation into adipocytes (Mahy, Perry and Bickmore, 2002; Williams *et al.*, 2002; Ragozczy *et al.*, 2003; Scheuermann *et al.*, 2004; Galiová, Bártoová and Kozubek, 2004; Chambeyron and Bickmore, 2004; Chambeyron *et al.*, 2005; Szczerbal, Foster and Bridger, 2009).



- image source: Misteli, 2007

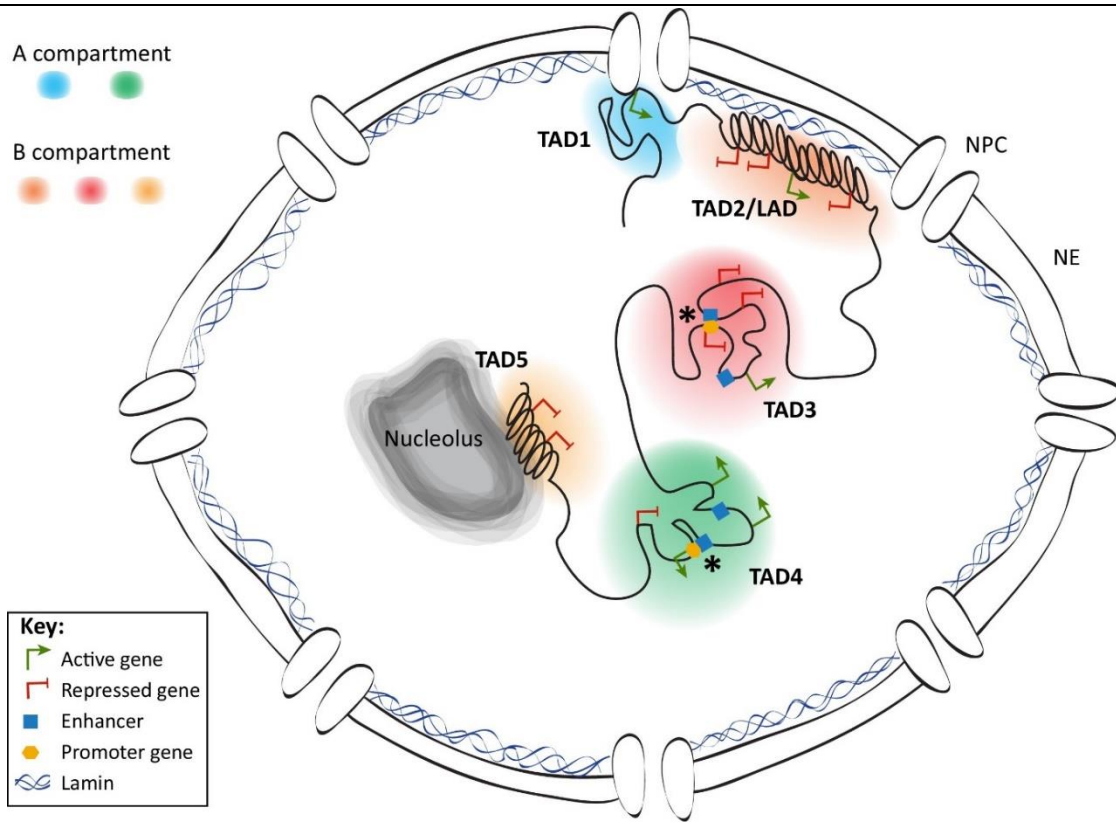
**Figure 1. 13 Chromosome Out-Looping:**

Gene cluster extending out of its CT via the formation of a large chromatin loop.

Loci out-looping (thought to be facilitated via the inter-chromosome domain (ICD) but, challenged by Branco and Pombo, 2006) are usually directed towards active RNA Pol II, Cajal bodies and splicing speckles/SC35 domains, that is affected when RNA polymerase II transcription is inhibited suggesting purpose in expression (Boyle *et al.*, 2001; Fedorova and Zink, 2008; Heard and Bickmore 2007; Bickmore, 2013). Looping has led to the reconsideration of CTs to include the 'territory core' visualised with standard chromosome 'paints' and the 'territory corona' the surrounding territory visualised by FISH using locus-specific probes or gene-dense chromatin probes (Bickmore and van Steensel, 2013). In this framework, looping starts from the core into the one own's corona into the corona of a neighbouring territory (Bickmore and van Steensel, 2013). A base for tethering is also required as findings have shown this type of associations with the nuclear periphery, nuclear pore complex, nucleolus and the abundant transcription/replication factories that they loop towards (Ishii *et al.*, 2002; Cook, 2002; Byrd and Corces, 2003; Yusufzai *et al.*, 2004; Chakalova *et al.*, 2005; Noma *et al.*, 2006; Misteli, 2007). Extensive chromatin looping is more prevalent than thought, as it is an energetically and functionally favourable arrangement (Branco and Pombo, 2006; Marenduzzo, Micheletti and Cook, 2006).

### **1.2.1.7 Topologically Associated Domains (TADs)**

Chromatin are also organised into TADs categorised with the A/B compartmentalisation (figure [1.14](#)) (Gonzalez-Sandoval and Gasser, 2016). Each TAD is evolutionary conserved and enriched for certain proteins to express a subset of genes specific to the identity of the cell (Gonzalez-Sandoval and Gasser, 2016; Valton and Dekker, 2016). There are also regions insulated against TADs to limit 3D interactions of distant regulatory regions (reviewed in Azagra *et al.*, 2020). Dynamic long-range interactions are detected in TADs among promoters and enhancers to regulate the activation or repression of transcription (Gonzalez-Sandoval and Gasser, 2016). The disruption of TAD boundaries reveals genes to unsuitable regulatory elements resulting in abnormal gene expression (Valton and Dekker, 2016; Campbell, 2019). Carcinogenesis as a result of TAD disruption can take place via two mechanisms; one where the boundaries are deleted or mutated leading to the fusion of two adjacent TADs and the other that includes genomic rearrangements that breaks up the TADs, creating new ones while the boundary remains unaltered (reviewed in Valton and Dekker, 2016). This highlights the vital role in understanding the mechanisms and long-range chromatin control of TADs and how mutations, deletions and rearrangements can lead to the dysregulation of TSGs and oncogenes.



- image source: Gonzalez-Sandoval and Gasser, 2016.

**Figure 1. 14 Topologically Associating Domains (TADs):**

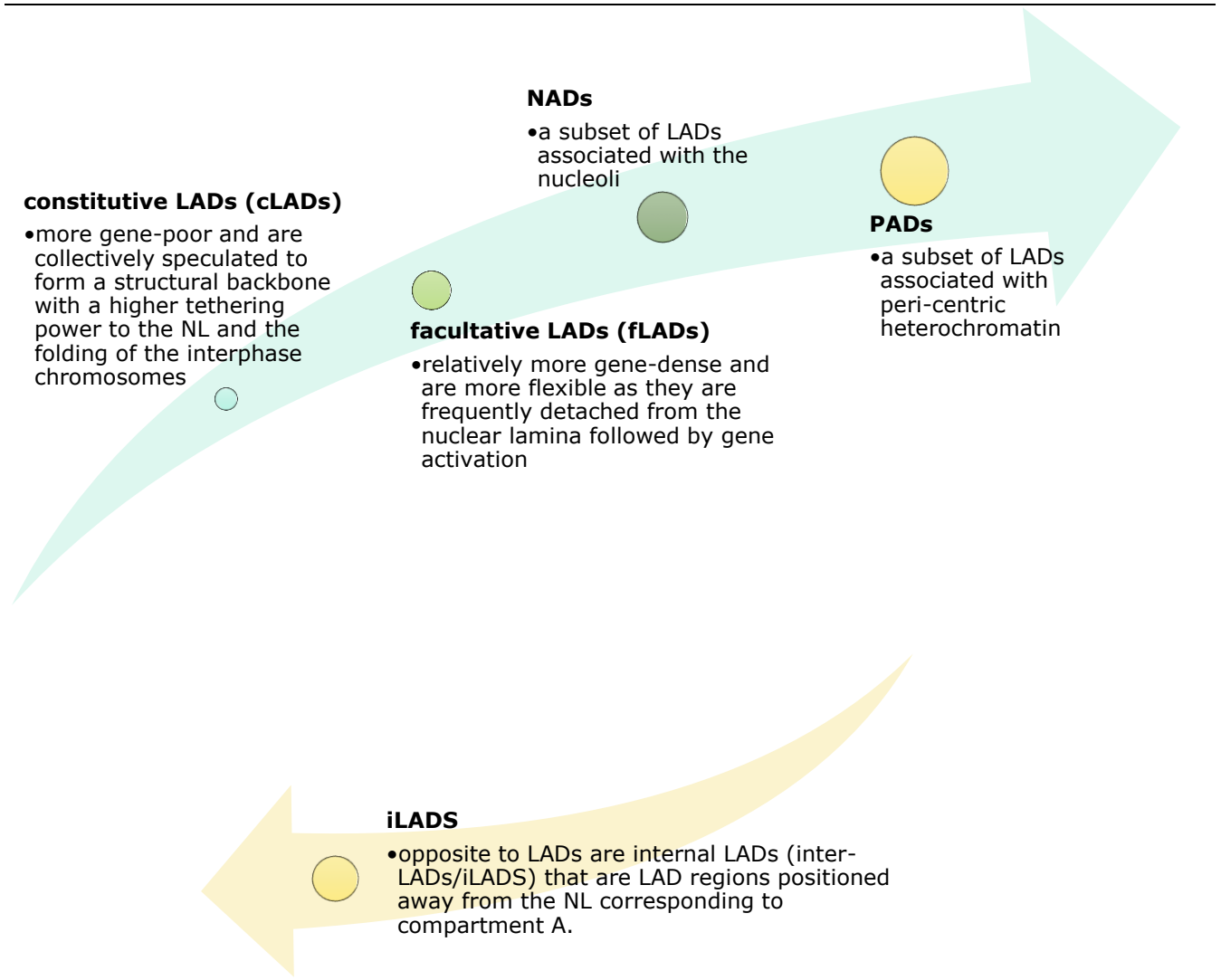
TADs classified into two compartments: A-type (active) or B-type (inactive) (orange, red, yellow). Within a given TAD is an enrichment of specific proteins for tailored gene expression. \* - TADs encompass long-range chromatin interactions that are detected between promoters and enhancers, leading to the activation or repression of genes. NPC - nuclear pore complex and NE - nuclear envelope.

TADs with NL association have also been defined as LADs; therefore, a LAD can encompass a few TADs, and a TAD can encompass a one or more LADs (Gonzalez-Sandoval and Gasser, 2016). LADs overlap to a more significant extent with B compartments (Gonzalez-Sandoval and Gasser, 2016).

### 1.2.1.8 LADs

LADs are genomic regions that interact with the NL exhibiting roles in anchoring, organisation and gene repression. LADs form a condensed dynamic layer of chromatin lining at the NL moving to and from the periphery and partially randomised after each mitosis (van Steensel and Belmont, 2017). In mammalian cells, there are ~1,000 – 1,500 LADs covering more than one-third of the genome, and in murine embryonic stem cells they were found to lower expression by 1000-fold compared to genes located elsewhere; rendering them noteworthy (reviewed in Irianto *et al.*, 2016; van Steensel and Belmont, 2017). Their features are typical of heterochromatin as they are less transcriptionally active with a low gene-density and found to overlap to a larger extent with B compartments (figure [1.15](#)) (Guelen *et al.*, 2008).

Both LADs and the NL are polymeric entities that result in multivalent interactions that stably secures chromosomes to the periphery via non-overlapping regions, NE transmembrane proteins (NETs) and barrier-to-autointegration factor (BAF) (reviewed in van Steensel and Belmont, 2017). However, whether and how lamins play a role is still an open question as they were found to play zero roles in facilitating genome-wide LAD organisation in murine ES cells further suggesting that lamins are not a significant determinant of LADs, instead roles of other non-lamin NE components such as lamin-associated proteins (LAPs) and NETs (Amendola and van Steensel, 2015; reviewed in Irianto *et al.*, 2016; van Steensel and Belmont, 2017).



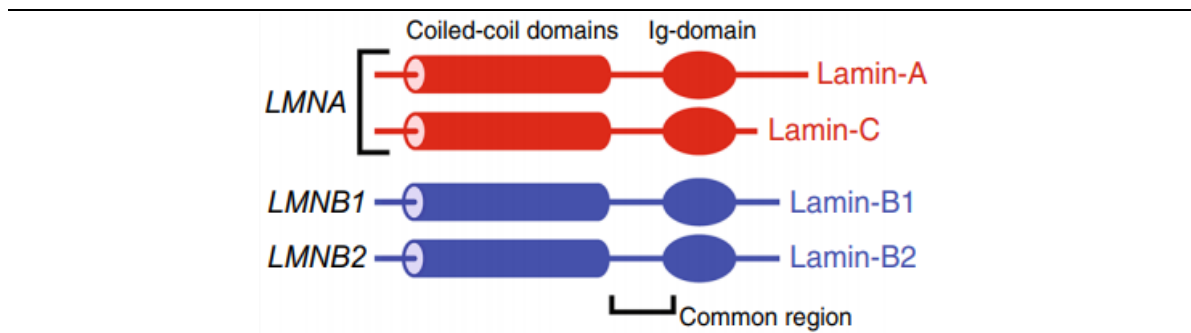
- image info: reviewed in van Steensel and Belmont, 2017.

**Figure 1. 15 Summary of Sub-LADs Hierarchy:**

NADs and PADs have substantial overlap with LADs, not identical; however, may have the same preserved outcome; hence complete silencing is not dependant on peripheral location (van Steensel and Belmont, 2017). iLADs can be actively recruited to the nuclear interior while still attached by neighbouring LADs to the NL; this results in a 'tug of war' mechanism or 'chromatin stretching' through a possible force-generating mechanism (Khanna *et al.*, 2014).

### 1.2.2 Lamins

Since 40% of the genome associates with lamin proteins, genome organisation cannot be investigated without exploring related roles of lamins (Guelen *et al.*, 2008). The lamin family consist of A-type (Lamin-A, -C, -C<sub>2</sub>, and -A<sub>Δ10</sub>) and B-type (lamin-B<sub>1</sub>, -B<sub>2</sub> and -B<sub>3</sub>) lamins encoded by genes three genes *LMNA*, *LMNB1*, and *LMNB2* (figure 1.16) (Stuurman, Heins and Aebi, 1998). Lamin-C<sub>2</sub> and -B<sub>3</sub> are testis-specific and Lamin-A<sub>Δ10</sub> although it is somatic, its expression profile is uncertain.



- image source: Irianto *et al.*, 2016.

**Figure 1. 16 The Major Forms of Lamins (in somatic cells of human, mice and most other vertebrates):**

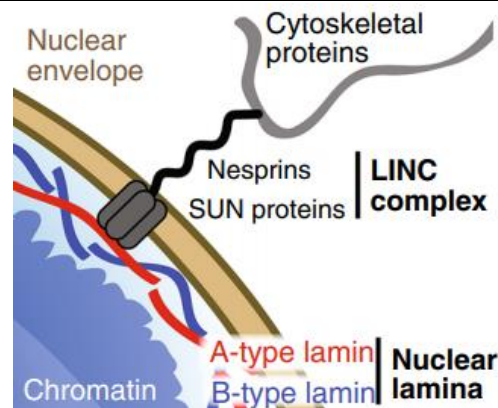
*LMNA* gene produces lamins A and C via alternative splicing whereas *LMNB1* and *LMNB2* separately encode Lamin B<sub>1</sub> and B<sub>2</sub> respectively. Lamins share common regions or amino acids but differ in their post-translational modifications.

A-type lamins are not expressed in early neuronal, embryonic or stem cells, whereas all nucleated cells express B-type lamins, indicative of both their essential roles in the lamina (reviewed in Burke and Stewart, 2013; Chen *et al.*, 2019). When Lamin B<sub>1</sub> and B<sub>2</sub> were knocked down in HeLa cells, it resulted in arrested growth and apoptosis and though lamin A/C is suggested to be non-essential at the cellular level, has been linked to at least 12 different diseases in addition to cancer (Burke and Stewart, 2013). Additionally, in murine keratinocyte or hepatocyte cells, lamin A/C role was fortified when lamin B<sub>1</sub> and B<sub>2</sub> was knocked down, the cells did not exhibit severe pathology as they expressed high levels of lamin A/C (Yang *et al.*, 2011a; Yang *et al.*, 2011b). Furthermore, in neuronal cells that exhibit little to no lamin A/C, a knockdown of lamin B<sub>1</sub> or B<sub>2</sub> rendered the cell



more susceptible to nuclear membrane rupture (Yang *et al.*, 2011a; Yang *et al.*, 2011b; Chen *et al.*, 2019). It is possible that A-type lamins step in when deficient in B-type lamins; however, while the role is not found reciprocated, there is still more research required.

The NE is dotted with nuclear pore complexes (NPCs) that are responsible for the transport of molecules between the nucleus and cytoplasm (Rout *et al.*, 2000). Within the envelope is the perinuclear space that houses the Linker of Nucleoskeleton and Cytoskeleton (LINC) complex. The LINC complex spans the entire membrane and directly connects the cytoskeleton with the NL possibly conveying mechanical signals to alter chromosomes (figure 1.17) (Rout *et al.*, 2000; de Lanorelle, 2012; Osmanagic-Myers *et al.*, 2015).



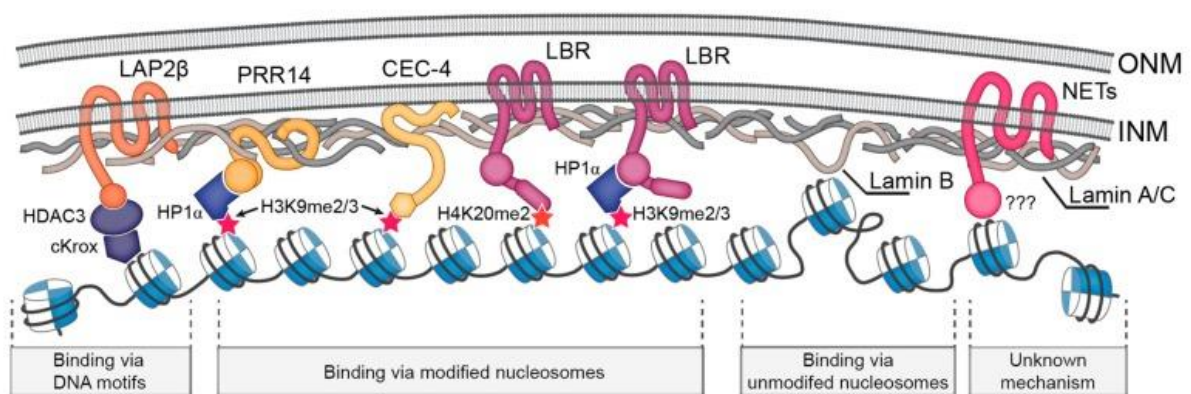
- image source: Irianto *et al.*, 2016.

#### Figure 1. 17 Continuity from the Cytoskeleton to the Nucleoskeleton:

The cytoskeletal network interacts with the lamins (juxtaposed networks on the inner NE) that may act as a mechanotransduction bridge between the chromosomes and the extracellular environment.

The architecture and regulation within the nucleus begin at the filamentous network of lamins primarily through tethering at the periphery via LADs relaying the signal to other nuclear proteins within the nucleoplasm. The mechanism of chromosomal regions attaching to the lamins via tethering constrains them in the nuclear peripheral region, through which approximately 500 loci are regulatorily silenced, a mechanism that remains unclear (figure 1.18) (Heun *et al.*, 2001; Chubb

*et al.*, 2002; Finlan, 2008; Fedorova and Zink, 2008; Shevelyov and Ulianov, 2019).



- image source: Shevelyov and Ulianov, 2019.

**Figure 1. 18 A Schematic Representation of the Three Assumed Lamina-Chromatin Tethering Mechanisms:**

The lamina components may bind with either specific DNA motifs, modified nucleosomes or unmodified nucleosomes present in LADs of the genome (Shevelyov and Ulianov, 2019).

Chromatin anchoring may be more intricate than originally thought since NE proteins and LADs show tissue-specific expression and cell-type variability, tethering could differ amongst cell types (van Steensel and Belmont, 2017; Burke and Stewart, 2013). Not all lamin-tethered genes are repressed, and the involvement other proteins have been suggested peripheral activation (Fedorova and Zink., 2008; Ibarra and Hetzer, 2015; Randise-Hinchliff and Brickner, 2016). Aberrant tethering or the lack of becomes a concern when carcinogenic pathways are set off due to abnormal transcriptional silencing of oncogenes and TSGs (Kazanets *et al.*, 2016; Burke and Stewart, 2013).

### 1.2.2.1 Lamin and Cancer

Lamins provide structural support for the nuclear membrane in addition to influencing the nuclear shape and when over or under-expressed profound disease implications are presented (Zink *et al.*, 2004; Bridger *et al.*, 2007; Burke and Stewart, 2013). Most notably the premature ageing disease Hutchinson-Gilford progeria syndrome (HGPS), attributed to a mutant lamin A (progerin), resulting

in radial organisation disruption, which is attractive as ageing is amongst the highest risk factors for cancer (Bridger *et al.*, 2007; Bickmore, 2013; reviewed in Irianto *et al.*, 2016). Normal nuclei have a regular ellipsoid shape but, in many cancers, an irregular sometimes tissue type-specific contour is observed and correlations are beginning to emerge between the dysmorphic nuclei (nuclear atypia) in cancers and lamins (table 1.3) (Zink *et al.*, 2004; reviewed in Irianto *et al.*, 2016).

**Table 1. 3 Changes in the Levels of A-type and B-type Lamins in Cancer:**

Type of cancer	A-type lamins	B-type lamins
Ovarian serous	↑	
Ovarian	↓	↑
Lung	↓	
Breast	↓	↓
Colon	↓	↓
Colorectal	↑	↑
Colonic and gastric	↓	
Primary gastric	↓	
Basal cell skin	↓	
Skin	↑	
Leukaemia	↓	
Prostate	↓	↑
Liver cancer		↑
Pancreatic cancer		↑

- adapted from Irianto *et al.*, 2016

Lamins fluctuations may indirectly affect cancer progression through chromosome conformation and tethering via LADs as well as fluctuating gene expression through transcriptional regulators (reviewed in Irianto *et al.*, 2016). Luxton *et al.*, 2010; Folker *et al.*, 2011 showed that cells absent of A-type lamins was incapable of nuclear re-positioning and centrosome polarisation. Lamins also serve to protect the genome by preventing chromosomal aneuploidies and regulate their spatial excursions within the nucleus as seen in the colorectal cancer cell line (DLD1) upon Lamin A/C and B<sub>2</sub> depletion (Ranade *et al.*, 2017). In the same cell line, Camps *et al.*, 2014 showed CT

decompaction and increased abnormal nuclear shapes in the absence of lamin B<sub>1</sub> and Sengupta and Sengupta, 2017 also revealed alterations in nucleolar morphology and nucleoplasmic dynamics upon lamin B<sub>2</sub> depletion.

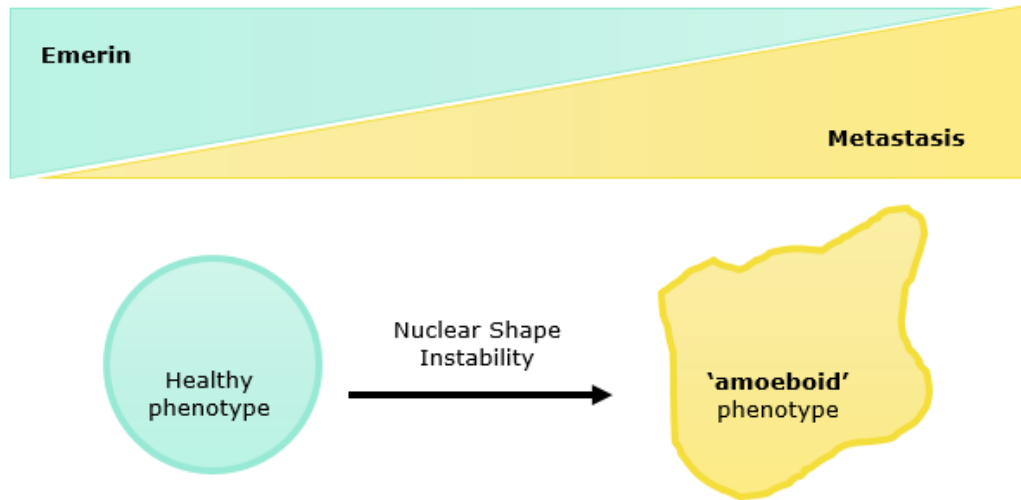
Previous studies have demonstrated the vital role of microenvironment mechanics in cancer progression which makes lamins particularly interesting since they were shown to be mechanosensitive and implicated in the hypothetical nuclear motor complex that includes nuclear myosin (Mehta *et al.*, 2008; reviewed in Irianto *et al.*, 2016). In 3D, lamins have shown roles in modulating cancer cell migration with impact on tumour growth. In Xenograft models, perturbed lamin A showed increased migration and overexpressed lamin A reflected a pro-survival function (Harada *et al.*, 2014). Lamins mirror tissue stiffness (a 'mechanostat') where the nucleus of stiffer tissues with also be stiffer due to a higher lamin content, as demonstrated *in-vitro* when lung cancer and primary mesenchymal stem cells were grown in a stiffer matrix, their lamin A/C levels were higher (reviewed in Irianto *et al.*, 2016). A-type lamins affect the morphology and visco-elastic properties of the nucleus in a way that over-expression increases nuclear stiffness (Osmanagic-Mayers *et al.*, 2016). While studies have shown that this might increase its nuclear integrity, it may also reduce invasive migration as the transient knockdown of lamin A/C led to the initial rapid growth of tumours and softer nuclei, with greater efficiency of migrating through small micro-pores (Osmanagic-Mayers *et al.*, 2016).

Currently, the cancer-related findings on lamins are limited, and further investigation is required for its mechanistic link, therapeutic, diagnostic and even its prognostic value as higher lamin A in breast cancer has been associated with better clinical outcomes and low lamin A with the recurrence of colon cancer (Wang *et al.*, 2009; Belt *et al.*, 2011; Capo-chichi *et al.*, 2011; de las Heras, Batrakou and Schirmer, 2013). Numerous lamin-cancer connections raise many possibilities in its role from epigenetic modifications that lead to oncogene activation, or migration inhibition of tumour suppressors or by even protecting the genome from damage.

### 1.2.3 Emerin

To organise the structure of the nucleus and chromatin, the lamina must complex with other proteins to relay signals. Emerin interacts with the inner nuclear membrane, as it can bind to chromatin both directly and indirectly, (possibly with a role in chromatin tethering due to its binding and co-localisation with both A-type and B-type lamin) and interact with NET proteins, BAF and chromatin (Holaska and Wilson, 2006; Berk, Tiffit and Wilson, 2013). Emerin also binds to nuclear actin and in the disease Emery-Dreifuss Muscular Dystrophy (EDMD), emerin suffers a missense mutation, and its binding to F-actin is disrupted (Holaska and Wilson, 2006).

Emerin, together with lamin and LADs, has been implicated in maintaining the structural integrity of the nucleus and progression of the cell cycle and its mutation is associated with many degenerative diseases including cancer (Reis-Sobreiro *et al.*, 2018; Urciuoli *et al.*, 2020). Abnormalities in emerin are associated with mechanical weakness as its loss may disrupt the actin-based, lamin-reinforcing system required for nuclear integrity which may be responsible for the 'amoeboid' tumour phenotype in cancers (Reis-Sobreiro *et al.*, 2018) (figure [1.19](#)). In breast and prostate cancer cells (*in-vitro*), human prostate cancer tissue and circulating tumour cells (*in-vivo*), the depletion lamin A/C leads to nuclear shape instability with a correlated gain in malignancy characterised the reduction and/or mis-localisation of emerin (Reis-Sobreiro *et al.*, 2018). Differential expression of lamins and emerin were also correlated to tumour aggressiveness in the osteosarcoma cell lines (Urciuoli *et al.*, 2020).



- adapted from Reis-Sobreiro et al., 2018

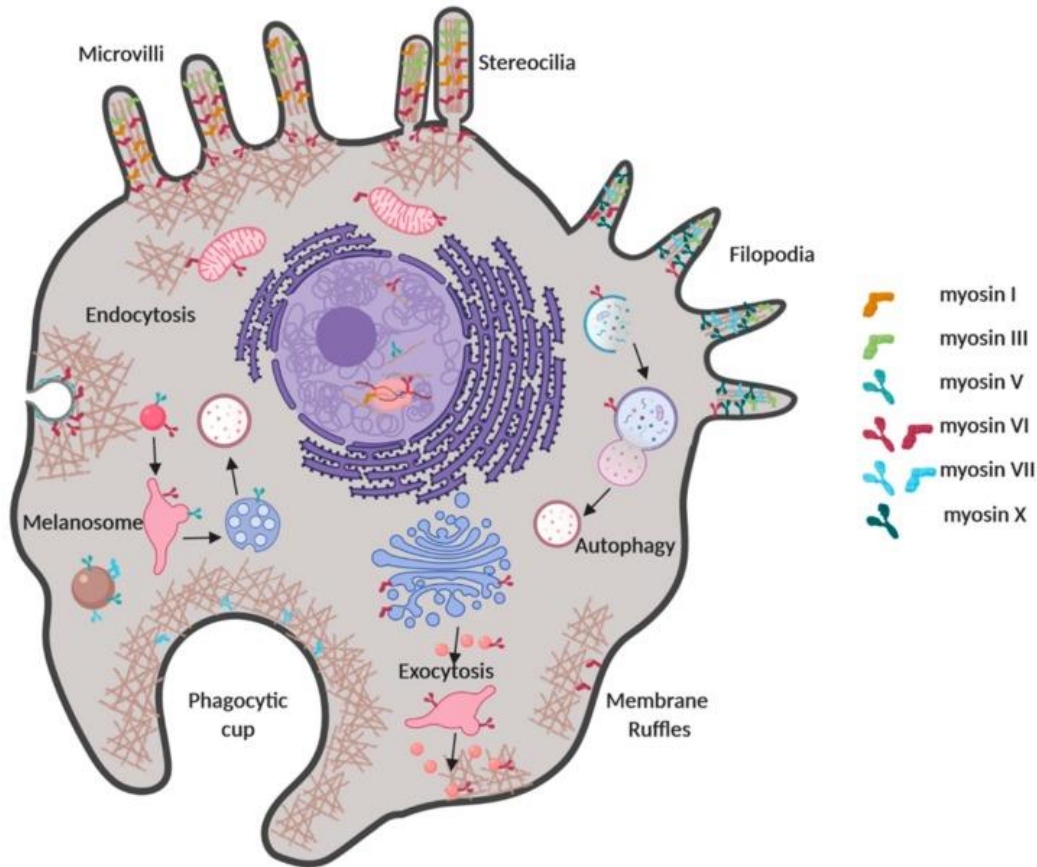
**Figure 1. 19 Emerin Nucleus in Cancer:**

Reduction and/or mis-localisation of emerin corresponds to a gain in malignancy. Emerin contributes to nuclear shape stability where aberrations can lead to 'amoeboid' tumour phenotype of the nucleus and the cell that aids in migration.

---

### 1.2.4 Nuclear Myosins

The two significant aspects of genome organisation are location and relocation. Aside from being functionally compartmentalised, chromosomes are functionally moved in response to proliferation and differentiation and some cases as a result of disease, as spatial positioning regulates gene expression at some level (Finlan *et al.*, 2008; Meaburn and Misteli, 2008). In the interphase nuclei of various organisms' genomes are non-randomly organised that can rapidly relocate upon a stimulus as shown by Mehta *et al.*, 2010 and Bridger, 2011, where within 15 minutes, chromosomes relocated after serum removal. Chuang *et al.*, 2006 showed that chromosomes move in a unidirectional, curvilinear path perpendicular to the NE at velocities of approximately 0.1-0.9 $\mu\text{m}/\text{min}$  covering distances over 1-5 $\mu\text{m}$ . The nucleus is a highly organised organelle, and while its contents are dynamic, phase organisation does not account for the energy-requiring process of CTs or 'biomolecular condensates' functionally moving. The motor protein family of myosins that exist in the cytoplasm are also found in the nucleoplasm, with roles in transportation, anchorage and tension sensing depending on structural and mechano-enzymatic characteristics (figure [1.20](#)) (Fili and Toseland, 2019).



- image source: Fili and Toseland, 2019.

**Figure 1. 18 Schematic Representation of Unconventional Myosins Fulfilling Multiple Roles in Vital Cellular Processes:**

The myosins partake in a wide range of intracellular roles and thus require spatial and temporal regulation.

Myosin structure consists of one or two **motor heads** (conserved 80kDa) where ATP hydrolysis, nucleotide-binding and actin-binding occurs; a **neck region** (of variable lengths; depending on the number isoleucine–glutamine (IQ) motifs) that amplifies conformational changes during the ATPase cycle creating the 'power-stroke', and a **tail domain** (coiled-coil, helical lever or single  $\alpha$ -helix) that determines the myosin conformation, dimerization and mediates interaction with cargo and lipids (McGurk *et al.*, 2006; reviewed in Fili and Toseland, 2019). The head domain can bind to actin and contains a specialised ATPase that hydrolyses ATP to ADP slowly in the absence of actin and 4-5x faster in its presence (Lodish *et al.*, 2000). Facilitating the conformational changes required for the power-stroke is an IQ domain on the neck region that binds calmodulin (CaM) (Fili and Toseland, 2019). The tail domain is positively charged and binds specific negatively charged cargo which



includes lipids and DNA with models proposing that the strength of this binding allows DNA to remain attached during the actomyosin power-stroke (Lodish *et al.*, 2000; de Lanerolle, 2012). Variation in the head and neck domain reveal that myosins could potentially play critical motor roles not only on cargo but also localisation (Cook, Gough and Toseland, 2020). Myosins use the energy produced from ATP hydrolysis for mechanical work along the actin within the cell to move proteins and aid in holding the cell together through anchorage and contractile tension (Vreugde *et al.*, 2006; Kapoor *et al.*, 2017). The proper functioning of myosin requires it to be activated at the right time, appropriate conformation, suitable binding partner, cargo, and lastly at the correct location.

### 1.2.4.1 Functional Diversity of Nuclear Myosins:

Conventional myosins encompass cardiac muscle myosin, smooth muscle myosin and non-muscle myosin II. Unconventional myosins account for 2/3 of myosin genes perform roles in endo-/exocytosis, intracellular trafficking and morphology, cell adhesion and motility and transcription (Cook, Gough and Toseland, 2020). Non-muscle myosin was discovered after observing ATP-dependent contractile events in non-muscle cells leading to the discovery of 18 'unconventional' subtypes of the conventional muscle myosin (Vreugde *et al.*, 2006). After being under scepticism for three decades, it is now clear that nuclear myosin (NM) exists in addition to its popular counterpart actin carrying out distinctly essential functions in the nucleus.

**Table 1. 4 Summary of Nuclear Myosins and their Genes**

<b>Name</b>	<b>Gene</b>
Nuclear Myosin I	<i>MYO1C – Isoform B</i>
Myosin I	<i>MYO1C – Isoform A and C</i>
Non-muscle myosin IIA	<i>MYH9</i>
Non-muscle myosin IIB	<i>MYH10</i>
Myosin Va	<i>MYO5A</i>
Myosin Vb	<i>MYO5B</i>
Myosin VI	<i>MYO6</i>
Myosin X	<i>MYO10</i>
Myosin XVI	<i>MYO16</i>
Myosin XVIIIβ	<i>MYO18β</i>

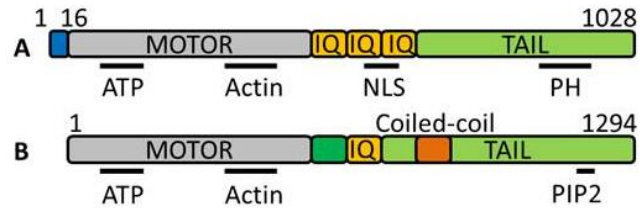
*-reviewed in Cook, Gough and Toseland, 2020*

In the early 1990s, the roman nomenclature for myosin was proposed as the family began to grow unexpectedly (Mooseker & Foth, 2007). To date, there are more than seven classes of the superfamily that have been discovered in the nucleus most notably I, II, V, VI, X, XVI and XVIII (table 1.4) (de Lanerolle, 2012). This research focuses on two NMs: NMI (NM1) and NMVI (NM6) recognised for their roles in the spatial organisation within the nucleus and briefly highlights NMVa and NMVb (NM5a and 5b), NMXVI (NM16) and NMVXIIIβ (NM18β) due to roles in the genome and OC.

**NM1**

NM1 was the first NM discovered and have been relatively well-studied and is the most prominently expressed NM in vertebrates (reviewed in Mooseker and Foth, 2008). NM1 plays conventional roles in the directed movement of interphase chromosome regions in addition to its ability to attach to chromatin remodelling complex and participate in transcription through direct interaction with RNA Pol I and II, mediating the phosphodiester bond formation during transcription initiation (reviewed in Mooseker and Foth, 2008). Philimonenko *et al.*, 2010 highlights an additional transcription role of NM1 involving rRNA, where the nucleolar positioning of actin and NMI is responsible for rRNA maturation and maintenance of the nucleolar structure where it is was further stated that the distribution of NM1 in the nucleolus, closely relates to the transcription process. The ATPase activity of NM1 is required for the initiation of transcription and the formation of the first phosphodiester bond validating its role as a transcription factor (Philimonenko *et al.*, 2010; Hofmann *et al.*, 2006.)

Studies have found that NMI and actin are tightly connected by separate but supporting roles, yet its mechanism remains unclear. Chuang *et al.*, 2006 also showed the inhibition of rapid long-range chromosome movements when mutant NM and actin was expressed, which emphasised significant roles in the motor arm of regulation. Mutational studies of nuclear actin and myosin rendered them necessary for efficient rRNA transcription and powering the active process of chromosome re-positioning (reviewed in de Lanerolle, 2012). Actin and NM1 were also necessary for activating genes on multiple chromosomes by estradiol, re-positioning of the gene locus, and chromosome re-positioning after serum starvation (Hu *et al.*, 2008; Mehta *et al.*, 2010). Mehta *et al.*, 2010 showed that chromosome relocation takes place upon the removal and addition of serum facilitated by NM1. This was demonstrated by direct inhibition of NM1, via RNAi of NM1 and through the inhibition of ATP and GTP.



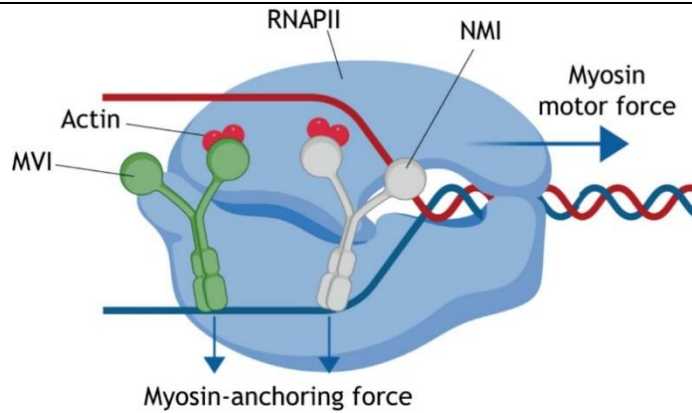
- image source: Toseland Lab: <http://toselandlab.mechanicsanddynamics.com>.

### Figure 1. 19 Simplified Structure of NM1 and NM6:

**A.** NM1 the Nuclear localisation sequence (NLS) in the IQ motif that contains CaM binding sites. PH domain for lipid binding in the tail. **B.** there is a short coiled-coil in the tail of NM6 and PIP2 domain for lipid binding.

## NM6

In the mammalian cell, NM6 is found in nuclear extracts, and in several cancer cell lines, it was immunolocalised in discrete foci in interphase nuclei (Mooseker and Foth, 2008). NM6 is the only member of the superfamily that moves backwards as it moves toward the minus end on the actin track (Dunn *et al.*, 2006). NM6 co-localises and co-immunoprecipitates with mRNA, promoters of the target genes and RNA Pol II in the nucleus during active transcription, implicating its role as a direct transcription factor (Vreugde *et al.*, 2006; Mooseker and Foth, 2008). Additionally, NM6 depletion led to a decrease in the target mRNA steady-state, and its inhibition halted transcription (Vreugde *et al.*, 2006; Mooseker and Foth, 2008). The complex formed by NM6 and RNA Pol II also includes NM1; however, NM6 differs in its ability to dimerise, its large and extensively variable step size in addition to being able to act as an anchor for immense mechanical loads; therefore, the mechanism could be totally different to NM1 (reviewed in de Lanerolle and Serebryanny, 2011; Fili and Toseland., 2019). While NM1 has been implicated in the spatial organisation of chromosomes, NM6 has been hypothesised to be a spatial organiser of transcription (Mehta *et al.*, 2010; Fili and Toseland., 2019). The shared interaction of NM1 and NM6 with RNA Pol II raises many questions to whether they are working alone, together, or against when bound to RNA Pol II (Figure 1.22).



- image Source: Cook, Gough and Toseland, 2020

### Figure 1. 20 Anchoring/transport of RNA polymerase II by Nuclear myosin:

NM1 and NM6 can bind to DNA directly via their C-terminal tail domain and indirectly to RNA Pol II through actin, by their motor domain (Cook, Gough and Toseland, 2020). This model suggests that myosin could either anchor RNA Pol II or transport it along the DNA. However, the question remains to whether NM1 and NM6 are working alone, together, or against when bound to RNA Pol II.

### NM5a and NM5b

The splice variant isoform NM5a has been observed in the nucleus of spermatocytes, where both NM5a and NM5b in the nucleus of ovarian mouse cells (Sun *et al.*, 2010; McGurk *et al.* 2006). Li and Yang, 2016 hypothesised that NM5a interacts with chromosomes as other NMs have been found too. Pranchevicius *et al.*, 2008 presented roles for NM5a in transcription, nuclear compartmentalisation and localises at RNA processing sites (nuclear speckles) raising possible roles in splicing. NM5a also has a valuable role in viral replication transporting viral particles by interacting with its capsid proteins, and some viruses go further into promoting the formation of the required actin filaments (reviewed in de Lanerolle, 2012). NM5b, often less studied but is attracting attention in the transcription process as it was found present in the nucleolus interacting with RNA Pol I,  $\beta$ -actin and newly transcribed rRNA (Lindsay and McCaffrey, 2009). Its association with RNA Pol I was altered when an RNA Pol I blocker was used (Lindsay and McCaffrey, 2009).

## **NM16**

NM16 is unique as it is exclusively expressed in the nucleus and localises primarily in the nucleolus (Reck-Peterson, Novick and Mooseker, 1999). NM16 is seen in the cytoplasm after being exported as a result of DNA replication stress, resulting in a reduction in the nucleus whereas an over-expression following either DNA damage, nucleotide insufficiency or DNA pol suppression, delays cell cycle progression into the S-phase (Cameron, Liu and Pihkala, 2013; Li and Yang, 2016). The C-terminal tail is responsible for localisation, and the N-terminal head interacts with stress-induced nuclear actin rods; however, the function of NM16 in interphase is not known (reviewed in Mooseker and Foth, 2008).

## **NM18**

NM18 was immunolocalised in the cytoplasm of undifferentiated myoblast, and upon differentiation, part of the NM18 enters the nuclei (Salamon *et al.*, 2003). A similar observation was found in primary skeletal muscles cells and cardiomyocytes (Salamon *et al.*, 2003). NM18 is required for microfibrillar development and a candidate TSG after being associated with lung and OC (Yanaihara *et al.*, 2004; de Lanerolle and Serebryanny, 2015). NM18 gene is found on chromosome arm 22q that contains three other TSGs linked with several other mammalian cancers, which were found either reduced, mutated or hypermethylated in lung and OC cell lines (Yanaihara *et al.*, 2004). Yanaihara *et al.*, 2004 showed the isoform NM18b had reduced expression in all four ovarian cell lines used and in 71% of the 17 primary cell line used. Though its nuclear role is undefined, when NM18 was restored using 5-aza-2-deoxycytidine and/or trichostatin A, anchorage-dependent growth of several tumour cell lines was suppressed, thus reinforcing its TSG role in human carcinogenesis (Ajima *et al.*, 2007).

### 1.2.5 Nuclear Actin

A unique feature of NM is that it does not interact with microfilaments like conventional myosins thus impacting the traditional concept of just being an actin-based motor using actin filaments for translocation (Li and Yang, 2016). As microfilaments do not constitutively exist in the nucleus, but only appear adaptively, myosins must, therefore, interact with the established nuclear actin (Baarlink *et al.*, 2013). The entire myosin superfamily contains actin-activated ATPase that tethers and move organelles along actin filaments through cycles of attachment and detachment to actin (reviewed in Cook, Gough and Toseland, 2020). Its interaction with RNA Pol II increases its activity 8-fold and thus considered a transcription factor (Hofmann *et al.*, 2004; Grummt, 2006). Upon the binding of actin and myosin, the tail is directed towards a nuclear cargo to bind; this co-binding produces a strain on myosin where it is then conveyed along actin (Hofmann *et al.*, 2006, de Lanerolle, 2012; reviewed in Cook, Gough and Toseland, 2020). Whether actin is present in the nucleus in monomeric, polymeric or filamentous forms; the exact state that actin interacts with NMs is still uncertain (reviewed in Cook, Gough and Toseland, 2020).

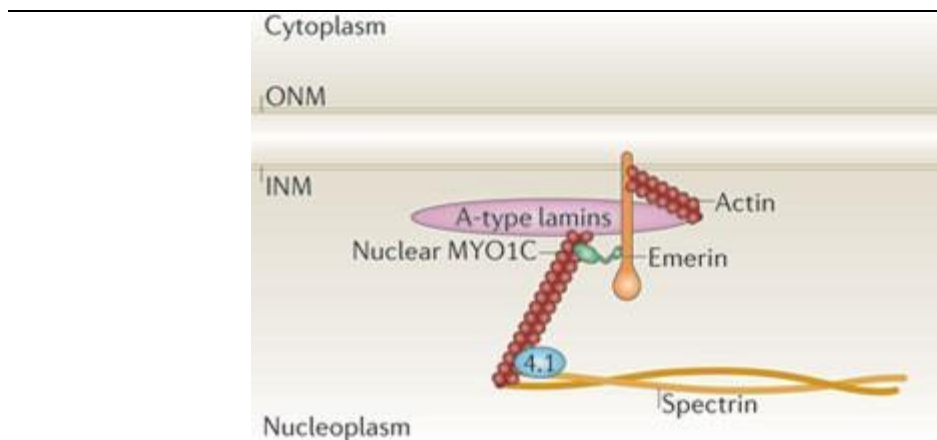
Actin tracks can now be observed in the nucleus, interact with several classes of NM, form actomyosin for contractility during translocation through narrow spaces, and regulatory roles in transcription and cell cycle (de Lanerolle, 2012; Serebryannyy *et al.*, 2016; Davidson *et al.*, 2020). Nuclear myosin has also been observed driving the movement of heterochromatin breaks towards the periphery while long-range actin filaments are also observed extending from the heterochromatin DNA damage sites to the nuclear periphery (Caridi *et al.*, 2018). An independent nuclear role proposed for actin is that it relaxes chromatin structure giving way for out-looping and possibly transcription, but not necessarily moving the chromosome (Fedorova and Zink, 2008). Furthermore, the perturbation of actin polymerisation through a *G13R* mutation or latrunculin A drug results in loss of movement in CTs, rearrangements and transcriptional stimulation (Chuang *et al.*, 2006; Dundr *et al.*, 2007; Mehta *et al.*, 2010). These data show that multiple actin subunits

are required for the movement of nuclear entities by NMs.



### 1.2.6 Hypothetical Motor Complex:

A study by Mehta *et al.*, 2008 proposed a hypothetical complex of nuclear proteins that are presently considered part of the NE and nucleoskeleton that could also be functionally present in roles involving transcriptional regulation (figure 1.23). Rapid repositioning of the CTs during interphase appears to be facilitated by NM and actin that falls within a nuclear motor complex. The Bridger lab has also found that required or expected chromosome re-positioning is altered or absent in cells that possess mutant lamin A or emerin deficiency and upon inhibition of myosin and actin (Mehta *et al.*, 2008 and Bridger *et al.*, 2014).



- image source: Simon and Wilson, 2011.

#### Figure 1. 21 Possible Arrangement of the Hypothetical Motor Complex:

Showing interactions of NM1 (nuclear MYO1C) with emerin and actin as well as A-type lamins with emerin and actin. This complex and its protein may be important for maintaining the nucleoskeleton dynamics and anchorage. Nuclear MYO1C binds emerin and actin to produce tension in a similar way to cytoplasmic MYO1C in ear hair cell stereocilia. INM -inner nuclear membrane and ONM-outer nuclear membrane.

For the hypothetical nuclear motor complex to hold, these four proteins must be connected, though are not limited to them. Although not currently visualised, de Lanerolle, 2012 pointed out that NMI then interacts with chromosomes to facilitate its movement with the mechanical aid of actin.

### **1.2.7 Outlook**

The information on the molecular cancer mechanisms is growing rapidly; however, the discovery of novel and effective drug targets to improve the therapeutic outcomes is lacking. In OC, there is currently no standard practice, and the biomarkers in current clinical use still present a substantial number of false negatives and false positives, while the field is rapidly progressing for better treatment predictions and preventing unnecessary surgeries. The challenge increases as the disease experience MDR (multidrug resistance), resulting in the need to include it in all fields of research equally. The plethora of nuclear roles and disease association have been studied for decades, but full genetic knowledge will also require investigating the 3D arrangement of the chromosomes.

#### **Research Objective:**

This research started by investigating the disease-related altered positioning of CTs (of chromosomes 1, 13, 17 and X) in four OC cell lines (SKOV-3, PEO-1, PEO4 and MDAH-2774) while also addressing their nuclear distribution and levels of NM1 and NM6, and a brief highlight on A-type and B-type lamin discrepancies within the disease. Since NM are responsible for the most significant input into movement within the hypothetical nuclear motor complex, the altered CTs were compared to the post knockdown CTs following NM1 and NM6 RNAi. Then finally, to address the gap in research of chemoresistant-related alterations, CTs were mapped on a lab-created platinum-resistant OC line also followed by RNAi of NM1 and NM6 that investigated the potential of re-sensitisation.

## CHAPTER 2

# CHROMOSOME SPATIAL ORGANISATION AND NUCLEAR MOTORS IN OC

### 2.1 INTRODUCTION

OC is the deadliest amongst gynaecological cancers, and in this field of study to date, breast and prostate cancers have taken the forefront. While well-funded breast and prostate, amongst other non-gynaecological cancers, are over-diagnosed and over-treated, the opposite is taking place for under-funded OC (Welch and Black, 2010). Challenging the shortage of additional prognostic markers to identify aggressive to indolent cancers can benefit both sets of patients by reducing the healthcare costs of treating over-diagnosed and over-treated cancers so that under-diagnosed and under-treated cancers can benefit.

Advances in gene regulation in cancer research are sometimes unsuccessful and not well understood because part of the picture is missing since functional chromosome positioning is over-looked. The unique oncogene *MECP2* exemplifies this, found on the inactive female chromosome X, *MECP2* that is unmutated, yet overexpressed in 18% of cancers through an unknown mechanism (Neupane *et al.*, 2016). As the acceptance and relevance of spatial chromosome positioning are emerging in diseases, it is crucial to re-evaluate diseases with gene regulation and expression discrepancies. The aggressive nature of OC provides a good starting point to understand the disease further with

the potential to understand other cancers in addition to nucleopathies.

### 2.1.1 Spatial Chromosomal Organisation in Cancer

Chromosomes non-randomly occupy spatial territories in interphase nuclei and re-position in response to changes in the functional requirements of the nucleus. For instance, in the absence of serum, chromosomes 18 and 13 relocated from the nuclear periphery to the nuclear interior, chromosome 10 from the intermediate nuclear region to the periphery and chromosome X remained at the nuclear periphery in primary human dermal fibroblasts when serum was removed (Mehta *et al.*, 2010; Bridger *et al.*, 2014). The spatial organisation can both reflect and contribute expression, and changes within the nuclei as in the case of chromosome 7 in leukemic cells (Brickner, 2017; Federico *et al.*, 2019). Chromosome 7 changed its spatial location in response to breakage on its q-arm caused by abnormalities that may have contributed to its altered transcriptional activity due to accompanied re-positioned genes (Federico *et al.*, 2019). Aside from influence by transcription factors and chromatin changes on spatial organisation, proximity to the nuclear periphery can also affect expression as exemplified by Finlan *et al.*, 2008 who showed tethering chromosomes to a protein of the inner nuclear membrane reversibly induced suppressed some (but not all) genes as they also depended on histone deacetylases (that removes the acetyl from histone allowing the DNA to wrap more tightly and thus rendering it inactive).

When compared to their healthy counterparts, **cancer-specific** re-positioning of gene loci is observed in both reproductive cancers breast and prostate (Zeitz *et al.*, 2013; Meaburn *et al.*, 2016; Leshner *et al.*, 2016). Although 94% and 57% of the genes mapped in prostate and breast cancer have non-altered positions, it is essential to recognise the ones that do (Meaburn *et al.*, 2009; Leshner *et al.*, 2016). Interestingly, in thyroid, colon and cervical cancers, chromosome 18 re-positions internally, and chromosome 19 re-positions away from the nuclear interior (Cremer *et al.*, 2003; Murata *et al.*, 2007; Wiech *et al.*, 2009). However, one must keep in mind, where genes such

as *FLI1* re-positions in 100% and 92.9% of breast and prostate cancers respectively, it is difficult to stratify aggressive and indolent cancers with this gene, so it becomes a matter of finding the right chromosomes and genes to exploit clinically (Meaburn *et al.*, 2016; Leshner *et al.*, 2016).

### **2.1.2 NM cancer-specificity**

The nucleus is the largest organelle in the cell, and movements of components within this highly organised space requires the use of motor proteins such as myosins. Nuclear myosins also change their distribution in response to functional requirements; in proliferating cells, NM1 is seen throughout the nucleoplasm, concentrated around the nucleoli, and regulating long-range chromosome dynamics during interphase that changes into aggregates when the serum is removed (induced quiescence) (Pestic-Dragovich *et al.*, 2000; Chuang *et al.*, 2006; Hofmann *et al.*, 2006; Mehta *et al.*, 2010; Kulashreshtha *et al.*, 2016). Building on the rapid re-location of chromosomes within 15 minutes of serum-removal and restoration of NM1, Mehta *et al.*, 2010 observed the relocation resumed only after 24-36 hrs as the proliferating distribution of NM1 was restored.

NM6 has not been directly linked to spatial chromosome organisation but has been shown to organise RNA Pol II spatially and is overexpressed in all the reproductive cancers; prostate, ovarian and breast (Dunn *et al.*, 2006; Yoshida *et al.*, 2004; Wang *et al.*, 2015; Hari-Gupta *et al.*, 2020). NM6 is the only myosin in the superfamily of myosins that moves towards the minus end of actin, and the unique property to move backwards enables its involvement in migration, endo-/exocytosis and RNA Pol II-dependent transcription (Wells *et al.*, 1999; Roberts *et al.*, 2004; Vreugde *et al.*, 2006). When NM6 is inhibited or knocked down, it perturbs the spatial organisation of RNA Pol II, affecting the anchorage of their chromatin clusters and gene/promoter associations which can be useful drug targets in cancer and understanding its biochemistry (Hari-Gupta *et al.*, 2020).

### 2.1.3 Lamins

Nuclear myosins alone cannot explain the complex biomechanical roles of spatial chromosome organisation. Nuclear myosins are known to bind DNA and are involved in transcription; however, they also complex with other nuclear proteins, such as emerin and actin (reviewed in Mehta *et al.*, 2008; Cook, Gough and Toseland, 2020). These two proteins bind to each other but, also together they bind to lamin on their other end, forming a **hypothetical nuclear motor complex** (Mehta *et al.*, 2008). Through this complex, a series of mechano-transduction events, including histone modifications; the cell cycle status can influence functional genome repositioning events (reviewed in Mehta *et al.*, 2008). Lamins in concert with other structural nuclear proteins such as actin maintain the nuclei's structural and genome integrity, where dysregulation in these proteins leads to dysmorphic nuclei and genome instability (reviewed in Irianto *et al.*, 2016). DNA interactions with the NL have been mapped in human, *Drosophila* and murine cells in large domains (LADs) instead of foci, and through a tethering mechanism to transcriptionally inactive sites of the NL, these LADs assume a repressive role (Guelen *et al.*, 2008; Pickersgill *et al.*, 2006; Peric-Hupkes *et al.*, 2008; van Steensel and Dekker, 2010). With more than 1,000 of these domains, their disputed influence under lamins, and the characteristic dysmorphic nuclei in cancer, it is vital to address lamins in OC (Guelen *et al.*, 2008).

### 2.1.4 Why these chromosomes?

**Chromosome 1** contains the TSG gene *ARID1A* that is mutated in 62% of OC cases and found deficient in 86-100% of OC cases are in *ARID1A* protein (Aunoble *et al.*, 2000). What also makes *ARID1A* interesting is its role in spatially partitioning chromosomes through its role in B-compartment formation and weakening of the border strength in topologically associated domains (TADs) in accordance with gene expression (Wu *et al.*, 2019). Furthermore, *ARID1A* knockouts increased the volume of the nucleus and chromosomes in addition to the **intermixing** of small

chromosomes 19 and 22 (Wu *et al.*, 2019). This would possibly mean intermixing of chromosomes/CTs in OC, by and large, downstream effects in transcription.

**Chromosome 13** contains the TSG *BRCA2* while **chromosome 17** contains TSG *BRCA1* and *p53* in addition to the oncogene *HER2*. 5-10% OC cases are due to *BRCA1/2* mutations, while 79% of all cases have *p53* mutations and 30% have *HER2* amplification (Aunoble *et al.*, 2000). These genes are also implicated in breast, cervical and prostate cancers and could provide translational value to other cancers. **Chromosome X** was used as a spatial reference chromosome as it occupies a peripheral region in the nuclei of cells such as HeLa, lymphocytes, primary human dermal fibroblasts and mouse embryonic fibroblasts (Kurz *et al.*, 1996; Cremer and Cremer, 2001; Mehta *et al.*, 2010; Deng *et al.*, 2015). However, in OC, it shows a preferential trend towards monosomy, and recently the paternal X-chromosome was linked to OC, making it an intriguing inclusion to this study (Eng *et al.*, 2018).

### 2.1.5 Outlook

Spatial genome repositioning events are orchestrated by a plethora of complexes and proteins, one of these; is the hypothetical nuclear motor complex that holds both motor and anchoring roles (Mehta *et al.*, 2010). Disruption in the anchoring and motor activities can, in turn, interrupt the cell cycle influence on the organisation, leading to chromosomes with unstimulated repositioning (high NM), unresponsive to functional repositioning (low NM), high repressory anchorage (high lamins) or lack of repressory anchorage (low lamins), all eventually leading to disease-related effects on gene regulation. Spatial chromosomal and gene positions are conserved throughout the cell cycle, and any alterations could allow the diagnosis of specific diseases and then possibly avenues to treatment (Tanabe *et al.*, 2002; Meaburn, 2016).

Even though there is growing evidence of oncogenic genomic spatial organisation, there is still a deficit in information to produce a reliable biomarker panel. The infrastructure for FISH in clinics already exists and can be used by integrating tissue samples already removed from patients (no additional invasiveness required) could be extended to diagnostics and prognostics. There are many probes sets available for a cancer diagnosis; for instance, Abbot Molecular currently manufactures FISH kits for bladder and lung cancer diagnosis based on translocation rearrangements. However, if this design can implement proximity positioning of silent culprits (healthy genes such as *MECP2*), new ways of diagnosing, prognosing and treating the OC can be personalised in addition to rectifying ineffective treatment and toxic dosing.

This chapter sets out to test the **hypothesis** of cancer-associated spatial chromosomal repositioning events in OC by positioning of 3 significant chromosomes (1, 13 and 17) containing prevalent TSGs and oncogenes related to OC and challenging chromosome X as a proximity control, at least in OC. The spatial territories of these four chromosomes were positioned in 4 cancer cell lines SKOV-3, PEO-4, MDAH-2774, PEO-1. Since epithelial OC accounts for approximately 80-90% of cases, a non-



immortalised control epithelial cell (HOSEpi) was used. This chapter also aimed to validate the **hypothesis** that irregularities in NM and lamins correlate with cancer-associated chromosomal repositioning events by examining the nuclear distribution of 6 proteins: NM1, NM6, lamin A, lamin C, lamin B<sub>1</sub> and lamin B<sub>2</sub>.

With FISH, the potential for a CT biomarker panel for OC construction was investigated, and with just four whole chromosomal OC-specific repositioning events it was possible to extract trends between each cell line, clonally related lines and those that possessed chemoresistance. The inclusion of indirect immunofluorescence (indirect-IF) and western blots (WB) showed inconsistencies in nuclear proteins, providing explanations to the dysfunctional spatial organisation in OC.

## 2.2 METHODS

### 2.2.1 Cell Culture

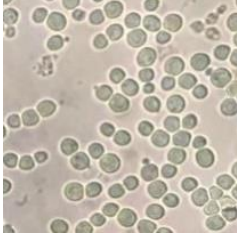
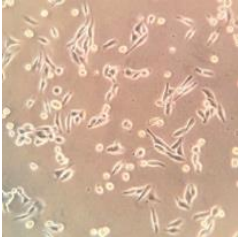
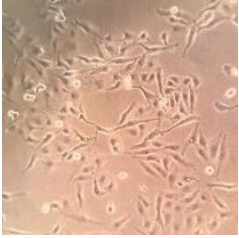
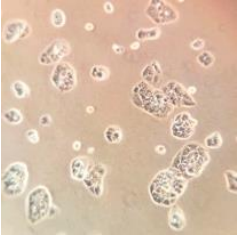
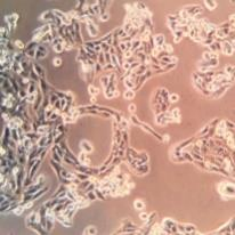
Human epithelial OC cell lines SKOV-3, PEO-1, PEO-4 and MDAH-2774 were gifted from the Karteris group, Brunel University London (attained from ATCC). Cells were cultured in supplemented Roswell Park Memorial Institute (RPMI) 1640 medium (Gibco) containing 10% FBS, 2mM L-glutamine (Sigma) and 50U/mL penicillin / 50 µg/mL streptomycin (Gibco) in a humidified 5% CO<sub>2</sub> incubator at 37°C. They were frozen in 5% DMSO, new batches were removed from liquid nitrogen every 8-12 weeks, and after two weeks stocks were made.

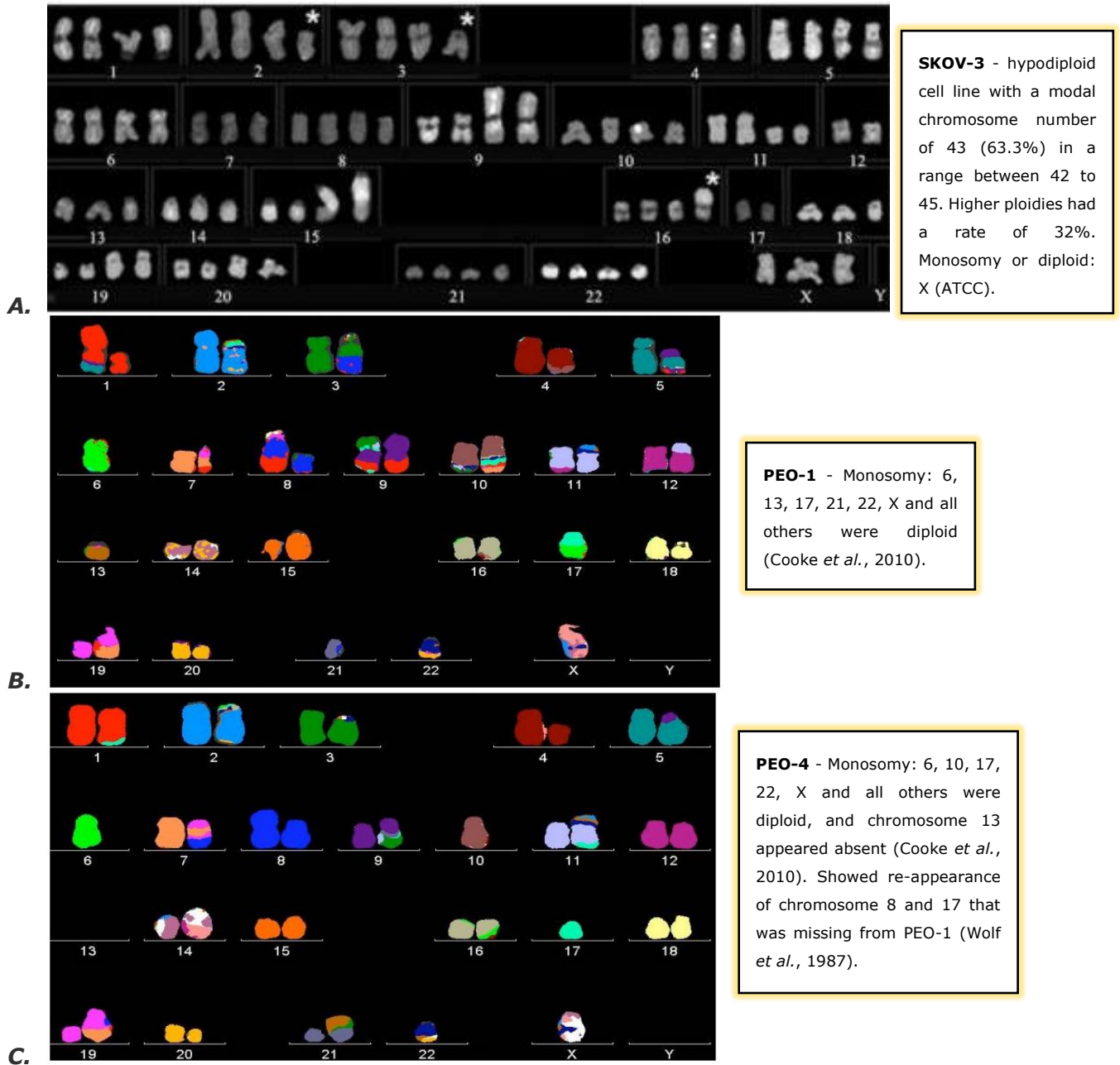
Healthy human ovarian surface epithelial (HOSEpi) cell line (SC-7310) was purchased from ScienCell research laboratories and cultured onto glass coverslips for use in 2.2.3 (IF). These are non-adherent cells; therefore, the flasks/ wells were treated before seeding with poly-L-lysine (2µg/cm<sup>2</sup>) that is 15µL of poly-L-lysine stock (10mg/mL) in 10mL sterile water at 37°C overnight (or minimum 1hr) in the incubator, then rinsed twice with sterile water. Cells were initially grown in Ovarian Epithelial Cell Medium (OEpiCM) (ScienCell), however, for bulking up they were grown in complete RPMI 1640 in suspension.

From another purchased pellet of 5x10<sup>6</sup> cells, 2x10<sup>6</sup> was fixed for FISH, and 2x10<sup>6</sup> was used to make lysates for WB.

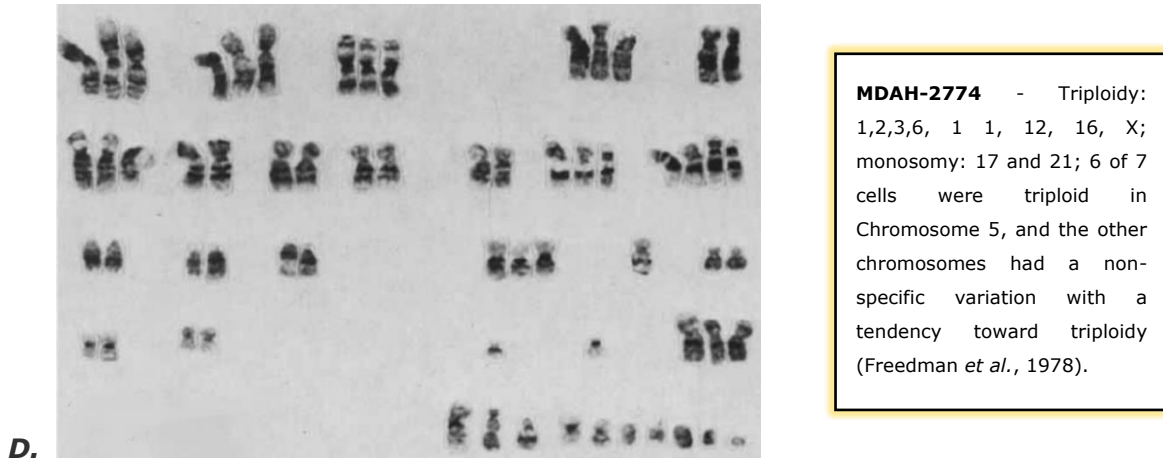
**Table 2. 1 Ovarian Cell Lines Summary:**

Images were taken using an iPhone on a light microscope of control cell line **HOSEpi**, and OC cell lines **SKOV-3**, **PEO-1**, **PEO-4** and **MDAH-2774**. Highlights the history of tumour cells that were all adenocarcinomas derived from ascites fluid, doubling time (t) and genetic variations (Beaufort *et al.*, 2014 and Hernandez *et al.*, 2016). These cell lines were a kind gift from the Karteris Group (Brunel University London).

<b>HOSEpi</b> (ScienCell) Healthy epithelial control Doubling t: 120 hrs			
			
400X			
<b>SKOV-3</b> (ATCC) Doubling t: 34 hrs Serous	<b>PEO-1</b> (ATCC) Stage 3 Doubling t: 84 hrs Serous	<b>PEO-4</b> (ATCC) Stage 3 Platinum-Resistant Doubling t: 106 hrs Serous	<b>MDAH-2774</b> (ATCC) Platinum-Sensitive Doubling t: 27 hrs Endometrioid
			
100X	100X	100X	100X
Derived from a 64yr old Caucasian woman from ascites fluid in 1973.  <b>TP53, NF1, PIK3CA, HRAS, ARID1A, ERBB2 (Amplification)</b>	PEO-1, PEO-4 and PEO6 were extracted from one patient by Dr Simon Langdon in February 1982, November 1982, and February 1983, respectively. PEO-1 was extracted after one chemotherapy treatment while still showing sensitivity.  <b>TP53, BRCA2</b>	PEO-4 was extracted when the disease had become resistant against cisplatin, chlorambucil and 5-fluorouracil treatments (Langdon <i>et al.</i> , 1988 and Wolf <i>et al.</i> , 1987). Contains a secondary mutation restoring BRCA function that was lost in its predecessor cell line PEO-1 (Cooke <i>et al.</i> , 2010).  <b>TP53, BRCA2 (Silent)</b>	Taken from a female patient in January 1972 it showed tumorigenicity in inoculated nude mice.  <b>TP53, BRCA1 (Silent), BRCA2 (Silent), PIK3CA, KRAS, ARID1A</b>



-continued on next page



This research uses 4 ovarian cancer cell lines that displayed a unique karyotype from each other. When compared to a normal karyotype, they showed high chromosomal instability (structural and numerical); however, the karyotype remains relatively stable when established in cell culture as highest instability takes place during carcinogenesis and does not persist in continued growth (Roschke *et al.*, 2002). Roschke *et al.*, 2002 showed this in colorectal and ovarian cell lines, including SKOV-3 for 25 passages. PEO-6, the platinum-resistant successor of PEO-4, was taken from the patient 3 months after and showed high similarity where only 4% of their genome differed (Cooke *et al.* 2010). MDAH-2774 Karyotype remained constant after 50 metaphases (Freedman *et al.*, 1978).

**Figure 2. 1 Karyotype Background**

**A.** SKOV-3: 10 Metaphases (Image source: Roschke *et al.*, 2002). **B.** PEO-1: 19 Metaphases (Image source: Cooke *et al.*, 2010). **C.** PEO-4: 23 Metaphases (Image source: Cooke *et al.*, 2010). There was a reappearance of healthy copies of chromosome 1, 9, 11 and 17 in PEO-4 that was previously absent in PEO-1. **D.** MDAH-2774: 7 Metaphases (Image source: Freedman *et al.*, 1978).

## 2.2.2 Fluorescence *in-situ* Hybridisation (FISH)

### 2.2.2.1 Probe Preparation:

Biotin-labelled chromosome probes were made by degenerate-oligonucleotide-primed PCR (DOP-PCR) using sequence pools (micro-dissected whole chromosome arm templates, a kind gift from Dr Michael Bittner) of chromosomes 1, 13, 17 and X (Telenius *et al.*, 1992). Two rounds of amplification were performed first without labelling and second with biotin-16-UTP (1mM, Roche) labelling.

**Table 2. 2 The DOP-PCR Reagents:**

Run 1 (without biotin-16-UTP labelling) and run 2 (with biotin-16-UTP labelling). Master mixes were scaled up proportionally.

REAGENTS	RUN 1: without biotin-16-UTP	RUN 2: with biotin-16-UTP
5X DOP-PCR Buffer	10	10
dACGTP (2mM)	5	5
dTTP (2mM)	5	2
DOP primer (20µM)	5	5
Taq (20U/µL)	1	1
Water	23	12
Template	1	5
biotin-16-UTP	-	10
TOTAL	50	50

**Table 2. 3 DOP-PCR Cycle Conditions:**

Run 1 (with 30 cycles) and run 2 (with 34 cycles).

PHASE	CYCLE	TEMPERATURE (°C)	TIME
Initial Denaturation	1	95	3 mins
Denaturation	Run 1: 30	98	20 secs
Primer Annealing	Run 2: 34	62	1 min
Extension		72	30 secs
Final Extension	1	72	5 mins
Cooling / Collection		4	∞

The amplified products were confirmed by performing a 1% agarose gel electrophoresis. 1g Agarose was dissolved in 100mL 1X Tris-acetate-EDTA (TAE, w/v) and then 5µL of SYBR® Safe (Invitrogen 10,000X) was added to the warmed mixture. It was poured into a gel tray fixed with a 12-well comb and left to solidify. 1X TAE was poured into the electrophoresis tray with the solid gel till fully submerged. The samples were prepared by combining 5µL of PCR product and 1µL of loading dye.

3 $\mu$ L of the 1 kb DNA ladder (50 $\mu$ g/ml, BioLabs) was added into the first well, followed by the other samples. The gels were run for 40 mins at 80V. Visualisation of the products was performed with the Bio-Rad Molecular Imager Gel Doc XRS (Image Lab Software). The secondary template was stored at -20°C until required and labelled probes were precipitated with ethanol or also stored until required.

### **2.2.2.2 Ethanol Precipitation:**

To the biotin-labelled probe mixture for every 200-400 $\mu$ g (per slide) of labelled chromosome 7 $\mu$ g of Co<sub>t</sub>-1 DNA (1 $\mu$ g/1 $\mu$ l, Roche), 3 $\mu$ g of Herring Sperm (Invitrogen), (1/10 v/v) of 3M Sodium Acetate (pH5.2), 200% ethanol and incubated at -80°C for at least 30 mins followed by 30 mins centrifugation at 4°C at (14,000rpm). The supernatant was removed, and the pellet was washed with 70% ethanol, followed by 15 mins centrifugation at 4°C (14,000rpm). The supernatant was removed, and the pellet was allowed to dry on a 50°C hot block. 12 $\mu$ L of hybridisation mix (50% Formamide, 10% 20X SSC and 1% Tween 20) per slide was added to resuspend the dried pellet (overnight at room temperature).

### **2.2.2.3 Cells for Sample Preparation:**

Trypsinised cells in solution were pelleted by centrifugation at 300-400g for 5 mins, incubated for 15 mins in a hypotonic solution (0.56% w/v) KCl solution, re-pelleted and fixed using ice-cold (3:1 v/v) Methanol:Acetic Acid solution on ice or -20°C for at least an hour. The fixation steps were repeated until minimal cytoplasm was observed under a light microscope.

Cells were dropped onto dampened glass microscope slides, baked at 70°C for 60 mins followed by 5 min serial dehydration in 70%, 90% and 100% ethanol solutions. They were heated at 70°C for 5 mins in a dry oven and then transferred to 70% formamide (pH 7.0 v/v) solution at 70°C for exactly 2 mins. Ice-cold 70% ethanol was used to fix the open DNA in place. Then the slides were

placed on a 37°C warming plate ready for hybridisation.

#### **2.2.2.4      *Hybridisation:***

To the denatured cells upon slides, 12µL (per slide) of probe labelled with Biotin was denatured at 72°C for 10 min and allowed to re-anneal for 10 mins (min) to 120 mins (max) at 37°C. 12µL was dropped onto a slide, sealed with a coverslip and rubber cement, then incubated in a humidified chamber at 37°C for minimum 18 hrs.

#### **2.2.2.5      *Washes:***

After 48 hrs, post-hybridisation washes were initiated thrice in 50% formamide (pH 7.0) at 45°C for 5 mins each followed by 0.1X Sodium Saline Citrate (SSC, Na<sub>3</sub>C<sub>6</sub>H<sub>5</sub>O<sub>7</sub>) (pH 7.0) washes at 60°C for 5 mins each and finally cooled in 4X SSC at room temperature. Cooled slides were blocked with 4% BSA in 4xSSC for 10 mins then incubated with streptavidin-conjugated-cyanine3 (Cy3) (ThermoFisher) in 1% BSA (1:200) for 1 hr in a dark humidified chamber at room temperature. A final wash was performed with 0.05% Tween20 in 4X SSC for 5 mins at 42°C. The edge of the slides was blotted on a tissue to remove excess liquid and mounted in Vectashield containing 4,6-diamidino-2-phenylindole (DAPI) (Vector Labs) and stored at 4°C until use.

#### **2.2.2.6      *Image and Analysis:***

Using the LEICA DM4000 microscope, epifluorescence microscopy was performed on each slide using 40X and 100X (in immersion oil (Immersol™)). For each chromosome of each cell line, 50-100 images were captured using "LAS AF" Leica Software.

From each data set at least 50 images were randomly selected in IPLab Spectrum Software on a Macintosh Apple Computer (MAC) to analyse the whole chromosome positions using erosion script analysis (Croft *et al.*, 1999; Boyle *et al.*, 2001). DAPI signal area (total nucleus) was divided into



five equal concentric shells from the periphery to the nuclear centre (1 to 5) as depicted in figure [2.2](#). Cy3 conjugated streptavidin was used to reveal the annealed chromosome painting probes, and its bright red colour was pseudo-coloured green for software detection.

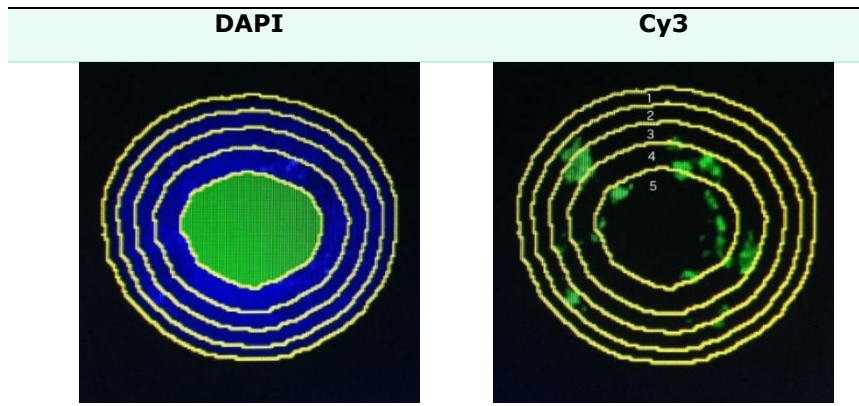


**Figure 2. 2 Erosion Analysis Representation:**

The erosion software divides the nucleus into five equal concentric rings called 'shells'. The chromosome signal for each shell (in green) is divided by the area of that shell (in blue) that then represents the estimated occupancy of the chromosome relative to the periphery or centre.

The script determined the pixel intensity of DAPI and the Cy3 (chromosome signal) which was normalised by division: % Cy3 pixel intensity / % DAPI Pixel Intensity for the five shells in Microsoft Excel. The output of the analysis was tabulated, graphed with  $\pm$  error bars (SEM), and two-tailed student's t-test ( $p < 0.5$ ) was performed on excel (Croft *et al.*, 1999).

It is also noteworthy that the occupancy is **not absolute** and most often partial in nearby shells (figure [2.3](#)) (Meaburn and Misteli, 2007). Signal concentration in shells 1 and 2 represented a preferred peripheral occupancy of that chromosome, shell 3 an intermediate preference and shells 4 and 5 a central preference.

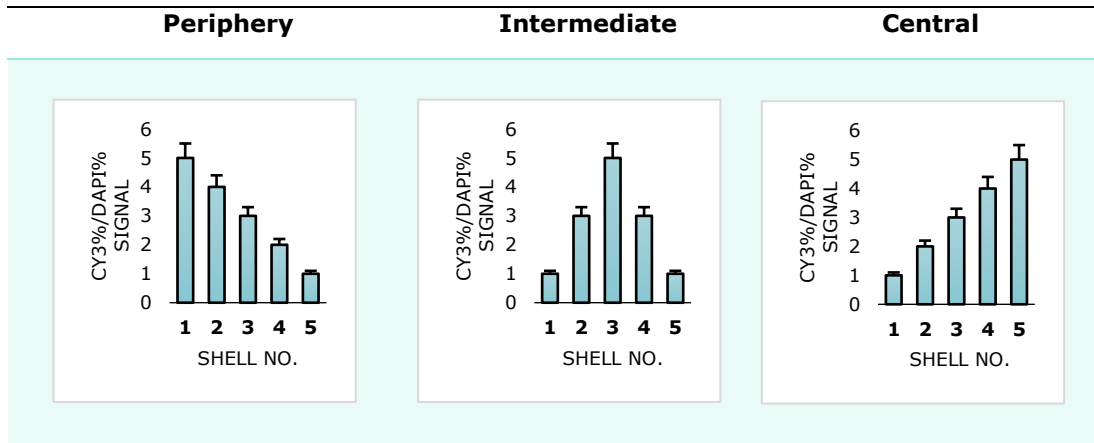


**Figure 2. 3 Erosion Analysis Sample Output:**

Depicting the output post-analysis of the tabulated numbers representing a chromosome that is preferentially located in the periphery, intermediate or the central position.

### 2.2.3 Indirect Immunofluorescence

Cells were grown for 48 hrs on glass coverslips, washed 3 times with 1X phosphate-buffered saline (PBS) (Sigma:1 tablet in 200mL), fixed with methanol: acetone (1:1 v/v) for 10 minutes on ice, and then washed again with 3 times PBS 1X. 20 $\mu$ L of primary antibody diluted in 1% FCS in PBS (v/v) was placed on the coverslips overnight at 4°C, 1hr at room temperature or 30 mins at 37°C. After incubation, the coverslips were washed 27 times in 1X PBS and returned to the humidified chamber. The coverslip was then covered with 20 $\mu$ L of the secondary antibody and incubated in the dark for 1hr at room temperature. The coverslips were washed in 27 times PBS 1X followed by 3 times in ddH<sub>2</sub>O, blotted on a tissue to remove excess liquid and mounted with DAPI.

**Table 2. 4 Antibody List:**

Primary and secondary antibodies and their dilutions used for indirect immunofluorescence.

Primary Ab	Dilution	Secondary Ab	Dilution
Rabbit anti-Myo IB (Thermofisher)	1:100	Donkey anti-rabbit-Cy3 (Merck MiliPore, UK)	1:500
Rabbit anti-Myo VI (Thermofisher)	1:100	Donkey anti-rabbit-Cy3 (Merck MiliPore, UK)	1:500
Mouse anti-Ki67 (Thermofisher)	1:100	Goat anti-mouse-FitC (Jackson Laboratories, USA)	1:1000
Rabbit anti-Lamin B1	1:500	Donkey anti-rabbit-Cy3 (Merck MiliPore, UK)	1:500
Mouse anti-Lamin B2	1:400	Goat anti-mouse-FitC (Jackson Laboratories, USA)	1:1000
Mouse anti-Lamin A (Abcam, UK)	1:100	Goat anti-mouse-FitC (Jackson Laboratories, USA)	1:1000
Rabbit anti-Lamin C (ThermoFisher, UK)	1:200	Donkey anti-rabbit-Cy3 (Merck MiliPore, UK)	1:500

The HOSEpi cells are non-adherent cells, so they were fixed in solution with 1mL methanol: acetone (1:1, v/v) for 10 minutes on ice, centrifuged and washed once 1mL PBS 1X, incubated with 1mL primary antibody overnight at 4°C, 1hr at room temperature or 30 mins at 37°C, washed once again 1mL PBS 1X, then incubated 1mL secondary antibody for 1hr in the dark at room temperature. The cells were washed once again with PBS 1X and attached to slides using Shandon Cytospin 2 (Marshall Scientific) (400g).

Coverslips were mounted onto slides with DAPI for epifluorescence microscopy using the Leica DM4000 microscope. All slides were analysed for specific patterns of NM distribution in 200 nuclei.

Images of representative patterns were captured of the patterns scored, which were: dispersed foci, aggregate foci, dispersed and aggregate foci and negative.

### 2.2.4 Western Blot Assay

Trypsinised cells were fractionated for nuclei; a pellet of approximately  $2 \times 10^6$  cells was resuspended in 100uL hypotonic buffer for 15 mins at 37°C to swell the cytoplasm of the cell to aid douncing. The mixture was transferred to a microcentrifuge tube, spun at 800rpm for 6 mins and the supernatant was removed as the cytoplasmic extract. The pellet washed in another 100uL of the hypotonic buffer and checked under a light microscope for cytoplasm residue (in the case of excess cytoplasm, the wash was repeated). 100µL of 2X Laemmli buffer (Sigma-Aldrich; 20% glycerol, 10% 2-mercaptoethanol, 4% SDS, 0.004% bromophenol blue and 0.125M Tris HCl, pH6.8) was then added to both the final pellet (nuclear extract) and the first supernatant (cytoplasmic extract) and stored in -80°C until use.

Before loading, the samples were heated to 90°C for 10 mins. Two 10-well 10% SDS-PAGE Bio-Rad pre-cast gels were placed into the tank and filled with running buffer (3.02% TRIS, 14.4% Glycine and 1% SDS). To each well, on one gel, 10µL of the cytoplasmic sample and on another gel, 5 µL of the nuclear extract was loaded and ran at a current of 80mA (40mA for one gel) and 300V for approximately 40 mins.

In a tray, 800mL ice-cold transfer buffer (3.01% TRIS and 14.06% Glycine) and 200mL of methanol were mixed. The gel was removed from the plates and mounted into the blot 'sandwich' (Black side, sponge, 2x filter paper, gel, nitrocellulose membrane, 2x filter paper, sponge, transparent side). The sandwich was fitted into the tank and kept cool with an ice block in the tank and surrounded by ice tray. Current was applied at 400mA and 300V for 1hr and 30 mins, respectively.

The membranes with the transferred proteins were placed into blocking buffer (1g milk powder in 20mL TBS 1X 0.1% Tween<sub>20</sub>) in a sealed dark chamber on an orbital shaker overnight at 4°C. The membranes were then washed with TBS 1X 0.1% T<sub>20</sub> and incubated with 5mL of the primary antibody (diluted in 5% BSA in TBS 1X with 0.1% T<sub>20</sub>) in a sealed dark chamber on an orbital shaker

---

overnight at 4°C. On the control membrane, GAPDH antibodies were added and on the second gel antibodies for NM1 and NM6 were added.

**Table 2. 5 Li-Cor Antibody List:**

Used for the WB of NM1 (Myo1B) and NM6 (MyoVI) and their dilutions.

<b>Primary Ab</b>	<b>Dilution</b>	<b>Secondary Ab</b>	<b>Dilution</b>
Rabbit anti-Myo Ib (ThermoFisher)	1:1,000	Donkey anti-rabbit IRDye 800CW/680RD (Li-Cor, UK)	1:15,000
Rabbit anti-Myo VI (ThermoFisher)	1:1,000	Donkey anti-rabbit IRDye 800CW/680RD (Li-Cor, UK)	1:15,000
Rabbit anti-GAPDH (ThermoFisher)	1:2,000	Donkey anti-rabbit IRDye 800CW/680RD (Li-Cor, UK)	1:15,000

The membranes were washed 3 X in TBS 1X 0.1% T<sub>20</sub> (15 mins each) and incubated with 5mL of the secondary antibody (Li-Cor 800cw/680RD DkxRb diluted 1:15,000 in 1% BSA in TBS 1X with 0.1% T<sub>20</sub>) for 1hr at room temperature in a dark chamber. The membranes were washed 3 times for 5 mins with PBS, then visualized with the Li-Cor Odyssey Imaging System (Li-Cor, UK) at wavelengths 800 nm (green) and 700 nm (red). The images from the membranes were uploaded to ImageJ software (Version 1.53a) to calculate the band intensities.

## 2.3 RESULTS

### 2.3.1 Spatial Chromosomal Organisation in OC:

To characterise the disease-related spatial chromosome organisation in OC, four key chromosomes were chosen (based on the oncogenes and TSGs found mutated in OC) to be mapped using FISH and erosion analysis software: chromosome 1, chromosome 13, chromosome 17 and chromosome X. This was performed on four tumour cells (SKOV-3, PEO-1, PEO-4 and MDAH-2774) and compared to one control cell line (HOSEpi) (figure [2.3](#) and [2.4](#)).

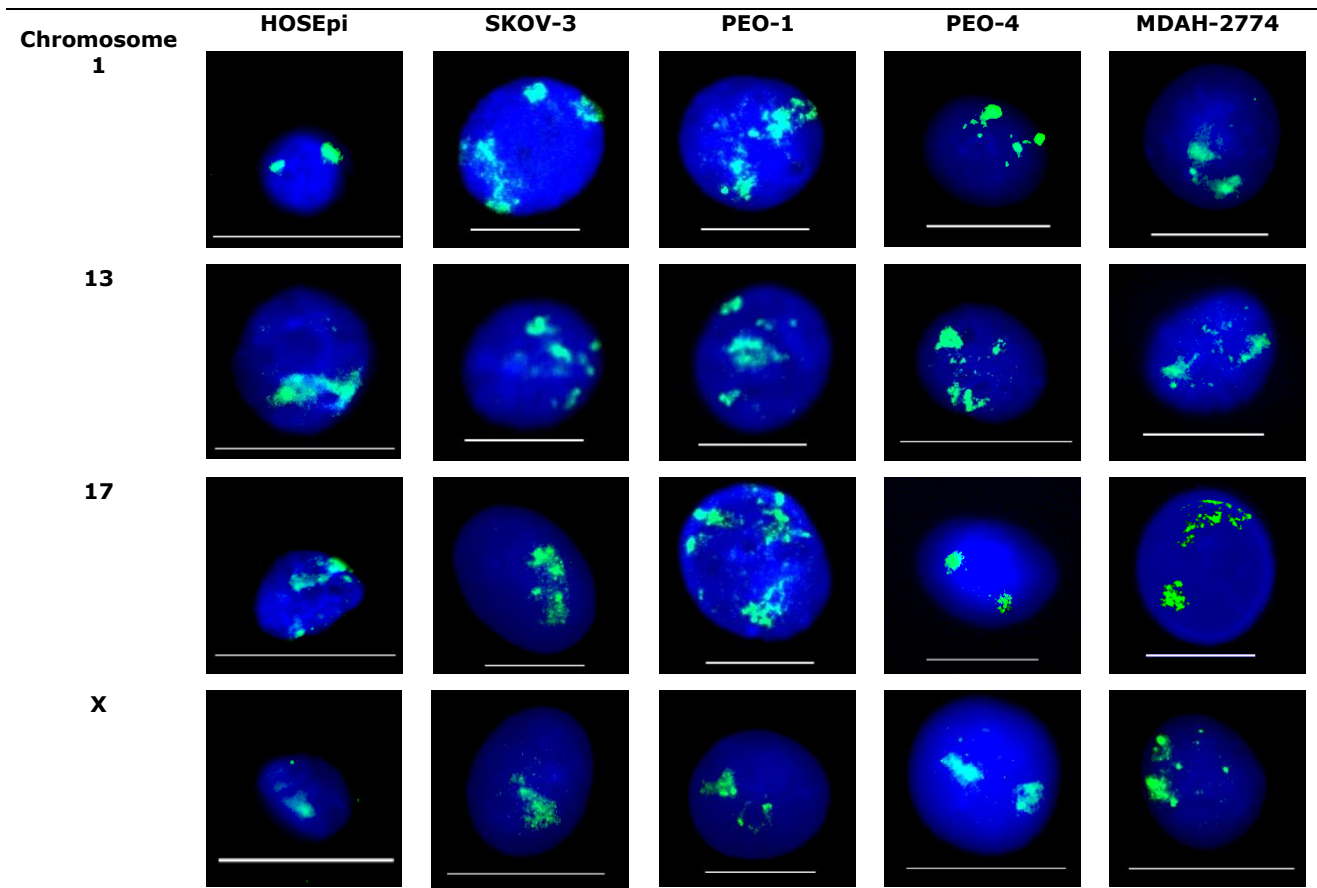


**Figure 2. 4 Chromosome Spatial Positioning:**

Images for the nuclear localisations of chromosomes 1, 13, 17 and X in OC cell lines SKOV-3, PEO-1, PEO-4 and MDAH-2774 and the *control* cell line HOSEpi (non-cancer) delineated using 2D-FISH. Nuclear DNA is blue-stained with DAPI, and whole chromosome signals were visualised via Cy3 and converted to green for software recognition. Magnification x400 / x1000. Scale bars represent 25 $\mu$ m.

To quantify these changes, 50-100 images were analysed using an IPLab erosion software method as described in section 2.2.2.6 (Croft *et al.*, 1999; Boyle *et al.*, 2001; Clements *et al.*, 2016) that creates a mask around the nuclear DAPI signal and then divides the nuclei into five concentric shells and then calculates the % of chromosome (green) signal in each shell. Shell 1 signifies the outermost periphery and shell 5 signifies the centre, as shown in figure 2.2. Cy3 dye was used, and the greyscale image for it converted to green for software detection. The output of the analysis was tabulated, plotted with  $\pm$  error bars (standard error of the mean, SEM), and a 2-tailed student's t-test (unpaired, unequal variances) was performed on excel (table 2.6). Signal concentration in shells



1 and 2 represented a preferred peripheral occupancy of that chromosome, shell 3 an intermediate preference and shells 4 and 5 a central preference. A graphical panel comparing the control cell HOSEpi against the four tumour cells was constructed using the output graphs from MS excel (figure [2.4](#)).

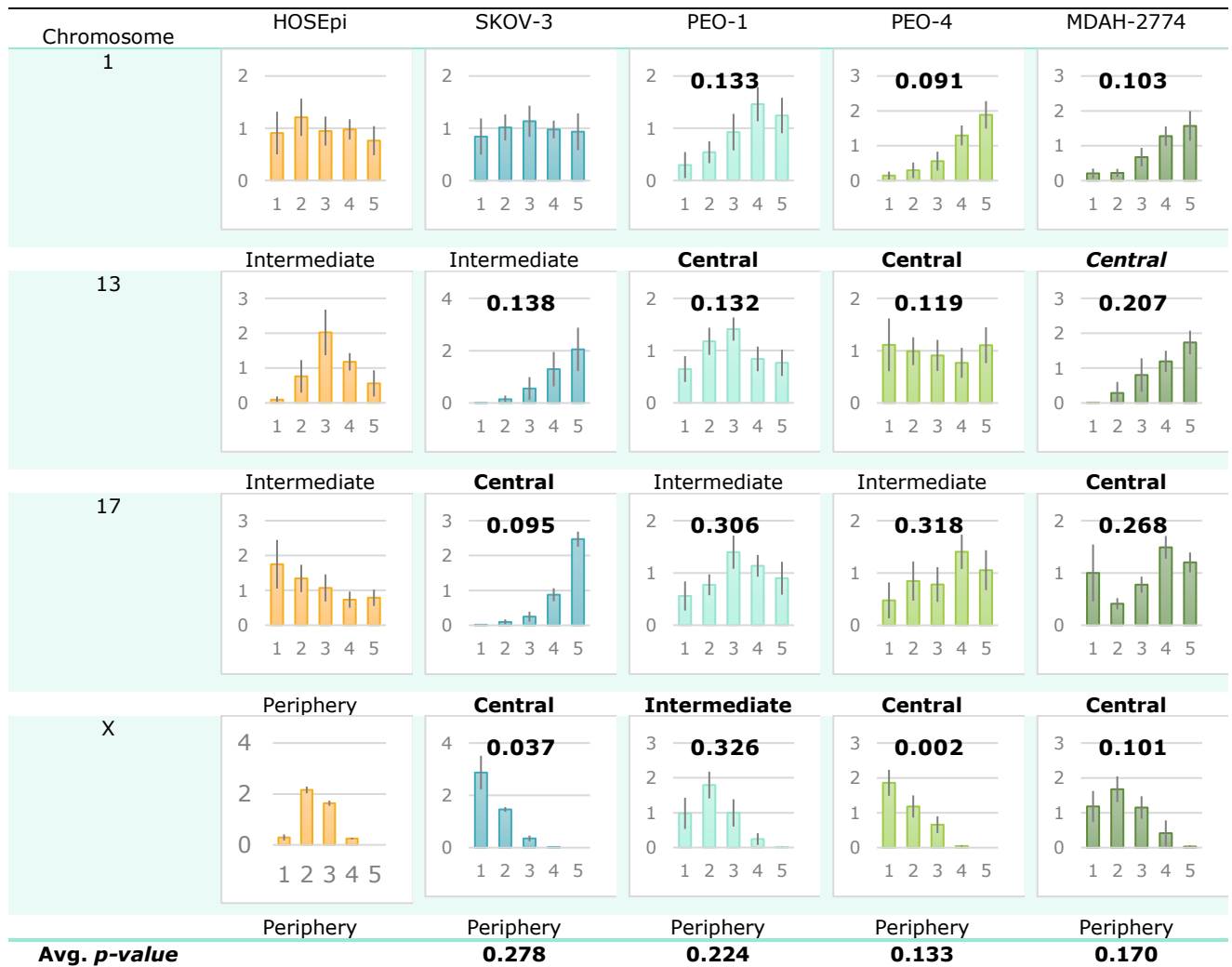


**Figure 2. 5 Image Analysis: Chromosome Spatial Positioning:**

These histograms demonstrate the nuclear localisation of chromosomes 1, 13, 17 and X in OC cell lines SKOV-3, PEO-1, PEO-4 and MDAH-2774 and the control cell line HOSEpi (non-cancer), visualised using 2D-FISH and positioned by erosion analysis software [section 2.2.5] (Croft *et al.*, 1999, Boyle *et al.*, 2001 and Clements *et al.*, 2016). The bars and error bars signify means and standard error of the mean of 50-100 nuclei, respectively. Y-Axis represents % Cy3 whole chromosome probe signal / % DAPI nuclear signal, and the X-axis represents the nuclear periphery to the nuclear interior location (1 to 5). Student's t-test of all cancer cells performed against the wild-type (healthy HOSEpi) for each shell [*p*-value above each histogram].

	SKOV-3	PEO-1	PEO-4	MDAH-2774
<b>Chromosome 1</b>				
Shell 1	0.887	0.133	0.065	0.098
Shell 2	0.704	0.050	0.019	0.005
Shell 3	0.972	0.360	0.047	0.083
Shell 4	0.954	0.031	0.316	0.289
Shell 5	0.691	0.091	0.005	0.038
AVG →	<b>0.842</b>	<b>0.133</b>	<b>0.091</b>	<b>0.103</b>
<b>Chromosome 13</b>				
Shell 1	0.079	0.010	0.021	0.097
Shell 2	0.002	0.132	0.409	0.022
Shell 3	0.000	0.052	0.003	0.001
Shell 4	0.608	0.101	0.081	0.917
Shell 5	0.000	0.362	0.083	0.000
AVG →	<b>0.138</b>	<b>0.132</b>	<b>0.119</b>	<b>0.207</b>
<b>Chromosome 17</b>				
Shell 1	0.048	0.166	0.178	0.531
Shell 2	0.001	0.104	0.303	0.008
Shell 3	0.004	0.250	0.371	0.339
Shell 4	0.421	0.070	0.009	0.012
Shell 5	0.001	0.941	0.732	0.447
AVG →	<b>0.095</b>	<b>0.306</b>	<b>0.318</b>	<b>0.268</b>
<b>Chromosome X</b>				
Shell 1	0.149	0.105	0.000	0.035
Shell 2	0.017	0.311	0.005	0.149
Shell 3	0.012	0.060	0.002	0.006
Shell 4	0.008	0.975	0.004	0.253
Shell 5	0.000	0.178	0.000	0.062
AVG →	<b>0.037</b>	<b>0.326</b>	<b>0.002</b>	<b>0.101</b>

**Table 2. 6  $p$ -values against HOSEpi:**

Shells that showed no significant differences with  $p > 0.5$  are highlighted in red, the shells that showed statistical differences with  $p > 0.5$  are unhighlighted, and the shells that showed statistical differences with  $p < 0.05$  are highlighted in green. The average values listed below; the red value represents no significant differences [ $p > 0.5$ ]; the black values are significantly different [ $p > 0.5$ ] and the green values significantly different [ $p < 0.05$ ].

15/16 tumour chromosomes were significantly different from the position of comparable chromosomes within the control cell line ( $p > 0.5$ ) where chromosome 1 of tumour cell line SKOV-3 showed a high  $p$ -value of 0.842. Chromosome X of all cell lines was preferentially located at the periphery, which complies with previous literature of the preferred occupancy (Belmont *et al.*, 1986; Kurz *et al.*, 1996; Boyle *et al.*, 2001; Cremer and Cremer, 2001; Mehta *et al.*, 2010; Deng *et al.*, 2015).

### 2.3.2 Nuclear Myosin Presence and Distribution in OC:

To investigate the drivers behind this tumorigenic change in CT, the distribution network of nuclear motors was investigated through indirect-IF. This can elucidate dysfunctional roles as NM1 that have shown a motor role in chromosomal movement and is known to associate with proteins of the nucleoli and nucleoplasmic speckles, and NM6 has also been found elevated in OC cells that also associates with nucleoplasmic speckles and proteins therein (Percipalle *et al.*, 2006; Vreugde *et al.*, 2006).

A scoring system of specific patterns was devised of dispersed foci (nucleoplasmic speckles patterns), aggregate foci (nucleoli pattern), dispersed and aggregate foci and negative (Figure [2.4](#), [2.5](#) and [2.6](#)). The distribution score of the tumour cells was compared to that of the control cell line to highlight the presence of dysfunctional distribution.

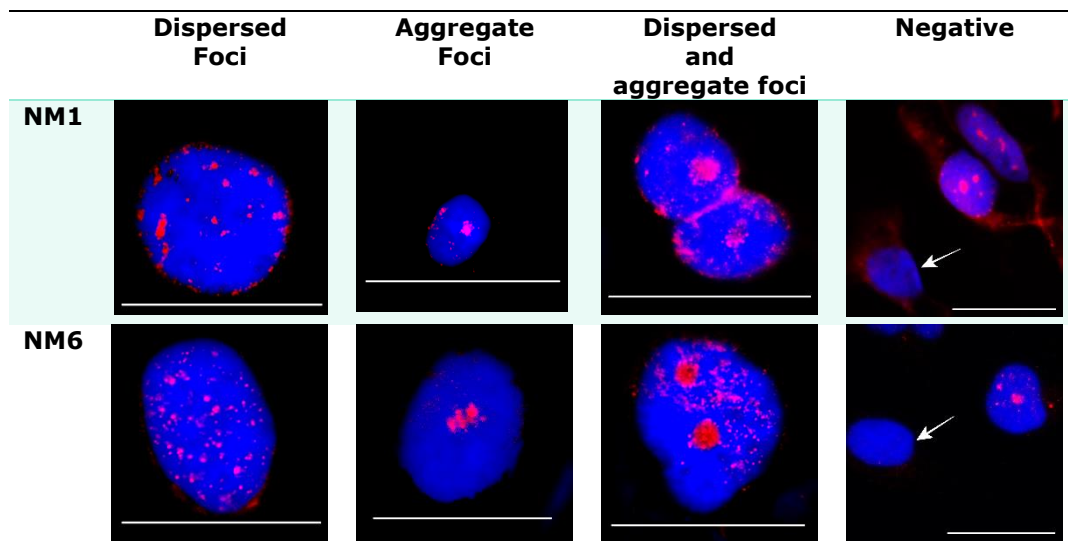


**Figure 2. 6 NM1 and NM6 Distribution Patterns Images:**

Representative images of the nuclear distribution pattern (dispersed foci, aggregate foci, dispersed and aggregate foci and negative) were captured in 4 OC cell lines SKOV-3, PEO-1, PEO-4 and MDAH-2774 and a control cell line (non-cancer). DNA was stained using DAPI (blue), and the NM1 protein was revealed by indirect IF with a Cy3 conjugated secondary antibody. Magnification x400 / x1000. Scale bars represent 25µm.

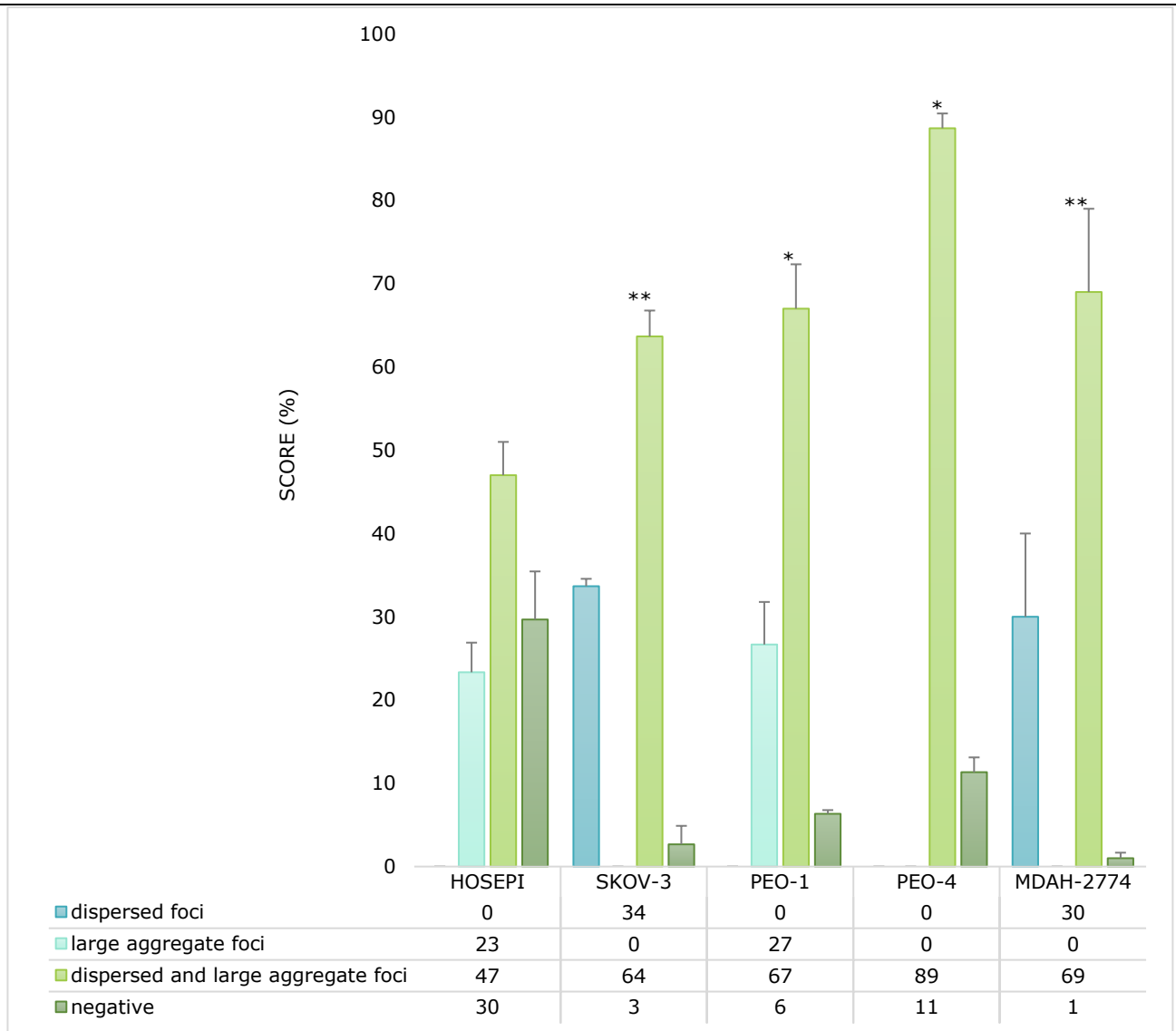


**Figure 2. 7 NM1 Distribution Patterns Score:**

Bar graph shows the score of 4 NM1 patterns (dispersed foci, aggregate foci, dispersed and aggregate foci and negative) in 4 OC cell lines SKOV-3, PEO-1, PEO-4 and MDAH-2774 and a control cell line (non-cancer). The bars and error bars for each cell line (X-axis) represents means of 3 replicate slides and SEM for a total of 200 nuclei as a percentage (% / Y-axis). Student's *t*-test of the cancer cells patterns was performed against the wild-type (healthy HOSEpi).

\* - denotes statistically different by one confidence interval (0.5) and \*\* - denotes statistically different by two confidence intervals (0.05 and 0.5).

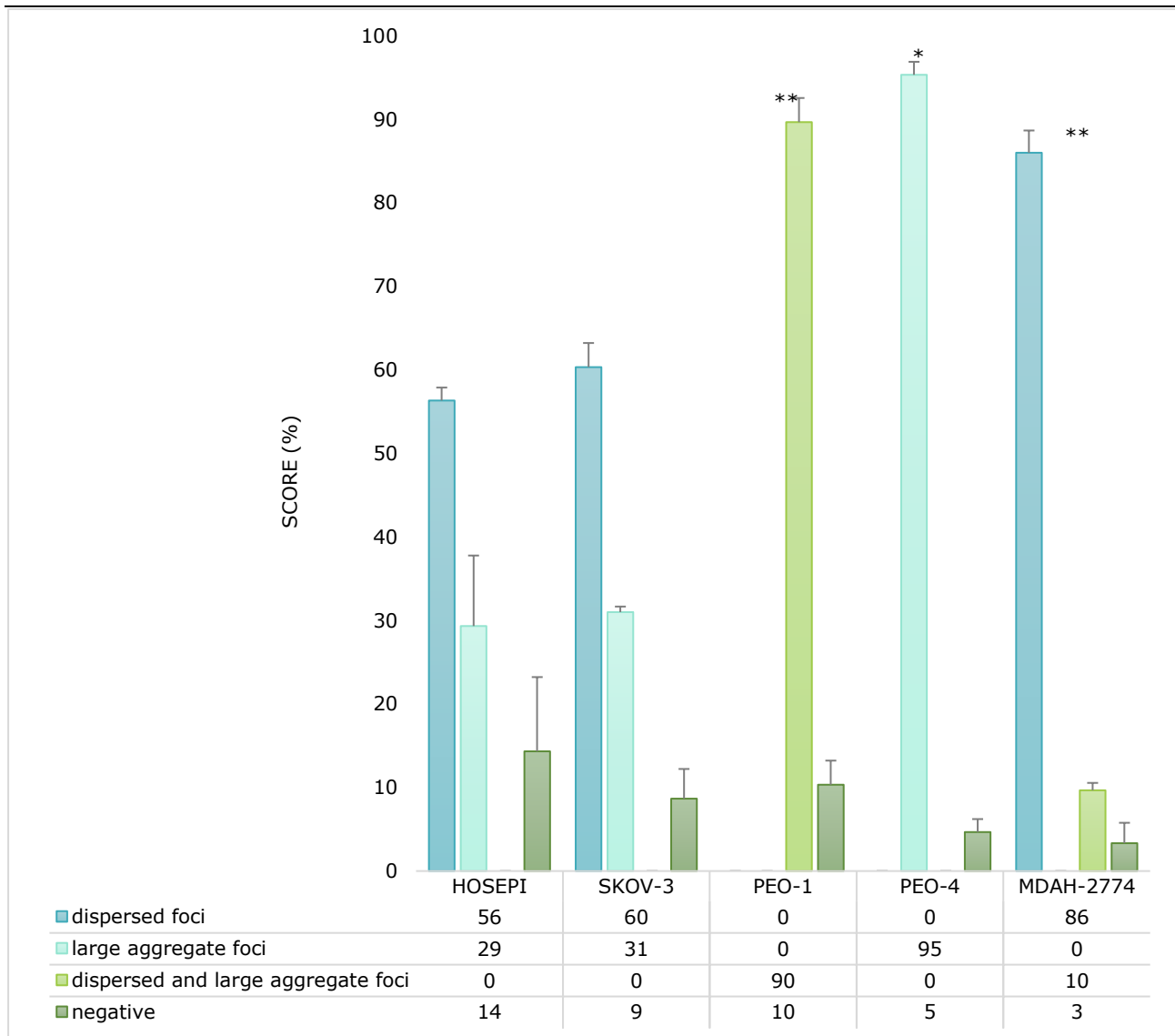


**Figure 2. 8 NM6 Distribution Patterns Score:**

Bar graph shows the score of 4 NM6 patterns (dispersed foci, aggregate foci, dispersed and aggregate foci and negative) in 4 OC cell lines SKOV-3, PEO-1, PEO-4 and MDAH-2774 and a control cell line (non-cancer). The bars and error bars for each cell line (X-axis) represents means and SEM for a total of 200 nuclei as a percentage (% / Y-axis). Student's t-test of the cancer cells patterns was performed against the wild-type (healthy HOSEpi).

\* - denotes statistically different by one confidence interval (0.5) and \*\* - denotes statistically different by two confidence intervals (0.05 and 0.5). SKOV-3 showed no statistical difference.

NM1 is directly involved with complexes of RNA Pol I (nucleoli) and RNA Pol II (nucleoplasmic speckles) transcription, post-initiation steps and chromatin remodelling (Percipalle *et al.*, 2006). Vreugde *et al.*, 2006 found high levels of NM6 in the nucleus of OC cells with RNA Pol II complex association. Therefore, we expected to see predominantly aggregate and dispersed foci for NM1 and dispersed foci for NM6. NM1 aggregates and dispersed foci had the highest frequency in all the cell lines; however, NM6 dispersed foci was observed in all cell lines except PEO-4.

Hudson, 2007 demonstrated that lamins A/C showed normal distribution using indirect IF; however, it was found over-expressed in OC tissues using protein microarrays. Therefore, it was imperative to quantify the protein levels of NM1 and NM6. NM1 and NM6 have recently been found in substantial amounts in the cytoplasm; thus for the WBs, nuclear extracts were made thus reflecting the nuclear protein content only (Venit *et al.*, 2016; Vreugde *et al.*, 2006) (figure [2.8](#) and [2.9](#)). Corresponding cytoplasmic extracts for the nuclear extracts were also used so the nuclear proteins can be normalised against GAPDH as lamins have been found abnormally expressed in cancer cells, including ovarian, prostate and breast cancers, thus unreliable (as reviewed by Guinde *et al.*, 2018).

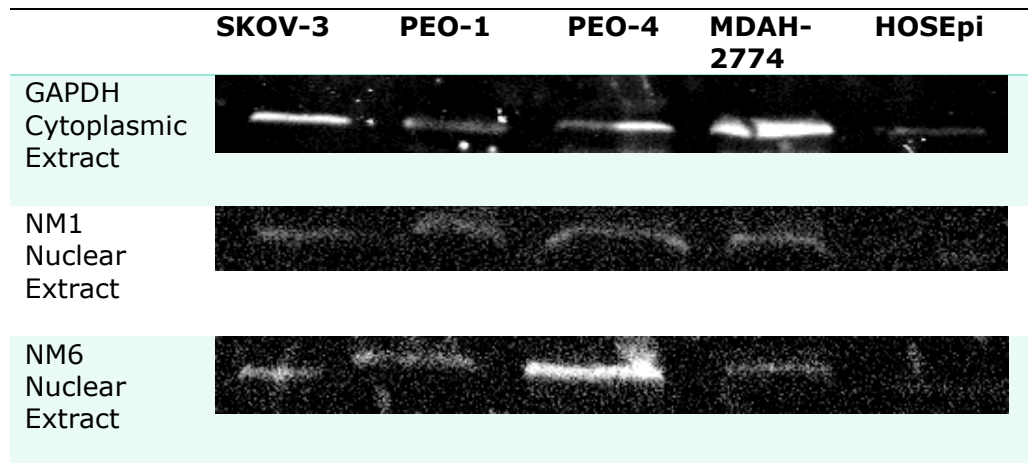


**Figure 2. 9 NM1 and NM6 Levels (Li-Cor Images):**

Cytoplasmic and Nuclear extracts of 4 OC cell lines SKOV-3 (lane 1), PEO-1 (lane 2), PEO-4 (lane 3) and MDAH-2774 (lane 4) and a control cell line (lane 5) were quantified by WB on the Li-Cor Odyssey for NM1 and NM6 using ImageJ software (Version 1.53a), the band intensities were calculated. The quantities were normalised against GAPDH levels (first band) in the corresponding cytoplasmic extracts.

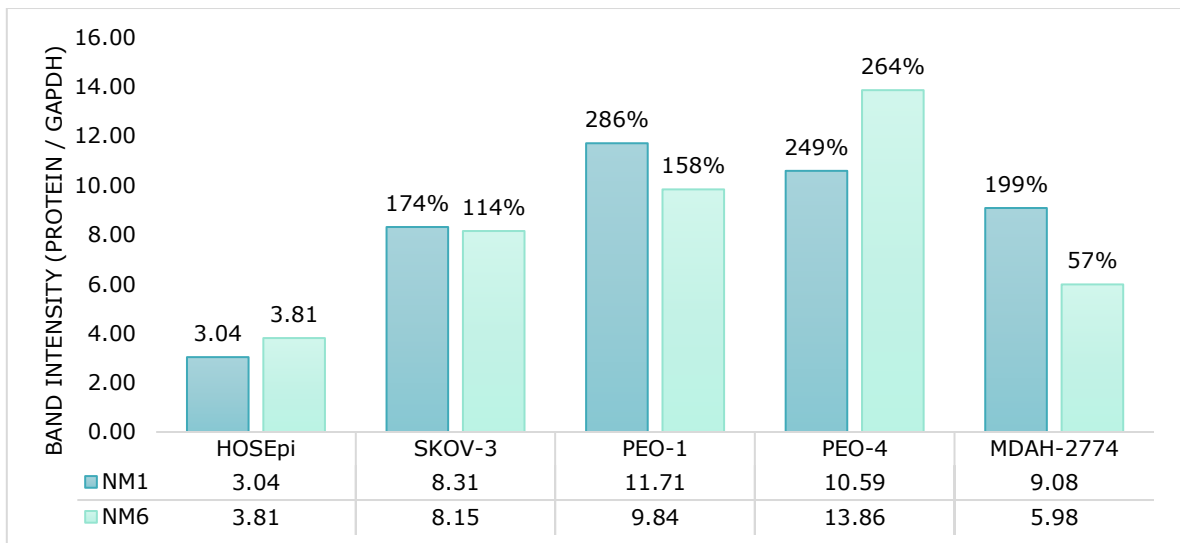


**Figure 2. 10 NM1 and NM6 Band Intensities:**

The fluorescence Li-Cor image of the membrane was uploaded to ImageJ software (Version 1.53a) to calculate the band intensities. The bars represent protein signal intensity / corresponding GAPDH signal intensity = X-axis. Above each cancer cell bar is the % increase; SKOV-3 (174%,114%), PEO-1 (286%,158%), PEO-4 (149%,264%) and MDAH-2774 (199%,57%) when compared to the healthy levels of the HOSEpi cell (n=1).



The distribution pattern scores of all cancer cells were statistically different ( $p < 0.5$ ) from the control cell except for NM6 patterns of SKOV-3. When the confidence interval was reduced to  $p < 0.05$ , PEO-4 was found not significantly different despite the largely incoherent patterns to the control cell. On the other hand, the fast-growing MDAH-2774 showed the highest statistical difference (with the lower confidence  $p < 0.05$ ) in both NM1 and NM6 distribution but exhibited low protein elevations when compared to the other cell lines.

Despite the lack of 0.05 confidence statically significant differences in PEO-4 patterns, the protein levels revealed an interesting observation: while SKOV-3, PEO-1 and MDAH-2774 showed a higher increase in NM1, the slow-growing platinum-resistant cell line PEO-4 had higher levels of NM6 instead, reflecting the levels by the ratio in that of the control cell.

Aside from the NM6 level of MDAH-2774, both nuclear proteins showed an elevation of  $> 100\%$  for all cell lines, highlighting a probable role in the tumorigenic chromosomal arrangement of the cancer cells, by and large, the disease. If this is the case, it would be valuable to investigate the effects of reducing these proteins on the spatial chromosomal arrangement in OC cells (chapter 3).

## 2.4 DISCUSSION

OC lethality lies heavily within its late diagnosis and chemoresistance. Signs and symptoms of the disease are not clear; therefore, the disease needs to be understood much more deeply and earlier. There are many known OC-associated TSGs and oncogenes, some with pathways yet to be understood, and by investigating the spatial organisation of some critical chromosomes associated with its disease progression broadens our understanding. This chapter investigated the spatial organisation of chromosomes 1, 13, 17 and X in 4 OC cell lines SKOV-3, PEO-1, PEO-4 and MDAH-2774. The distribution and levels of NM1 and NM6 were also investigated due to their evident roles in cancer and genome organisation (Mehta *et al.*, 2010; Große-Berkenbusch *et al.* 2020).

### 2.2.5 Chromosomes

To study the diagnostic value and functional change of whole chromosome spatial organisation in OC cells, using FISH probes, their nuclear distribution was mapped and assessed against a control cell. The cell lines had a total average  $p$ -value of 0.201, establishing a significant difference (with  $p < 0.5$ ) between cancer and non-cancer spatial organisation in OC.

#### 2.4.1.1 Chromosome X as a Proximity Control

In Mehta's study, chromosome X showed no change in position regardless of the presence of serum or not (Mehta *et al.*, 2010). Inactive chromosome X is known to occupy the nuclear periphery in female cells, and active chromosome X of both male and female fibroblasts also have a peripheral occupancy; however, its use as a control is challenged as the paternal X it has recently been linked to OC (Belmont *et al.*, 1986; Boyle *et al.*, 2001; Eng *et al.*, 2018). Figure 2.4 showed the control cell line, chromosome X was appeared peripheral with a predominance in shell 2 followed by shell 3, hinting towards an intermediate occupancy similar to tumour lines PEO-1 and MDAH-2774. In SKOV-3 and PEO-4, chromosome X showed a substantial peripheral occupancy (shell 1). In

mammals, chromosome organisation is not absolute as it represents the most probable 'preferred' location within a variable population as this increase with genes due to their higher dynamics (Croft *et al.*, 1999; Boyle *et al.*, 2001). While none of the cell lines showed chromosome X favouring interior localisation, the cancer cell lines showed stronger peripheral preferences than the control cell and, based on this and emerging studies; chromosome X remains disputed as an absolute control.

#### **2.4.1.2 Chromosome 1 (Key gene: ARID1A)**

There are two chromosome spatial positioning theories; size-based and gene-density-based, where size predominates in non-proliferating cells and gene-density in proliferating primary cells (Habermann *et al.*, 2001; Federico *et al.*, 2004; Mayer *et al.*, 2005; Tanabe *et al.*, 2005; Bridger *et al.*, 2000; Cremer *et al.*, 2001; Croft *et al.*, 1999; Sun, Shen and Yokota, 2000; Boyle *et al.* 2001; Bolzer *et al.*, 2005; Meaburn *et al.*, 2007; Bridger *et al.*, 2014). Chromosome positioning correlation to size was also observed in human dermal fibroblasts, where chromosome 1 was at the edge in non-proliferating state and moved to the intermediate location during proliferation (Mehta *et al.*, 2010). The control cell had the largest chromosome in the genome, chromosome 1, at an intermediate position with a skew to the periphery. Aside from SKOV-3 that showed no significant difference to chromosome 1 of the control cell, chromosome 1 of the other OC cell lines occupied the interior.

#### **2.4.1.3 Chromosome 13 (Key gene: BRCA2)**

A whole chromosome is not confined to its territory as it may stay at its silenced region but have an essential gene looped out to an active region (Volpi *et al.*, 2000; Branco and Pombo, 2006). Mehta *et al.*, 2010 showed while with serum, chromosome 13 occupied the periphery but part of its CT extended towards the interior, presumably linked to nucleoli via NADs. In this study, chromosome 13 of HOSEpi, PEO-1 and PEO-4 predominated the intermediate position; however, in

the fluorescent 2D FISH images CT extension is observed (Figure [2.3](#) and [2.11](#)). This was also observed in part of the population of SKOV-3 and MDAH-2774, but much of the population shifted towards the interior, possibly placing the chromosome in an unwarranted active location, perhaps favourable to cancer progression (refer to figure 2.16).

#### **2.4.1.4 Chromosome 17 (Key genes: BRCA1, p53, HER2)**

Chromosome 17 was found at the nuclear periphery in the control line, an area which is often associated with gene repression and transcriptional inactivity; however, this does not render a chromosome or gene totally inactive nor remote (Andrulis *et al.*, 1998; Brickner and Walter, 2004; Casolari *et al.*, 2004; Cabal *et al.*, 2006; Taddei *et al.*, 2006). Chromosome 17 in **all cell lines** showed a shift away from the periphery possibly accompanied by higher transcriptional activity. Remarkably, for MDAH-2774, chromosome 17 showed bi-modal occupancy; however, the images showed this was due to part of the population having interior occupancy and part having peripheral occupancy.

#### **2.4.1.5 Cancer Cell Characterisation by Chromosome**

The spatial organisation of chromosome 1, 13, 17 and X of platinum-resistant PEO-4 has the highest significant difference against the control cell line, followed by the fast-growing MDAH-2774. Then compared against each other; PEO-4 and MDAH-2774 show no significant differences (table [2.7](#)). Table [2.7](#) also displays stronger statistical relationships between MDAH-2774 and PEO-1/PEO-4 and weaker statistical relationships with SKOV-3. However, this weak statistical relationship amongst the cancer cells was balanced as SKOV-3 has the most robust statistical relationship with the control cell line (table [2.6](#)).

**Table 2. 7 Inter-cell comparisons among the OC lines: SKOV-3, PEO-1, PEO-4 And MDAH-2774**

Means of 50-100 nuclei. **Red bold** – denotes higher  $p$ -value than three others (including wild-type), **Green bold** – denotes higher  $p$ -value than two others (including wild-type), **Black**– denotes higher  $p$ -value than wild-type HOSEpi.

Chromosome	SKOV-3 vs PEO-1	SKOV-3 vs PEO-4	SKOV-3 vs MDAH-2774	PEO-1 vs PEO-4	PEO-1 vs MDAH-2774	MDAH-2774 vs PEO-4
1	<b>0.172</b>	0.081	0.103	<b>0.261</b>	<b>0.337</b>	<b>0.703</b>
13	0.021	0.066	<b>0.437</b>	<b>0.403</b>	0.029	<b>0.178</b>
17	0.058	0.093	0.078	<b>0.546</b>	<b>0.269</b>	<b>0.654</b>
Avg. $p$ -value	<b><u>0.084</u></b>	<b><u>0.080</u></b>	<b><u>0.206</u></b>	<b><u>0.403</u></b>	<b><u>0.212</u></b>	<b><u>0.511</u></b>

### 2.4.6 Nuclear Lamins

In primary lymphoblasts, chromosome 1 and 17 have been found in a central nuclear position, while chromosome 13 was enriched at the periphery (Boyle *et al.*, 2001). Chromosome 17 was also found in the central position of healthy breast cells, MCF-10A (immortalised) and 3/4 breast cancer cells (Hassan-Ahmed, 2013). To investigate chromosomes' 1 and 17 peripheral positionings in ovarian tissue that opposes internal positionings in non-ovarian tissue required a closer look, which revealed a stretching or extension into the interior accompanied by a peripheral localisation (possibly tethered to the NE) in chromosome 13 and 17 (figure [2.6](#)).

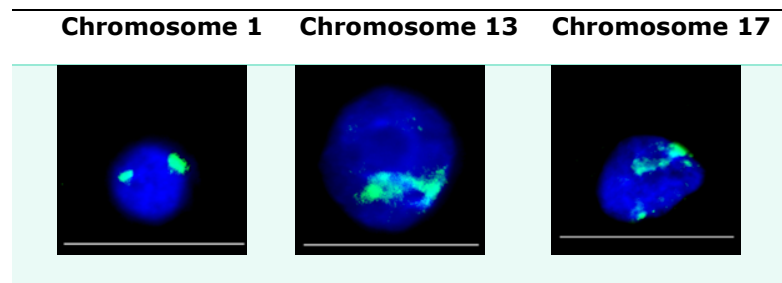


**Figure 2. 11 'Chromosome Stretching' in HOSEpi:**

Images of nuclear localisations of chromosomes 1, 13 and 17 in control cell line HOSEpi delineated using 2D-FISH. No tethering or stretching patterns were seen in chromosome 1; they were either central or peripheral. Nuclear DNA is blue stained with DAPI, and whole chromosome signals were visualised via Cy3 and converted to green for software recognition. Magnification x1000 on Leica DM4000.

'Chromatin stretching' occurs when a region is tethered peripherally through LADs (gene-poor and repressory) but also associates internally with Inter-LADs (gene-rich and transcriptionally active) (Pickersgill *et al.*, 2006; van Steensel and Belmont, 2017). The cancer cells (SKOV-3, PEO-1, PEO-4 and MDAH-2774) may have lacked this chromosome tethering and stretching mechanism most likely due to their aberrant lamin distributions highlighted in figure [2.11](#) and [2.12](#) causing them to occupy only internal positions. A review by Shevelyov and Ulianov, 2019 highlight studies in *Drosophila* and mammals where the loss of tethering resulted in chromatin occupying a more interior position further mentioning that NE attachment during interphase stretches the chromosomes. They further proposed that interactions within TADs and macromolecular crowding result in chromosome

contraction upon NL tethering loss (Shevelyov and Ulianov, 2019). Systemic chromosome stretching was recently described in *Caenorhabditis elegans* where the organisation of the A/B compartments relied on the tethering of lamins to stretch the chromosome and detachment resulted in chromosome compaction and A/B compartment intermingling (Sawh *et al.*, 2020).

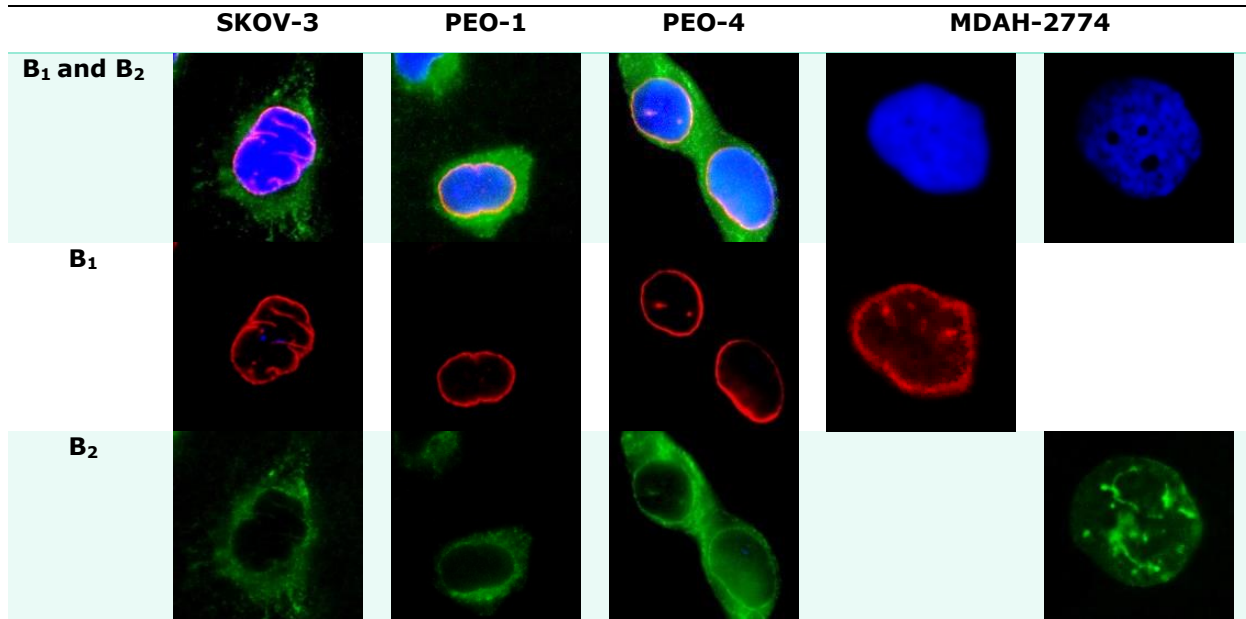


**Figure 2. 12 B-type Lamin Distribution Patterns:**

Images of the nuclear distribution pattern of Lamin B<sub>1</sub> (red Cy3) and Lamin B<sub>2</sub> (green FitC) was captured in 4 OC cell lines SKOV-3, PEO-1, PEO-4 and MDAH-2774. DNA was blue-stained using DAPI. Magnification x1000 on Leica DM4000.

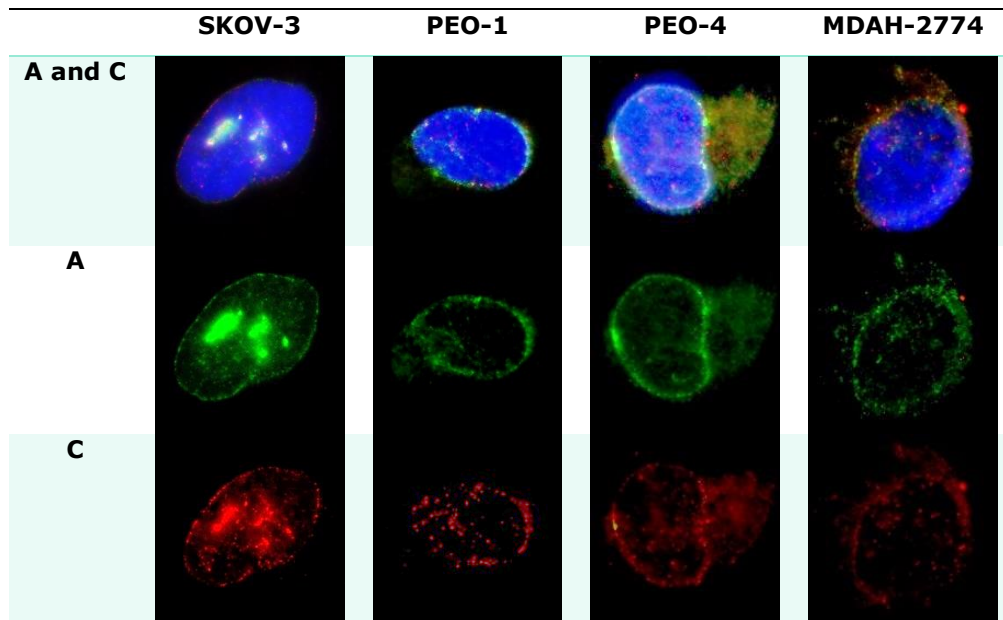


**Figure 2. 13 A-type Lamin Distribution Patterns:**

Images of the nuclear distribution pattern of Lamin A (green FitC) and Lamin C (red Cy3) was captured in 4 OC cell lines SKOV-3, PEO-1, PEO-4 and MDAH-2774. DNA was blue-stained using DAPI. Magnification x100 on Leica DM4000.



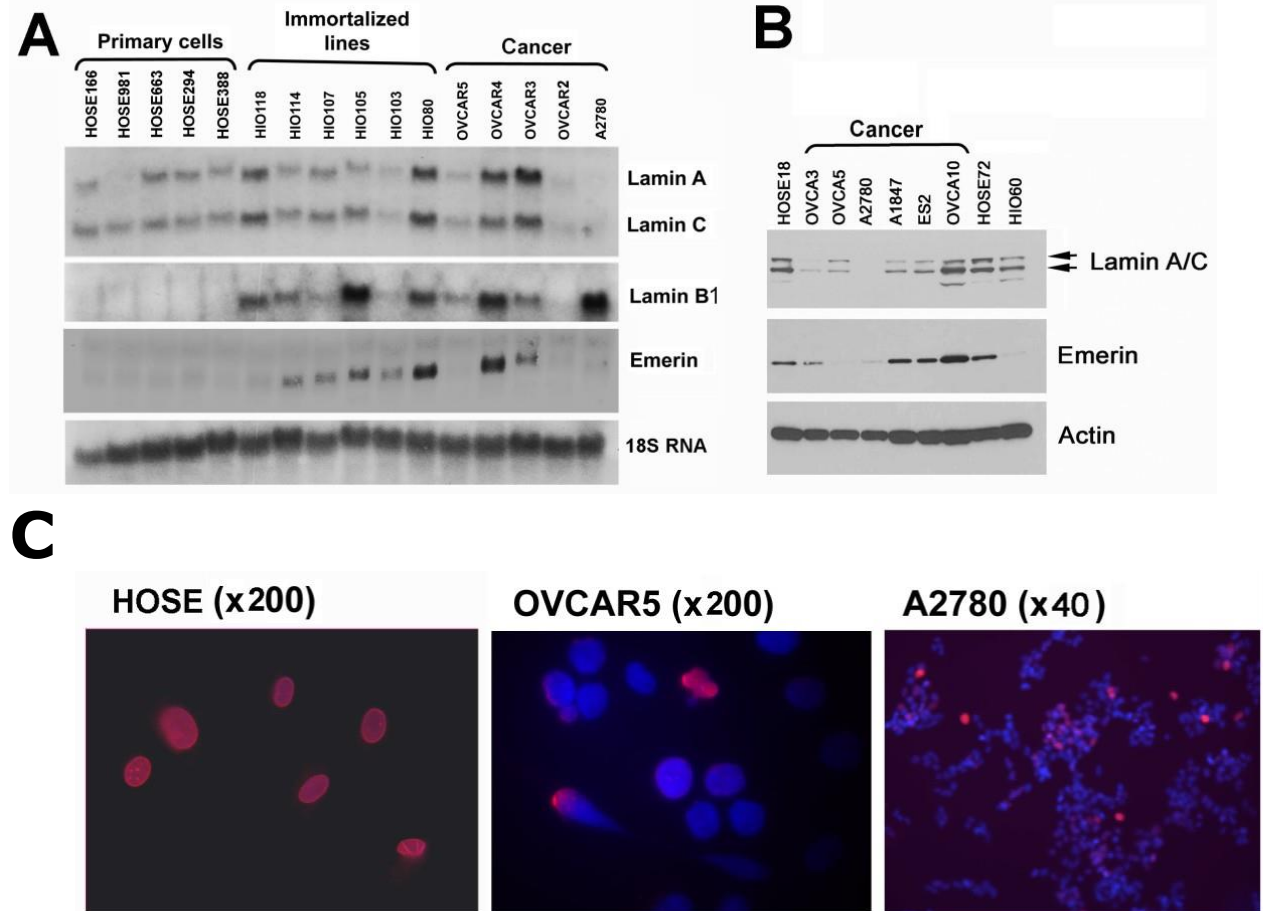


**Figure 2. 14 Lamin A/C and B<sub>1</sub> levels:**

In control cell line (HOSE) and OC cell lines OVCAR5 and A2780 by Capo-Chichi *et al.*, 2011. **A.** Northern blot of lamin A/C, B<sub>1</sub> and emerin in healthy and cancer cell lines showing a general increase of lamin B<sub>1</sub> and emerin mRNA while there was a variation in lamin A/C mRNA **B.** WB of Lamin A/C in 6 OC cell lines showing a general decrease in lamin A/C. **C.** IF of Lamin A/C (red) and DAPI (blue) in control cell line HOSE and OC cell line OVCAR5 and A2780.

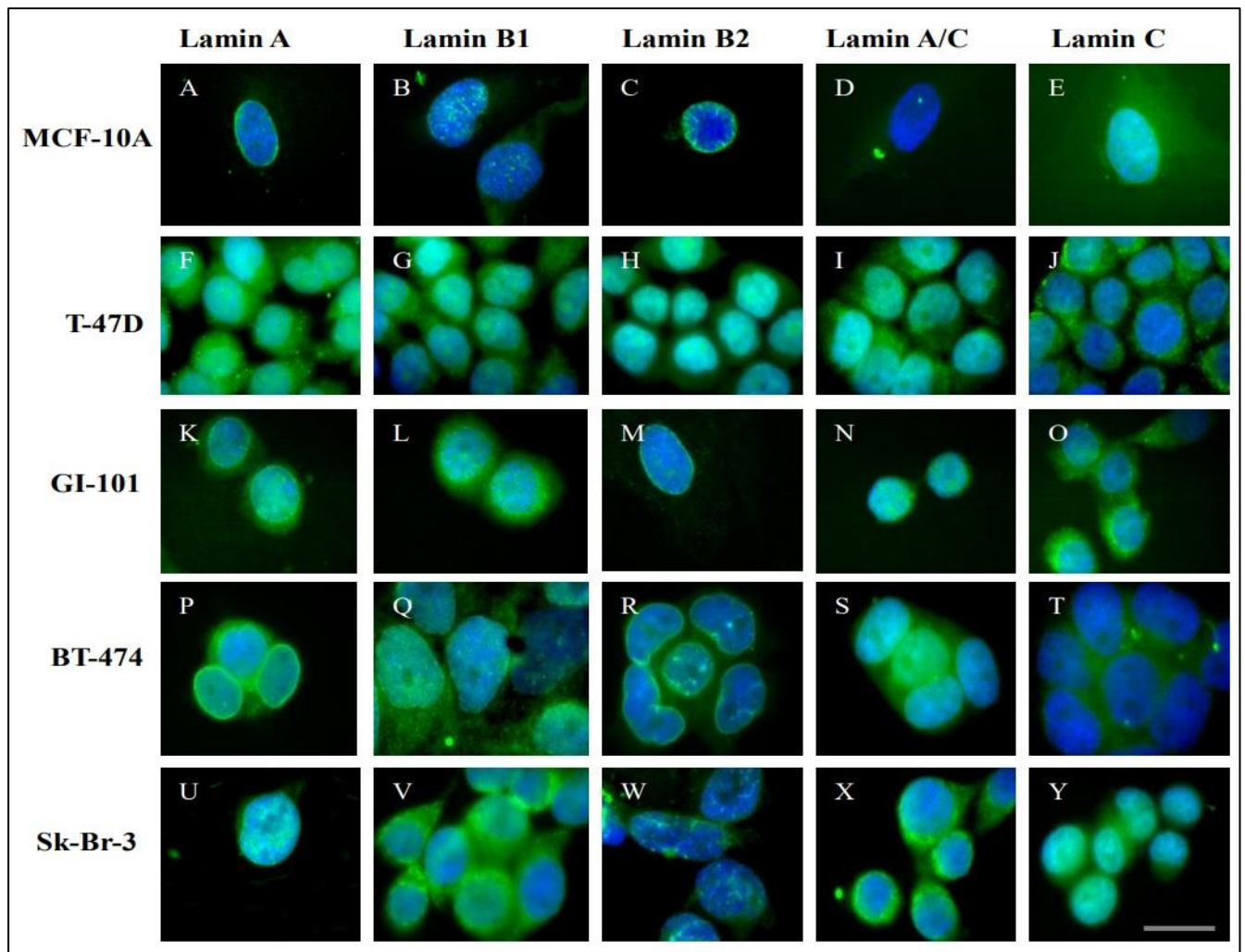


**Figure 2. 15 Lamin Distribution in Breast Cancer:**

In healthy breast cell lines (MCF-10A) and breast cancer cell lines T-47D, GI-101 BT-474 and Sk-Br-3 by Hassan-Ahmed, 2013. Indirect IF of lamin A, B<sub>1</sub>, B<sub>2</sub>, A/C, and C (green) and DNA/DAPI (blue) in healthy and cancer cell lines.

Capo-Chichi *et al.*, 2011 revealed discrepancies in lamin expression and quantity where lamin B<sub>1</sub> was higher in the cancer cells (OVCAR5 and A2780), and lamin A/C showed a reduction when compared to the control cell (HOSE) (figure 2.14). Lamin B<sub>1</sub> in the 4 OC cells has strong rim stains consistent with the over-expression.

Using epithelial breast cell MCF-10A lamins stains from Hassan-Ahmed, 2013 to depict healthy

distribution (figure [2.15](#)), lamin B<sub>2</sub>, appeared highly compromised in the OC cells, deficient in SKOV-3 and PEO-1, and as solid aberrated stains inside the nucleus in MDAH-2774 (figure [2.12](#)). Lamin B<sub>2</sub> depletion can lead to chromosomal instability and aneuploidies in colorectal cancer cells while its knockdown showed specific transcriptionally deregulated chromosomes and repositioning of a candidate gene (*ZNF570*) away from the NL that resulted in increased gene expression (RNA-FISH and qRT-PCR) (Kuga *et al.*, 2014; Ranade *et al.*, 2017). Lamin A and C show strong rim-stains in the healthy distribution, however in MDAH-2774, there were irregularities in lamin A, and with all the cell lines, lamin C showed rim-deficiency with internal foci.

Swift *et al.* 2013 mentioned the ratio of A-type and B-type lamins determining the mechanical properties of nuclei where the relative stoichiometry of A/B-type lamins is cell-type specific in most cases. In addition to the breakdown of “chromosome stretching”, the disruption of healthy ratio may have also led to downstream effects with associated proteins in addition to those within the hypothetical nuclear motor complex resulting in compensatory elevation levels of emerin found by Capo-Chichi *et al.*, 2011 and then possibly the increase of NM1 and NM6 observed here and by others (Ranade *et al.*, 2019).

### 2.4.7 Nuclear Myosins

To study the diagnostic value and functional change of NM1 and NM6 in OC cells and set the basis for subsequent manipulation of whole chromosome spatial organisation, using Indirect IF and WB the nuclear distribution and levels were determined and assessed against control ovarian cells.

Each cell line except PEO-4 showed a significant difference ( $p < 0.05$ ) to at least one protein; however, with the appearance of a different distribution in PEO-4 when significant difference considered at  $p < 0.5$  confidence level, PEO-4 was significantly different (table 2.8). After the warranted protein quantification, PEO-4 had significant NM1 and NM6 elevations, but unlike the other cell lines, it was proportional to the control cell line, i.e., more NM6 than NM1 (table 2.9). This observation is particularly interesting as it is a slow-growing platinum-resistant cell line. Chemoresistant tissues are known to morphologically adapt to resemble the control cell allowing them to evade therapy (Rosa *et al.*, 2014; Bell & Gilan, 2020).

**Table 2. 8 Control Cell vs Cancer Cell:**

Cell Lines SKOV-3, PEO-1, PEO-4 and MDAH-2774 Compared Against the Control HOSEpi (IF): NM1 and NM6 distribution patterns for 200 nuclei. The **red** value represents no significant differences ( $p < 0.5$ ); the **black** values are significantly different ( $p < 0.5$ ), and the **green** values significantly different ( $p < 0.05$ ).

Cell Line	SKOV-3	PEO-1	PEO-4	MDAH-2774	AVG Protein $p$ -value
<b>NM1</b>	0.005	0.424	0.336	0.026	<b>0.198</b>
<b>NM6</b>	0.511	0.009	0.335	0.010	<b>0.216</b>
<b>AVG Cell Line <math>p</math>-value</b>	<b>0.258</b>	<b>0.217</b>	<b>0.336</b>	<b>0.018</b>	-

MDAH-2774, on the other hand, showed highest statistical differences in both protein distributions despite having relatively lower NM1 and NM6 elevations. This event increases the equal importance of protein distribution when investigating fast replicating cancer cell lines. Quite often, the levels of the protein take precedence, and its localisations are over-looked.

**Table 2. 9 NM1 and NM6 % Elevation:**

Cell lines SKOV-3, PEO-1, PEO-4 and MDAH-2774 compared against HOSEpi: [Extracted from **figure 2.9**].

Cell Line	SKOV-3	PEO-1	PEO-4	MDAH-2774	AVG %
<b>NM1</b>	174	286	249	199	<b>227</b>
<b>NM6</b>	114	158	264	57	<b>148</b>
<b>AVG</b>	<b>144</b>	<b>222</b>	<b>257</b>	<b>128</b>	-

These results not only indicate that NM distribution and levels are contributory factors to cancer but also their stoichiometry. This is supported by possibly shared roles of NM1 and NM6 with RNA Pol II (as they have been anticipated to not work together in different complementary capacities but rather in two separate pools of RNA Pol II) (figure 1.22) and compensatory isoforms of NM1 even within cytoplasmic and nuclear NM1 (Venit *et al.*, 2013; Cook, Gough and Toseland, 2020). Toseland's lab even proposed a compensation mechanism between NM1 and NM6 in the perturbation of either protein as NM6-associated RNA Pol II clusters were still present after NM6 was perturbed (Fili *et al.*, 2019; Hari-Gupta *et al.*, 2020; Große-Berkenbusch *et al.* 2020). Additionally, NM1 was found higher in the faster-growing OC cell lines while nuclear NM6 was higher in the slower-growing and platinum-resistant cell line which perhaps may be hinting towards an NM1/NM6 stoichiometry related growth rate and chemoresistance (see doubling times in table 2.1). Taken together, protein stoichiometry and compensation may explain the cases of SKOV-3 and PEO-1 (figure 2.6 and 2.7), as one protein is abnormally distributed (NM1 in SKOV-3 and NM6 in PEO-1), the other is relatively distributed normally (NM6 in SKOV-3 and NM1 in PEO-1), probably in a compensatory capacity.

### 2.4.7.1 A Failed Compensation/Feedback Mechanism: a TSG Solution Becomes an Oncogene Problem

Overall, in healthy ovarian cells, chromosomes 1, 17 and X predominate at the nuclear periphery and chromosome 13 at the intermediate location while the tumour cell lines showed relocalisations toward the interior (active) for all chromosomes. Table [2.1](#) shows all these cell lines have varied TSG mutations (*p53*, *BRCA1/2* and *ARID1A*), which are usually active in cancer cells. However, mutated TSGs producing incorrect proteins, is as if it had not been produced (or 50% product in monoallelic mutations). Aiding this is maybe dysregulated lamin repressory tethering and possible hypermotility by elevated NM levels. They are altogether pulling or releasing the entire chromosome also accompanied by its oncogenes into the active site, which may have been the case for SKOV-3 chromosome 17 that contains TSG mutations and experience oncogene *HER2* amplification.

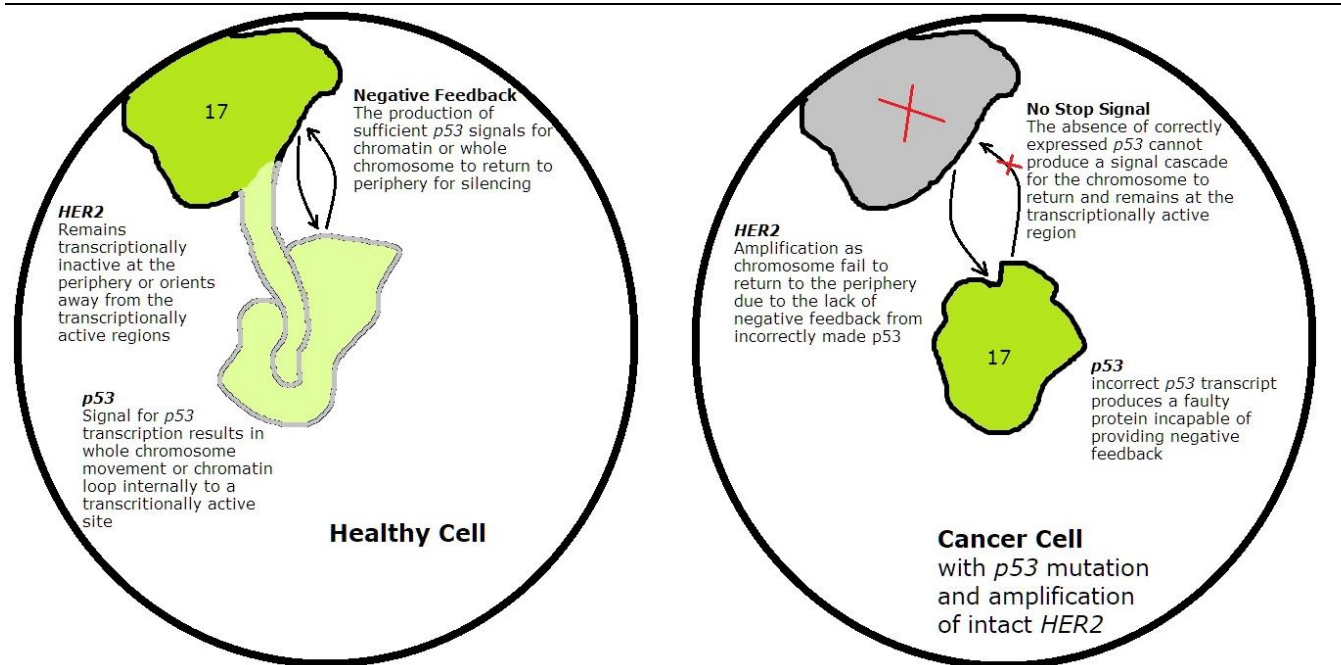


**Figure 2. 16 Hypothetical Schematic: Failed Compensation/Feedback Mechanism:**

**Heavy green** represents predominant CT occupancy; **light green** represents temporary CT upon *p53* transcriptional activation that will return to its repressed territory and **grey** entity represents CT void of the previous chromosome which will now house another chromosome in its place.

### 2.4.8 Conclusion

This research offers another layer of information when understanding the progression of OC through the analysis of well-studied nuclear proteins. Not only has this lead to a deeper understanding of OC, but it has potentially also introduced chromosome spatial positioning as a biomarker panel with diagnostic and prognostic implications, such as has been done for breast cancer - see Meaburn *et al.*, 2009 and 2016. Cancer cells are highly proliferative, which may explain why their levels of NMs (1 and 6) were higher and distribution altered compared to healthy cells, possibly causing unstimulated or hyperactive chromosomal spatial re-organisations. However, aberrations in nuclear lamin presence and distribution also highlight a lack of control, possibly causing disrupted tethering to repressive sites. There is currently no way of predicting what repositioning occurs, but from this study, NMs in addition to lamins highlight a more significant role of the hypothetical nuclear motor complex and superfamily stoichiometry.

The OC cell lines showed higher similarities amongst each other and different when compared to the control line, not only concluding that spatial organisation is altered non-randomly in OC, but subtypes may share drivers to this disorganisation that can be clinically relevant in diagnostics, targeted therapy, prognostics and predicting resistance. In the clinics, chemoresistant cancers are treated with therapies for sensitive cancers; however, different cancers require different treatments. This study contributes towards tailoring therapies, for fast-growing cancers by reducing NM1 while reducing NM6 in chemoresistant cancer may be more useful.

The study of genomic spatial positioning in OC is at its beginning, and even though a fraction of the genome was investigated, we have started to see patterns emerge to drive a plethora of investigations encompassing more cell/tissues types, chromosomes, and genes. The work by Mehta and Bridger, 2010 showed that concomitant with NM1 restoration post-inhibition or knockdown, chromosomes were repositioned back to a proliferative distribution. Moreover, while NM6 has not

been linked directly to spatial organisation, it exhibits anchorage properties as a response to force and is proposed to share compensatory roles with NM1 through their RNA Pol II associations (Fili *et al.*, 2020 and Hari-Gupta *et al.*, 2020). The next chapter, however, investigates further into the role of NM1 and NM6 in spatial genome organisation using RNAi to reduce their levels in OC cells.



## CHAPTER 3

# RESTORING CHROMOSOME SPATIAL POSITIONING IN OC CELLS VIA RNAI OF NUCLEAR MYOSINS 1 AND 6

### 3.1 INTRODUCTION

Chromosomes and genes organise and reorganise depending on the requirements of the cell, by employing the nuclear motor complex to move towards the transcriptionally active interior upon activation or towards the periphery where it is transcriptionally less active (Brown *et al.*, 1997; Shaklai *et al.*, 2007; Szczerbal, Foster and Bridger, 2009; Van de Vosse *et al.*, 2011). Myosins motor ability in transporting biomolecules is well known in the cytoplasm; NM1 functions in concert with RNA Pol I and II and influences spatial genome organisation, while NM6 have so far been associated with RNA Pol II complexes and its role in spatial genome organisation is just emerging (Vreugde *et al.*, 2006; Mehta *et al.*, 2010; Venit *et al.*, 2016; Fili *et al.*, 2019; Cook, Gough and Toseland, 2020). These associations can influence their distribution and functions, however when their levels are perturbed it gets relayed to their distribution and function that alters to suit the perturbation (Vreugde *et al.*, 2006; Mehta *et al.*, 2010; Venit *et al.*, 2016; Fili *et al.*, 2019). These and other NM isoforms myosins (NM2, NM5, NM9 and NM10) have been implicated via over-expression in many cancers (breast, colorectal, prostate and ovarian) in areas of cell migration and invasion (Ouderkirk

and Krendel, 2014).

### **3.1.1 RNA interference (RNAi) of NM1 and NM6 in Cancer**

RNAi is an indispensable tool in cancer genomics which is being used to identify treatment targets. The method transiently suppresses the expression of proteins by introducing constructs of the target RNA into the cell, that then recruits the RNA induced silencing complex (RISC), and together these two entities cleave the mRNA of the target (in this case NM1 and NM6), thus suppressing the protein expression without affecting the DNA (Iorns *et al.*, 2007). This is especially important when the protein to be suppressed is essential under normal circumstances (Iorns *et al.*, 2007).

Ranade *et al.*, 2019 found that lamin A/C and emerin co-knockdown in colorectal cancer cells increased cytoplasmic actin while decreasing nuclear actin which may have potentially affected NM1 activity to enhance chromobility. They further reinforced the intricate crosstalk within the hypothetical nuclear motor complex through NM1 inhibition and actin depolymerisation (in addition to the lamin A/C and emerin co-knockdown) which led to a restoration of the enhanced chromobility (caused by lamin A/C and emerin depletion). Interestingly the knockdown of lamin A/C or emerin individually was not enough to alter spatial territory of chromosome 19 (interior) and chromosome 18 (peripheral), however, a co-knockdown repositioned chromosome 19 away from the nuclear interior while chromosome 18 remained unaltered (Ranade *et al.*, 2017/2019). This raises the question when knocking down myosin, would an individual knockdown be sufficient in cancer? Or require an associate protein for co-knockdown? Chapter 1 and 2 also cited the vital role RNAi played in an individual knockdown of NM1 that was sufficient to investigate the link between NM1 role in rapid chromosome spatial organisation (in young proliferating HDF) by Mehta *et al.*, 2010.

The elevation of NM has also been studied for its tumorigenic value in many cancers through RNAi. siRNA knockdown of NM1 reduced the migratory and invasive potential of prostate cancer cells (PC-

3) and for NM6 led to a 3-fold reduction in NM6 activity in breast cancer cells (MCF-7) (Maly *et al.*, 2017; Fili *et al.*, 2017). NM6 showed cancer-specific expression in prostate cancer cells (LNCaP), and upon siRNA knockdown, cells had significantly reduced migration potential (Dunn *et al.*, 2006). Wang *et al.*, 2015 even performed a lentivirus-mediated RNA interference knockdown of NM6 in breast cancer cells (ZR-75-30 and MDA-MB-231) and found reduced viability and proliferation, in addition to cell cycle suppression.

A role for NM6 in chromosome behaviour and dynamics has not been studied by RNAi; it has been studied for its role in whole chromosome movement by Zorca *et al.*, 2015 who found that chromosome 17 was not able to move when transcription was stimulated in NM6 deficient T-helper cells. Zorca *et al.*, 2015 concluded a possible dual role for NM6 in genome organisation upon gene activation and transition modulator for RNA Pol II from pause to elongation for a rapid transcriptional response. The constant cell activation cycles of cancerous cells may be the reason NMs are elevated; however, while it may be favourable for some chromosomes, it may be causing unstimulated relocations of other chromosomes.

### **3.1.2 Outlook**

In retrospect, while related research into the deadliest of gynaecological cancers is deficient, some have focused on knocking down NM1 and NM6 to learn about its mechanism regarding migratory and proliferation potential of cancers (Dunn *et al.*, 2006; Ouderkirk and Krendek, 2014; Maly *et al.*, 2017;). Chapter 2 showed discrepancies in NM1 and NM6 levels and distribution, which may be linked to their function in the altered spatial genome organisation in OC cells. The identification of chromosomes that improve their spatial positions with a protein knockdown is valuable for finding new drug targets. However, not one size fits all; therefore, this chapter aims to target the hypothetical nuclear complex through its NMs end and assess the restorative value that temporarily reducing the level of NM1 and NM6 through siRNA may have on spatial chromosome organisation (of chromosome 1, 13, 17 and X) in OC cells (SKOV-3, PEO-4, MDH-2774, PEO-1).

## 3.2 METHODS

### 3.2.1 RNA interference

#### 3.2.1.1 *Making the siRNA Transfection media (1mL):*

100 $\mu$ L of 15nM siRNA solution (0.75 $\mu$ L of 20 $\mu$ M siRNA\* stock, 4.25 $\mu$ L siRNA Buffer 1X and 95 $\mu$ L serum-free media) and 100 $\mu$ L of transfection reagent (3 $\mu$ L of dharmaFECT1 (Dharmacon) and 97 $\mu$ L serum-free media) was made. They were both incubated at room temperature for 5 mins separately and then for another 20 mins combined (200 $\mu$ L). 800 $\mu$ L of supplemented complete media was added to the 200 $\mu$ L to make 1mL.

\*Control (ON-TARGETplus Non-targeting Control Pool) (Dharmacon)

\*NM1 (ON-TARGETplus Human MYO1b siRNA – SMARTpool) (Dharmacon)

\*NM6 (ON-TARGETplus Human MYO6 siRNA – SMARTpool) (Dharmacon)

#### 3.2.1.2 *Transfection*

The freshly trypsinised cells were re-suspended in the transfection medium (scaled accordingly) and plated. After 48 hours, the media was replaced with freshly made siRNA transfection medium. This was performed on all cell lines (SKOV-3, PEO-1, PEO-4 and MDAH-2774) in 24-well plates three times and then scaled up (x5 for T25 and x3 for 6-well plates) to collect material for WB (T25), FISH (T25) and IF (coverslips in 6-well plates) after 96 hrs.

### **3.2.2 Cell Culture – refer to section 2.2.1**

Plating densities were  $7.5 \times 10^3$ ,  $2.5 \times 10^5$  and  $5.0 \times 10^5$  for 96-well, 6-well and T25 respectively. 96-well plates were used initially for trials and optimization, 6-well dishes were used to grow cells on glass coverslips for IF and T25 to scale up for WBs and 2D-FISH.

### **3.2.3 FISH – refer to section 2.2.2**

Post knockdown cells were left in the hypotonic solution were left for 15-20 mins instead of 10 mins as the cytoplasm became challenging to remove. This was discovered by Venit *et al.*, 2016 in NM1 knockdown cells showed 50% more elasticity with 25% higher resistance to swelling.

### **3.2.4 Indirect IF – refer to section 2.2.3**

### **3.2.5 WB – refer to section 2.2.4**

## 3.3 RESULTS

### 3.3.1 Knockdown of NM1 and NM6 in 4 OC Cell Lines:

Chromosomes 1, 13 and 17 displayed significant differences in their spatial organisation in the OC cells to that of the control cell line and in addition, also have a significant increase in the protein levels of NM1 and NM6. To investigate whether there is any relationship between the spatial occupancy of interphase chromosomes and NM1 and NM6 levels in OC, the proteins were individually reduced by RNAi in the cancer cells then nuclear positions for chromosomes 1, 13 and 17 nuclear positions were examined post-knockdown. The siRNA constructs were obtained from Dharmacon who also outlined a protocol involving plating the cells and replacing the media after 24 hrs with the transfection media. This method was not allowing a sufficient knockdown without affecting the control, as it required high concentrations of the siRNA reagents (50-100nM). To improve the efficiency, the 'reverse transfection method' outlined by ThermoFisher was used that involved plating the cells at 0 hrs with the transfection media (15nM siRNA) and replacing the media with freshly made transfection media (15nM siRNA) after 48 hrs. This economised and reduced the potential toxic load of the method.

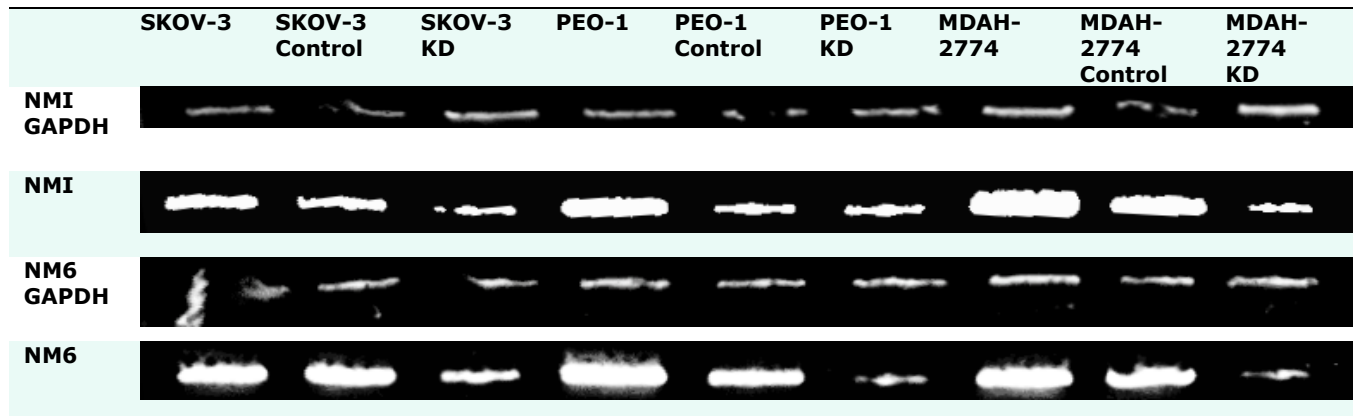


**Figure 3. 1 NM1 and NM6 Levels Pre- and Post-knockdown of NM1 and NM6 in Cell Lines SKOV-3, PEO-1 and MDAH-2774:**

Cytoplasmic and Nuclear extracts of 3 OC cell lines SKOV-3 (lane 1,2 and 3), PEO-1 (lane 4, 5 and 6) and MDAH-2774 (lane 7, 8 and 9) post siRNA of NM1 and NM6 were analysed by WB on the Li-Cor Odyssey for band intensity quantification via the ImageJ software (Version 1.53a). The quantities were normalised against the loading control GAPDH (top band) in their corresponding cytoplasmic extracts (n=1).

The band intensities were calculated using the ImageJ application and normalised against their control to estimate their knockdown level. The aim was a 50% knockdown to combat the elevation but not make the cell devoid of the protein.



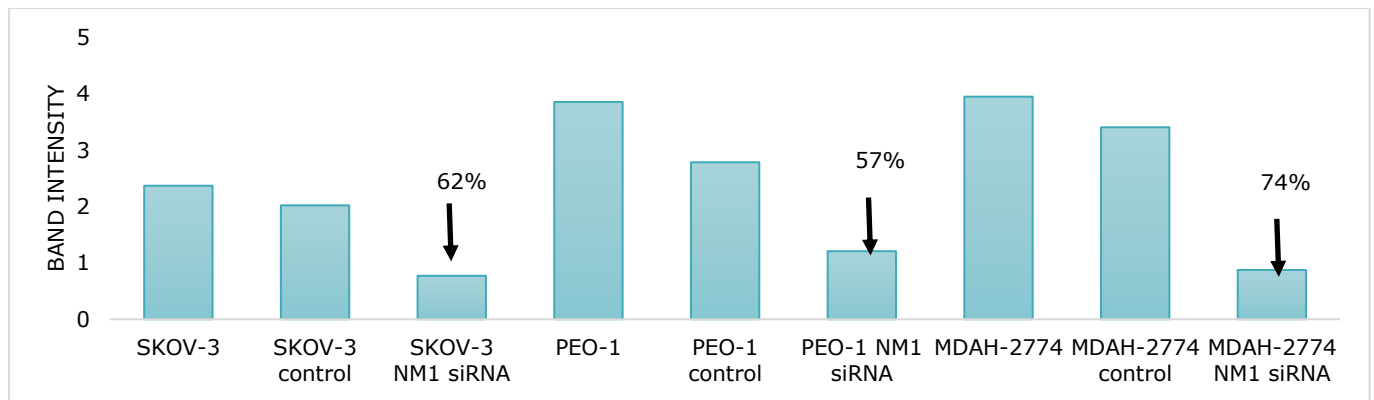


**Figure 3. 2 NM1 Band Intensities:**

Showing the reduction of NM1 following siRNA knockdown of NM1 (ON-TARGETplus Human MYO1b siRNA – SMARTpool) in cell lines SKOV-3, PEO-1 and MDAH-2774 quantified by band intensities (NM1 / GAPDH) calculated using the ImageJ software (Version 1.53a) and normalised with the loading control GAPDH. SKOV-3, PEO-1 and MDAH-2774 were reduced to 38%, 43% and 26% of the original NM1 amount respectively that was estimated against the control (ON-TARGETplus Non-targeting Control Pool).

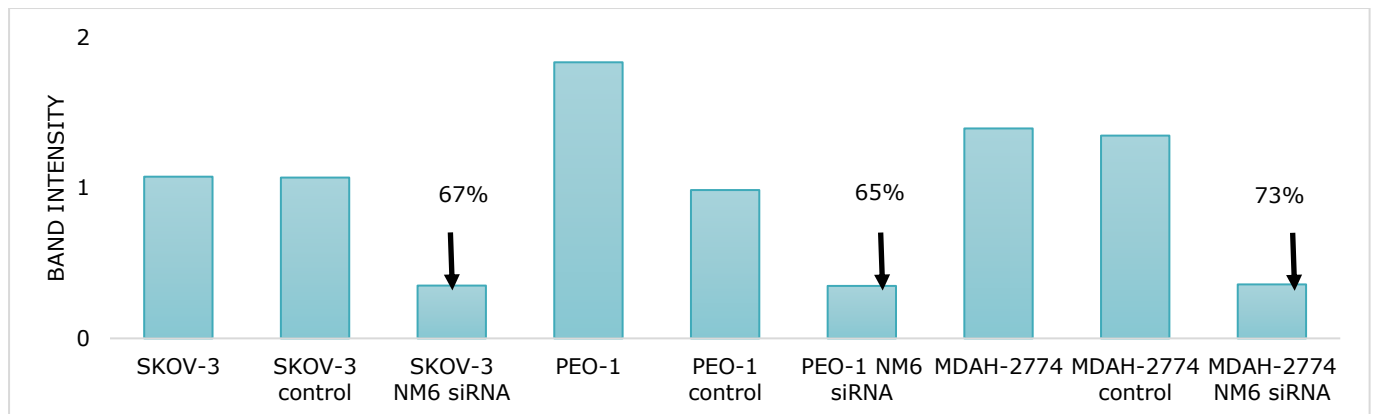
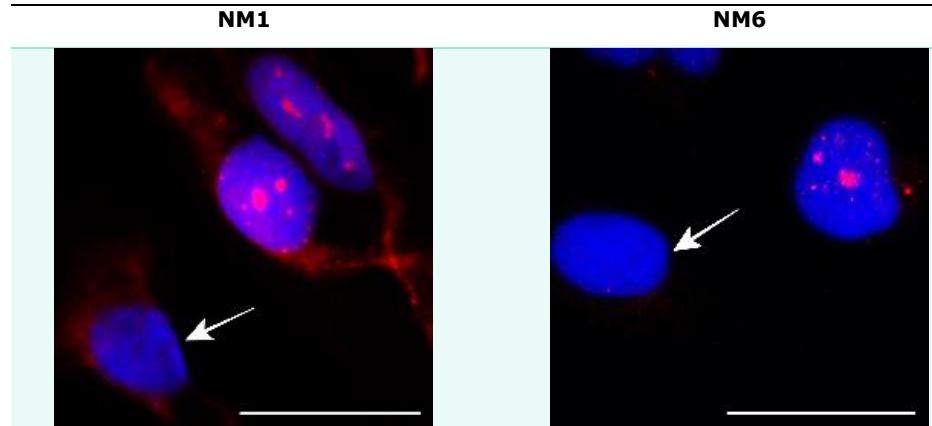


**Figure 3. 3 NM6 Band Intensities:**

Showing the reduction of NM1 following siRNA knockdown of NM6 (ON-TARGETplus Human MYO6 siRNA – SMARTpool) in cell lines SKOV-3, PEO-1 and MDAH-2774 quantified by band intensities (NM6 / GAPDH) calculated using the ImageJ software (Version 1.53a) and normalised with the loading control GAPDH. SKOV-3, PEO-1 and MDAH-2774 were reduced to 33%, 35% and 27% of the original NM6 amount respectively that was estimated against the control (ON-TARGETplus Non-targeting Control Pool).

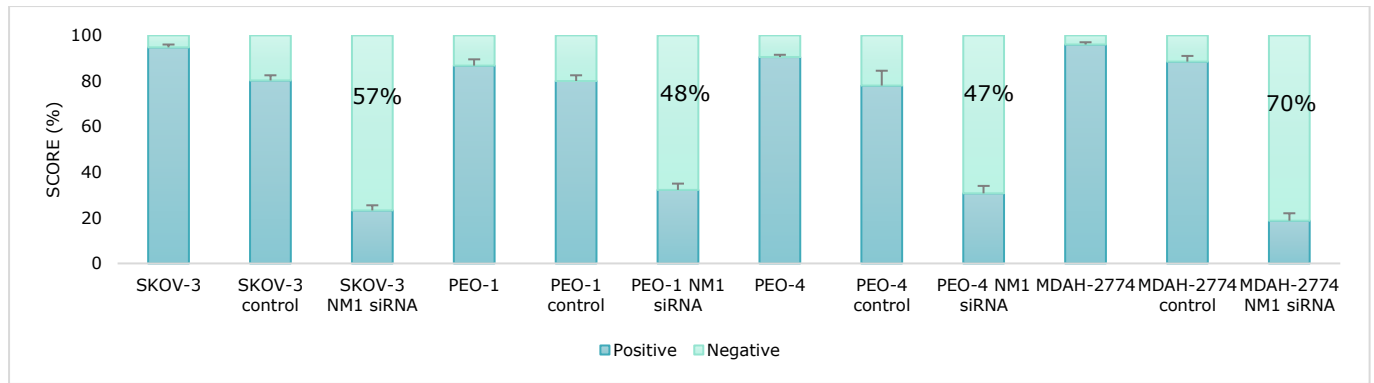
The knockdown effect was also evident by microscopy, which afforded the scoring of the positively and negatively stained nuclei, thus providing a subjective estimation for the knockdown. This was especially useful as a suitable WB for PEO-4 knockdown could not be provided (due to SARS-CoV-

2). The protein levels of the IF proportionally reflected the protein levels of the other cell lines on the WB; therefore, the FISH of PEO-4 cell line has been assumed to have had a knockdown efficiency of 47% and 32% in NM1 and NM6 respectively.



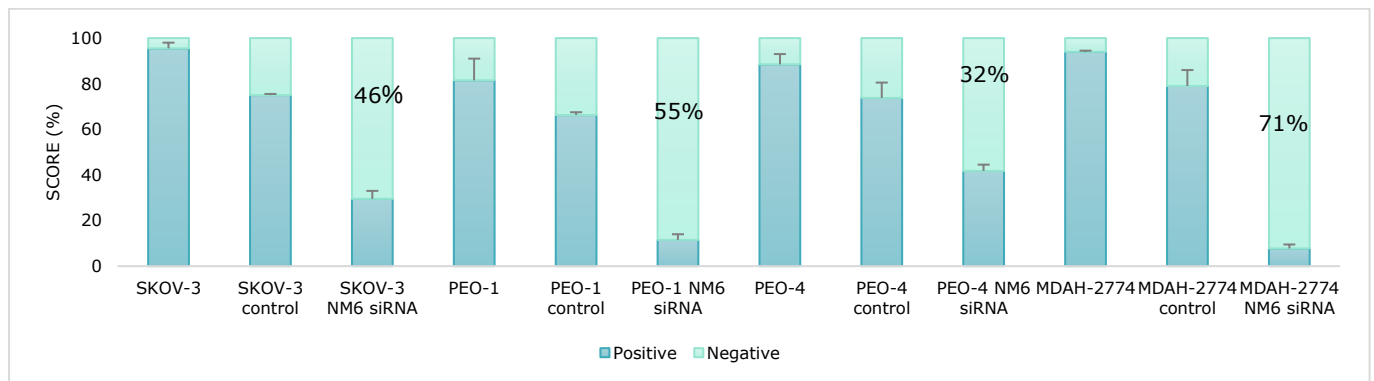
**Figure 3. 4 NM1 and NM6 Positively and Negatively Stained Nuclei:**

Representative images of the positively and negatively stained nucleus in OC cells to score the level of knockdown in the 4 OC cell lines SKOV-3, PEO-1, PEO-4 and MDAH-2774. DNA was stained using DAPI (blue), and the NM1 and NM6 protein were revealed by Indirect IF with a Cy3 conjugated secondary antibody. The arrows point to negative nuclei—magnification x400. Scale bars represent 25 $\mu$ m.



**Figure 3. 5 NM1 Levels Pre- and Post-Knockdown of NM1 in Cell Lines SKOV-3, PEO-1, PEO-4 and MDAH-2774 as Estimated by Indirect-IF:**

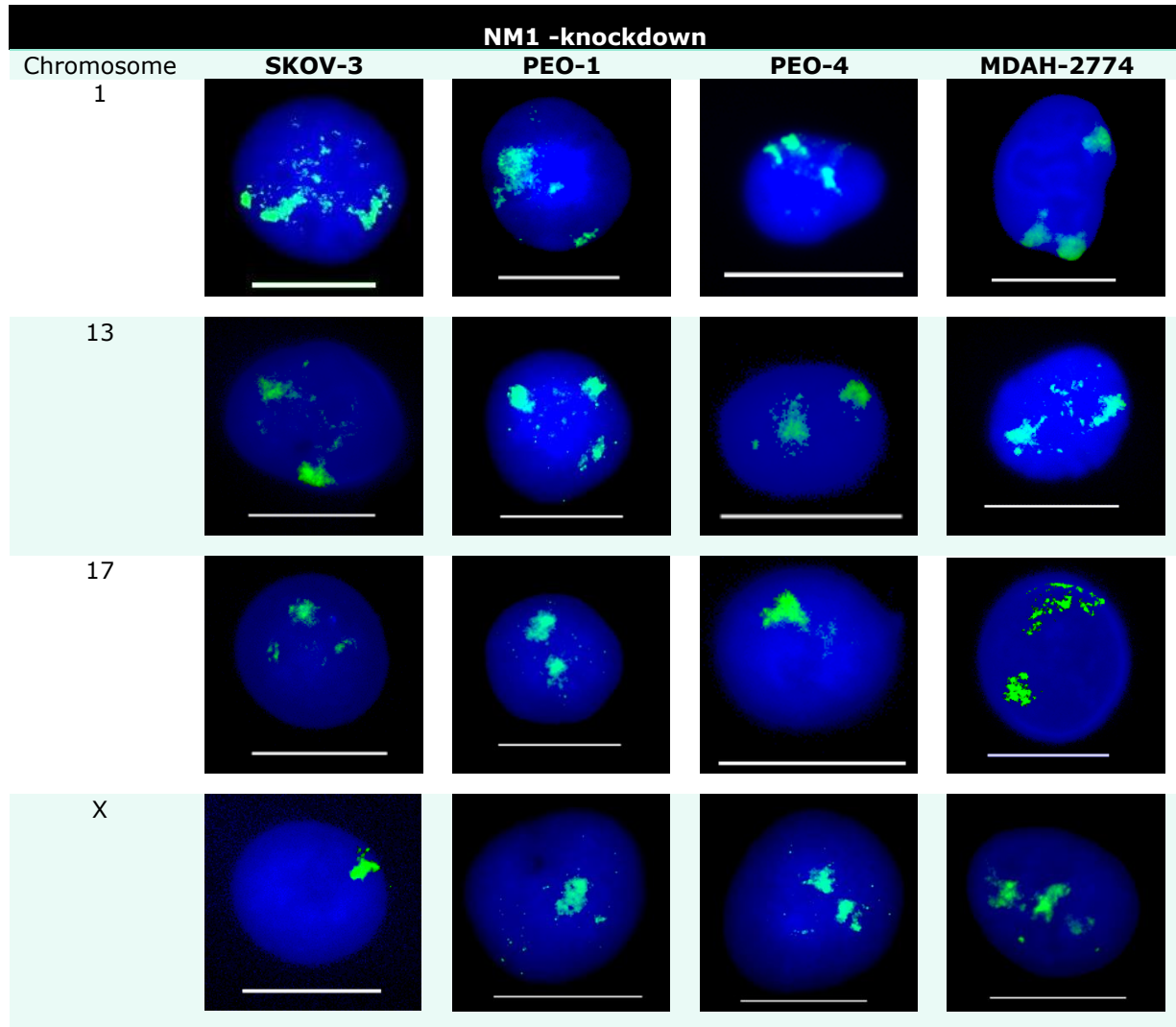
The bars and error bars for each cell line (X-axis) represents means and standard error of the mean for a total of 200 nuclei as a percentage (% / Y-axis) of positive and negative stained cells before and after NM1 knockdown NM1 (ON-TARGETplus Human MYO1b siRNA – SMARTpool). SKOV-3, PEO-1, PEO-4 and MDAH-2774 were reduced to 43%, 52%, 53% and 30% of the original NM1 amount respectively that was normalised against the control (ON-TARGETplus Non-targeting Control Pool) (n=2).



**Figure 3. 6 NM1 Levels Pre and Post Knockdown of NM1 in Cell Lines SKOV-3, PEO-1, PEO-4 and MDAH-2774 as Estimated by Indirect-IF:**

The bars and error bars for each cell line (X-axis) represents means and standard error of the mean for a total of 200 nuclei as a percentage (% / Y-axis) of positive and negative stained cells before and after NM6 knockdown NM6 (ON-TARGETplus Human MYO6 siRNA – SMARTpool). SKOV-3, PEO-1, PEO-4 and MDAH-2774 were reduced to 54%, 55%, 68% and 29% of the original NM6 amount respectively that was normalised against the control (ON-TARGETplus Non-targeting Control Pool) (n=2).

Once satisfactory knockdown was obtained by assessing both the WB and immunofluorescence, the spatial positioning of chromosomes 1, 13, 17 were analysed as outlined in chapter 2 with re-positionings attributed to NM1/NM6 decreased.

**3.3.2 Spatial Chromosome Organisation Post-NM1 and -NM6 Knockdown:****Figure 3. 7 Post-NM1 Knockdown Chromosome Spatial Positioning Images:**

Fluorescence images for the nuclear localisations of chromosomes 1, 13, 17 and X in OC cell lines SKOV-3, PEO-1, PEO-4 and MDAH-2774 positioned using 2D-FISH post NM1 knockdown. Nuclear genetic material stained blue with DAPI and whole chromosome signals were stained red with Cy3 and converted to green for software recognition. Magnification x400 / x1000. Scale bars represent 25µm.

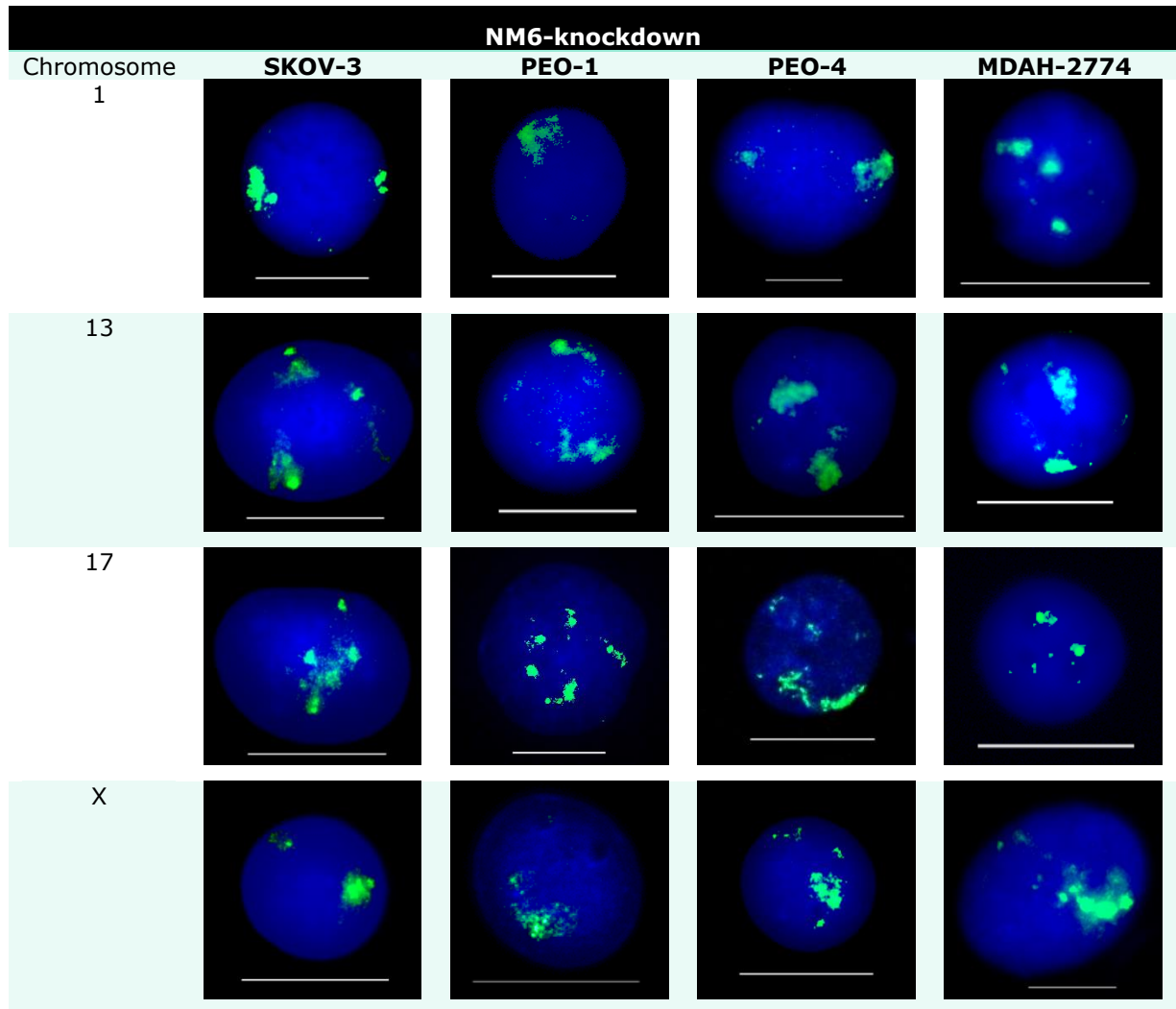


**Figure 3. 8 Post-NM6 Knockdown Chromosome Spatial Positioning Images:**

Fluorescence images for the nuclear localisations of chromosomes 1, 13, 17 and X in OC cell lines SKOV-3, PEO-1, PEO-4 and MDAH-2774 positioned using 2D-FISH post NM6 knockdown. Nuclear genetic material stained blue with DAPI and whole chromosome signals were stained red with Cy3 and converted to green for software recognition. Magnification x400 / x1000. Scale bars represent 25µm.



**Figure 3. 9 Graphical Representation: Image Analysis Chromosome Spatial Positioning Post-NM1 Knockdown:**

Histograms show the nuclear localisations of chromosomes 1, 13, 17 and X in OC cell lines SKOV-3, PEO-1, PEO-4 and MDAH-2774 before (light blue) and after (dark green) siRNA knockdown of NM1, positioned using 2D-FISH and analysed by erosion analysis software [section 2.2.2]. The bars and error bars signify means and standard error of the mean of 50-100 nuclei, respectively. Y-Axis represents % Cy3 whole chromosome probe signal / % DAPI nuclear signal, and the X-axis represents periphery to the central position (1 to 5). Student's *t*-test of all cancer cells performed against their origin cell and to the wild-type (healthy HOSEpi) [*p*0.5 considered as significant].

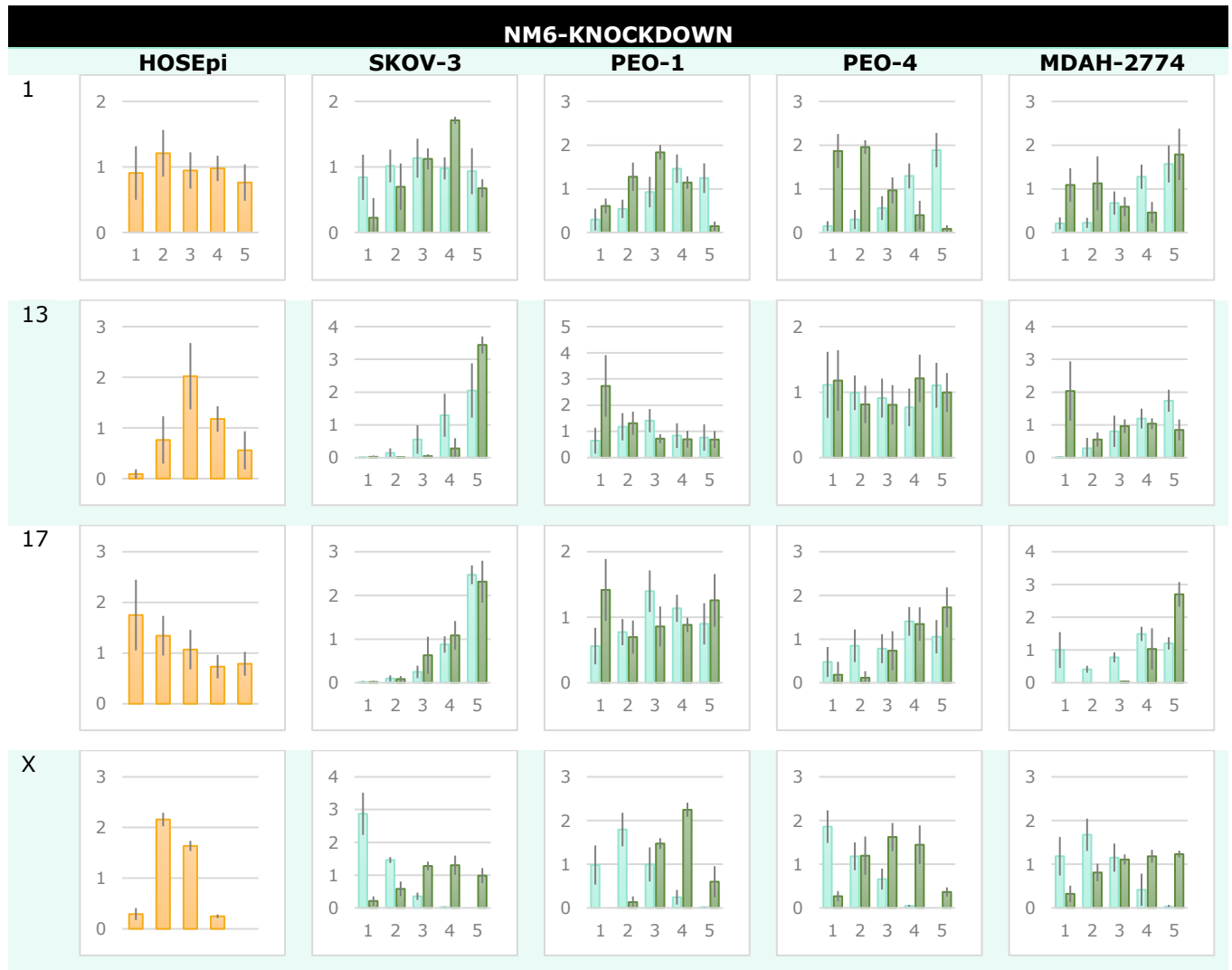


**Figure 3. 10 Graphical Representation: Image Analysis Chromosome Spatial Positioning Post-NM6 Knockdown:**

Histograms show the nuclear localisations of chromosomes 1, 13, 17 and X in OC cell lines SKOV-3, PEO-1, PEO-4 and MDAH-2774 before (light blue) and after (dark green) siRNA knockdown of NM6, positioned using 2D-FISH and analysed by erosion analysis software [section 2.2.2]. The bars and error bars signify means and standard error of the mean of 50-100 nuclei, respectively. Y-Axis represents % Cy3 whole chromosome probe signal / % DAPI nuclear signal, and the X-axis represents periphery to the central position (1 to 5). Student's *t*-test of all cancer cells performed against their origin cell and to the wild-type (healthy HOSEpi) [ $p < 0.5$  considered as significant].

Each shell of each OC cell line was statistically compared to the corresponding shell of the control cell and then categorised by **no** significant difference ( $p0.5$ ), a significant difference ( $p0.5$ ) and a significant difference ( $p0.05$ ) (table 3.1).

**Table 3. 1 p-values Post-NM1 and NM6 Knockdown Against HOSEpi:**

Each shell was calculated in MS Excel and the below. Shells that showed no significant differences with  $p0.5$  are highlighted in **red**, the shells that showed statistical differences with  $p0.5$  are unhighlighted, and the shells that showed statistical differences with  $p0.05$  are highlighted in **green**. The average values listed below; the **red** value represents no significant differences [ $p0.5$ ]; the black values are significantly different [ $p0.5$ ] and the **green** values significantly different [ $p0.05$ ].

<b>NM1 KNOCKDOWN</b>				
	SKOV-3	PEO-1	PEO-4	MDAH-2774
<b>Chromosome 1</b>				
Shell 1	0.626	0.754	0.214	0.789
Shell 2	0.922	0.103	0.603	0.621
Shell 3	0.486	0.890	0.198	0.854
Shell 4	0.417	0.064	0.000	0.351
Shell 5	0.630	0.790	0.978	0.633
AVG →	0.616	0.520	0.399	0.650
<b>Chromosome 13</b>				
Shell 1	0.336	0.022	0.012	0.210
Shell 2	0.329	0.106	0.142	0.242
Shell 3	0.107	0.018	0.000	0.119
Shell 4	0.021	0.761	0.000	0.015
Shell 5	0.004	0.299	0.000	0.595
AVG →	0.160	0.241	0.031	0.236
<b>Chromosome 17</b>				
Shell 1	0.047	0.287	0.669	0.968
Shell 2	0.012	0.331	0.838	0.210
Shell 3	0.376	0.325	0.600	0.000
Shell 4	0.089	0.261	0.108	0.195
Shell 5	0.048	0.811	0.106	0.007
AVG →	0.114	0.403	0.464	0.276
<b>Chromosome X</b>				
Shell 1	0.361	0.095	0.415	0.052
Shell 2	0.392	0.000	0.001	0.016
Shell 3	0.091	0.047	0.008	0.002
Shell 4	0.900	0.106	0.004	0.059
Shell 5	0.500	0.022	0.009	0.415
AVG →	0.449	0.054	0.087	0.109

<b>NM6 KNOCKDOWN</b>				
	SKOV-3	PEO-1	PEO-4	MDAH-2774
<b>Chromosome 1</b>				
Shell 1	0.142	0.482	0.162	0.771
Shell 2	0.285	0.785	0.028	0.980
Shell 3	0.924	0.044	0.660	0.122
Shell 4	0.000	0.495	0.285	0.174
Shell 5	0.602	0.014	0.005	0.187
AVG →	0.391	0.364	0.228	0.447
<b>Chromosome 13</b>				
Shell 1	0.200	0.040	0.146	0.125
Shell 2	0.001	0.269	0.901	0.436
Shell 3	0.000	0.000	0.013	0.003
Shell 4	0.015	0.199	0.952	0.490
Shell 5	0.000	0.720	0.336	0.422
AVG →	0.043	0.245	0.470	0.295
<b>Chromosome 17</b>				
Shell 1	0.049	0.778	0.074	0.047
Shell 2	0.001	0.266	0.001	0.001
Shell 3	0.203	0.755	0.383	0.000
Shell 4	0.112	0.481	0.033	0.562
Shell 5	0.002	0.660	0.059	0.003
AVG →	0.073	0.588	0.110	0.122
<b>Chromosome X</b>				
Shell 1	0.752	0.088	0.888	0.873
Shell 2	0.035	0.004	0.108	0.003
Shell 3	0.210	0.387	0.973	0.011
Shell 4	0.140	0.044	0.067	0.011
Shell 5	0.120	0.339	0.031	0.003
AVG →	0.251	0.172	0.413	0.180



These data were summarised and compared to their pre-knockdown state on a heat-map (figure 3.4) and a statistical table with entire nuclear averages (table 3.2).

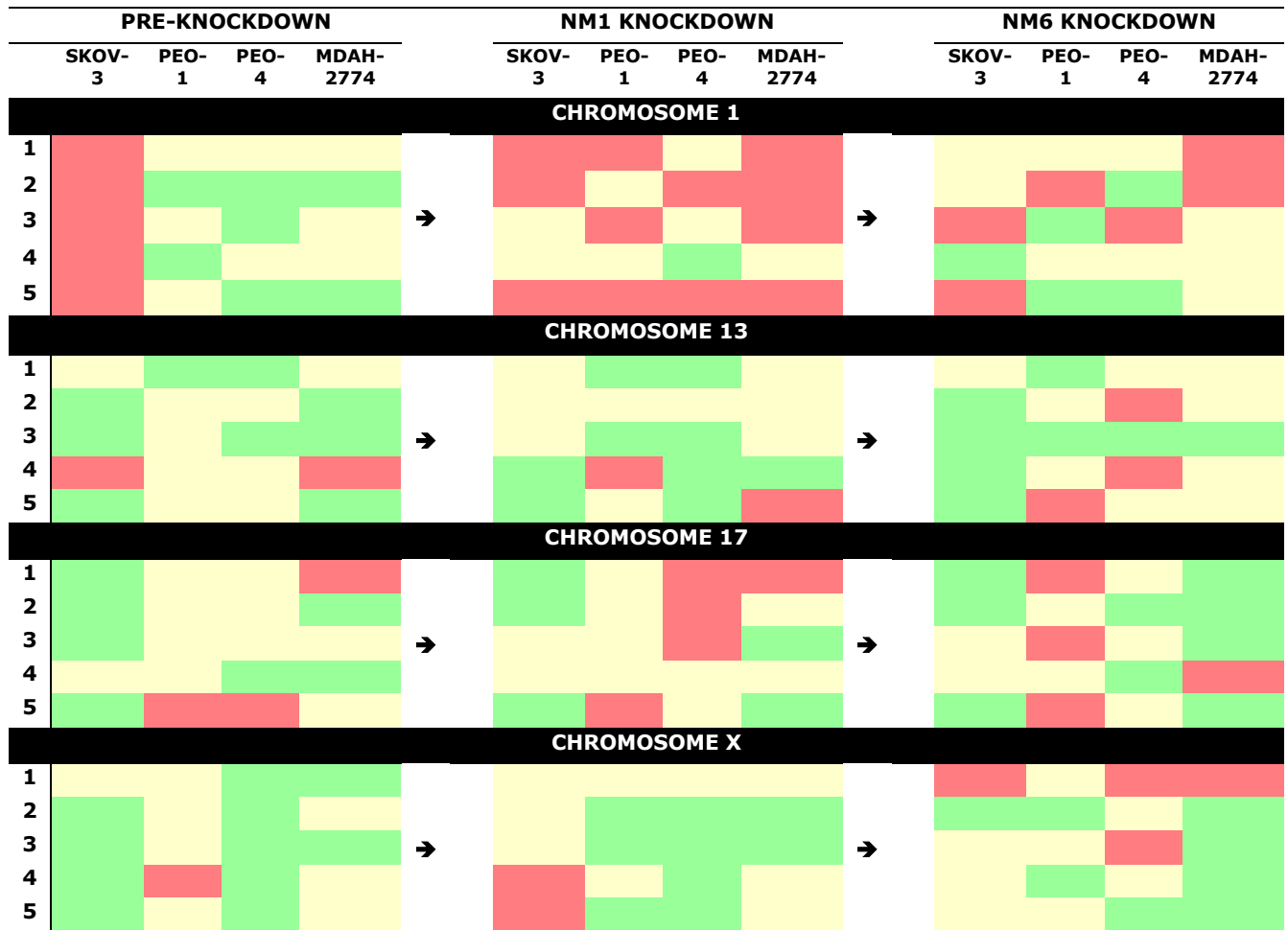


**Figure 3. 11 Heat-Map of Post-Knockdowns Effect Using  $p$ -values Against HOSEpi:**

Blocks highlighted in red are shells that showed no significant differences ( $p > 0.5$ ), highlighted in green are shells that showed statistical differences with  $p < 0.05$ , and the yellow shells showed statistical differences ( $p < 0.5$ ). The higher similarity to the control cells is reflected by more red blocks and the lowest similarities reflected by more green blocks.

**Table 3. 2 Summary of *p*-values Post-Knockdown Cancer Cells vs Control Cell:**

After the siRNA knockdown of NM1 and NM6 for cell lines SKOV-3, PEO-1, PEO-4, and MDAH-2774 their chromosome positions analysed for improvements statistically. **Red bold** – denotes higher *p*-value than pre-knockdown implicative of CTs re-positioning in locations closer to those adopted by the control cell. Means of 50-100 nuclei.

Chromosome	Cell Line	Pre-Knockdown	NM1 knockdown	NM6 knockdown
<b>1</b>	SKOV-3	0.842	0.616	0.391
	PEO-1	0.133	<b>0.520</b>	<b>0.364</b>
	PEO-4	0.091	<b>0.399</b>	<b>0.228</b>
	MDAH-2774	0.103	<b>0.650</b>	<b>0.447</b>
<b>13</b>	SKOV-3	0.138	<b>0.160</b>	0.043
	PEO-1	0.132	<b>0.241</b>	<b>0.245</b>
	PEO-4	0.119	0.031	<b>0.470</b>
	MDAH-2774	0.207	<b>0.236</b>	<b>0.295</b>
<b>17</b>	SKOV-3	0.095	<b>0.114</b>	0.073
	PEO-1*	0.306	<b>0.403</b>	<b>0.588</b>
	PEO-4	0.318	<b>0.464</b>	0.110
	MDAH-2774	0.268	<b>0.276</b>	0.122
<b>X</b>	SKOV-3	0.037	<b>0.449</b>	<b>0.251</b>
	PEO-1*	0.326	0.037	0.172
	PEO-4	0.002	<b>0.087</b>	<b>0.413</b>
	MDAH-2774	0.101	<b>0.109</b>	<b>0.180</b>

Post-knockdown showed 13/16 chromosome positions of NM1 knockdown and 10/16 chromosome positions NM6 had CTs re-positioning in locations closer to that adopted by the control cell when compared to the pre-knockdown position (table 3.2). **Chromosome 17** of the NM6 knockdowns showed the least restored shifts overall (1/4) and **chromosome 1** of SKOV-3 stood no chance of restoration as its pre-knockdown state was already close to ideal with no significant difference to the control cell line. However, the heat map showed that each shell had an overall improvement (increase in red), more so in NM1 knockdown (figure 3.4). This led to questioning the extent of re-location causing these improvements. Table 3.3 shows a summary of *p*-value averages from the chromosome position of the same cell line after the knockdown against its own position pre-knockdown or 'knockdown gap'.

**Table 3. 3 Knockdown Gap: Magnitude of Change from Original Territory to Post Knockdown in OC cells**

After the siRNA knockdown of NM1 and NM6 for cell lines SKOV-3, PEO-1, PEO-4, and MDAH-2774, their new chromosome positions were compared to the previous positions statistically [p0.5]. The higher the *p*-value, the smaller the 'knockdown gap' and vice versa.  $P > 0.250$  was considered a small gap, and  $p < 0.250$  was considered a large gap—means of 50-100 nuclei.

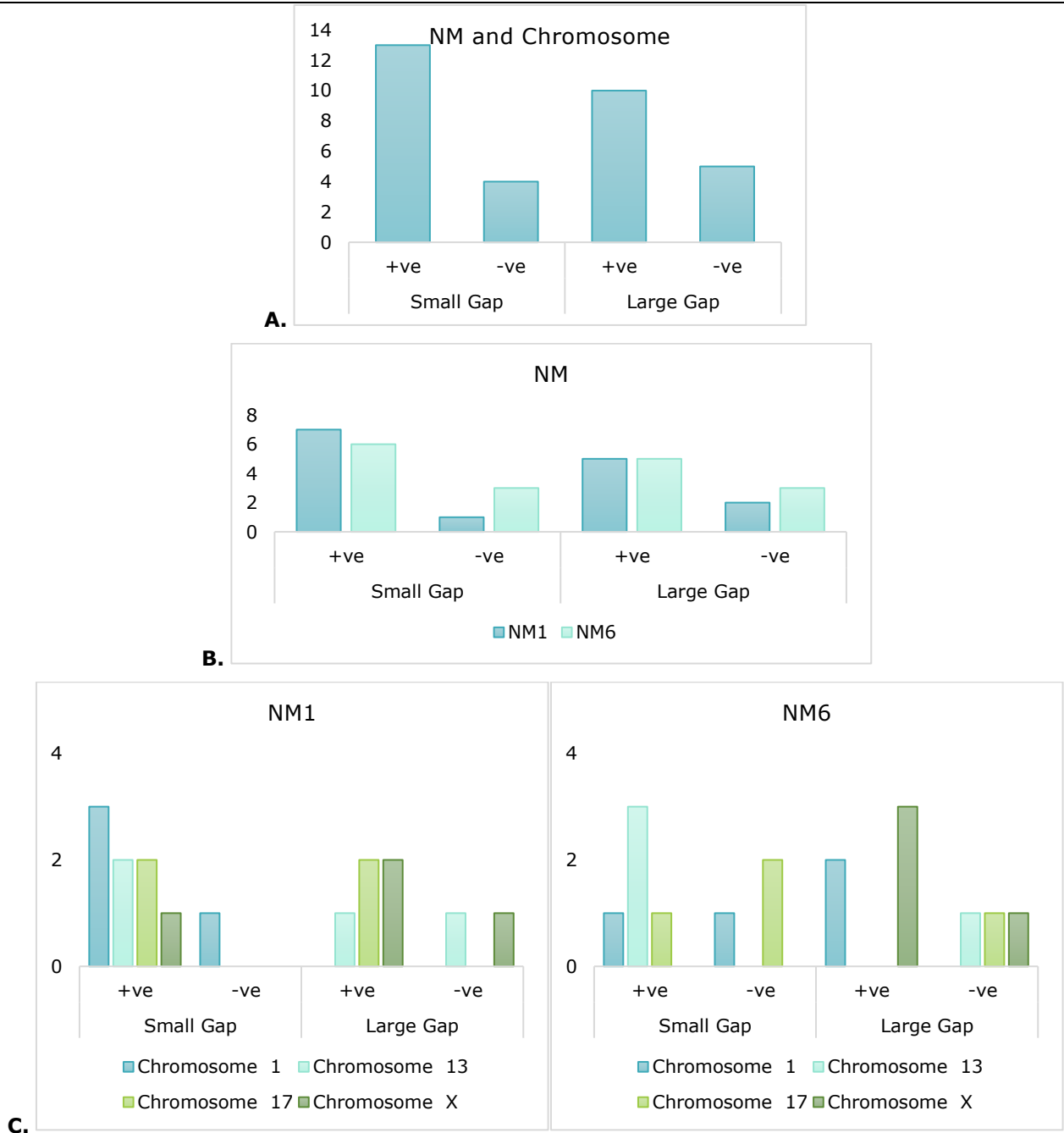
\*- small gap with positive change

\*\* - large gap with positive change

\*\*\*- small gap with negative change

\*\*\*\*- large gap with negative change

Chromosome	Cell Line	NM1 knockdown	NM6 knockdown
<b>1</b>	SKOV-3	<b>0.676***</b>	0.368***
	PEO-1	0.496*	0.152**
	PEO-4	0.348*	0.127**
	MDAH-2774	0.265*	0.408*
<b>13</b>	SKOV-3	0.271*	0.116****
	PEO-1	0.334*	0.489*
	PEO-4	0.129****	<b>0.734*</b>
	MDAH-2774	0.060**	0.294*
<b>17</b>	SKOV-3	0.240**	<b>0.600***</b>
	PEO-1*	<b>0.748*</b>	<b>0.528*</b>
	PEO-4	0.422*	0.484***
	MDAH-2774	0.190**	0.149****
<b>X</b>	SKOV-3	<b>0.601*</b>	0.099**
	PEO-1	0.038****	0.108****
	PEO-4	0.131**	0.225**
	MDAH-2774	0.171**	0.170**



-continued next page

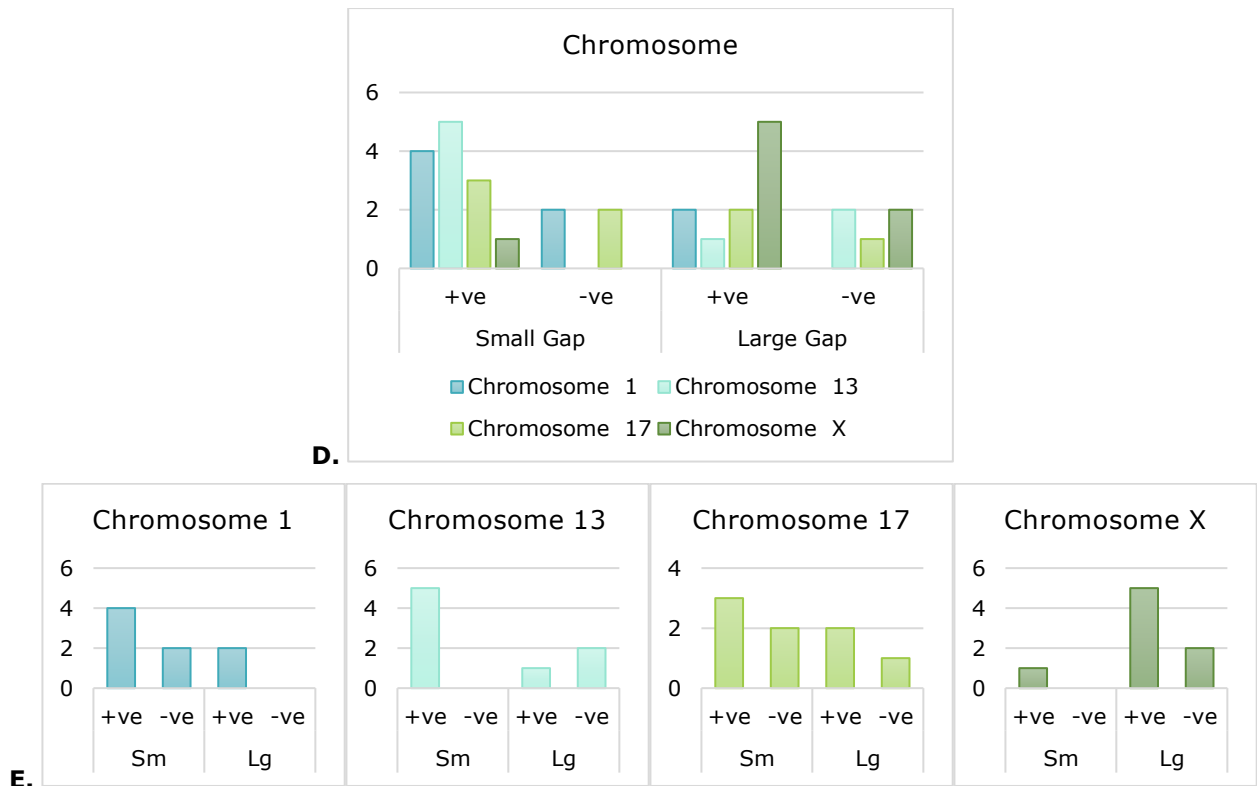


**Figure 3. 12 Knockdown Gap Influence:**

The knockdown gap (small or large) influence on the outcome of CTs re-positioning in locations closer to that adopted by the control cell, i.e., positive or negative. **A.** the overall influence of small and large gaps on positive and negative outcomes that were then **B.** categorised into NM and further **C.** divided into NM and chromosomes. **D.** categorised the influence according to overall chromosomes and **E.** showed the influence in individual chromosomes.

Overall, more positive relocalisations came from smaller gaps compared to larger gaps (figure 3.11A) which was also the same between NM1 and NM6 (figure 3.11B/C). The same trend was also observed was also observed amongst the chromosomes, except for chromosome X that had more large changes resulting in positive relocalisations (figure 3.11D/E). Chromosome 17 showed exhibited the four variations of influence, but the trend of positive relocalisations from smaller gaps remained the highest. In table 3.2, the *p*-values >0.5 that showed no significant difference to the control cell all originated from small gaps.

### 3.4 DISCUSSION

Spatial territories of chromosomes and genes have altered positions in many cancers (breast, cervical, colon, lymphocytes, and melanoma) that are orchestrated by many proteins, including a family of nuclear motor myosins and together with chapter 2 findings, warranted further investigation (Cremer *et al.*, 2003; Meaburn, 2016). Chapter 2 showed that key chromosomes of OC had altered spatial positioning in nuclei when compared to their healthy counterpart. Moreover, nuclear motor proteins NM1 and NM6 were elevated in all of 4 cancer cell lines investigated. This presents NM1 and NM6 as favourable targets to investigate changes in chromosome positions (1, 13, 17 and X) post knockdown. To determine if these motor proteins influence disease-associated spatial alterations, NM1 and NM6 were knocked down in the 4 OC cell lines, and their positions were mapped.

Both NM1 and NM6 are detected in the cytoplasm and appeared to be constitutive due to the plethora of roles they encompass (Vreugde *et al.*, 2006; Venit *et al.*, 2016). For this reason, it was not favourable to completely rid the cells of proteins that otherwise have crucial roles at normal levels. It was also impossible to completely knock down NM1 and NM6 without harming the cells. A high concentration of reagents and high knockdown efficiency led to nuclear and cellular membranes with serrated edges. By changing the method to 'reverse transfection' where the cells are treated at the time of seeding and post -48 hrs, instead of just post-24 and -48 hrs, the reagent concentration was lowered from 50-100nM to 10-15nM for an aim of 50% knockdown efficiency.

### **3.4.1 Disruption of the tumorigenic superfamily stoichiometry of NM1/NM6**

The WBs of SKOV-3, PEO-1 and MDAH-2774 showed knockdowns of efficiency of 62%, 57% and 74% for NM1 and 67%, 65% and 73% for NM6, respectively. [was not able to perform the WB for PEO-4 due to SARS-CoV-2]. The IF of SKOV-3, PEO-1, PEO-4 and MDAH-2774 estimated knockdowns efficiency of 57%, 48%, 47% and 70% for NM1 and 46%, 55%, 32% and 71% for NM6 respectively. Through the correlation of the WB quantification and the Indirect IF scoring, an estimation (subjective) of PEO-4 knockdown was made.

The average knockdown effect of NM1 (64%) was relatively similar to that of NM6 (68%); and while the CTs did not show large re-positionings in some cases, NM1 knockdown led to a higher number of CTs adopting positions closer to that of the control cells, when compared to NM6 knockdown (table [3.2](#)). In chapter 2, NM6 was higher than NM1 in the control cell and chemoresistant tumour cell, however the opposite way around for all other tumour cell lines. Perhaps knocking down NM1 shifted to a healthy NM1/NM6 stoichiometry, and NM6 knockdown resulted in chaotic of the stoichiometry, also hinting that stoichiometry is just as or maybe more critical than having elevated levels; not only did it combatted high levels of the protein but also restored some balance between itself and NM6 (figure [3.6](#)).

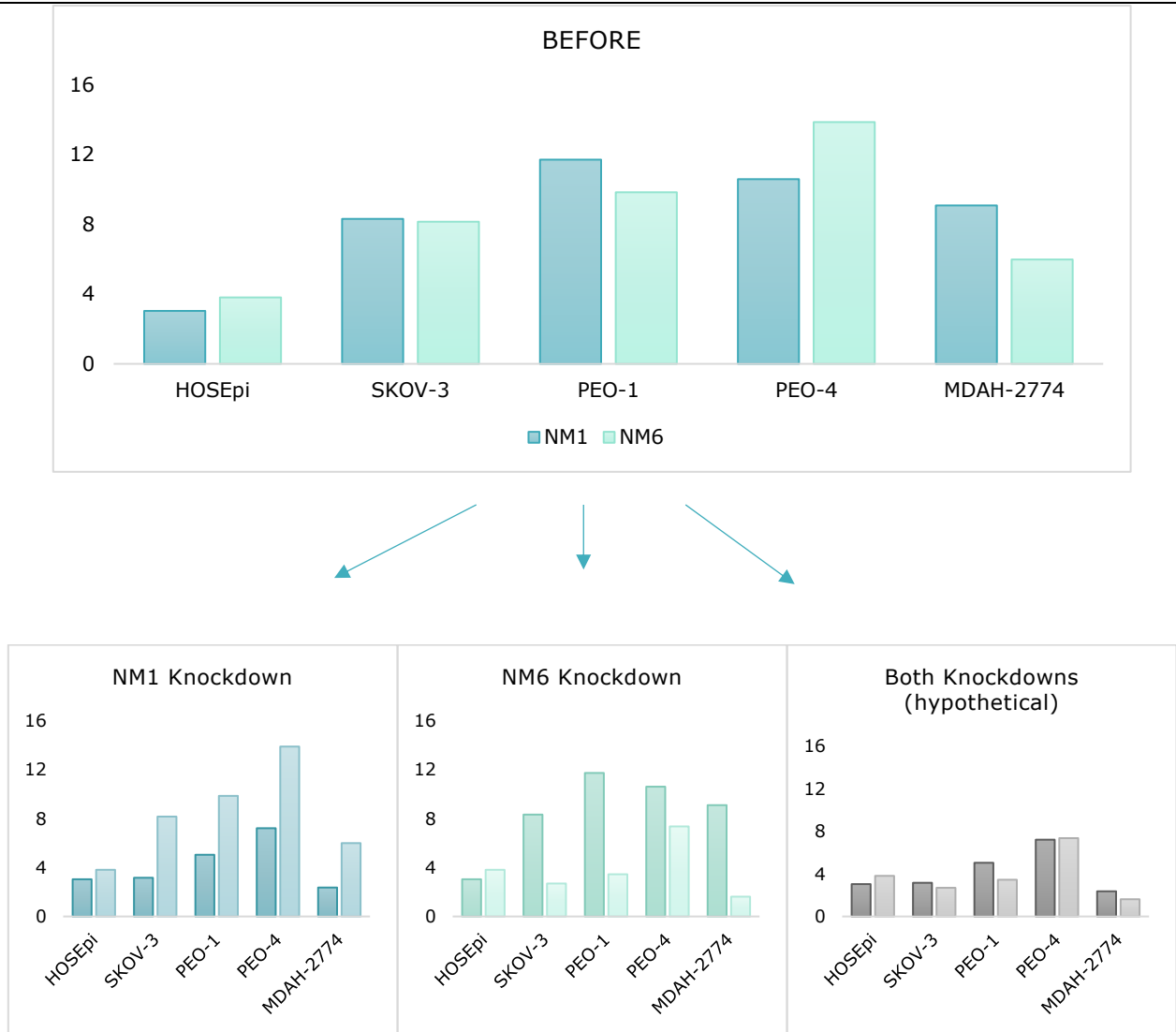


**Figure 3. 13 NM1 and NM6 Levels Before and After Knockdown:**

The before figure (extracted from figure 2.9) was amended using the per cent knockdown (extracted from figure 3.2, 3.3, 3.5 and 3.6) to depict what the post-knockdown levels of NM1/NM6 would look.



### 3.4.2 One size does not fit all

In the tumour cells, both knockdowns resulted in **CTs re-positioning in locations closer to that adopted by the control cells** as the new chromosome positions had lower statistical differences to the control cell in 13/16 and 10/16 instances for NM1 and NM6 respectively (table [3.2](#)).

Even though more positive adoption of CT location came from smaller gaps post-knockdown, compared to larger gaps (figure [3.11A](#)), one must consider the severity of the initial mispositioning and question the repositioning on large gaps, is it too much? For instance, chromosome 13 and 17 that was grossly altered initially would require a larger knockdown gap to reach a healthy position, and chromosome 1 would not require as much. The data shows that different chromosomes require different degrees of re-location to be beneficial as one size does not fit all, however, while some chromosomes require large-scale re-location, others revealed that too much might not be beneficial.

Intriguingly, **chromosome X** showed re-location from the periphery to intermediate or interior positions (figure [3.9](#) and [3.10](#)) leading to the hypothesis that NM knockdowns may have altered the stoichiometry, in turn, dysregulating the mechanotransduction signals amongst other associated structural proteins such as lamins. Together with LADs, this may result in the attachment of gene-poor areas of the essential chromosomes, thus displacing chromosome X. This type of chromosome X misplacement was also observed in atypical HGPS (expresses Lamin A, not progerin) cell line upon telomere elongation (immortalisation) by human telomerase reverse transcriptase (hTERT) (Bikkul *et al.*, 2019).

Assessing the **therapeutic value** of chromosome re-location via NM1/6 knockdown could possibly mean that patients with chromosome 1 and 13-associated TSGs and oncogenes will benefit from NM1 knockdown therapy and patients with chromosome 17-associated TSGs and oncogenes will benefit from either NM1 or NM6 knockdown therapy. A broad-range attempt that affects all myosins by blocking its ATP/GTP-derived energy source using enzymes ouabain (ATP inhibitor) and AG10

(GTP inhibitor) can be considered, as it also found overexpressed in the cytoplasm (Mehta *et al.*, 2010). However, ATP/GTP of healthy tissue becomes vulnerable and despite the overexpression of numerous NMs including NM2, NM5 $\alpha/\beta$ , NM9, NM10 in ovarian and other cancers, some NMs such as NM18 $\beta$  is found under-expressed in OC, and due to the relative specificity of RNAi, a siRNA pool of only overexpressed NMs for the requirement of particular cancers would be a more favourable clinical approach (Yanaihara *et al.*, 2004).

### **3.4.3 Conclusion**

The complex nature of the myosin superfamily provides a multifaceted target in drug discovery. Complementary and compensatory associations have been proposed as they both interact with RNA Pol II, and both possess motor functions. The forward moving NM1 has its own unique association with RNA Pol I while NM6 that moves backwards with anchorage properties gives no lesser superiority to either. However, it appears that NM1 levels are problematic in cancer cells as it may offset its stoichiometry with NM6, and considering the plethora of NM6 roles, more work needs to be done. Interestingly, the platinum-resistant cell retained the healthy stoichiometry of NM1/NM6 while also both being elevated. This warrants further investigation to assess its inclusivity to NM1 and NM6 therapy. Would a perturbation of this balance re-sensitise resistant cells, providing a rationale for NM1/NM6 knockdown in combating drug resistance?

## CHAPTER 4

# UNDERSTANDING CHEMORESISTANCE AND RE-SENSITISATION IN OC

### 4.1 INTRODUCTION

OC can be effectively treated with chemotherapy where taxols (e.g. paclitaxel) and platinols (e.g. cisplatin) are the chosen first-line drugs; however, due to the high toxicity and allergenic nature of taxols, patients are started and often limited to platinum-based drugs (Lheureux, Braunstein and Oza, 2019). Platinum-based drugs are highly effective in the first cycle, but with an intricate disease like OC with platinum resistance relapses, the patient is further rendered unsuitable for chemotherapy (Lheureux, Braunstein and Oza, 2019). Even though a patient might be able to tolerate taxols (with or without steroids), reoccurrence and resistance still occur as 75% of Taxol recipients eventually relapse after 18 months (Sherman-Baust *et al.*, 2011; Siegal *et al.*, 2011). Patients continue to go through the list of drugs until they are halted by multi-drug resistance (MDR). Wiech *et al.*, 2009 stated that transcription levels are altered with chromosome positioning, in which Meaburn and Misteli, 2008, added that it does not affect transcription levels in early disease states and therefore, it may be of more benefit to start from the advance states such as chemoresistance and work backwards.

### 4.1.1 Modelling a Lab-Grade Platinum-Resistant Cell Line

Development of drug-resistant cell lines *in-vitro* has always been of interest to scientists to study this poorly understood phenomenon. The first resistant cell line to be produced was in 1970 on Chinese hamster cells; before that, *in-vivo* models were used in the 1950s and 1960s (Biedler and Riehm, 1970). Developing such cell lines usually takes 3 to 18 months, and the method can vary between continuous and pulse treatments or a mixture of drugs (Penner-Goeke *et al.*, 2017). Pulse treatment of drugs (low doses below  $IC_{50}$  with recovery time) best mimics the clinical cycles a patient receives, however, the cell lines derived have low and unstable resistance with changes too subtle to detect and analyse (reviewed in Penner-Goeke *et al.*, 2017). Despite having lower clinical relevance, continuous treatments (high doses at  $IC_{50}$  or above then escalated with time) produces stable high-level resistant lines that are easier to maintain and molecular changes are more significant making them easier to study. This study will use a hybrid of both methods by treating the cells with its long-term  $IC_{50}$  once a week for 24 hrs, then 144 hrs recovery time, increasing the dose when doubling time returns, all within a duration of 3 months, in which Penner-Goeke *et al.*, 2017 also found as sufficient time for resistance acquisition in eOC cell lines from patients. This ensured a robust, resistant line in the shortest time possible.

Cell line groups such as PEO-1 (platinum-sensitive) / PEO-4 (platinum-resistant) are widely used for platinum-resistant research as they were derived from the same patient displaying common marker chromosomes (table [2.2](#)). However, PEO-4 shows a re-appearance of chromosome 8 and 17 that were missing in PEO-1 that instead suggests a clonal origin and then a divergence into a heterogeneous population (Langdon *et al.*, 1988; Wolf *et al.*, 1987). The best cell lines for comparative studies start with parental cell lines with no previous treatment or low  $IC_{50}$  values (Beaufort *et al.*, 2014). For this study, we employed the naïve cell line MDAH-2774 and created a new cisplatin-resistant line, MDAH-2774<sub>CR</sub>.

### 4.1.2 Understanding Drug Resistance by Spatial Chromosome Organisation

A disease with multiple re-occurrences, each accompanied by increasing resistance to chemotherapy, needs just as much attention as the sensitive form of the disease, as it cannot be treated the same. Drug metabolism, membrane transporters, modification in drug targets, cell cycle pathways, RNA transcription, epigenetics, oxidative stress, and oncogenes have all been linked to platinum drug resistance of OC (reviewed in Norouzi-Barough *et al.*, 2017; section [1.1.7](#)). All these factors are associated with either overexpression or mutations in genes, both poorly understood in OC and, due to the complexity of interactions, pinpointing one pathway may be unsuccessful. However, by broadening the scope and studying spatial genome organisation in drug-resistant cell lines, more can be understood while new targets or therapy could be discovered. To date, no prior literature addressing spatial genome organisation in chemoresistance, far less in OC can be found; however, Penner-Goeke *et al.*, 2017 found that well-studied carcinogenesis-associated chromosome instability (CIN) continues onto the chemoresistant and re-occurrent disease stages in OC cells.

### 4.1.3 Re-sensitisation using siRNA

Sun *et al.*, 2011 outlined the benefits of lower toxic doses as siRNA of polo-like kinase 1 (*Plk1*), and paclitaxel resulted in a synergistic tumour suppression in MDA-MB-435s inoculate in murine models resulting in requiring 1000-fold less paclitaxel compared to its monotherapy. In sensitive OC, Xue *et al.*, 2019 showed synergistic outcomes in SKOV-3 inoculated into nude mice with siRNA of ribonucleotide reductase M2 (*RRM2*), resulting in reduced tumour volume, as well as an increased growth inhibition rate, from 36% in siRNA only and 41% in cisplatin only, to 64% in siRNA combined with cisplatin group. Also seen in drug-resistant OC, Yang *et al.*, 2015 reported synergistic effects in OVCAR8TR (paclitaxel-resistant) and mice with siRNA of Multi-Drug Resistance Gene 1 (*MDR1*).

siRNA has been invaluable in discovering new drug targets, and in addition to its stand-alone effects, its synergistic effects have benefited disease response to drugs. siRNA treatment strategies fall into

two categories; discrimination against tumour growth (and angiogenesis) and drug-resistance (and cell survival) (van den Brand *et al.*, 2018). Chapter 2 and 3 used FISH and siRNA to understand tumour growth from the perspective of spatial chromosomal organisation, where this chapter builds on that to investigate drug-resistance.

#### **4.1.4 Outlook**

Dismantling the stability of chemoresistance cells through siRNA re-sensitisation provides a suitable and potential target in drug treatment and resistance, leading to lower drug doses and delayed drug resistance. This chapter aims to investigate the spatial territories of chromosomes 1, 13, 17 and X in addition to the protein level ratio of NM1/NM6 in a lab-created platinum-resistant cell line. This attempts to challenge the findings of chapter 2; where all the cancer cells had both NM1 and NM6 elevated levels, NM1 being higher; and on the other hand, the platinum-resistant cell line PEO-4 had NM6 higher a ratio also reflected by the control cell line (figure [2.9](#)). Chapter 3 demonstrated spatial chromosome re-positionings post-NM1 and -NM6 knockdown in PEO-4, that was ideal in some cases; however, this chapter explores combination treatments of siRNA and cisplatin through survival assays since NM1/NM6 knockdowns may be a better candidate in re-sensitisation over therapy.

## 4.2 METHODS

### 4.2.1 Sulforhodamine B (SRB) Calibration for use in Cytotoxicity Assays

In 96-well plates, 50% serial dilutions of  $1 \times 10^4$  cells (SKOV-3, PEO-4, PEO-1 and MDAH-2774) were grown. After 48 hrs, in one plate, the cells were fixed by adding 25 $\mu$ L of cold 50% TCA directly to the media (100 $\mu$ L) and incubated for an hour on ice. The TCA was gently removed, and the plates were gently washed by submersion into water 4 times then air-dried at room temperature. Once dried, 50 $\mu$ L of 0.04% SRB solution was added to each well and incubated for 1hr. This was then gently tapped out and rinsed by submersion in 1% acetic acid 4 times then air-dried at room temperature. Once ready to be analysed 100 $\mu$ L of 10mM TRIS base (pH10.5) was added to each well, and the plate was shaken on an orbital shaker for at least 10 mins, then analysed at 510nm using the CLARIOStar plate reader. The cells in the second plate were used to count cell numbers using the Countess (ThermoFisher); trypsinised cell suspension (50 $\mu$ L) was neutralised with 2% Trypan Blue media (50 $\mu$ L). The results of both methods were combined to create a calibration curve so that cell proliferation could be determined by the SRB assay onwards. Its linearity exceeds the likes of the Lowry and Bradford assays, and with the MTT assay, it is also faster, simpler and more sensitive, which provides several advantages for large-scale screening (NCI; Skehan *et al.* 1990).

### **4.2.2 50% Growth Inhibitory Concentration (IC<sub>50</sub>) Assay**

PEO-1, PEO-4 and MDAH-2774 ( $1.0 \times 10^3$  to  $1.0 \times 10^4$ ) were seeded in 96-well plates and assayed 120 hrs later to choose an appropriate cell density (near confluency) for drug treatment as shown in figure 4.2. From this, the ideal seeding density for 96-well plates was determined to be  $1.0 \times 10^4$  cells for PEO-4 and MDAH-2774<sub>CR</sub> and  $8.0 \times 10^3$  cells for PEO-1 and MDAH-2774. 5mM stocks of Cisplatin (Abcam/ab141398) were made using 0.09% NaCl and working concentrations were made before use by dissolving in complete RPMI media. The 50% Growth Inhibitory Concentration (IC<sub>50</sub>) values for MDAH-2774 and PEO-1 were determined. The cells were plated, and after 24 hrs, plates were treated with varying drug concentrations (20 $\mu$ M, 15 $\mu$ M, 10 $\mu$ M, 5 $\mu$ M, 2 $\mu$ M and 1 $\mu$ M). The media was refreshed with drug-free media, and after another 24 hrs and 72 hrs, they were fixed for the SRB assay.

### **4.2.3 Chemoresistance induction**

The naïve cell line MDAH-2774 was treated once a week for 24 hrs with the 96hr IC<sub>50</sub> cisplatin dose (1 $\mu$ M) for seven weeks and the last six weeks treated with 2 $\mu$ M, for a total of 3 months (Penner-Goeke *et al.*, 2017). Thus, cells for FISH, IF and WB were harvested on week 12.

### **4.2.4 Cytotoxic Assay**

Cells were plated in 96-well plates using the ideal cell density and treated with siRNA via the reverse transfection method (as described in section 3.2.1). After 48 hrs they were re-treated with siRNA. After another 24 hrs, the media was refreshed and selected wells treated with 1 $\mu$ M cisplatin (determined from the IC<sub>50</sub> assay). The media was refreshed in all wells after a further 24 hrs. After the final 24 hrs (120 hrs in total), the cells were fixed for the SRB assay.



**4.2.5 Cell Culture – refer to section 2.2.1**

**4.2.6 FISH – refer to section 2.2.2**

Combinations containing post knockdown cells were left in the hypotonic solution for 15-20 mins instead of 10 mins since the cytoplasm became challenging to remove (refer to section 3.2.3).

**4.2.7 Indirect IF – refer to section 2.2.3**

**4.2.8 WB – refer to section 2.2.4**

**4.2.9 RNAi – refer to section 3.2.1**

## 4.3 RESULTS

Data presented in chapter 2 demonstrated both NM1 and NM6 protein elevation in all the cancer cells where NM1 was higher than NM6, however, the platinum-resistant cell-line PEO-4 and the control cell line had higher NM6 levels instead than NM1. This delicate balance prompted the investigation into OC chemoresistance. Due to the divergence in using PEO-1/PEO-4 for chemosensitive studies, the chemo-naïve cell line MDAH-2774 was used to create a novel chemoresistance cell line for an absolute baseline of, before and after, within the same lineage.

### **4.3.1 Creation of a Platinum-Resistant MDAH-2774, MDAH-2774<sub>CR</sub>:**

Firstly, a long-term IC<sub>50</sub> had to be determined so that the naïve cell-line could be treated with cisplatin in 12 weeks while remaining sufficiently viable. Several assays had to be done to determine the cell survival in large cohorts, and so SRB assays were performed. Basically, at the time of analysis, the floating (dead) cells were removed, the live adherent cells were fixed, dyed and washed to exclude excess dye and the protein-bound dye was re-solubilised in 100µL of 10mM TRIS base, pH10.5 and read at 510 nm (ideal for SRB). The absorbance increases linearly with cell numbers (figure [4.1](#)).

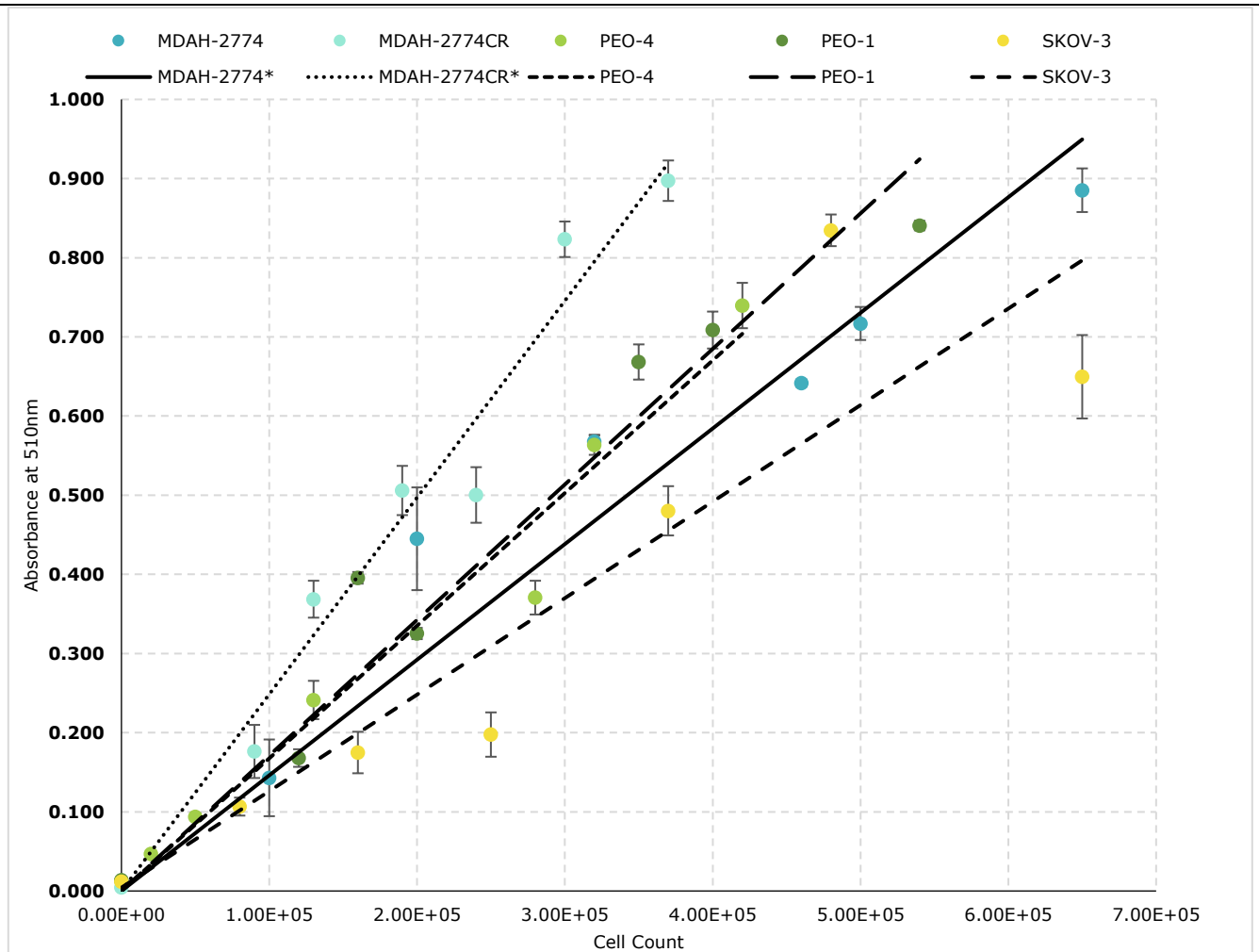


**Figure 4. 1 SRB Calibration:**

The linear correlation with SRB dye and cell density for cell line MDAH2774, MDAH-2774<sub>CR</sub>, PEO-4, PEO-1 and SKOV-3. After 48 hrs of growth, varying plate densities were subjected to spectrophotometric analysis post-SRB staining and correlated with duplicates quantified by the countess. The absorbencies were normalised, and the intercept was set at zero, the gradient (MDAH-2774 =  $1.45 \times 10^6$ , MDAH-2774<sub>CR</sub> =  $2.49 \times 10^6$ , PEO-4 =  $1.71 \times 10^6$ , PEO-1 =  $1.72 \times 10^6$  and SKOV-3 =  $1.24 \times 10^6$ ) can be used to convert absorbencies to cell numbers. This index also illustrates the relative protein content of the cell, where SKOV-3 contains the least, PEO-1 and PEO-4 are similar and MDAH-2774 has an increase as it gains resistance. The data represent normalised means (n=3).

The survival assays and combination treatment experiments were set-up to take place within a 6-day (120 hrs) block, and un-treated control cells had to be able to grow to that time frame healthily. The cell lines to be experimented on were plated at different densities, and the seeding density that resulted in maximum growth before the curve plateaued at day 6 was selected as the density to seed upcoming experiments. Fast-growing cell lines MDAH-2774 and PEO-1 were plated at  $8 \times 10^3$ ,

and slower-growing PEO-4 and MDAH-2774<sub>CR</sub> were plated at  $1 \times 10^4$  in 96-well plates. MDAH-2774<sub>CR</sub> data was included from work post-IC<sub>50</sub> experiments.

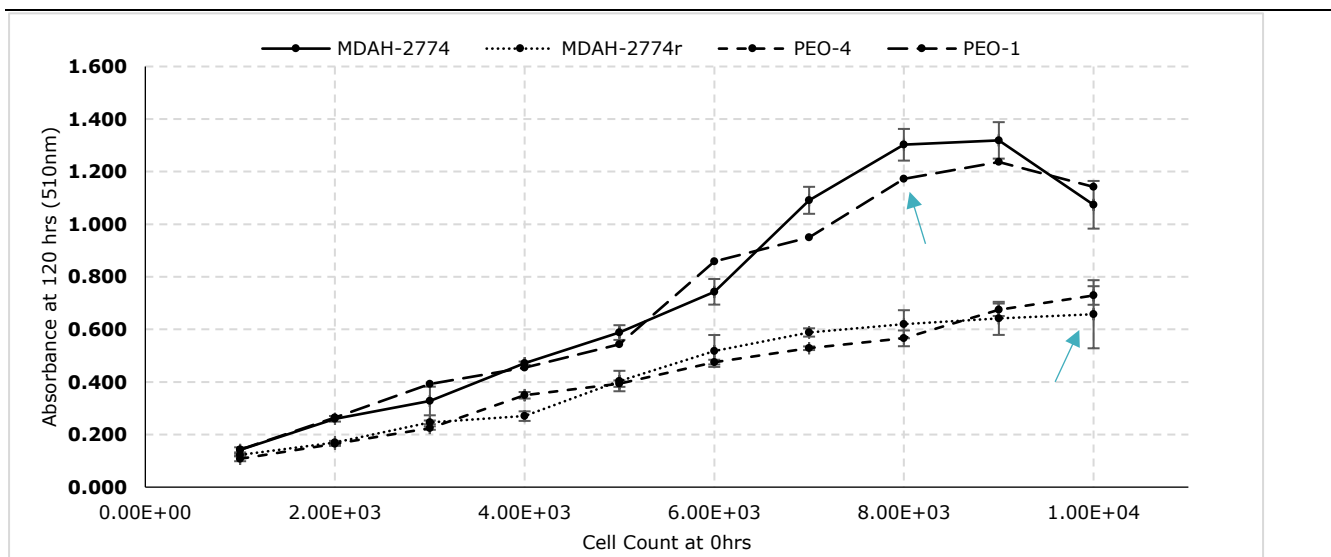


**Figure 4. 2 Seeding Density Determination for Cytotoxic Assay:**

Cell growth after 120 hrs to determine near confluence for cell lines MDAH2774, MDAH-2774<sub>CR</sub>, PEO-4, and PEO-1. Varying cell densities between  $1 \times 10^3$  to  $1 \times 10^4$  were plated, and after 120 hrs of growth, the cells were subjected to spectrophotometric analysis post-SRB staining to determine the lowest plating density near full confluence (before plateau). The arrows indicate MDAH-2774 and PEO-1 at  $8.0 \times 10^3$  and MDAH-2774<sub>CR</sub> and PEO-4 at  $1.0 \times 10^4$ . The data represent normalised means ( $n=4$ )

From this,  $8 \times 10^3$  MDAH-2774 and PEO-1 cells were seeded (0 hrs) and after 24 hrs treated with different concentrations of cisplatin for another 24 hrs at which point the media was refreshed with drug-free media. The absorbance was taken at 72 hrs and 120 hrs (6 days). The absorbance that reflected 50% survival was used as the IC<sub>50</sub>. At 48 hrs the IC<sub>50</sub> of MDAH-2774 and PEO-1 was  $5 \mu\text{M}$  which was almost halved for the long-term IC<sub>50</sub> at  $1 \mu\text{M}$  and  $2 \mu\text{M}$  for MDAH-2774 and PEO-1 respectively.

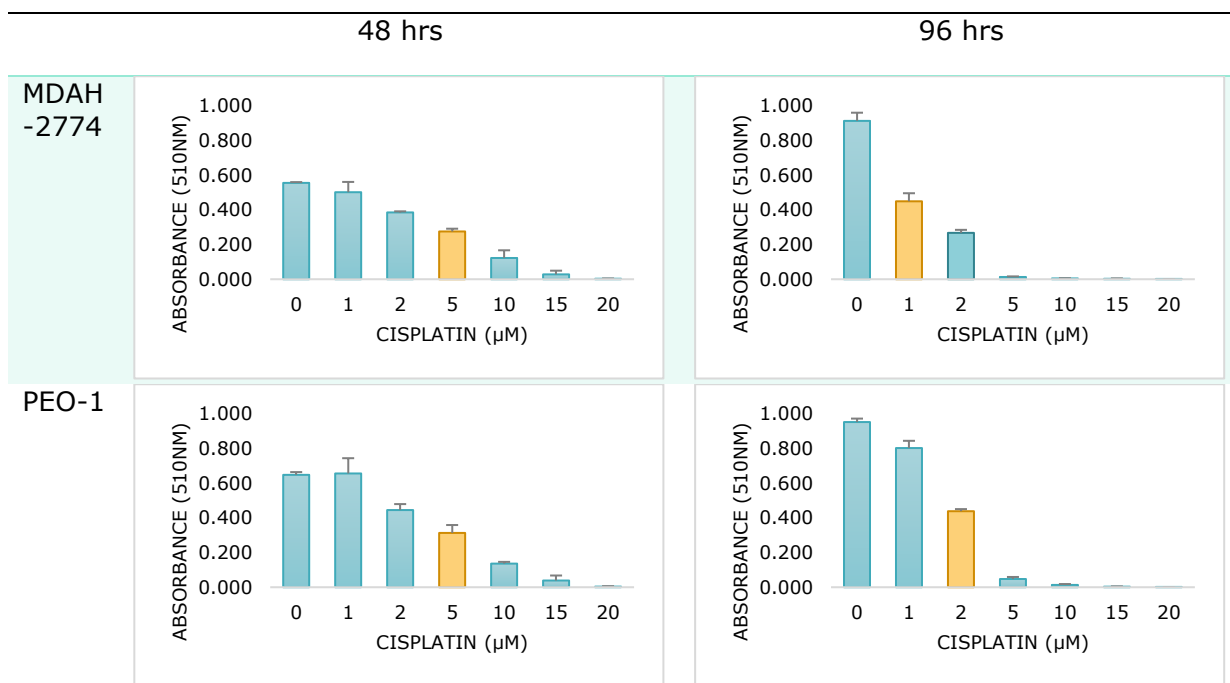


**Figure 4. 3 IC<sub>50</sub> for MDAH-2774 and PEO-1:**

Spectral analysis post-SRB staining for cell line MDAH2774 and PEO-1 after treating with varying cisplatin concentrations (1μM, 2μM, 5μM, 10μM, 15μM and 20μM), incubated for 24 hrs, refreshed and after 24 hrs and 72 hrs, then subjected to spectral analysis post-SRB staining to determine the IC<sub>50</sub> (concentration at approximately 50% survival). The yellow bar represents the approximate IC<sub>50</sub> which decreases (MDAH-2774: 5μM to 1μM and PEO-1 5μM to 2μM) the longer the culture it is treated (48 hrs vs 96 hrs respectively). The data represents normalised means (n=3).

Using the long-term IC<sub>50</sub>, for seven weeks, once a week, MDAH-2774 was treated with 1μM cisplatin for 24 hrs. In the last six weeks, this was increased to 2μM. They were passaged twice a week as usual, and in the last month, they were passaged once a week. At the end of 12 weeks, they were now recognised as MDAH-2774<sub>CR</sub>. MDAH-2774<sub>CR</sub> was subjected to SRB calibration and plating density experiments (included in figure 4.1 and 4.2)

### 4.3.2 NMI and NM6 Distribution and Quantity of newly created Platinum-Resistant MDAH-2774CR:

Before starting combination treatments with cisplatin and siRNA, NM1 and NM6 distribution (dispersed foci, aggregate foci, dispersed and aggregate foci and negative; see figure 2.5 for representative images) and protein levels of MDAH-2774<sub>CR</sub> were analysed using IF and WB respectively (figure 4.4/4.5 and 4.6/4.7).

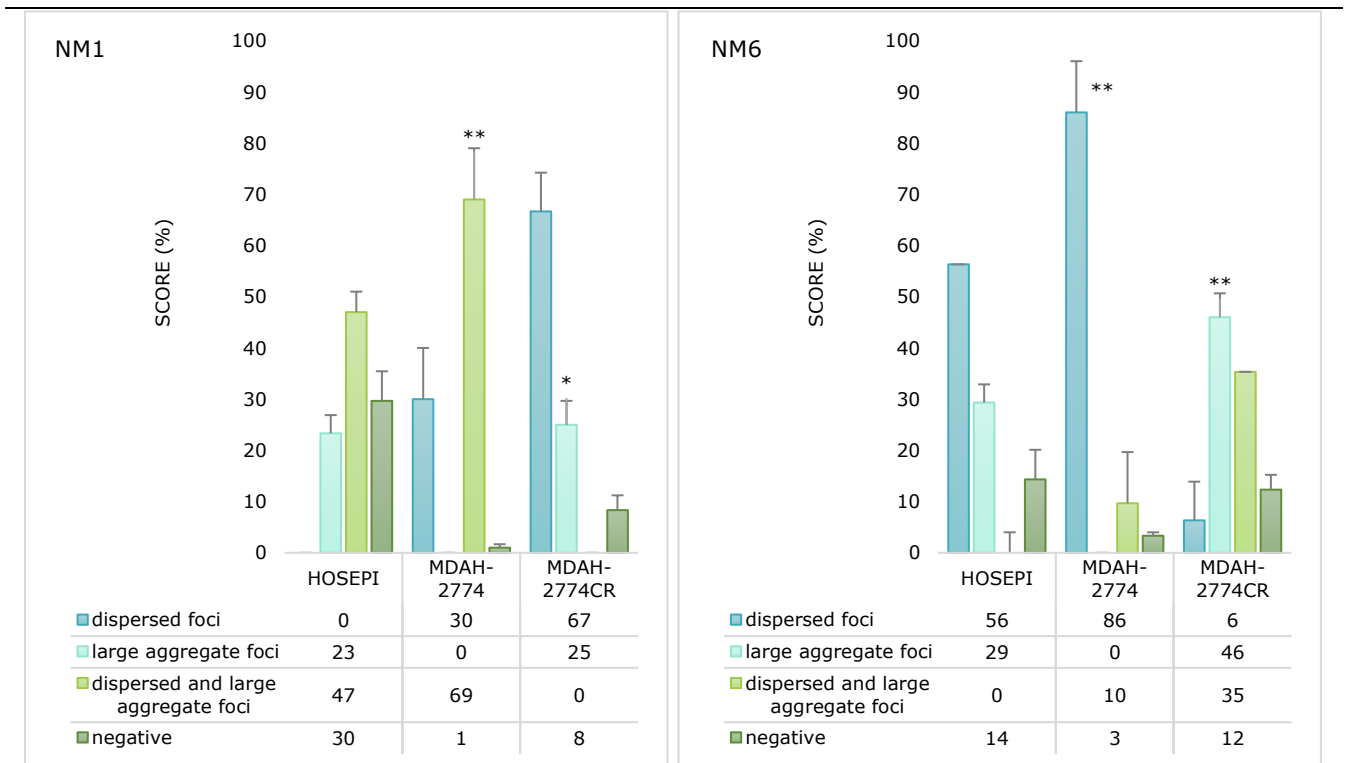


**Figure 4. 4 NM1 and NM6 Distribution Patterns Score:**

Bar graphs show the score of 4 NM1 patterns (dispersed foci, aggregate foci, dispersed and aggregate foci and negative) in cell lines MDAH-2774 and MDAH-2774<sub>CR</sub>. The bars and error bars for each cell line (X-axis) represents means of 3 replicate slides and SEM for a total of 200 nuclei as a percentage (% / Y-axis). Student's *t*-test of the cancer cells NM1 and NM6 patterns was performed against the wild-type (control HOSEpi) *p*-values: 0.026\*\* and 0.010\*\* for MDAH-2774 and 0.125\* and 0.032\*\* MDAH-277<sub>CR</sub> respectively.

\* - denotes statistically different by one confidence interval (0.5) and \*\* - denotes statistically different by two confidence intervals (0.05 and 0.5).

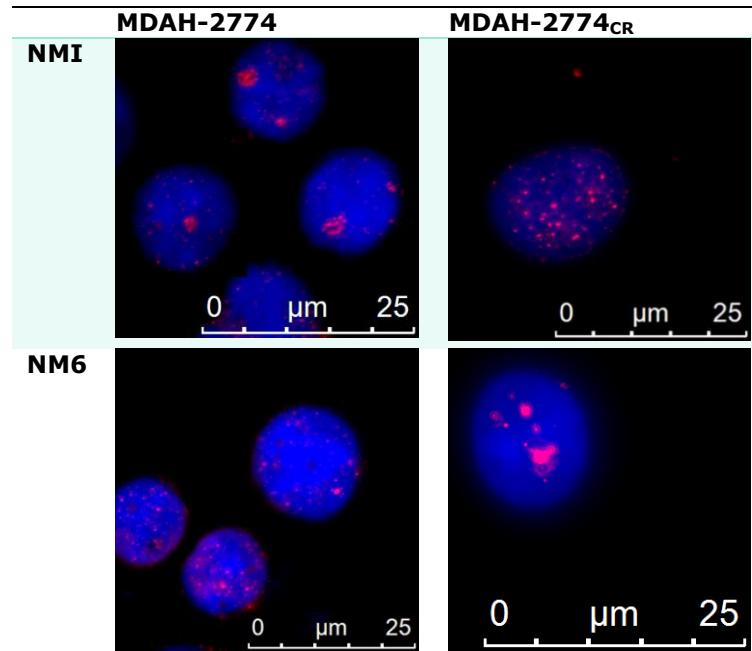


**Figure 4. 5 NM1 and NM6 Distribution Patterns Images:**

Representative images of the nuclear most prevalent distribution pattern captured in cell lines MDAH-2774 and MDAH-2774<sub>CR</sub>. DNA was stained using DAPI (blue), and the NM1/NM6 protein was revealed by Indirect IF with a Cy3 conjugated secondary antibody. Magnification x400 / x1000. Scale bars represent 25µm.

IF revealed the platinum-resistant cell MDAH-2774<sub>CR</sub> had a unique distribution that displayed features of both its sensitive counterpart MDAH-2774 and the control cell line. Figure 4.4 shows the re-emergence of NM1 and NM6 (both large-aggregate foci) patterns in the resistant cell that was absent in the tumour cell and present in the control cell. Additionally, the modal pattern of NM1 (dispersed and aggregate) and NM6 (dispersed) in the control cell elevated in the tumour cell but then declined as it acquired resistance to the point where dispersed and aggregate patterns of NM1 were absent in the platinum-resistant cell. Lastly, NM1 (dispersed) and NM6 (dispersed and aggregate) patterns that were absent in the control cells, were present in the tumour cell and amplified further in the platinum-resistant cell. Interestingly, the increase in negative cells was not expected as there were protein elevations in the platinum-resistant line as the tumour line (figure 4.6 and 4.7).

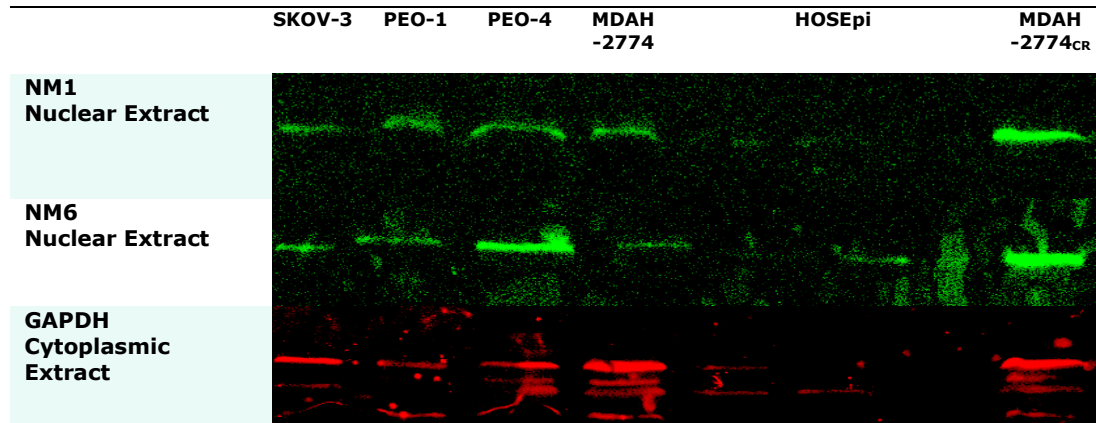


**Figure 4. 6 NM1 and NM6 Levels:**

Cytoplasmic and Nuclear extracts of cell line MDAH-2774 (lane 4) and MDAH-2774<sub>CR</sub> (lane 8) were quantified by WB on the Li-Cor Odyssey for NM1 and NM6 using ImageJ software (Version 1.53a), the band intensities were calculated. The quantities were normalised against GAPDH levels (first band) in the corresponding cytoplasmic extracts. Lane 5, 6 and 7 are the control HOSEpi.

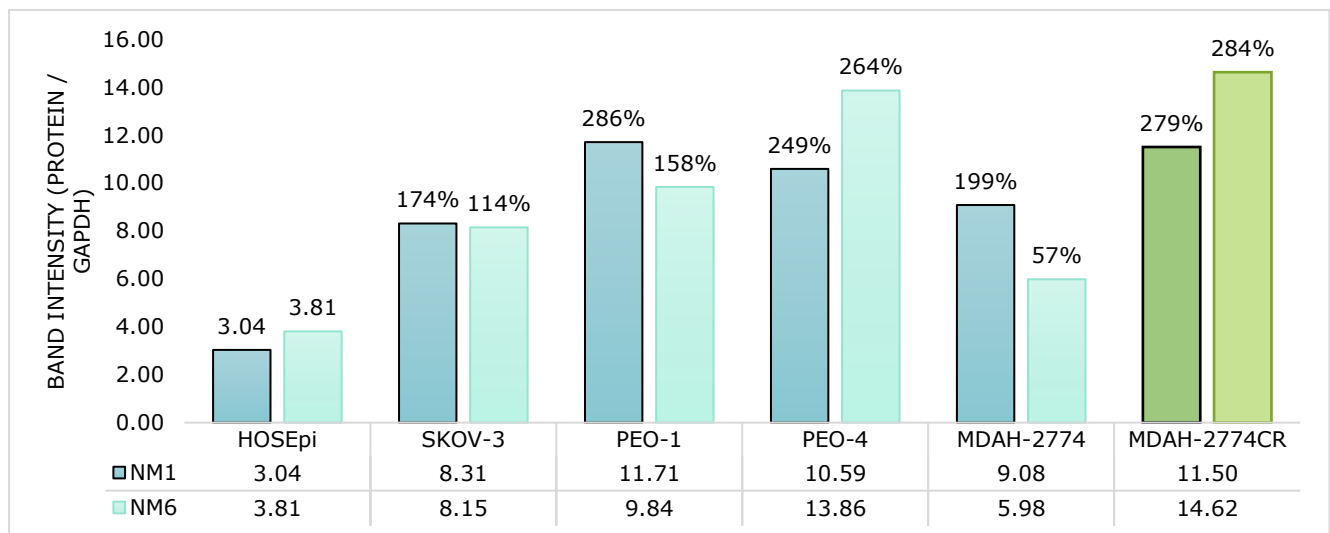


**Figure 4. 7 NM1 and NM6 Band Intensities:**

The fluorescence Li-Cor image of the membrane was uploaded to ImageJ software (Version 1.53a) to calculate the band intensities. The bars represent protein signal intensity / corresponding GAPDH signal intensity = X-axis. Above each cancer cell bar is the % increase; SKOV-3 (174%,114%), PEO-1 (286%,158%), PEO-4 (149%,264%), MDAH-2774 (199%,57%) and MDAH-2774<sub>CR</sub> (279%, 284%) when compared to the healthy levels of the HOSEpi cell.

NM1/NM6 protein levels for MDAH-2774<sub>CR</sub> conformed to the findings of chapter 2 as it not only showed an elevation of the proteins when compared to both the control cell and its originator cell,



MDAH-2774, but also that NM6 was higher than NM1 in HOSEpi, PEO-4 and MDAH-2774<sub>CR</sub>.

### 4.3.3 Investigating Re-Sensitisation of MDAH-2774<sub>CR</sub> through Combination Treatments of siRNA and Cisplatin:

To investigate the potential synergy of siRNA and traditional chemotherapy combined to combat unresponsiveness to drugs by resistant forms of diseases, siRNA of NM1 and NM6 was used to reduce their levels in the resistant cell lines followed by treatment with cisplatin and then they were assayed for cell survival. The knockdown efficiency was 39% and 38% for NM1 and NM6 respectively by estimating by scoring the positive and negative cells from IF (see figure 3.7 for positive and negatively stained representative images). [Figure 4.10/4.11 could not be completed due to SARS-CoV-2]

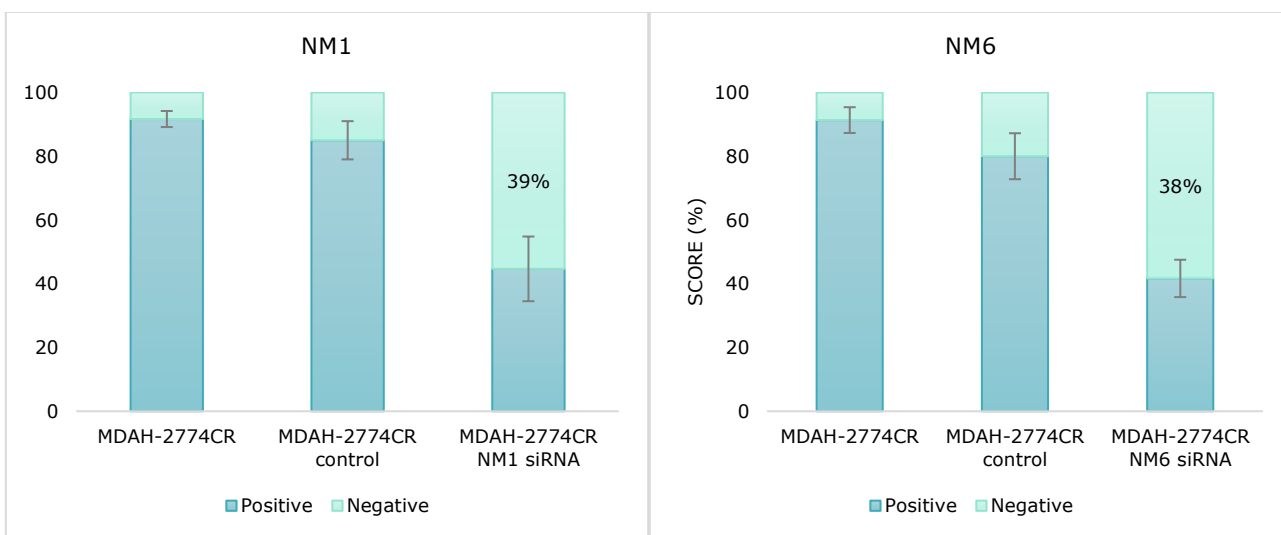


**Figure 4. 8 MDAH-2774<sub>CR</sub> NM1 and NM6 levels:**

Pre- and post-siRNA knockdown of NM1 and NM6 as estimated by Indirect IF. The bars and error bars for each cell line (X-axis) represent means and standard error of the mean for a total of 200 nuclei as a percentage (% / Y-axis) of positive and negative stained cells before and after NM1/NM6 knockdown (ON-TARGETplus Human MYO1b and MYO6 siRNA – SMARTpool). MDAH-2774<sub>CR</sub> NM1 and NM6 were reduced to **61%** and **62%** of the original amount, respectively, that was normalised against the control (ON-TARGETplus Non-targeting Control Pool) (n=3).

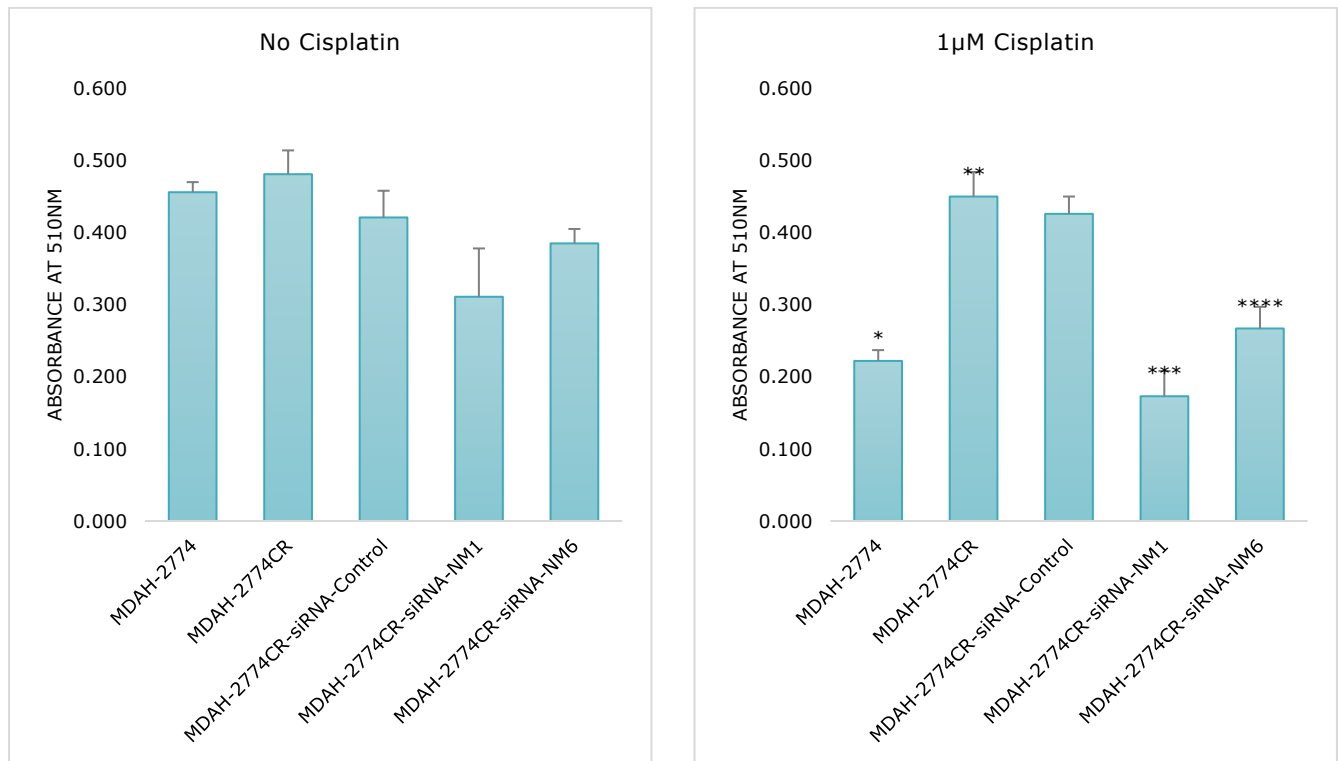


**Figure 4.9 Cisplatin Cytotoxic Assay:**

Cell survival following different combination of cisplatin treatments and NM1/NM6 siRNA. Sensitive and resistant paired cell line (MDAH-2774/MDAH-2774<sub>CR</sub>) were subjected to a series of treatments. At the end of 120 hrs, they were assessed by spectral analysis post-SRB staining. The bars for each condition (X-axis) represent means and standard error of the mean (Y-axis; Absorbance @510nm) of triplicates wells.

When the cells were treated with IC<sub>50</sub> MDAH-2774 (1µM) cisplatin, there was \*49% survival (desired outcome) in the sensitive cell line and \*\*94% survival (unwanted outcome) in the resistant cell line. The knockdown of NM1 and NM6 reduced the survival to 77% and 93% respectively (with the control knockdown consideration). However, when the knockdown of NM1 and NM6 was combined with 1µM of cisplatin, survival was reduced to \*\*\*47% (exceeding the desired outcome) and \*\*\*\*67% respectively (with the control knockdown consideration). Exceeding the desired outcome is valuable as the effect is reduced when phased into clinics, and this result also highlights the role of NM in chemoresistance and its potential in therapy.

#### 4.3.4 The Role of Spatial Chromosomal Organisation in Platinum-Resistance and Re-Sensitisation:

To understand how MDAH-2774<sub>CR</sub> became resistant and re-sensitized to cisplatin treatments through NM1 knockdown, the spatial territories of chromosomes 1, 13, 17 and X were investigated in MDAH-2774<sub>CR</sub> pre- and post-NM1 knockdown.

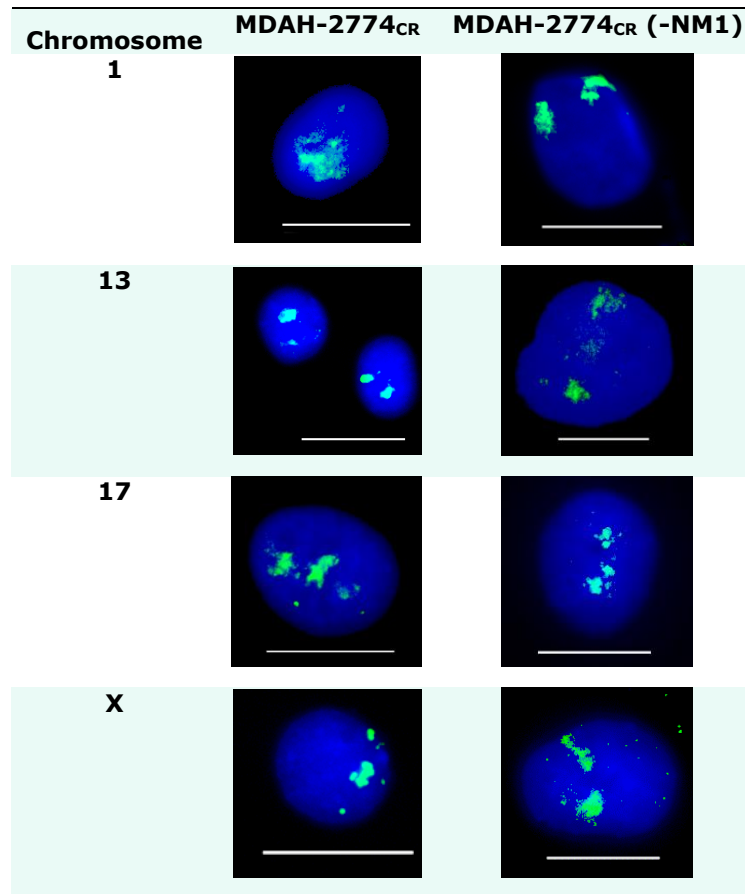


**Figure 4. 100 Chromosome Spatial Positioning Images: MDAH-2774<sub>CR</sub> Pre- and Post-NM1 Knockdown:**

Fluorescence images for the nuclear localisations of chromosomes 1, 13, 17 and X in cell lines MDAH-2774<sub>CR</sub> positioned using 2D-FISH pre/post NM1 knockdown. Nuclear genetic material blue-stained using DAPI and whole chromosome signals were red-stained with Cy3 and converted to green for software recognition. Magnification x400 / x1000. Scale bars represent 25µm. Images from fluorescent microscopy following 2D-FISH of MDAH-2774<sub>CR</sub> and MDAH-2774<sub>CR-NM1</sub> were then analysed by erosion analysis and compared against their originator MDAH-2774 and the control cell line using *p*-values from the students' *t*-test (figure 4.13 and table 4.1).

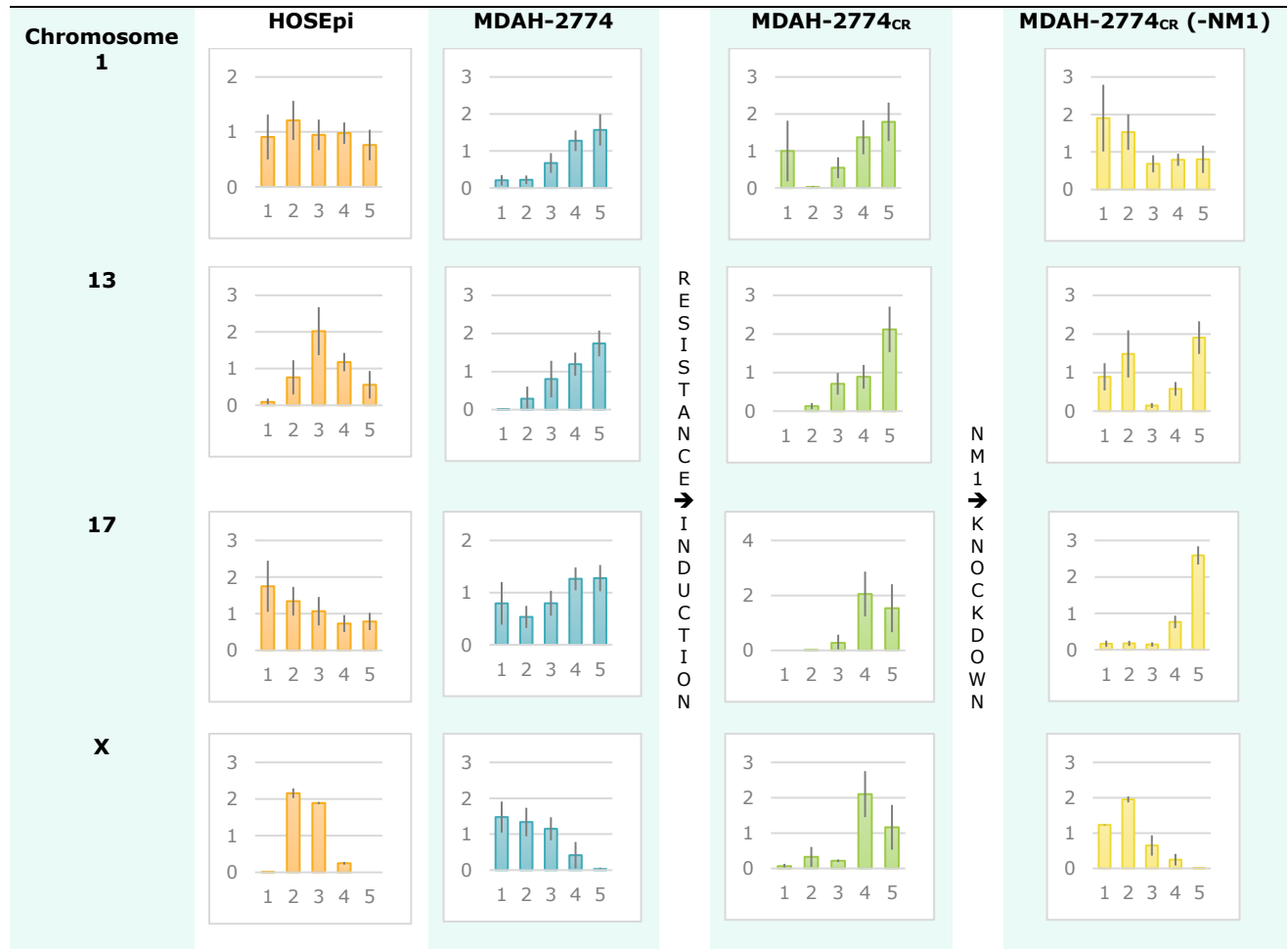


**Figure 4. 11 Graphical Representation: MDAH-2774<sub>CR</sub> Image Analysis Chromosome Spatial Positioning Pre- and Post-NM1 Knockdown:**

Histograms show the nuclear localisations of chromosomes 1, 13, 17 and X in cell line MDAH-2774<sub>CR</sub> before (light green) and after (dark green) siRNA knockdown of NM1, positioned using 2D-FISH and analysed by erosion analysis software [section 2.2.2]. The bars and error bars signify means and standard error of the mean of 50-75 nuclei, respectively. Y-Axis represents  $\% \text{ Cy3 whole chromosome probe signal} / \% \text{ DAPI nuclear signal}$ , and the X-axis represents periphery to the interior position (1 to 5). Student's *t*-test of all cancer cells performed against their origin cell and to the wild-type (healthy HOSEpi) [ $p < 0.5$  considered as significant].

Upon chemoresistance acquisition, Chromosome 1 in MDAH-2774 altered from internal to bi-modal (internal and periphery population), chromosome 13 stayed central, chromosome 17 moved further central and chromosome X from periphery to central. However, when NM1 was knocked down in MDAH-2774<sub>CR</sub>, only chromosome 1 and X showed reversion to intermediate and periphery respectively as the control cell while Chromosome 13 became bi-modal and chromosome 17 predominated internally.

**Table 4. 1  $p$ -values for MDAH-2774<sub>CR</sub> and Post-NM1 Knockdown Against HOSEpi:**

Each shell was calculated in MS Excel and the below. Shells that showed no significant differences with  $p > 0.5$  are highlighted in red, the shells that showed statistical differences with  $p < 0.5$  are unhighlighted, and the shells that showed statistical differences with  $p < 0.05$  are highlighted in green. The average values listed below; the red value represents no significant differences [ $p > 0.5$ ]; the black values are significantly different [ $p < 0.5$ ] and the green values significantly different [ $p < 0.05$ ].

	MDAH-2774 <sub>CR</sub>	MDAH-2774 <sub>CR</sub> -NM1 KNOCKDOWN
<b>Chromosome 1</b>		
Shell 1	0.925	0.482
Shell 2	0.001	0.594
Shell 3	0.046	0.262
Shell 4	0.315	0.499
Shell 5	0.023	0.990
AVG →	0.262	0.565
<b>Chromosome 13</b>		
Shell 1	0.057	0.421
Shell 2	0.004	0.654
Shell 3	0.007	0.000
Shell 4	0.467	0.278
Shell 5	0.070	0.325
AVG →	0.121	0.336
<b>Chromosome 17</b>		
Shell 1	0.279	0.069
Shell 2	0.028	0.002
Shell 3	0.352	0.001
Shell 4	0.015	0.812
Shell 5	0.315	0.001
AVG →	0.198	0.177
<b>Chromosome X</b>		
Shell 1	0.138	0.009
Shell 2	0.062	0.243
Shell 3	0.001	0.161
Shell 4	0.215	0.997
Shell 5	0.317	0.500
AVG →	0.147	0.382

**Table 4. 2  $p$ -values of MDAH-2774<sub>CR</sub> Pre- and Post-NM1 Knockdown Against HOSEpi:**

Summarised from table 4.1 - MDAH-2774<sub>CR</sub> had a higher significant difference to the control cell line before the knockdown and a lower significant difference after the knockdown. Means of 50-100 nuclei.

Chromosome	MDAH -2774 <sub>CR</sub>	NM1 siRNA	MDAH -2774 <sub>CR</sub> (-NM1)
<b>1</b>	0.262	→	0.565
<b>13</b>	0.121		0.336
<b>17</b>	0.198		0.177
<b>X</b>	0.147		0.382
<b>AVG</b>	<b>0.182</b>		<b>0.365</b>

The  $p$ -values of spatial chromosomal organisation showed that the created resistant MDAH-2774<sub>CR</sub> had an unexpected decrease in its statistical similarities to the control cell line. However, when NM1 was knocked down, its statistical similarity increases with large contributions from chromosome 1 and X.

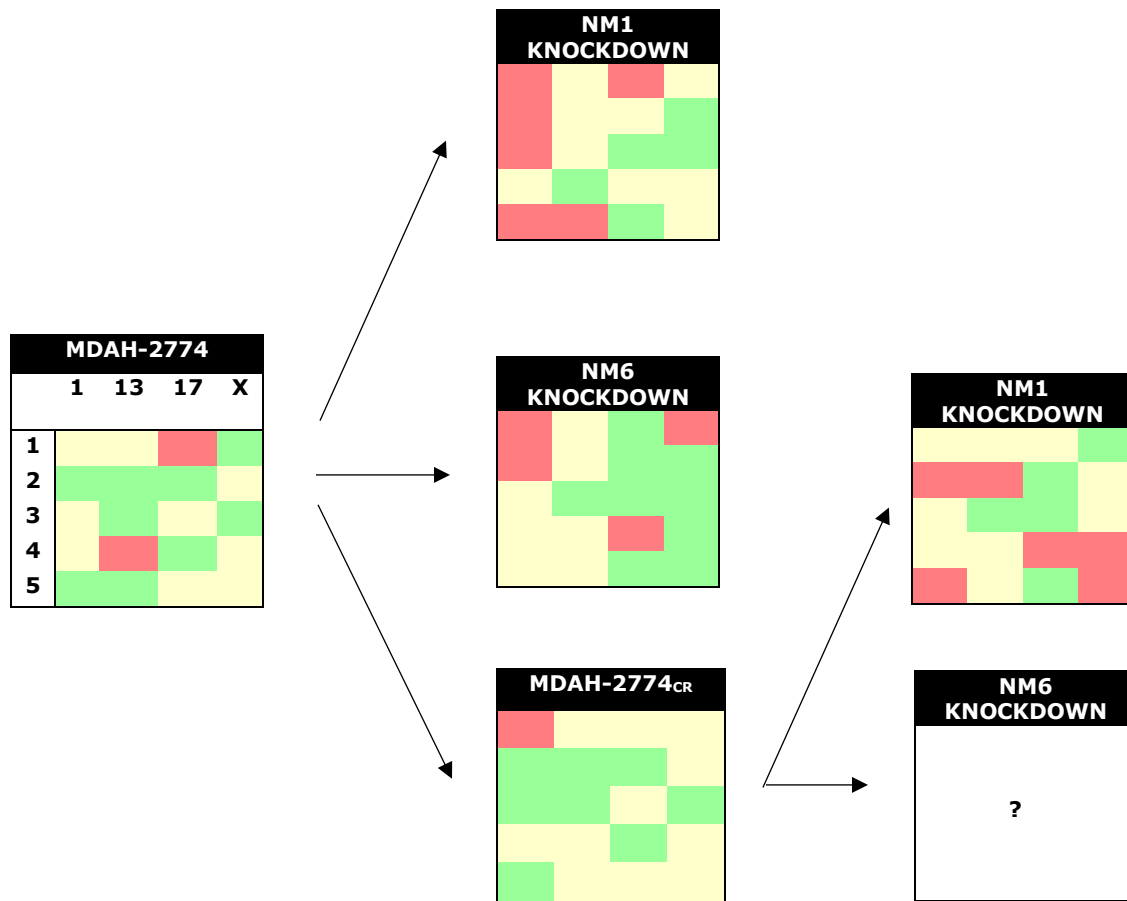


**Figure 4. 12 Post-Knockdown Effect by  $p$ -values Against HOSEpi:**

Heat-maps represent the level of shifts from the control cell that MDAH-2774 experiences when NM1 and NM6 are knocked down, when it acquires chemoresistance and when its resistant progeny undergoes NM1 knockdown. Blocks highlighted in **red** are shells that showed no significant differences with  $p > 0.5$ , highlighted in **green** are shells that showed statistical differences with  $p < 0.05$  and the **yellow** shells showed statistical differences with  $p < 0.5$ . The higher similarity to the control cells

The heat maps showed that post NM1 knockdown resulted in both MDAH-2774<sub>CR</sub> and MDAH-2774 having increased statistical similarities to the control cell line.

## 4.4 DISCUSSION

A major problem in treating a disease commonly diagnosed at a late stage is reoccurrence and cumulative chemoresistance. At this point, the disease is still cancerous, but its response is not the same as it has a new collection of properties allowing it to evade treatment despite a change in drug and dosage. Chemoresistant cancers cannot be treated as sensitive cancers; thus, greater understanding and therapy is required. This chapter aims to investigate the spatial arrangement and myosin level alterations that an OC cell undergoes upon the acquisition of chemoresistance and explore the synergistic effects of combining chemotherapy with siRNA.

### 4.4.1 NM1/NM6 Role in Acquiring Chemoresistance.

Chapter 2 presented altered CT positionings and NM distributions in the cancer cell lines. However, although elevated as in the other cell lines, PEO-4 NM1/NM6 stoichiometry stood out as it was similar to the control cell stoichiometry (NM6 higher than NM1; figure [2.9](#)). In chapter 3, when NM1 was knocked down, NM6 then also became higher in the cancer cells, which was accompanied by a slightly more significant improvement in the localisation of chromosomal territories when compared to the control cells. This led to the production of a lab-grade cisplatin-resistant cell line (MDAH-2774<sub>CR</sub>), in which a similar characteristic stoichiometry was found (NM6 higher than NM1; figure [4.7](#)). In the family of NMs, NM2 was also found overexpressed in drug-resistant OC, increasing the migratory potential of the disease and has been proposed as a potential suppression target (Kapoor *et al.*, 2018). This research also presents an exciting role for NM6 in chemoresistance.

Data presented in chapter 2 also found that PEO-4 NM1 and NM6 distribution was inconsistent with the distribution in the control cells (figure [2.7](#)). MDAH-2774<sub>CR</sub> on the other hand, while it had inconsistent distribution in both NM1 and NM6 when compared to both its originator cell line and control cell line, a **decline** of the modal tumour-specific patterns, an **emergence** of patterns associated with normal control cells and an **amplification** of sporadic tumour-cell associated

patterns (figure 4.4). The selective pressure *in-vitro* may have been intense compared to *in-vivo*, which may have resulted in extreme perturbations in NM1 and NM6 distribution patterns in MDAH-2774<sub>CR</sub> versus the *in-vivo* line PEO-4.

#### 4.4.2 Synergy

Nuclear myosins were also targeted to investigate its role in resistance-related chromosomal reorganisation. This required over-expressed NM1 and NM6 to be knocked down in the platinum-resistant line and then treated as the sensitive line would be. Figure 4.11 showed that sensitive MDAH-2774 had 49% survival while the resistant MDAH-2774<sub>CR</sub> had 94% survival when treated with cisplatin alone, however when combined with NM1 or NM6 knockdown, MDAH-2774<sub>CR</sub> survival reduced to had 47% and 67% survival respectively, where the NM1 knockdown combination surpassed the expected outcome of the sensitive line highlighting exceptional synergy of combining chemotherapy with the reduction of NM.

The knockdown effect observed in NM1 (39%) was similar to NM6 (38%), and as the resistant cell line does have higher levels of both proteins compared when to the control cell and its tumour originator, NM6 is also higher than NM1 before the knockdown, therefore the magnitude of RNA interference would have to be greater for NM6.

#### 4.4.3 Chemoresistance and Spatial Chromosomal Organisation

Chromosomes may move to advantageous locations favouring drug efflux/metabolism-related transcription, but are they staying there permanently or more likely the elevated levels of motor proteins causing them to move rapidly? Upon the acquisition of chemoresistance and the successful re-sensitisation by NM1 knockdown, chromosomes 1, 13, 17 and X territories were mapped to deduce correlations with the spatial organisation. When MDAH-2774 acquired resistance, it surprisingly had a small increase in its *p*-value when compare to the control cell, and interestingly



when NM1 was knocked down, its  $p$ -value unexpectedly increased, both circumstances going against the 'resistance principle' (figure 4.14 and table 4.2). Under the 'resistance principle', resistant cells evade drugs by adopting features resembling control cells while also accumulating tumorigenic traits; therefore, it was expected that MDAH-2774<sub>CR</sub> would have shown larger similarities to HOSEpi (see resistance principle section 1.1.8). The lack of templates of control cells may be the reason *in-vitro* experiments have been unsuccessfully translated into therapy, and future studies should consider spiking chemo-induction treatments with control cells. It was also expected that for re-sensitisation, MDAH-2774<sub>CR-NM1</sub> would have shown similarities to MDAH-2774 rather than HOSEpi. Intriguingly, the only chromosome that had this expected repositioning was chromosome X. The consensus is that the re-sensitisation should push the resistant cell to such vulnerability to be destroyed by the drug, and this may have been achieved by the chaos of chromosomes adopting abnormal and normal positions.

#### **4.4.4 Conclusion**

Co-delivery to treat and combat resistance using a multifunctional nanoparticle-based delivery system that delivers drugs and siRNA targets has been used to investigate many multi-drug resistant cancers and has been found to inhibit growth drastically (Saad *et al.*, 2008). However, after first discovered in 2004, the wave of optimism died as delivery techniques faced challenges to translate into clinics in addition to innate immune responses and off-target effects (Wang *et al.*, 2017). This caused suspension of numerous RNAi clinical trials, including the first RNAi drug Bevasiranib (Garba and Mousa, 2010). Introducing RNAi in clinical therapies heavily relies on nanoparticle biology, and as research design and standards improve, RNAi-based anticancer therapies will soon become available. In August 2018, the first RNAi drug, Onpattro (patisiran), that knocks down transthyretin (*TTR*) was approved for polyneuropathy in hATTR amyloidosis, then in November 2019, Givlaari (givosiran), that knocks down aminolevulinate synthase 1 (*ALAS1*) for acute hepatic porphyria (*AHP*), both by Alnylam Pharmaceuticals.

Additionally, when combating drug resistance through RNAi, a technique that rarely provides 100% knockdown needs to be directed to a protein that is required at reduced levels coupled with a synergistic treatment. This study reduced the protein, whereas other studies approach targets by complete eradication of a gene/protein (perhaps CRISPR might be required instead). This chapter also showed that the spatial organisation of just four chromosomes was able to reveal information about resistance in OC, while its role in re-sensitisation warrants further studies. NM1/NM6 knockdowns may also be a better candidate in re-sensitisation over therapy but can potentially reduce toxic drug doses and delay resistance. More work needs to be done to include more parameters such as time, more chromosomes, cell lines and further understand NM role in re-sensitisation.

## CHAPTER 5

# GENERAL DISCUSSION

This project aimed to bridge the gap in research by investigating the nuclear organisation of four chromosomes and two NMs in four OC cell lines, as well as highlight their relevance of chemoresistance in hopes of improving the prognosis of OC. Widening the gap by possibly delaying chemoresistance through improved therapy or a prognostic prediction may allow a patient extended time and/or better quality of life. While the management of OC has improved over the decades, it remains the deadliest female gynaecological cancer as it continues to be shadowed by other cancers in terms of funding and research.

### 1. **Chromosome X**

This research began by reserving the use of chromosome X as a control for chromosome 1, 13 and 17 in FISH as it is known to occupy the periphery, however, with recent findings of the paternal X chromosome being linked to OC, we continued investigations in the knockdown where instability emerged as chromosome X moved internally in 7/8 instances (Belmont *et al.*, 1986; Boyle *et al.*, 2001; Eng *et al.*, 2018). Though some of these were positive relocations, it was not expected based on Mehta's study where chromosome X showed no change in position regardless of the presence of serum or not (Mehta *et al.*, 2010). Moreover, chromosome X did not occupy the absolute periphery

in the control cells and may imply a yet to be elucidated correlations with its position and roles in OC.

Throughout this project, the knockdown by NM showed favourable outcomes when the knockdown gap (the spatial difference in CT pre- and post-knockdown) was small, and despite having relatively similar knockdown efficiencies, a more significant number of CTs adopted new positions post-NM1 knockdown that were similar to the control cells, even in the cisplatin-resistant cells when compared to NM6 knockdown. Interestingly, chromosome X is the only chromosome of the four to show higher favourable outcomes with larger knockdown gaps (Figure 3.11E). The re-location of CTs varied widely with knockdowns, where one chromosome that seemed to respond in a rehabilitative way (figure 3.11) was chromosome 1 (more significant in NM1). However, in the cisplatin-resistant line, chromosome 1 was not alone as chromosome X also showed the same rehabilitative response (figure 4.13).

Chromosome X may no longer be a suitable reference when investigating CT, at least in OC as it may have a role in the development and progression of the disease. This unsuitability stems from the observation of the escape of X chromosome inactivation (XCI) by inactive chromosome X ( $X_{\text{inactive}}$ ) due to interaction with the active form of chromosome X ( $X_{\text{active}}$ ) (Laskowski *et al.*, 2019).  $X_{\text{inactive}}$  is more peripherally positioned in a distinct, condensed and spherical structure known as a Barr body and perhaps the  $X_{\text{active}}$  may also influence the position of the  $X_{\text{inactive}}$  making it less peripheral further explaining the loss of Barr bodies in cancer cells (Pageau *et al.*, 2007; Jowhar *et al.*, 2018; Etter *et al.*, 2020).

X chromosome interactions and influence have been found to exacerbate disease response in autoimmune diseases coherent with the supernumerary of X, thus the higher prevalence of X-linked diseases (i.e. 10% of diseases with a mendelian inheritance pattern) in women than in men (Ross *et al.*, 2005; Jowhar *et al.*, 2018; Laskowski *et al.*, 2019). X chromosome interactions and escaping

XCI is problematic for oncogenic X-linked genes, for example, the "cancer-testis" genes that are typically expressed in adult testes tissue, are also expressed by many tumours, including the ovary (Dezhong *et al.*, 2003; Etter *et al.*, 2020). Even XCI has been observed in high-grade serous tumours, patterns of OC-related XCI remains largely unknown (Winham *et al.*, 2019).

## **2. Characterisation of whole chromosome spatial organisation**

Chromosome 1, particularly interesting as the ARID1A it possesses roles in chromosome partitioning, so while its position may show partial agreement to the size-based theory of chromosome organisation rather than the gene-density based, this is beginning to be disputed as more information on individual chromosomes with various specificities (tissue and cell state) is emerging, thus, may also be considered on an individual basis. However, with the emergence 'chromosome stretching' or CT extension as possibly displayed by chromosome 13 and 17 and the element of the lack of complete repression of at the periphery, this large gene-rich chromosome 1 can still be active while near or tethered to the periphery and stretched into the centre. Also interesting is that spatial position of chromosome 1 and NM6 distribution in SKOV-3 showed no significant difference to the control cells. However, this was followed with aberrance its other chromosomes 13, 17 and X presenting larger  $p$ -values than the other cell lines and both its NM1 and NM6 also having >100% elevations as the other tumour lines (figure 2.9 and 3.11). Amongst the OC tumour lines and the lab-created cisplatin-resistant line MDAH-2774<sub>CR</sub>, there was a frequent re-location of the chromosome to the centre, especially in the case of chromosome 17 (Figure 2.4 and 4.13). Chromosome 17 contains the oncogene *HER2*, which may be problematic in the transcriptionally active centre.

### 3. ***Tethering versus Anchorage Stoichiometry***

This then shifts focus on a dysregulation at the nuclear periphery in which we found irregularities in lamin staining, particularly lamin B<sub>2</sub> was deficient or mis-localised internally, and lamin C was also deficient, that may have disrupted LAD tethering. Also, the possible chromosome stretching that peripheral chromosome experience requires an internal opposite force in which we attributed to the force-generating and anchorage properties of NM1 and NM6, both of which were found elevated and irregularly distributed. Therefore, while lamin tethering was deficient chromosome stretching was overpowered by the elevated pull by NM towards the active centre likely carrying oncogenes with it. Just as stoichiometry within the lamin and myosin superfamily is important, stoichiometry with the hypothetical nuclear motor complex is as well (Swift *et al.*, 2013).

### 4. ***Superfamily/Supercomplex stoichiometry***

Swift *et al.* 2013 mentioned the cell-type-specific stoichiometry of A/B-type lamins determines the mechanical properties of nuclei and disruption of this ratio can have downstream effects to other protein and lead to diseases. Lamin B<sub>2</sub> and C showed irregular characteristic lamin staining that may have disrupted the ratio within A-type and B-type lamins and the superfamily, with probable downstream effects on the proteins of the hypothetical nuclear motor complex such as NM1 and NM6 that was found elevated and irregularly distributed. The tumour cells showed a different stoichiometry to the control cell where NM1 was higher opposed to NM6 being higher in the control cell, which may also be accompanied by downstream effects. Additionally, there is compensation within the superfamily where A-type lamins step in during B-type lamin deficiency; which is also observed between nucleoplasmic and cytoplasmic isoforms of NM1, and also between NM1 and NM6 when NM6 was perturbed (Yang *et al.*, 2011a/b; Venit *et al.*, 2013; Chen *et al.*, 2019; Cook, Gough and Toseland, 2020). Whether disruption in the lamin stoichiometry affected NM stoichiometry or vice versa would require further investigation that perturbs the one protein and assess the other.

### 5. Other Nuclear Myosins

My work also included other NMs that uncovered some interesting patterns that paves the way for future research (figure 5.1). While NM16 and NM18b showed patterns similar to the "dispersed" and "aggregates" as for NM1 and NM6 staining, a further pattern was apparent whereby NM was located at the nuclear rim, thus, making an exciting future co-study. NM18b showed a high number of negative stains consistent with its reduced expression report in OC justifying restorative investigations and its levels in the resistant disease (Yanaihara *et al.*, 2004; Ajima *et al.*, 2007). Though NM5b showed a uniform splicing speckles pattern (due to proposed roles in transcription splicing) throughout all the cell lines, it is understudied, and its emerging in transcription is attracting attention (Pranchevicius *et al.*, 2008).

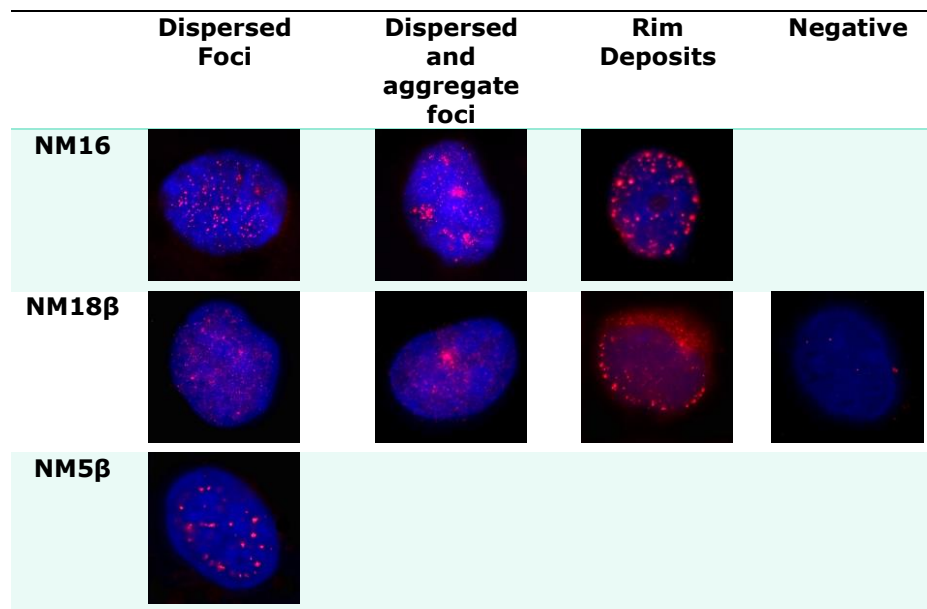


**Figure 5. 1 NM16, NM18β and NM5β:**

Representative images of the nuclear distribution pattern (dispersed, dispersed and aggregate, rim deposits and splicing speckles) were captured in 4 OC cell lines SKOV-3, PEO-1, PEO-4 and MDAH-2774. DNA was stained using DAPI (blue), and the NM1 protein was revealed by Indirect IF with a Cy3 conjugated secondary antibody. Magnification x400 / x1000.

## 6. Chemoresistance

The NM1/NM6 stoichiometry stood out in the platinum-resistant PEO-4 that showed similarities of control cells, which may have given it the resistant advantage. The lab-created cisplatin-resistant also showed the same stoichiometry, which was expected. We anticipated the platinum-resistant line, according to 'the resistant principle' to encompass mesh of healthy and tumorigenic properties; however, the principle lies on the fact that *in-vivo* a healthy template is available that enables this to take place, so it was not astonishing when the following expectations were not met during chemoresistant acquisition and re-sensitisation. Following the acquisition of chemoresistance MDAH-2774<sub>CR</sub> showed very little shift in CT that was similar to the control cell; instead, the CTs become more central. Moreover, when MDAH-2774<sub>CR</sub> re-sensitised through NM1 knockdown, an expectation is that it would resemble the sensitive tumour line; however, it showed higher similarities to the control cell. These outcomes may have been due to the lack of template during resistance acquisition and creation of such chaos instead through re-sensitisation that it did not matter which CT was at a healthy territory or not.

Furthermore, even though no healthy template was available, the cisplatin-resistant MDAH-2774<sub>CR</sub> showed a re-emergence of NM patterns that were not seen its tumour originator cell MDAH-2774 but observed in the control cell. Interestingly, this was also accompanied by a decline of the modal tumour-specific patterns and an increase in sporadic tumour-cell associated patterns (figure 4.4), highlighting the lineage advantage of the naïve cell and *in-vitro* chemoresistant line (Penner-Goeke *et al.*, 2017). This novel investigation opens the avenues for research into chemoresistance concerning CTs and protein stoichiometry within the nucleus. However, the field of studying chemoresistance *in-vitro* requires control experiments to address the validity of the resistance principle by spiking resistance induction with control cells.



## 7. Conclusion

While the irregularities of lamins and NM may have resulted in the detachment of some CTs from the periphery and to repositioning to the centre, this may have led to the displacement of chromosome X territory to the periphery. Following the NM knockdown, the anchorage effect was relaxed, resulting in the return of chromosome 17 to the periphery and pushing chromosome X back to its intermediate position. Perhaps restoring lamin with its tethering property and reducing NM with their anchorage would be ideal. However, the individual reduction of NM provided a remarkable response providing clinical possibilities with co-manipulations.

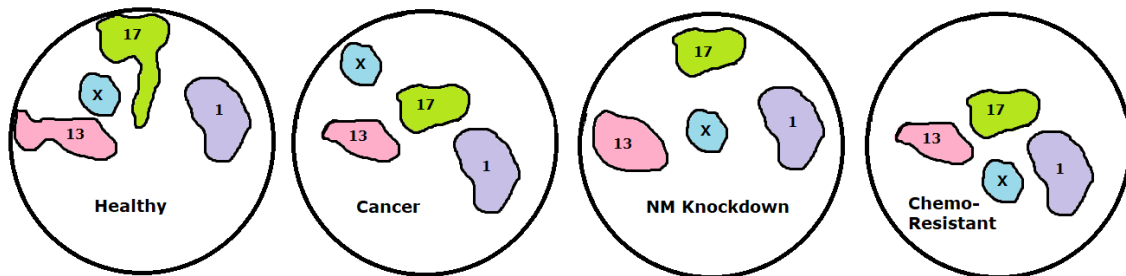


**Figure 5. 2 Summary of the CT Re-Positionings from Healthy to Cancer to NM Knockdown and Chemoresistance:**

In the control cell, Chromosome 17 (green) and 13 (pink) exhibited chromosome stretching, chromosome 1 (lilac) and X (blue) occupied with intermediate spaces. In the cancer cell chromosome X occupied the periphery while chromosomes 1, 13 and 17 had a relatively more internal occupancy. In the NM knockdown, chromosome 17 reverted towards the periphery, chromosome 1 also reverted towards the periphery. Chromosome 13 varied with its occupancy; thus, a trend could not be summarised; however, there were some instances where it moves back outwards. The platinum-resistant line exhibited bi-modalism in its chromosome 1 population, but all four chromosomes predominated in the centre.

The re-locations of these CTs may have displaced each other, however in the platinum-resistant line, they all showed central occupancy and thus begged the question of what CTs have they displaced? The vast amount of information extracted from 4 chromosomes indicates that there is a vast potential for expansion in this field to investigate other chromosomes including genes to understand the tumour biology of OC and with a clinical role in prognosis. It also would be interesting

to investigate the speed at which chromosomes move with differing myosin quantities at each stage of the disease, and under cisplatin, during and upon resistance acquisition and knockdown treatment conditions via real-time FISH. This research was also able to combine pulse and continuous methods in chemoresistant induction to create a robust and stable resistant line, thus saving months of resources; however, this may not be applicable to every cell line. It must also be considered that investigations need to go beyond in-vitro, which reduces the time producing research material and provides a comprehensive portrait of nuclear and sub-nuclear organization, however, this will require novel high-throughput assays that preserves the spatial information.

In terms of diagnosis, acquiring cells to diagnose OC efficiently is a challenge due to the location of the disease and organ; however, just as non-invasive (clinically) blood samples employed in CA-125 tests, samples can be enriched for circulating tumour cells (CTCs). CTCs can reveal valuable in-vivo insights into CTs and NM levels, distribution, and roles at every stage of the disease, including resistance. Simultaneously, research is required for clinical transitioning relating to drug safety regarding RNAi and nanoparticle technology.

## 6 REFERENCES

- Adriaens, C., Serebryanny, L. A., Feric, M., Schibler, A., Meaburn, K. J., Kubben, N., Trzaskoma, P., Shachar, S., Vidak, S., Finn, E. H., Sood, V., Pegoraro, G., & Misteli, T. (2018). Blank spots on the map: some current questions on nuclear organization and genome architecture. *Histochemistry and Cell Biology*, 150(6), 579–592. <https://doi.org/10.1007/s00418-018-1726-1>
- Ajima, R., Kajiya, K., Inoue, T., Tani, M., Shiraishi-Yamaguchi, Y., Maeda, M., Segawa, T., Furuichi, T., Sutoh, K., & Yokota, J. (2007). HOMER2 binds MYO18B and enhances its activity to suppress anchorage independent growth. *Biochemical and Biophysical Research Communications*. <https://doi.org/10.1016/j.bbrc.2007.03.060>
- Akhtar, A., & Gasser, S. M. (2007). The nuclear envelope and transcriptional control. In *Nature Reviews Genetics* (Vol. 8, Issue 7, pp. 507–517). Nature Publishing Group. <https://doi.org/10.1038/nrg2122>
- Alnylam® Pharmaceuticals*. (n.d.). Retrieved August 8, 2020, from <https://www.alnylam.com/>
- Amendola, M., & van Steensel, B. (2015). Nuclear lamins are not required for lamina-associated domain organization in mouse embryonic stem cells. *EMBO Reports*, 16(5), 610–617. <https://doi.org/10.15252/embr.201439789>
- Andrulis, E. D., Neiman, A. M., Zappulla, D. C., & Sternglanz, R. (1998). Perinuclear localization of chromatin facilitates transcriptional silencing. *Nature*, 394(6693), 592–595. <https://doi.org/10.1038/29100>
- Aunoble, B., Sanches, R., Didier, E., & Bignon, Y. J. (2000). Major oncogenes and tumor suppressor genes involved in epithelial ovarian cancer (review). In *International journal of oncology* (Vol. 16, Issue 3, pp. 567–576).
- Azagra, A., Marina-Zárate, E., Ramiro, A. R., Javierre, B. M., & Parra, M. (2020). From Loops to Looks: Transcription Factors and Chromatin Organization Shaping Terminal B Cell Differentiation. *Trends in Immunology*, 41(1), 46–60. <https://doi.org/https://doi.org/10.1016/j.it.2019.11.006>
- Baarlink, C., Wang, H., & Grosse, R. (2013). Nuclear actin network assembly by formins regulates the SRF coactivator MAL. *Science*. <https://doi.org/10.1126/science.1235038>
- Banani, S. F., Lee, H. O., Hyman, A. A., & Rosen, M. K. (2017). Biomolecular condensates: organizers of cellular biochemistry. *Nature Reviews Molecular Cell Biology*, 18(5), 285–298. <https://doi.org/10.1038/nrm.2017.7>
- Banerjee, S., & Kaye, S. B. (2013). New Strategies in the Treatment of Ovarian Cancer: Current Clinical Perspectives and Future Potential. *Clinical Cancer Research*, 19(5), 961 LP – 968. <https://doi.org/10.1158/1078-0432.CCR-12-2243>
- Bártová, E., Harničarová, A., Pacherník, J., & Kozubek, S. (2005). Nuclear topography and expression of the BCR/ABL fusion gene and its protein level influenced by cell differentiation and RNA interference. *Leukemia Research*, 29(8), 901–913. <https://doi.org/https://doi.org/10.1016/j.leukres.2005.01.011>
- Bártová, E., & Kozubek, S. (2006). Nuclear architecture in the light of gene expression and cell differentiation studies. *Biology of the Cell*, 98(6), 323–336. <https://doi.org/10.1042/BC20050099>
- Bártová, E., Kozubek, S., Jirsová, P., Kozubek, M., Gajová, H., Lukášová, E., Skalníková, M., Gaňová, A., Koutná, I., & Hausmann, M. (2002). Nuclear structure and gene activity in human differentiated cells. *Journal of Structural Biology*, 139(2), 76–89.
- Bártová, E., Kozubek, S., Kozubek, M., Jirsová, P., Lukášová, E., Skalníková, M., Cafourková, A., & Koutná, I. (2000). Nuclear topography of the c-myc gene in human leukemic cells. *Gene*, 244(1), 1–11. [https://doi.org/https://doi.org/10.1016/S0378-1119\(99\)00572-7](https://doi.org/https://doi.org/10.1016/S0378-1119(99)00572-7)

- Beaufort, C. M., Helmijr, J. C. A., Piskorz, A. M., Hoogstraat, M., Ruigrok-Ritstier, K., & Bessenlink, N. (2015). Ovarian cancer cell line panel (OCCP): clinical importance of in vitro morphological subtypes (vol 9, e103988, 2014). *PLoS One*, *10*(3).
- Bell, C. C., & Gilan, O. (2020). Principles and mechanisms of non-genetic resistance in cancer. In *British Journal of Cancer* (Vol. 122, Issue 4, pp. 465–472). Springer Nature. <https://doi.org/10.1038/s41416-019-0648-6>
- Belmont, A. S., Bignone, F., & Ts' O, P. O. P. (1986). The relative intranuclear positions of barr bodies in XXX non-transformed human fibroblasts. *Experimental Cell Research*, *165*(1), 165–179. [https://doi.org/10.1016/0014-4827\(86\)90541-0](https://doi.org/10.1016/0014-4827(86)90541-0)
- Belt, E. J. T., Fijneman, R. J. A., van den Berg, E. G., Bril, H., Delis-van Diemen, P. M., Tijssen, M., van Essen, H. F., de Lange-de Klerk, E. S. M., Beliën, J. A. M., Stockmann, H. B. A. C., Meijer, S., & Meijer, G. A. (2011). Loss of lamin A/C expression in stage II and III colon cancer is associated with disease recurrence. *European Journal of Cancer*, *47*(12), 1837–1845. <https://doi.org/10.1016/j.ejca.2011.04.025>
- Berk, J. M., Tift, K. E., & Wilson, K. L. (2013). The nuclear envelope LEM-domain protein emerlin. In *Nucleus (United States)* (Vol. 4, Issue 4). Taylor & Francis. <https://doi.org/10.4161/nucl.25751>
- Bickmore, W. A. (2013). The Spatial Organization of the Human Genome. *Annual Review of Genomics and Human Genetics*, *14*(1), 67–84. <https://doi.org/10.1146/annurev-genom-091212-153515>
- Bickmore, W. A., & van Steensel, B. (2013). Genome Architecture: Domain Organization of Interphase Chromosomes. *Cell*, *152*(6), 1270–1284. <https://doi.org/https://doi.org/10.1016/j.cell.2013.02.001>
- Biedler, J. L., & Riehm, H. (1970). Cellular Resistance to Actinomycin D in Chinese Hamster Cells in Vitro: Cross-Resistance, Radioautographic, and Cytogenetic Studies. *Cancer Research*, *30*(4).
- Bikkul, M. U., Faragher, R. G. A., Worthington, G., Meinke, P., Kerr, A. R. W., Sammy, A., Riyahi, K., Horton, D., Schirmer, E. C., Hubank, M., Kill, I. R., Anderson, R. M., Slijepcevic, P., Makarov, E., & Bridger, J. M. (2019). Telomere elongation through hTERT immortalization leads to chromosome repositioning in control cells and genomic instability in Hutchinson-Gilford progeria syndrome fibroblasts, expressing a novel SUN1 isoform. *Genes, Chromosomes and Cancer*, *58*(6), 341–356. <https://doi.org/10.1002/gcc.22711>
- Bioprognos*. (n.d.). 2020. Retrieved August 17, 2020, from <https://www.bioprognos.com/en/oncoovarian-dx-ovarian-cancer-diagnosis-test/>
- Boivin, M., Lane, D., Piché, A., & Rancourt, C. (2009). CA125 (MUC16) tumor antigen selectively modulates the sensitivity of ovarian cancer cells to genotoxic drug-induced apoptosis. *Gynecologic Oncology*. <https://doi.org/10.1016/j.ygyno.2009.08.007>
- Bolzer, A., Kreth, G., Solovei, I., Koehler, D., Saracoglu, K., Fauth, C., Müller, S., Eils, R., Cremer, C., & Speicher, M. R. (2005). Three-dimensional maps of all chromosomes in human male fibroblast nuclei and prometaphase rosettes. *PLoS Biol*, *3*(5), e157.
- Boveri, T. (1909). Die Blastomerenkerne von *Ascaris megalocephala*. *Archiv Für Zellforschung*, *3*, 181.
- Boyle, S., Gilchrist, S., Bridger, J. M., Mahy, N. L., Ellis, J. A., & Bickmore, W. A. (2001). The spatial organization of human chromosomes within the nuclei of normal and emerlin-mutant cells. *Human Molecular Genetics*, *10*(3), 211–220. <https://doi.org/10.1093/hmg/10.3.211>
- Branco, M. R., & Pombo, A. (2006). Intermingling of chromosome territories in interphase suggests role in translocations and transcription-dependent associations. *PLoS Biol*, *4*(5), e138.
- Brickner, J. (2017). Genetic and epigenetic control of the spatial organization of the genome. *Molecular Biology of the Cell*, *28*(3), 364–369. <https://doi.org/10.1091/mbc.E16-03-0149>
- Brickner, J. H., & Walter, P. (2004). Gene recruitment of the activated INO1 locus to the nuclear membrane. *PLoS Biology*, *2*(11), e342.
- Bridger, J M, Boyle, S., Kill, I. R., & Bickmore, W. A. (2000). Re-modelling of nuclear architecture in quiescent and senescent human fibroblasts. *Current Biology*, *10*(3), 149–152.
- Bridger, Joanna M., Arican-Gotkas, H. D., Foster, H. A., Godwin, L. S., Harvey, A., Kill, I. R., Knight, M., Mehta, I. S., & Ahmed, M. H. (2014). The non-random repositioning of whole chromosomes and individual gene loci in interphase nuclei and its relevance in disease, infection, aging, and cancer. *Advances in Experimental Medicine and Biology*. [https://doi.org/10.1007/978-1-4899-8032-8\\_12](https://doi.org/10.1007/978-1-4899-8032-8_12)
- Bridger, Joanna M., & Bickmore, W. A. (1998). Putting the genome on the map. In *Trends in Genetics*. [https://doi.org/10.1016/S0168-9525\(98\)01572-8](https://doi.org/10.1016/S0168-9525(98)01572-8)
- Brown, J. S., O'Carrigan, B., Jackson, S. P., & Yap, T. A. (2017). Targeting DNA repair in cancer: Beyond PARP inhibitors. In *Cancer Discovery* (Vol. 7, Issue 1, pp. 20–37). American Association for Cancer Research Inc. <https://doi.org/10.1158/2159-8290.CD-16-0860>

- Brown, K. E., Guest, S. S., Smale, S. T., Hahm, K., Merckenschlager, M., & Fisher, A. G. (1997). Association of transcriptionally silent genes with Ikaros complexes at centromeric heterochromatin. *Cell*, *91*(6), 845–854. [https://doi.org/10.1016/S0092-8674\(00\)80472-9](https://doi.org/10.1016/S0092-8674(00)80472-9)
- Burke, B., & Stewart, C. L. (2013). The nuclear lamins: Flexibility in function. In *Nature Reviews Molecular Cell Biology* (Vol. 14, Issue 1, pp. 13–24). Nature Publishing Group. <https://doi.org/10.1038/nrm3488>
- Byrd, K., & Corces, V. G. (2003). Visualization of chromatin domains created by the gypsy insulator of Drosophila. *The Journal of Cell Biology*, *162*(4), 565–574. <https://doi.org/10.1083/jcb.200305013>
- Cabal, G. G., Genovesio, A., Rodriguez-Navarro, S., Zimmer, C., Gadal, O., Lesne, A., Buc, H., Feuerbach-Fournier, F., Olivio-Marin, J.-C., & Hurt, E. C. (2006). SAGA interacting factors confine sub-diffusion of transcribed genes to the nuclear envelope. *Nature*, *441*(7094), 770–773.
- Cameron, R. S., Liu, C., & Pihkala, J. P. S. (2013). Myosin 16 levels fluctuate during the cell cycle and are downregulated in response to DNA replication stress. *Cytoskeleton*, *70*(6), 328–348. <https://doi.org/10.1002/cm.21109>
- Campbell, M. J. (2019). Tales from topographic oceans: Topologically associated domains and cancer. In *Endocrine-Related Cancer* (Vol. 26, Issue 11, pp. R611–R626). BioScientifica Ltd. <https://doi.org/10.1530/ERC-19-0348>
- Cancer survival in England - Office for National Statistics*. (n.d.). Retrieved July 30, 2020, from <https://www.ons.gov.uk/peoplepopulationandcommunity/healthandsocialcare/conditionsanddiseases/bulletins/cancersurvivalinengland/nationalestimatesforpatientsfollowedupto2017>
- Capo-chichi, C. D., Cai, K. Q., Simpkins, F., Ganjei-Azar, P., Godwin, A. K., & Xu, X.-X. (2011). Nuclear envelope structural defects cause chromosomal numerical instability and aneuploidy in ovarian cancer. *BMC Medicine*, *9*(1), 28. <https://doi.org/10.1186/1741-7015-9-28>
- Caridi, C. P., Ryu, T., Zapotoczny, G., Delabaere, L., Li, X., Khodaverdian, V. Y., Amaral, N., Lin, E., Rau, A., & Chiolo, I. (2018). Nuclear F-actin and myosins drive relocalization of heterochromatic breaks Actin nucleators drive DSB relocalization. *Nature*. <https://doi.org/10.1038/s41586-018-0242-8>
- Carrillo, A. M., Hicks, M., Khabele, D., & Eischen, C. M. (2015). Pharmacologically increasing Mdm2 inhibits DNA repair and cooperates with genotoxic agents to kill p53-inactivated ovarian cancer cells. *Molecular Cancer Research*. <https://doi.org/10.1158/1541-7786.MCR-15-0089>
- Casolari, J. M., Brown, C. R., Komili, S., West, J., Hieronymus, H., & Silver, P. A. (2004). Genome-wide localization of the nuclear transport machinery couples transcriptional status and nuclear organization. *Cell*, *117*(4), 427–439.
- Chakalova, L., Debrand, E., Mitchell, J. A., Osborne, C. S., & Fraser, P. (2005). Replication and transcription: Shaping the landscape of the genome. *Nature Reviews Genetics*, *6*(9), 669–677. <https://doi.org/10.1038/nrg1673>
- Chambeyron, S., & Bickmore, W. A. (2004). Chromatin decondensation and nuclear reorganization of the HoxB locus upon induction of transcription. *Genes & Development*, *18*(10), 1119–1130. <https://doi.org/10.1101/gad.292104>
- Chambeyron, S., Da Silva, N. R., Lawson, K. A., & Bickmore, W. A. (2005). Nuclear re-organisation of the Hoxb complex during mouse embryonic development. *Development*, *132*(9), 2215–2223.
- Chen, M., Yao, S., Cao, Q., Xia, M., Liu, J., & He, M. (2016). The prognostic value of Ki67 in ovarian high-grade serous carcinoma: an 11-year cohort study of Chinese patients. *Oncotarget*, *8*(64), 107877–107885. <https://doi.org/10.18632/oncotarget.14112>
- Chen, N. Y., Yang, Y., Weston, T. A., Belling, J. N., Heizer, P., Tu, Y., Kim, P., Edillo, L., Jonas, S. J., Weiss, P. S., Fong, L. G., & Young, S. G. (2019). An absence of lamin B1 in migrating neurons causes nuclear membrane ruptures and cell death. *Proceedings of the National Academy of Sciences*, *116*(51), 25870 LP – 25879. <https://doi.org/10.1073/pnas.1917225116>
- Chuang, C.-H., Carpenter, A. E., Fuchsova, B., Johnson, T., de Lanerolle, P., & Belmont, A. S. (2006). Long-Range Directional Movement of an Interphase Chromosome Site. *Current Biology*, *16*(8), 825–831. <https://doi.org/https://doi.org/10.1016/j.cub.2006.03.059>
- Chubb, J. R., Boyle, S., Perry, P., & Bickmore, W. A. (2002). Chromatin Motion Is Constrained by Association with Nuclear Compartments in Human Cells. *Current Biology*, *12*(6), 439–445. [https://doi.org/https://doi.org/10.1016/S0960-9822\(02\)00695-4](https://doi.org/https://doi.org/10.1016/S0960-9822(02)00695-4)
- Clements, C. S., Bikkul, U., Ahmed, M. H., Foster, H. A., Godwin, L. S., & Bridger, J. M. (2016). Visualizing the spatial relationship of the genome with the nuclear envelope using fluorescence in situ hybridization. In *Methods in Molecular Biology* (Vol. 1411, pp. 387–406). Humana Press Inc. [https://doi.org/10.1007/978-1-4939-3530-7\\_24](https://doi.org/10.1007/978-1-4939-3530-7_24)
- Clemson, C. M., Hall, L. L., Byron, M., McNeil, J., & Lawrence, J. B. (2006). The X chromosome is organized into a gene-rich outer rim and an internal core containing silenced nongenic sequences. *Proceedings of the National Academy of Sciences*, *103*(20), 7688 LP – 7693. <https://doi.org/10.1073/pnas.0601069103>
- Cook, A. W., Gough, R. E., & Toseland, C. P. (2020). Nuclear myosins – roles for molecular transporters and anchors. *Journal of Cell Science*, *133*(11), jcs242420. <https://doi.org/10.1242/jcs.242420>

- Cook, P. R. (2002). Predicting three-dimensional genome structure from transcriptional activity. *Nature Genetics*, 32(3), 347–352. <https://doi.org/10.1038/ng1102-347>
- Cooke, S. L., Ng, C. K. Y., Melnyk, N., Garcia, M. J., Hardcastle, T., Temple, J., Langdon, S., Huntsman, D., & Brenton, J. D. (2010). Genomic analysis of genetic heterogeneity and evolution in high-grade serous ovarian carcinoma. *Oncogene*, 29(35), 4905–4913. <https://doi.org/10.1038/onc.2010.245>
- Coticchia, C. M., Yang, J., & Moses, M. A. (2008). Ovarian cancer biomarkers: current options and future promise. *Journal of the National Comprehensive Cancer Network: JNCCN*, 6(8), 795–802. <https://doi.org/10.6004/jnccn.2008.0059>
- Cremer, C., Cremer, T., Zorn, C., & Schoeller, L. (1976). Effects of laser UV-microirradiation ( $\lambda = 2573 \text{ \AA}$ ) on proliferation of Chinese hamster cells. *Radiation Research*, 66(1), 106–121.
- Cremer, M., Küpper, K., Wagler, B., Wizelman, L., Hase, J. v., Weiland, Y., Kreja, L., Diebold, J., Speicher, M. R., & Cremer, T. (2003). Inheritance of gene density-related higher order chromatin arrangements in normal and tumor cell nuclei. *Journal of Cell Biology*, 162(5), 809–820. <https://doi.org/10.1083/jcb.200304096>
- Cremer, T., Kurz, A., Zirbel, R., Dietzel, S., Rinke, B., Schrock, E., Speicher, M. R., Mathieu, U., Jauch, A., Emmerich, P., Scherthan, H., Ried, T., Cremer, C., & Lichter, P. (1993). Role of chromosome territories in the functional compartmentalization of the cell nucleus. *Cold Spring Harbor Symposia on Quantitative Biology*, 58, 777–792. <https://doi.org/10.1101/SQB.1993.058.01.085>
- Cremer, Thomas, & Cremer, C. (2001). Chromosome territories, nuclear architecture and gene regulation in mammalian cells. *Nature Reviews Genetics*, 2(4), 292–301.
- Croft, J. A., Bridger, J. M., Boyle, S., Perry, P., Teague, P., & Bickmore, W. A. (1999). Differences in the Localization and Morphology of Chromosomes in the Human Nucleus. *Journal of Cell Biology*, 145(6), 1119–1131. <https://doi.org/10.1083/jcb.145.6.1119>
- Crosetto, N., & Bienko, M. (2020). Radial Organization in the Mammalian Nucleus. In *Frontiers in Genetics* (Vol. 11, p. 33). Frontiers Media S.A. <https://doi.org/10.3389/fgene.2020.00033>
- Dakubo, G. D. (2017). Ovarian Cancer Biomarkers in Circulation. In *Cancer Biomarkers in Body Fluids* (pp. 371–398). Springer International Publishing. [https://doi.org/10.1007/978-3-319-48360-3\\_13](https://doi.org/10.1007/978-3-319-48360-3_13)
- Davidson, P. M., Battistella, A., Déjardin, T., Betz, T., Plastino, J., Borghi, N., Cadot, B., & Sykes, C. (2020). Nesprin-2 accumulates at the front of the nucleus during confined cell migration. *EMBO Reports*, 21(7), e49910. <https://doi.org/10.15252/embr.201949910>
- De Lanerolle, P. (2012). Nuclear actin and myosins at a glance. *Journal of Cell Science*. <https://doi.org/10.1242/jcs.099754>
- De Lanerolle, P., Johnson, T., & Hofmann, W. A. (2005). Actin and myosin I in the nucleus: what next? *NATURE STRUCTURAL & MOLECULAR BIOLOGY*, 12(9). <https://doi.org/10.1038/nsmb983>
- De Lanerolle, P., & Serebryanny, L. (2011). Nuclear actin and myosins: Life without filaments. In *Nature Cell Biology*. <https://doi.org/10.1038/ncb2364>
- de las Heras, J. I., Batrakou, D. G., & Schirmer, E. C. (2013). Cancer biology and the nuclear envelope: A convoluted relationship. *Seminars in Cancer Biology*, 23(2), 125–137. <https://doi.org/https://doi.org/10.1016/j.semcancer.2012.01.008>
- Denais, C., & Lammerding, J. (2014). Nuclear mechanics in cancer. *Advances in Experimental Medicine and Biology*, 773, 435–470. [https://doi.org/10.1007/978-1-4899-8032-8\\_20](https://doi.org/10.1007/978-1-4899-8032-8_20)
- Deng, X., Ma, W., Ramani, V., Hill, A., Yang, F., Ay, F., Berletch, J. B., Blau, C. A., Shendure, J., Duan, Z., Noble, W. S., & Distèche, C. M. (2015). Bipartite structure of the inactive mouse X chromosome. *Genome Biology*, 16(1), 152. <https://doi.org/10.1186/s13059-015-0728-8>
- Dixon, J. R., Selvaraj, S., Yue, F., Kim, A., Li, Y., Shen, Y., Hu, M., Liu, J. S., & Ren, B. (2012). Topological domains in mammalian genomes identified by analysis of chromatin interactions. *Nature*, 485(7398), 376–380. <https://doi.org/10.1038/nature11082>
- Duan, G., Tang, Q., Yan, H., Xie, L., Wang, Y., Zheng, X. E., Zhuge, Y., Shen, S., Zhang, B., Zhang, X., Wang, J., Wang, W., & Zou, X. (2017). A Strategy to Delay the Development of Cisplatin Resistance by Maintaining a Certain Amount of Cisplatin-Sensitive Cells. *Scientific Reports*, 7(1), 432. <https://doi.org/10.1038/s41598-017-00422-2>
- Dundr, M. (2012). Nuclear bodies: multifunctional companions of the genome. *Current Opinion in Cell Biology*, 24(3), 415–422. <https://doi.org/10.1016/j.ceb.2012.03.010>
- Dundr, M., Ospina, J. K., Sung, M.-H., John, S., Upender, M., Ried, T., Hager, G. L., & Matera, A. G. (2007). Actin-dependent intranuclear repositioning of an active gene locus in vivo. *The Journal of Cell Biology*, 179(6), 1095–1103. <https://doi.org/10.1083/jcb.200710058>
- Dunn, T. A., Chen, S., Faith, D. A., Hicks, J. L., Platz, E. A., Chen, Y., Ewing, C. M., Sauvageot, J., Isaacs, W. B., De Marzo,

- A. M., & Luo, J. (2006). A novel role of myosin VI in human prostate cancer. *The American Journal of Pathology*, 169(5), 1843–1854. <https://doi.org/10.2353/ajpath.2006.060316>
- Ellis, L. M. (2006). Mechanisms of Action of Bevacizumab as a Component of Therapy for Metastatic Colorectal Cancer. *Seminars in Oncology*, 33(SUPPL. 10), S1–S7. <https://doi.org/10.1053/j.seminoncol.2006.08.002>
- Eng, K. H., Szender, J. B., Etter, J. L., Kaur, J., Poblete, S., Huang, R. Y., Zhu, Q., Grzesik, K. A., Battaglia, S., Cannioto, R., Krolewski, J. J., Zsiros, E., Frederick, P. J., Lele, S. B., Moysich, K. B., & Odunsi, K. O. (2018). Paternal lineage early onset hereditary ovarian cancers: A Familial Ovarian Cancer Registry study. *PLoS Genetics*, 14(2). <https://doi.org/10.1371/journal.pgen.1007194>
- Etter, J. L., Moysich, K., Kohli, S., Lele, S., Odunsi, K., & Eng, K. H. (2020). Transmission of X-linked Ovarian Cancer: Characterization and Implications. *Diagnostics*, 10(2), 90.
- Federico, C., Owoka, T., Ragusa, D., Sturiale, V., Caponnetto, D., Leotta, C. G., Bruno, F., Foster, H. A., Rigamonti, S., Giudici, G., Cazzaniga, G., Bridger, J. M., Sisu, C., Saccone, S., & Tosi, S. (2019). Deletions of chromosome 7q affect nuclear organization and HLXB9Gene expression in hematological disorders. *Cancers*, 11(4). <https://doi.org/10.3390/cancers11040585>
- Federico, C., Saccone, S., Andreozzi, L., Motta, S., Russo, V., Carels, N., & Bernardi, G. (2004). The pig genome: compositional analysis and identification of the gene-richest regions in chromosomes and nuclei. *Gene*, 343(2), 245–251.
- Fedorova, E., & Zink, D. (2008). Nuclear architecture and gene regulation. In *Biochimica et Biophysica Acta - Molecular Cell Research* (Vol. 1783, Issue 11, pp. 2174–2184). <https://doi.org/10.1016/j.bbamcr.2008.07.018>
- Fili, N., Hari-Gupta, Y., Aston, B., dos Santos, Á., Gough, R. E., Alamad, B., Wang, L., Martin-Fernandez, M. L., & Toseland, C. P. (2020). Competition between two high- And low-affinity protein-binding sites in myosin VI controls its cellular function. *Journal of Biological Chemistry*, 295(2), 337–347. <https://doi.org/10.1074/jbc.RA119.010142>
- Fili, N., Hari-Gupta, Y., dos Santos, Á., Cook, A., Poland, S., Ameer-Beg, S. M., Parsons, M., & Toseland, C. P. (2017). NDP52 activates nuclear myosin VI to enhance RNA polymerase II transcription. *Nature Communications*, 8(1), 1871. <https://doi.org/10.1038/s41467-017-02050-w>
- Fili, N., & Toseland, C. P. (2019). Unconventional Myosins: How Regulation Meets Function. *International Journal of Molecular Sciences*, 21(1), 67. <https://doi.org/10.3390/ijms21010067>
- Finlan, L. E., Sproul, D., Thomson, I., Boyle, S., Kerr, E., Perry, P., Ylstra, B., Chubb, J. R., & Bickmore, W. A. (2008). Recruitment to the Nuclear Periphery Can Alter Expression of Genes in Human Cells. *PLoS Genetics*, 4(3), e1000039–e1000039. <https://doi.org/10.1371/journal.pgen.1000039>
- Folker, E. S., Östlund, C., Luxton, G. W. G., Worman, H. J., & Gundersen, G. G. (2011). Lamin A variants that cause striated muscle disease are defective in anchoring transmembrane actin-associated nuclear lines for nuclear movement. *Proceedings of the National Academy of Sciences of the United States of America*, 108(1), 131–136. <https://doi.org/10.1073/pnas.1000824108>
- Foster, H. A., & Bridger, J. M. (2005). The genome and the nucleus: A marriage made by evolution. Genome organisation and nuclear architecture. In *Chromosoma* (Vol. 114, Issue 4, pp. 212–229). Springer. <https://doi.org/10.1007/s00412-005-0016-6>
- Freedman, R. S., Pihl, E., Kusyck, C., Gallager, H. S., & Rutledge, F. (1978). Characterization of an ovarian carcinoma cell line. *Cancer*, 42(5), 2352–2359. [https://doi.org/10.1002/1097-0142\(197811\)42:5<2352::AID-CNCR2820420536>3.0.CO;2-#](https://doi.org/10.1002/1097-0142(197811)42:5<2352::AID-CNCR2820420536>3.0.CO;2-#)
- Fritz, A. J., Barutcu, A. R., Martin-Buley, L., Van Wijnen, A. J., Zaidi, S. K., Imbalzano, A. N., Lian, J. B., Stein, J. L., & Stein, G. S. (2016). Chromosomes at Work: Organization of Chromosome Territories in the Interphase Nucleus. *Journal of Cellular Biochemistry*, 117(1), 9–19. <https://doi.org/10.1002/jcb.25280>
- Galiová, G., Bártová, E., & Kozubek, S. (2004). Nuclear topography of  $\beta$ -like globin gene cluster in IL-3-stimulated human leukemic K-562 cells. *Blood Cells, Molecules, and Diseases*, 33(1), 4–14. <https://doi.org/https://doi.org/10.1016/j.bcmd.2004.03.006>
- Garba, A. O., & Mousa, S. A. (2010). Bevasiranib for the Treatment of Wet, Age-Related Macular Degeneration. *Ophthalmology and Eye Diseases*, 2, OED.S4878. <https://doi.org/10.4137/oed.s4878>
- GIVLAARI® (givosiran) | Homepage. (n.d.). Retrieved August 8, 2020, from <https://www.givlaari.com/>
- Gonzalez-Sandoval, A., & Gasser, S. M. (2016). On TADs and LADs: Spatial Control Over Gene Expression. *Trends in Genetics*, 32(8), 485–495. <https://doi.org/10.1016/j.tig.2016.05.004>
- Gorkin, D. U., Leung, D., & Ren, B. (2014). The 3D genome in transcriptional regulation and pluripotency. In *Cell Stem Cell* (Vol. 14, Issue 6, pp. 762–775). Cell Press. <https://doi.org/10.1016/j.stem.2014.05.017>
- Grisham, R. N., Iyer, G., Garg, K., Delair, D., Hyman, D. M., Zhou, Q., Iasonos, A., Berger, M. F., Dao, F., Spriggs, D. R., Levine, D. A., Aghajanian, C., & Solit, D. B. (2013). BRAF Mutation is associated with early stage disease and



- improved outcome in patients with low-grade serous ovarian cancer. *Cancer*, 119(3), 548–554. <https://doi.org/10.1002/cncr.27782>
- Große-Berkenbusch, A., Hettich, J., Kuhn, T., Fili, N., Cook, A. W., Hari-Gupta, Y., Palmer, A., Streit, L., Ellis, P. J. I., Toseland, C. P., & Gebhardt, J. C. M. (2020). Myosin VI moves on nuclear actin filaments and supports long-range chromatin rearrangements. *BioRxiv*, 2020.04.03.023614. <https://doi.org/10.1101/2020.04.03.023614>
- Grummt, I. (2006). Actin and myosin as transcription factors. *Current Opinion in Genetics & Development*, 16(2), 191–196. <https://doi.org/https://doi.org/10.1016/j.gde.2006.02.001>
- Guelen, L., Pagie, L., Brasset, E., Meuleman, W., Faza, M. B., Talhout, W., Eussen, B. H., de Klein, A., Wessels, L., de Laat, W., & van Steensel, B. (2008). Domain organization of human chromosomes revealed by mapping of nuclear lamina interactions. *Nature*, 453(7197), 948–951. <https://doi.org/10.1038/nature06947>
- Guinde, J., Frankel, D., Perrin, S., Delecourt, V., Lévy, N., Barlesi, F., Astoul, P., Roll, P., & Kaspi, E. (2018). Lamins in Lung Cancer: Biomarkers and Key Factors for Disease Progression through miR-9 Regulation? *Cells*, 7(7), 78. <https://doi.org/10.3390/cells7070078>
- Habermann, F. A., Cremer, M., Walter, J., Kreth, G., Von Hase, J., Bauer, K., Wienberg, J., Cremer, C., Cremer, T., & Solovei, I. (2001). Arrangements of macro- and microchromosomes in chicken cells. *Chromosome Research*, 9(7), 569–584.
- Harada, T., Swift, J., Irianto, J., Shin, J.-W., Spinler, K. R., Athirasala, A., Diegmiller, R., Dingal, P. C. D. P., Ivanovska, I. L., & Discher, D. E. (2014). Nuclear lamin stiffness is a barrier to 3D migration, but softness can limit survival. *The Journal of Cell Biology*, 204(5), 669–682. <https://doi.org/10.1083/jcb.201308029>
- Hari-Gupta, Y., Fili, N., dos Santos, Á., Cook, A. W., Gough, R. E., Reed, H. C. W., Wang, L., Aaron, J., Venit, T., Wait, E., Grosse-Berkenbusch, A., Gebhardt, J. C. M., Percipalle, P., Chew, T.-L., Martin-Fernandez, M., & Toseland, C. P. (2020). Nuclear myosin VI regulates the spatial organization of mammalian transcription initiation. *BioRxiv*, 2020.04.21.053124. <https://doi.org/10.1101/2020.04.21.053124>
- Harničarová, A., Kozubek, S., Pacherník, J., Krejčí, J., & Bártová, E. (2006). Distinct nuclear arrangement of active and inactive c-myc genes in control and differentiated colon carcinoma cells. *Experimental Cell Research*, 312(20), 4019–4035. <https://doi.org/https://doi.org/10.1016/j.yexcr.2006.09.007>
- Hassan-Ahmed, M. M. (2013). *Discovery and Restoration of Aberrant Nuclear Structure and Genome Behaviour in Breast Cancer Cells*.
- Heard, E., & Bickmore, W. (2007). The ins and outs of gene regulation and chromosome territory organisation. *Current Opinion in Cell Biology*, 19(3), 311–316. <https://doi.org/https://doi.org/10.1016/j.ceb.2007.04.016>
- Hernandez, L., Kim, M. K., Lyle, L. T., Bunch, K. P., House, C. D., Ning, F., Noonan, A. M., & Annunziata, C. M. (2016). Characterization of ovarian cancer cell lines as in vivo models for preclinical studies. *Gynecologic Oncology*, 142(2), 332–340. <https://doi.org/10.1016/j.ygyno.2016.05.028>
- Heun, P., Laroche, T., Shimada, K., Furrer, P., & Gasser, S. M. (2001). Chromosome Dynamics in the Yeast Interphase Nucleus. *Science*, 294(5549), 2181 LP – 2186. <https://doi.org/10.1126/science.1065366>
- Hoffman, B., & Liebermann, D. A. (2008). Apoptotic signaling by c-MYC. In *Oncogene* (Vol. 27, Issue 50, pp. 6462–6472). Nature Publishing Group. <https://doi.org/10.1038/onc.2008.312>
- Hofmann, W. A., Johnson, T., Klapczynski, M., Fan, J.-L., & de Lanerolle, P. (2006). From transcription to transport: emerging roles for nuclear myosin I This paper is one of a selection of papers published in this Special Issue, entitled 27th International West Coast Chromatin and Chromosome Conference, and has undergone the Journal's usual peer review process. *Biochemistry and Cell Biology*, 84(4), 418–426. <https://doi.org/10.1139/o06-069>
- Hofmann, W. A., Stojiljkovic, L., Fuchsova, B., Vargas, G. M., Mavrommatis, E., Philimonenko, V., Kysela, K., Goodrich, J. A., Lessard, J. L., Hope, T. J., Hozak, P., & de Lanerolle, P. (2004). Actin is part of pre-initiation complexes and is necessary for transcription by RNA polymerase II. *Nature Cell Biology*, 6(11), 1094–1101. <https://doi.org/10.1038/ncb1182>
- Holaska, J. M., & Wilson, K. L. (2006). Multiple roles for emerin: Implications for Emery-Dreifuss muscular dystrophy. *The Anatomical Record Part A: Discoveries in Molecular, Cellular, and Evolutionary Biology: An Official Publication of the American Association of Anatomists*, 288(7), 676–680.
- Home | ONPATTRO® (patisiran) lipid complex injection 10 mg/5 mL. (n.d.). Retrieved August 8, 2020, from <https://www.onpattro.com/>
- Homepage | Figo. (n.d.). Retrieved July 30, 2020, from <https://www.figo.org/>
- Hu, Q., Kwon, Y.-S., Nunez, E., Cardamone, M. D., Hutt, K. R., Ohgi, K. A., Garcia-Bassets, I., Rose, D. W., Glass, C. K., Rosenfeld, M. G., & Fu, X.-D. (2008). Enhancing nuclear receptor-induced transcription requires nuclear motor and LSD1-dependent gene networking in interchromatin granules. *Proceedings of the National Academy of Sciences of the United States of America*, 105(49), 19199–19204. <https://doi.org/10.1073/pnas.0810634105>



- Ibarra, A., & Hetzer, M. W. (2015). Nuclear pore proteins and the control of genome functions. *Genes & Development*, 29(4), 337–349. <https://doi.org/10.1101/gad.256495.114>
- Iorns, E., Lord, C. J., Turner, N., & Ashworth, A. (2007). Utilizing RNA interference to enhance cancer drug discovery. *Nature Reviews Drug Discovery*, 6(7), 556–568. <https://doi.org/10.1038/nrd2355>
- Iqbal, N., & Iqbal, N. (2014). Human Epidermal Growth Factor Receptor 2 (HER2) in Cancers: Overexpression and Therapeutic Implications. *Molecular Biology International*, 2014. <https://doi.org/10.1155/2014/852748>
- Irianto, J., Pfeifer, C. R., Ivanovska, I. L., Swift, J., & Discher, D. E. (2016). Nuclear lamins in cancer. *Cellular and Molecular Bioengineering*, 9(2), 258–267. <https://doi.org/10.1007/s12195-016-0437-8>
- Ishii, K., Arib, G., Lin, C., Van Houwe, G., & Laemmli, U. K. (2002). Chromatin Boundaries in Budding Yeast: The Nuclear Pore Connection. *Cell*, 109(5), 551–562. [https://doi.org/https://doi.org/10.1016/S0092-8674\(02\)00756-0](https://doi.org/https://doi.org/10.1016/S0092-8674(02)00756-0)
- Jayson, G. C., Kohn, E. C., Kitchener, H. C., & Lederemann, J. A. (2014). Ovarian cancer. *The Lancet*, 384(9951), 1376–1388. [https://doi.org/https://doi.org/10.1016/S0140-6736\(13\)62146-7](https://doi.org/https://doi.org/10.1016/S0140-6736(13)62146-7)
- Jowhar, Z., Shachar, S., Gudla, P. R., Wangsa, D., Torres, E., Russ, J. L., Pegoraro, G., Ried, T., Raznahan, A., & Misteli, T. (2018). Effects of human sex chromosome dosage on spatial chromosome organization. *Molecular Biology of the Cell*, 29(20), 2458–2469. <https://doi.org/10.1091/mbc.E18-06-0359>
- Kapoor, A., Barai, A., Thakur, B., Das, A., Patwardhan, S. R., Monteiro, M., Gaikwad, S., Bukhari, A. B., Mogha, P., Majumder, A., De, A., Ray, P., & Sen, S. (2018). Soft drug-resistant ovarian cancer cells migrate via two distinct mechanisms utilizing myosin II-based contractility. *Biochimica et Biophysica Acta (BBA) - Molecular Cell Research*, 1865(2), 392–405. <https://doi.org/https://doi.org/10.1016/j.bbamcr.2017.11.012>
- Kazanets, A., Shorstova, T., Hilmi, K., Marques, M., & Witcher, M. (2016). Epigenetic silencing of tumor suppressor genes: Paradigms, puzzles, and potential. *Biochimica et Biophysica Acta (BBA) - Reviews on Cancer*, 1865(2), 275–288. <https://doi.org/https://doi.org/10.1016/j.bbcan.2016.04.001>
- Kelland, L. (2007). The resurgence of platinum-based cancer chemotherapy. *Nature Reviews Cancer*, 7(8), 573–584.
- Kelley, M. R., Logsdon, D., & Fishel, M. L. (2014). Targeting DNA repair pathways for cancer treatment: What's new? In *Future Oncology* (Vol. 10, Issue 7, pp. 1215–1237). Future Medicine Ltd. <https://doi.org/10.2217/fon.14.60>
- Kim, S. H., McQueen, P. G., Lichtman, M. K., Shevach, E. M., Parada, L. A., & Misteli, T. (2004). Spatial genome organization during T-cell differentiation. *Cytogenetic and Genome Research*, 105(2–4), 292–301. <https://doi.org/10.1159/000078201>
- Kosak, S. T., Skok, J. A., Medina, K. L., Riblet, R., Le Beau, M. M., Fisher, A. G., & Singh, H. (2002). Subnuclear Compartmentalization of Immunoglobulin Loci During Lymphocyte Development. *Science*, 296(5565), 158 LP – 162. <https://doi.org/10.1126/science.1068768>
- Kozar, I., Margue, C., Rothengatter, S., Haan, C., & Kreis, S. (2019). Many ways to resistance: How melanoma cells evade targeted therapies. *Biochimica et Biophysica Acta (BBA) - Reviews on Cancer*, 1871(2), 313–322. <https://doi.org/https://doi.org/10.1016/j.bbcan.2019.02.002>
- Kuga, T., Nie, H., Kazami, T., Satoh, M., Matsushita, K., Nomura, F., Maeshima, K., Nakayama, Y., & Tomonaga, T. (2014). Lamin B2 prevents chromosome instability by ensuring proper mitotic chromosome segregation. *Oncogenesis*, 3(3), e94–e94. <https://doi.org/10.1038/oncsis.2014.6>
- Kulashreshtha, M., Mehta, I. S., Kumar, P., & Rao, B. J. (2016). Chromosome territory relocation during DNA repair requires nuclear myosin 1 recruitment to chromatin mediated by  $\gamma$ -H2AX signaling. *Nucleic Acids Research*, 44(17), 8272–8291. <https://doi.org/10.1093/nar/gkw573>
- Kumaran, R. I., & Spector, D. L. (2008). A genetic locus targeted to the nuclear periphery in living cells maintains its transcriptional competence. *The Journal of Cell Biology*, 180(1), 51–65. <https://doi.org/10.1083/jcb.200706060>
- Küpper, K., Kölbl, A., Biener, D., Dittrich, S., von Hase, J., Thormeyer, T., Fiegler, H., Carter, N. P., Speicher, M. R., Cremer, T., & Cremer, M. (2007). Radial chromatin positioning is shaped by local gene density, not by gene expression. *Chromosoma*, 116(3), 285–306. <https://doi.org/10.1007/s00412-007-0098-4>
- Kurz, A., Lampel, S., Nickolenko, J. E., Bradl, J., Benner, A., Zirbel, R. M., Cremer, T., & Lichter, P. (1996). Active and inactive genes localize preferentially in the periphery of chromosome territories. *Journal of Cell Biology*, 135(5), 1195–1205.
- Langcôt, C., Cheutin, T., Cremer, M., Cavalli, G., & Cremer, T. (2007). Dynamic genome architecture in the nuclear space: regulation of gene expression in three dimensions. *Nature Reviews Genetics*, 8(2), 104–115. <https://doi.org/10.1038/nrg2041>
- Langdon, S. P., Lawrie, S. S., Hay, F. G., Hawkes, M. M., McDonald, A., Hayward, I. P., Schol, D. J., Hilgers, J., Leonard, R. C. F., & Smyth, J. F. (1988). Characterization and Properties of Nine Human Ovarian Adenocarcinoma Cell Lines. *Cancer Research*, 48(21), 6166 LP – 6172. <http://cancerres.aacrjournals.org/content/48/21/6166.abstract>

- Laskowski, A. I., Neems, D. S., Laster, K., Strojny-Okyere, C., Rice, E. L., Konieczna, I. M., Voss, J. H., Mathew, J. M., Leventhal, J. R., Ramsey-Goldman, R., Smith, E. D., & Kosak, S. T. (2019). Varying levels of X chromosome coalescence in female somatic cells alters the balance of X-linked dosage compensation and is implicated in female-dominant systemic lupus erythematosus. *Scientific Reports*, 9(1), 8011. <https://doi.org/10.1038/s41598-019-44229-9>
- Leshner, M., Devine, M., Roloff, G. W., True, L. D., Misteli, T., & Meaburn, K. J. (2016). Locus-specific gene repositioning in prostate cancer. *Molecular Biology of the Cell*, 27(2), 236–246. <https://doi.org/10.1091/mbc.E15-05-0280>
- Lever, E., & Sheer, D. (2010). The role of nuclear organization in cancer. *The Journal of Pathology*, 220(2), 114–125. <https://doi.org/10.1002/path.2651>
- Lheureux, S., Braunstein, M., & Oza, A. M. (2019). Epithelial ovarian cancer: Evolution of management in the era of precision medicine. *CA: A Cancer Journal for Clinicians*, 69(4), 280–304. <https://doi.org/10.3322/caac.21559>
- Li, Y.-R., & Yang, W.-X. (2016). Myosin superfamily: The multi-functional and irreplaceable factors in spermatogenesis and testicular tumors. *Gene*, 576(1, Part 2), 195–207. <https://doi.org/https://doi.org/10.1016/j.gene.2015.10.022>
- Liao, D. J., Du, Q., Yu, B. W., Grignon, D., & Sarkar, F. H. (2003). Novel Perspective: Focusing on the X Chromosome in Reproductive Cancers. *Cancer Investigation*, 21(4), 641–658. <https://doi.org/10.1081/CNV-120022385>
- Lieberman-Aiden, E., Van Berkum, N. L., Williams, L., Imakaev, M., Ragoczy, T., Telling, A., Amit, I., Lajoie, B. R., Sabo, P. J., Dorschner, M. O., Sandstrom, R., Bernstein, B., Bender, M. A., Groudine, M., Gnirke, A., Stamatoyannopoulos, J., Mirny, L. A., Lander, E. S., & Dekker, J. (2009). Comprehensive mapping of long-range interactions reveals folding principles of the human genome. *Science*, 326(5950), 289–293. <https://doi.org/10.1126/science.1181369>
- Lindsay, A. J., & McCaffrey, M. W. (2009). Myosin Vb localises to nucleoli and associates with the RNA polymerase I transcription complex. *Cell Motility and the Cytoskeleton*, 66(12), 1057–1072. <https://doi.org/10.1002/cm.20408>
- Lodish, H., Berk, A., Zipursky, S. L., Matsudaira, P., Baltimore, D., & Darnell, J. (2000). *Myosin: The Actin Motor Protein*. <https://www.ncbi.nlm.nih.gov/books/NBK21724/>
- Luxton, G. W. G., Gomes, E. R., Folker, E. S., Vintinner, E., & Gundersen, G. G. (2010). Linear arrays of nuclear envelope proteins harness retrograde actin flow for nuclear movement. *Science*, 329(5994), 956–959.
- Mahy, N. L., Perry, P. E., & Bickmore, W. A. (2002). Gene density and transcription influence the localization of chromatin outside of chromosome territories detectable by FISH. *The Journal of Cell Biology*, 159(5), 753–763. <https://doi.org/10.1083/jcb.200207115>
- Maly, I. V., Domaradzki, T. M., Gosy, V. A., & Hofmann, W. A. (2017). Myosin isoform expressed in metastatic prostate cancer stimulates cell invasion. *Scientific Reports*, 7(1), 8476. <https://doi.org/10.1038/s41598-017-09158-5>
- Marenduzzo, D., Micheletti, C., & Cook, P. R. (2006). Entropy-Driven Genome Organization. *Biophysical Journal*, 90(10), 3712–3721. <https://doi.org/https://doi.org/10.1529/biophysj.105.077685>
- Matsuo, K., Lin, Y. G., Roman, L. D., & Sood, A. K. (2010). Overcoming platinum resistance in ovarian carcinoma. In *Expert Opinion on Investigational Drugs* (Vol. 19, Issue 11, pp. 1339–1354). NIH Public Access. <https://doi.org/10.1517/13543784.2010.515585>
- Mavaddat, N., Peock, S., Frost, D., Ellis, S., Platte, R., Fineberg, E., Evans, D. G., Izatt, L., Eeles, R. A., Adlard, J., Davidson, R., Eccles, D., Cole, T., Cook, J., Brewer, C., Tischkowitz, M., Douglas, F., Hodgson, S., Walker, L., ... Easton, D. F. (2013). Cancer risks for BRCA1 and BRCA2 mutation carriers: Results from prospective analysis of EMBRACE. *Journal of the National Cancer Institute*. <https://doi.org/10.1093/jnci/djt095>
- Mayer, R., Brero, A., von Hase, J., Schroeder, T., Cremer, T., & Dietzel, S. (2005). Common themes and cell type specific variations of higher order chromatin arrangements in the mouse. *BMC Cell Biology*, 6, 44. <https://doi.org/10.1186/1471-2121-6-44>
- McDermott, M., Eustace, A. J., Busschots, S., Breen, L., Crown, J., Clynes, M., O'Donovan, N., & Stordal, B. (2014). In vitro Development of Chemotherapy and Targeted Therapy Drug-Resistant Cancer Cell Lines: A Practical Guide with Case Studies. *Frontiers in Oncology*, 4, 40. <https://doi.org/10.3389/fonc.2014.00040>
- McGurk, L., Tzolovsky, G., Spears, N., & Bownes, M. (2006). The temporal and spatial expression pattern of Myosin Va, Vb and VI in the mouse ovary. *Gene Expression Patterns*, 6(8), 900–907. <https://doi.org/https://doi.org/10.1016/j.modgep.2006.03.002>
- Meaburn, K. J. (2016). Spatial Genome Organization and Its Emerging Role as a Potential Diagnosis Tool. *Frontiers in Genetics*, 7, 134. <https://doi.org/10.3389/fgene.2016.00134>
- Meaburn, K. J., Cabuy, E., Bonne, G., Levy, N., Morris, G. E., Novelli, G., Kill, I. R., & Bridger, J. M. (2007). Primary laminopathy fibroblasts display altered genome organization and apoptosis. *Aging Cell*, 6(2), 139–153.
- Meaburn, K. J., Gudla, P. R., Khan, S., Lockett, S. J., & Misteli, T. (2009). Disease-specific gene repositioning in breast cancer. *Journal of Cell Biology*, 187(6), 801–812. <https://doi.org/10.1083/jcb.200909127>

- Meaburn, K. J., & Misteli, T. (2008). Locus-specific and activity-independent gene repositioning during early tumorigenesis. *The Journal of Cell Biology*, *180*(1), 39–50. <https://doi.org/10.1083/jcb.200708204>
- Mehta, I. S., Amira, M., Harvey, A. J., & Bridger, J. M. (2010). Rapid chromosome territory relocation by nuclear motor activity in response to serum removal in primary human fibroblasts. *Genome Biology*, *11*(1), R5. <https://doi.org/10.1186/gb-2010-11-1-r5>
- Mehta, I. S., Elcock, L. S., Amira, M., Kill, I. R., & Bridger, J. M. (2008). Nuclear motors and nuclear structures containing A-type lamins and emerin: Is there a functional link? *Biochemical Society Transactions*, *36*(6), 1384–1388. <https://doi.org/10.1042/BST0361384>
- Mehta, I. S., Eskiw, C. H., Arican, H. D., Kill, I. R., & Bridger, J. M. (2011). Farnesyltransferase inhibitor treatment restores chromosome territory positions and active chromosome dynamics in Hutchinson-Gilford progeria syndrome cells. *Genome Biology*. <https://doi.org/10.1186/gb-2011-12-8-r74>
- Mehta, I. S., Figgitt, M., Clements, C. S., Kill, I. R., & Bridger, J. M. (2007). Alterations to nuclear architecture and genome behavior in senescent cells. *Annals of the New York Academy of Sciences*. <https://doi.org/10.1196/annals.1395.027>
- Minotti, G., Menna, P., Salvatorelli, E., Cairo, G., & Gianni, L. (2004). Anthracyclines: Molecular advances and pharmacologic developments in antitumor activity and cardiotoxicity. In *Pharmacological Reviews* (Vol. 56, Issue 2, pp. 185–229). American Society for Pharmacology and Experimental Therapeutics. <https://doi.org/10.1124/pr.56.2.6>
- Misteli, T. (2007). Beyond the Sequence: Cellular Organization of Genome Function. In *Cell* (Vol. 128, Issue 4, pp. 787–800). Elsevier. <https://doi.org/10.1016/j.cell.2007.01.028>
- Misteli, T., & Soutoglou, E. (2009). The emerging role of nuclear architecture in DNA repair and genome maintenance. *Nature Reviews Molecular Cell Biology*, *10*(4), 243–254. <https://doi.org/10.1038/nrm2651>
- Mitelman, F., Johansson, B., & Mertens, F. (2007). The impact of translocations and gene fusions on cancer causation. In *Nature Reviews Cancer* (Vol. 7, Issue 4, pp. 233–245). Nat Rev Cancer. <https://doi.org/10.1038/nrc2091>
- Mooseker, M. S., & Foth, B. J. (2007). The Structural And Functional Diversity Of The Myosin Family Of Actin-Based Molecular Motors. In *Myosins* (pp. 1–34). Springer Netherlands. [https://doi.org/10.1007/978-1-4020-6519-4\\_1](https://doi.org/10.1007/978-1-4020-6519-4_1)
- Mucinous Adenocarcinoma of Ovary*. (n.d.). Retrieved July 30, 2020, from <https://www.dovemed.com/diseases-conditions/mucinous-adenocarcinoma-ovary/>
- Murata, S., Nakazawa, T., Ohno, N., Terada, N., Iwashina, M., Mochizuki, K., Kondo, T., Nakamura, N., Yamane, T., Iwasa, S., Ohno, S., & Katoh, R. (2007). Conservation and Alteration of Chromosome Territory Arrangements in Thyroid Carcinoma Cell Nuclei. *Thyroid*, *17*(6), 489–496. <https://doi.org/10.1089/thy.2006.0328>
- Naora, H., & Montell, D. J. (2005). Ovarian Cancer Metastasis: Integrating insights from disparate model organisms. *Nature Reviews Cancer*, *5*(5), 355–366. <https://doi.org/10.1038/nrc1611>
- National Ovarian Cancer Coalition*. (n.d.). Retrieved July 30, 2020, from <http://ovarian.org/>
- NCBI's genome browser for human (Homo sapiens) - Genome Data Viewer*. (n.d.). Retrieved August 4, 2020, from <https://www.ncbi.nlm.nih.gov/genome/gdv/>
- Neupane, M., Clark, A. P., Landini, S., Birkbak, N. J., Eklund, A. C., Lim, E., Culhane, A. C., Barry, W. T., Schumacher, S. E., Beroukhi, R., Szallasi, Z., Vidal, M., Hill, D. E., & Silver, D. P. (2016). MECP2 Is a Frequently Amplified Oncogene with a Novel Epigenetic Mechanism That Mimics the Role of Activated RAS in Malignancy. *Cancer Discovery*, *6*(1), 45–58. <https://doi.org/10.1158/2159-8290.CD-15-0341>
- NICE | The National Institute for Health and Care Excellence*. (n.d.). Retrieved July 30, 2020, from <https://www.nice.org.uk/>
- Noma, K., Cam, H. P., Maraia, R. J., & Grewal, S. I. S. (2006). A role for TFIIC transcription factor complex in genome organization. *Cell*, *125*(5), 859–872. <https://doi.org/https://doi.org/10.1016/j.cell.2006.04.028>
- Norouzi-Barough, L., Sarookhani, M. R., Sharifi, M., Moghbelinejad, S., Jangjoo, S., & Salehi, R. (2018). Molecular mechanisms of drug resistance in ovarian cancer. *Journal of Cellular Physiology*, *233*(6), 4546–4562. <https://doi.org/10.1002/jcp.26289>
- Orszynowicz, M., Lechniak, D., Pawlak, P., Kociucka, B., Kubickova, S., Cernohorska, H., & Madeja, Z. E. (2017). Changes in chromosome territory position within the nucleus reflect alternations in gene expression related to embryonic lineage specification. *PLOS ONE*, *12*(8), e0182398. <https://doi.org/10.1371/journal.pone.0182398>
- Osmanagic-Myers, S., Dechat, T., & Foisner, R. (2015). Lamins at the crossroads of mechanosignaling. *Genes & Development*, *29*(3), 225–237. <https://doi.org/10.1101/gad.255968.114>
- Ouderkirk, J. L., & Krendel, M. (2014). Non-muscle myosins in tumor progression, cancer cell invasion, and metastasis. In *Cytoskeleton* (Vol. 71, Issue 8, pp. 447–463). John Wiley and Sons Inc. <https://doi.org/10.1002/cm.21187>
- Ovarian, Fallopian Tube, and Primary Peritoneal Cancer—Patient Silver - National Cancer Institute*. (n.d.). Retrieved July 30, 2020, from <https://www.cancer.gov/types/ovarian>

- Ovarian cancer | Cancer Research UK. (n.d.). Retrieved July 30, 2020, from <https://www.cancerresearchuk.org/about-cancer/ovarian-cancer>
- Ovarian cancer | Target Ovarian Cancer charity. (n.d.). Retrieved July 30, 2020, from <https://www.targetovariancancer.org.uk/>
- Pageau, G. J., Hall, L. L., Ganesan, S., Livingston, D. M., & Lawrence, J. B. (2007). The disappearing Barr body in breast and ovarian cancers. *Nature Reviews Cancer*, 7(8), 628–633. <https://doi.org/10.1038/nrc2172>
- Palaia, I., Tomao, F., Santangelo, G., Di Pinto, A., Sassu, C. M., Perniola, G., Musella, A., Di Donato, V., Giancotti, A., & Benedetti Panici, P. (2019). The EOLO (End-of-Life Ovarian Cancer) Study: Approach to ovarian cancer patients at the end of life. *Oncology (Switzerland)*, 97(5), 306–310. <https://doi.org/10.1159/000501721>
- Penner-Goeke, S., Lichtensztejn, Z., Neufeld, M., Ali, J. L., Altman, A. D., Nachtigal, M. W., & McManus, K. J. (2017). The temporal dynamics of chromosome instability in ovarian cancer cell lines and primary patient samples. *PLOS Genetics*, 13(4), e1006707. <https://doi.org/10.1371/journal.pgen.1006707>
- Percipalle, P., Fomproix, N., Cavellán, E., Voit, R., Reimer, G., Krüger, T., Thyberg, J., Scheer, U., Grummt, I., & Farrants, A.-K. O. (2006). The chromatin remodelling complex WSTF-SNF2h interacts with nuclear myosin 1 and has a role in RNA polymerase I transcription. *EMBO Reports*, 7(5), 525–530. <https://doi.org/10.1038/sj.embor.7400657>
- Peric-Hupkes, D., Meuleman, W., Pagie, L., Bruggeman, S. W. M., Solovei, I., Brugman, W., Gräf, S., Flicek, P., Kerkhoven, R. M., van Lohuizen, M., Reinders, M., Wessels, L., & van Steensel, B. (2010). Molecular maps of the reorganization of genome-nuclear lamina interactions during differentiation. *Molecular Cell*, 38(4), 603–613. <https://doi.org/10.1016/j.molcel.2010.03.016>
- Perren, T. J., Swart, A. M., Pfisterer, J., Ledermann, J. A., Pujade-Lauraine, E., Kristensen, G., Carey, M. S., Beale, P., Cervantes, A., Kurzeder, C., Bois, A. du, Sehouli, J., Kimmig, R., Stähle, A., Collinson, F., Essapen, S., Gourley, C., Lortholary, A., Selle, F., ... Oza, A. M. (2011). A Phase 3 Trial of Bevacizumab in Ovarian Cancer. *New England Journal of Medicine*, 365(26), 2484–2496. <https://doi.org/10.1056/NEJMoa1103799>
- Pestic-Dravovich, L., Stojiljkovic, L., Philimonenko, A. A., Nowak, G., Ke, Y., Settlage, R. E., Shabanowitz, J., Hunt, D. F., Hozak, P., & de Lanerolle, P. (2000). A Myosin I Isoform in the Nucleus. *Science*, 290(5490), 337 LP – 341. <https://doi.org/10.1126/science.290.5490.337>
- Philimonenko, V. V., Janáček, J., Harata, M., & Hozák, P. (2010). Transcription-dependent rearrangements of actin and nuclear myosin i in the nucleolus. *Histochemistry and Cell Biology*, 134(3), 243–249. <https://doi.org/10.1007/s00418-010-0732-8>
- Pickersgill, H., Kalverda, B., de Wit, E., Talhout, W., Fornerod, M., & van Steensel, B. (2006). Characterization of the *Drosophila melanogaster* genome at the nuclear lamina. *Nature Genetics*, 38(9), 1005–1014. <https://doi.org/10.1038/ng1852>
- Plunkett, W., Huang, P., Xu, Y. Z., Heinemann, V., Grunewald, R., & Gandhi, V. (1995). Gemcitabine: Metabolism, mechanisms of action, and self-potentialiation. *Seminars in Oncology*, 22(4 SUPPL. 11), 3–10. <https://europepmc.org/article/med/7481842>
- Pranchevicius, M. C. S., Baqui, M. M. A., Ishikawa-Ankerhold, H. C., Lourenço, E. V., Leão, R. M., Banzi, S. R., Dos Santos, C. T., Barreira, M. C. R., Esprefico, E. M., & Larson, R. E. (2008). Myosin Va phosphorylated on Ser1650 is found in nuclear speckles and redistributes to nucleoli upon inhibition of transcription. *Cell Motility and the Cytoskeleton*. <https://doi.org/10.1002/cm.20269>
- Prat, J., Ribé, A., & Gallardo, A. (2005). Hereditary ovarian cancer. *Human Pathology*, 36(8), 861–870.
- Rabl Cerng, C. (1885). über Zellteilung. *Morphol Jahrb*, 10, 214–330.
- Ragoczy, T., Telling, A., Sawado, T., Groudine, M., & Kosak, S. T. (2003). A genetic analysis of chromosome territory looping: diverse roles for distal regulatory elements. *Chromosome Research*, 11(5), 513–525. <https://doi.org/10.1023/A:1024939130361>
- Ranade, D., Koul, S., Thompson, J., Prasad, K. B., & Sengupta, K. (2017). Chromosomal aneuploidies induced upon Lamin B2 depletion are mislocalized in the interphase nucleus. *Chromosoma*, 126(2), 223–244. <https://doi.org/10.1007/s00412-016-0580-y>
- Ranade, D., Pradhan, R., Jayakrishnan, M., Hegde, S., & Sengupta, K. (2019). Lamin A/C and Emerin depletion impacts chromatin organization and dynamics in the interphase nucleus. *BMC Molecular and Cell Biology*, 20(1), 11. <https://doi.org/10.1186/s12860-019-0192-5>
- Randise-Hinchliff, C., & Brickner, J. H. (2016). Transcription factors dynamically control the spatial organization of the yeast genome. *Nucleus*, 7(4), 369–374.
- Rao, S. S. P., Huntley, M. H., Durand, N. C., Stamenova, E. K., Bochkov, I. D., Robinson, J. T., Sanborn, A. L., Machol, I., Omer, A. D., Lander, E. S., & Aiden, E. L. (2014). A 3D Map of the Human Genome at Kilobase Resolution Reveals Principles of Chromatin Looping. *Cell*, 159(7), 1665–1680. <https://doi.org/10.1016/j.cell.2014.11.021>

- Reck-Peterson, S. L., Novick, P. J., & Mooseker, M. S. (1999). The tail of a yeast class V myosin, myo2p, functions as a localization domain. *Molecular Biology of the Cell*, *10*(4), 1001–1017. <https://doi.org/10.1091/mbc.10.4.1001>
- Reis-Sobreiro, M., Chen, J.-F., Novitskaya, T., You, S., Morley, S., Steadman, K., Gill, N. K., Eskaros, A., Rotinen, M., Chu, C.-Y., Chung, L. W. K., Tanaka, H., Yang, W., Knudsen, B. S., Tseng, H.-R., Rowat, A. C., Posadas, E. M., Zijlstra, A., Di Vizio, D., & Freeman, M. R. (2018). Emerin Deregulation Links Nuclear Shape Instability to Metastatic Potential. *Cancer Research*, *78*(21), 6086 LP – 6097. <https://doi.org/10.1158/0008-5472.CAN-18-0608>
- Reyes-González, J. M., Armaiz-Peña, G. N., Mangala, L. S., Valiyeva, F., Ivan, C., Pradeep, S., Echevarría-Vargas, I. M., Rivera-Reyes, A., Sood, A. K., & Vivas-Mejía, P. E. (2015). Targeting c-MYC in platinum-resistant ovarian cancer. *Molecular Cancer Therapeutics*. <https://doi.org/10.1158/1535-7163.MCT-14-0801>
- Roberts, R., Lister, I., Schmitz, S., Walker, M., Veigel, C., Trinick, J., Buss, F., & Kendrick-Jones, J. (2004). Myosin VI: cellular functions and motor properties. *Philosophical Transactions of the Royal Society of London. Series B, Biological Sciences*, *359*(1452), 1931–1944. <https://doi.org/10.1098/rstb.2004.1563>
- Roix, J. J., McQueen, P. G., Munson, P. J., Parada, L. A., & Misteli, T. (2003). Spatial proximity of translocation-prone gene loci in human lymphomas. *Nature Genetics*, *34*(3), 287–291. <https://doi.org/10.1038/ng1177>
- Roschke, A. V., Stover, K., Tonon, G., Schäffer, A. A., & Kirsch, I. R. (2002). Stable karyotypes in epithelial cancer cell lines despite high rates of ongoing structural and numerical chromosomal instability. *Neoplasia (New York, N.Y.)*, *4*(1), 19–31. <https://doi.org/10.1038/sj.neo.7900197>
- Ross, M. T., Grafham, D. V., Coffey, A. J., Scherer, S., McLay, K., Muzny, D., Platzer, M., Howell, G. R., Burrows, C., Bird, C. P., Frankish, A., Lovell, F. L., Howe, K. L., Ashurst, J. L., Fulton, R. S., Sudbrak, R., Wen, G., Jones, M. C., Hurles, M. E., ... Bentley, D. R. (2005). The DNA sequence of the human X chromosome. *Nature*, *434*(7031), 325–337. <https://doi.org/10.1038/nature03440>
- Rout, M. P., Aitchison, J. D., Suprpto, A., Hjertaas, K., Zhao, Y., & Chait, B. T. (2000). The yeast nuclear pore complex: Composition, architecture, transport mechanism. *Journal of Cell Biology*. <https://doi.org/10.1083/jcb.148.4.635>
- Roy, R., Chun, J., & Powell, S. N. (2012). BRCA1 and BRCA2: Different roles in a common pathway of genome protection. In *Nature Reviews Cancer*. <https://doi.org/10.1038/nrc3181>
- Saad, M., Garbuzenko, O. B., & Minko, T. (2008). Co-delivery of siRNA and an anticancer drug for treatment of multidrug-resistant cancer. *Nanomedicine*, *3*(6), 761–776. <https://doi.org/10.2217/17435889.3.6.761>
- Salamon, M., Millino, C., Raffaello, A., Mongillo, M., Sandri, C., Bean, C., Negrisolo, E., Pallavicini, A., Valle, G., Zaccolo, M., Schiaffino, S., & Lanfranchi, G. (2003). Human MYO18B, a novel unconventional myosin heavy chain expressed in striated muscles moves into the myonuclei upon differentiation. *Journal of Molecular Biology*. [https://doi.org/10.1016/S0022-2836\(02\)01335-9](https://doi.org/10.1016/S0022-2836(02)01335-9)
- Sawh, A. N., Shafer, M. E. R., Su, J.-H., Zhuang, X., Wang, S., & Mango, S. E. (2020). Lamina-Dependent Stretching and Unconventional Chromosome Compartments in Early *C. elegans* Embryos. *Molecular Cell*, *78*(1), 96–111.e6. <https://doi.org/10.1016/j.molcel.2020.02.006>
- Scheuermann, M. O., Tajbakhsh, J., Kurz, A., Saracoglu, K., Eils, R., & Lichter, P. (2004). Topology of genes and nontranscribed sequences in human interphase nuclei. *Experimental Cell Research*, *301*(2), 266–279. <https://doi.org/https://doi.org/10.1016/j.yexcr.2004.08.031>
- Sen Gupta, A., & Sengupta, K. (2017). Lamin B2 Modulates Nucleolar Morphology, Dynamics, and Function. *Molecular and Cellular Biology*, *37*(24), e00274–17. <https://doi.org/10.1128/MCB.00274-17>
- Sengupta, D., Nishan Ali, S., Bhattacharya, A., Mustafi, J., Mukhopadhyay, A., & Sengupta, K. (n.d.). *Nuclear Morphology Optimized Deep Hybrid Learning (NUMODRIL): A novel architecture for accurate diagnosis/prognosis of Ovarian Cancer*. <https://doi.org/10.1101/2020.11.23.393660>
- Serebryanny, L. A., Yuen, M., Parilla, M., Cooper, S. T., & de Lanerolle, P. (2016). The Effects of Disease Models of Nuclear Actin Polymerization on the Nucleus. *Frontiers in Physiology*, *7*, 454. <https://doi.org/10.3389/fphys.2016.00454>
- Shaklai, S., Amariglio, N., Rechavi, G., & Simon, A. J. (2007). Gene silencing at the nuclear periphery. *FEBS Journal*, *274*(6), 1383–1392. <https://doi.org/10.1111/j.1742-4658.2007.05697.x>
- Shayesteh, L., Lu, Y., Kuo, W. L., Baldocchi, R., Godfrey, T., Collins, C., Pinkel, D., Powell, B., Mills, G. B., & Gray, J. W. (1999). PIK3CA is implicated as an oncogene in ovarian cancer. *Nature Genetics*. <https://doi.org/10.1038/5042>
- Sherman-Baust, C. A., Becker, K. G., Wood III, W. H., Zhang, Y., & Morin, P. J. (2011). Gene expression and pathway analysis of ovarian cancer cells selected for resistance to cisplatin, paclitaxel, or doxorubicin. *Journal of Ovarian Research*, *4*(1), 21. <https://doi.org/10.1186/1757-2215-4-21>
- Shevelyov, Y. Y., & Ulianov, S. V. (2019). The Nuclear Lamina as an Organizer of Chromosome Architecture. *Cells*, *8*(2), 136. <https://doi.org/10.3390/cells8020136>
- Shih, I.-M., & Kurman, R. J. (2004). Ovarian Tumorigenesis: A Proposed Model Based on Morphological and Molecular Genetic Analysis. *The American Journal of Pathology*, *164*(5), 1511–1518. <https://doi.org/https://doi.org/10.1016/S0002->



9440(10)63708-X

- Shin, Y., & Brangwynne, C. P. (2017). Liquid phase condensation in cell physiology and disease. *Science*, 357(6357). <https://doi.org/10.1126/science.aaf4382>
- Shopland, L. S., Lynch, C. R., Peterson, K. A., Thornton, K., Kepper, N., Hase, J. von, Stein, S., Vincent, S., Molloy, K. R., & Kreth, G. (2006). Folding and organization of a contiguous chromosome region according to the gene distribution pattern in primary genomic sequence. *The Journal of Cell Biology*, 174(1), 27–38.
- Siegel, R., Ward, E., Brawley, O., & Jemal, A. (2011). Cancer statistics, 2011. *CA: A Cancer Journal for Clinicians*, 61(4), 212–236. <https://doi.org/10.3322/caac.20121>
- Simchoni, S., Friedman, E., Kaufman, B., Gershoni-Baruch, R., Orr-Urtreger, A., Kedar-Barnes, I., Shiri-Sverdlov, R., Dagan, E., Tsabari, S., Shohat, M., Catane, R., King, M.-C., Lahad, A., & Levy-Lahad, E. (2006). Familial clustering of site-specific cancer risks associated with BRCA1 and BRCA2 mutations in the Ashkenazi Jewish population. *Proceedings of the National Academy of Sciences of the United States of America*, 103(10), 3770–3774. <https://doi.org/10.1073/pnas.0511301103>
- Simon, D. N., & Wilson, K. L. (2011). The nucleoskeleton as a genome-associated dynamic “network of networks.” *Nature Reviews Molecular Cell Biology*, 12(11), 695–708. <https://doi.org/10.1038/nrm3207>
- Simonis, M., Klous, P., Splinter, E., Moshkin, Y., Willemsen, R., De Wit, E., Van Steensel, B., & De Laat, W. (2006). Nuclear organization of active and inactive chromatin domains uncovered by chromosome conformation capture-on-chip (4C). *Nature Genetics*, 38(11), 1348–1354. <https://doi.org/10.1038/ng1896>
- Skehan, P., Storeng, R., Scudiero, D., Monks, A., McMahon, J., Vistica, D., Warren, J. T., Bokesch, H., Kenney, S., & Boyd, M. R. (1990). New Colorimetric Cytotoxicity Assay for Anticancer-Drug Screening. *JNCI: Journal of the National Cancer Institute*, 82(13), 1107–1112. <https://doi.org/10.1093/jnci/82.13.1107>
- Skok, J. A., Brown, K. E., Azuara, V., Caparros, M.-L., Baxter, J., Takacs, K., Dillon, N., Gray, D., Perry, R. P., & Merckenschlager, M. (2001). Nonequivalent nuclear location of immunoglobulin alleles in B lymphocytes. *Nature Immunology*, 2(9), 848–854.
- Solovei, I., Kreysing, M., Lanctôt, C., Kösem, S., Peichl, L., Cremer, T., Guck, J., & Joffe, B. (2009). Nuclear Architecture of Rod Photoreceptor Cells Adapts to Vision in Mammalian Evolution. *Cell*, 137(2), 356–368. <https://doi.org/10.1016/j.cell.2009.01.052>
- Soutoglou, E., & Misteli, T. (2008). On the Contribution of Spatial Genome Organization to Cancerous Chromosome Translocations. *JNCI Monographs*, 2008(39), 16–19. <https://doi.org/10.1093/jncimonographs/lgn017>
- Strouboulis, J., & Wolffe, A. P. (1996). Functional compartmentalization of the nucleus. *Journal of Cell Science*, 109(8), 1991 LP – 2000. <http://jcs.biologists.org/content/109/8/1991.abstract>
- Stuurman, N., Heins, S., & Aebi, U. (1998). Nuclear Lamins: Their Structure, Assembly, and Interactions. *Journal of Structural Biology*, 122(1), 42–66. <https://doi.org/https://doi.org/10.1006/jsbi.1998.3987>
- Sun, H. B., Shen, J., & Yokota, H. (2000). Size-Dependent Positioning of Human Chromosomes in Interphase Nuclei. *Biophysical Journal*, 79(1), 184–190. [https://doi.org/10.1016/S0006-3495\(00\)76282-5](https://doi.org/10.1016/S0006-3495(00)76282-5)
- Sun, T. M., Du, J. Z., Yao, Y. D., Mao, C. Q., Dou, S., Huang, S. Y., Zhang, P. Z., Leong, K. W., Song, E. W., & Wang, J. (2011). Simultaneous delivery of siRNA and paclitaxel via a “two-in-one” micelle complex promotes synergistic tumor suppression. *ACS Nano*, 5(2), 1483–1494. <https://doi.org/10.1021/nn103349h>
- Sun, X., He, Y., Hou, L., & Yang, W.-X. (2010). Myosin Va Participates in Acrosomal Formation and Nuclear Morphogenesis during Spermatogenesis of Chinese Mitten Crab *Eriocheir sinensis*. *PLoS ONE*, 5(9), e12738. <https://doi.org/10.1371/journal.pone.0012738>
- Swift, J., Ivanovska, I. L., Buxboim, A., Harada, T., Dingal, P. C. D. P., Pinter, J., Pajerowski, J. D., Spinler, K. R., Shin, J.-W., Tewari, M., Rehfeldt, F., Speicher, D. W., & Discher, D. E. (2013). Nuclear Lamin-A Scales with Tissue Stiffness and Enhances Matrix-Directed Differentiation. *Science*, 341(6149), 1240104. <https://doi.org/10.1126/science.1240104>
- Swisher, E. M., Sakai, W., Karlan, B. Y., Wurz, K., Urban, N., & Taniguchi, T. (2008). Secondary BRCA1 mutations in BRCA1-mutated ovarian carcinomas with platinum resistance. *Cancer Research*, 68(8), 2581–2586. <https://doi.org/10.1158/0008-5472.CAN-08-0088>
- Szczerbal, I., Foster, H. A., & Bridger, J. M. (2009). The spatial repositioning of adipogenesis genes is correlated with their expression status in a porcine mesenchymal stem cell adipogenesis model system. *Chromosoma*, 118(5), 647–663.
- Taddei, A., Van Houwe, G., Hediger, F., Kalck, V., Cubizolles, F., Schober, H., & Gasser, S. M. (2006). Nuclear pore association confers optimal expression levels for an inducible yeast gene. *Nature*, 441(7094), 774–778.
- Takeda, T., Banno, K., Okawa, R., Yanokura, M., Iijima, M., Iriekunitomi, H., Nakamura, K., Iida, M., Adachi, M., Umene, K., Nogami, Y., Masuda, K., Kobayashi, Y., Tominaga, E., & Aoki, D. (2016). ARID1A gene mutation in ovarian and

- endometrial cancers (Review). In *Oncology Reports*. <https://doi.org/10.3892/or.2015.4421>
- Takizawa, T., Gudla, P. R., Guo, L., Lockett, S., & Misteli, T. (2008). Allele-specific nuclear positioning of the monoallelically expressed astrocyte marker GFAP. *Genes & Development*, *22*(4), 489–498. <https://doi.org/10.1101/gad.1634608>
- Tanabe, H., Küpper, K., Ishida, T., Neusser, M., & Mizusawa, H. (2005). Inter- and intra-specific gene-density-correlated radial chromosome territory arrangements are conserved in Old World monkeys. *Cytogenetic and Genome Research*, *108*(1–3), 255–261. <https://doi.org/10.1159/000080824>
- Tanabe, Hideyuki, Müller, S., Neusser, M., von Hase, J., Calcagno, E., Cremer, M., Solovei, I., Cremer, C., & Cremer, T. (2002). Evolutionary conservation of chromosome territory arrangements in cell nuclei from higher primates. *Proceedings of the National Academy of Sciences*, *99*(7), 4424–4429.
- Tanwar, P. S., Mohapatra, G., Chiang, S., Engler, D. A., Zhang, L. H., Kaneko-Tarui, T., Ohguchi, Y., Birrer, M. J., & Teixeira, J. M. (2014). Loss of LKB1 and PTEN tumor suppressor genes in the ovarian surface epithelium induces papillary serous ovarian cancer. *Carcinogenesis*. <https://doi.org/10.1093/carcin/bgt357>
- Telenius, Håk., Ponder, B. A. J., Tunnacliffe, A., Pelmar, A. H., Carter, N. P., Ferguson-Smith, M. A., Behmel, A., Nordenskjöld, M., & Pfragner, R. (1992). Cytogenetic analysis by chromosome painting using dop-pcr amplified flow-sorted chromosomes. *Genes, Chromosomes and Cancer*, *4*(3), 257–263. <https://doi.org/10.1002/gcc.2870040311>
- Toseland Lab. (n.d.). Retrieved August 8, 2020, from <http://toselandlab.mechanicsanddynamics.com/>
- Urciuoli, E., Petrini, S., D’Oria, V., Leopizzi, M., Rocca, C. Della, & Peruzzi, B. (2020). Nuclear Lamins and Emerin Are Differentially Expressed in Osteosarcoma Cells and Scale with Tumor Aggressiveness. *Cancers*, *12*(2), 443. <https://doi.org/10.3390/cancers12020443>
- Valton, A.-L., & Dekker, J. (2016). TAD disruption as oncogenic driver. *Current Opinion in Genetics & Development*, *36*, 34–40. <https://doi.org/10.1016/j.gde.2016.03.008>
- Van de Vosse, D. W., Wan, Y., Wozniak, R. W., & Aitchison, J. D. (2011). Role of the nuclear envelope in genome organization and gene expression. In *Wiley Interdisciplinary Reviews: Systems Biology and Medicine* (Vol. 3, Issue 2, pp. 147–166). NIH Public Access. <https://doi.org/10.1002/wsbm.101>
- van den Brand, D., Mertens, V., Massuger, L. F. A. G., & Brock, R. (2018). siRNA in ovarian cancer – Delivery strategies and targets for therapy. *Journal of Controlled Release*, *283*, 45–58. <https://doi.org/https://doi.org/10.1016/j.jconrel.2018.05.012>
- van Driel, R., Humbel, B., & de Jong, L. (1991). The nucleus: A black box being opened. *Journal of Cellular Biochemistry*, *47*(4), 311–316. <https://doi.org/10.1002/jcb.240470405>
- van Steensel, B., & Belmont, A. S. (2017). Lamina-Associated Domains: Links with Chromosome Architecture, Heterochromatin, and Gene Repression. *Cell*, *169*(5), 780–791. <https://doi.org/10.1016/j.cell.2017.04.022>
- van Steensel, B., & Dekker, J. (2010). Genomics tools for unraveling chromosome architecture. *Nature Biotechnology*, *28*(10), 1089–1095. <https://doi.org/10.1038/nbt.1680>
- Venit, T., Dzijak, R., Kalendová, A., Kahle, M., Rohožková, J., Schmidt, V., Rüllicke, T., Rathkolb, B., Hans, W., Bohla, A., Eickelberg, O., Stoeger, T., Wolf, E., Yildirim, A. Ö., Gailus-Durner, V., Fuchs, H., de Angelis, M. H., & Hozák, P. (2013). Mouse Nuclear Myosin I Knock-Out Shows Interchangeability and Redundancy of Myosin Isoforms in the Cell Nucleus. *PLOS ONE*, *8*(4), e61406. <https://doi.org/10.1371/journal.pone.0061406>
- Venit, T., Kalendová, A., Petr, M., Dzijak, R., Pastorek, L., Rohožková, J., Malohlava, J., & Hozák, P. (2016). Nuclear myosin I regulates cell membrane tension. *Scientific Reports*, *6*(1), 30864. <https://doi.org/10.1038/srep30864>
- Volpi, E. V., Chevret, E., Jones, T., Vatcheva, R., Williamson, J., Beck, S., Campbell, R. D., Goldsworthy, M., Powis, S. H., & Ragoussis, J. (2000). Large-scale chromatin organization of the major histocompatibility complex and other regions of human chromosome 6 and its response to interferon in interphase nuclei. *Journal of Cell Science*, *113*(9), 1565–1576.
- Vreugde, S., Ferrai, C., Miluzio, A., Hauben, E., Marchisio, P. C., Crippa, M. P., Bussi, M., & Biffo, S. (2006). Nuclear Myosin VI Enhances RNA Polymerase II-Dependent Transcription. *Molecular Cell*, *23*(5), 749–755. <https://doi.org/https://doi.org/10.1016/j.molcel.2006.07.005>
- Wang, H., Wang, B., Zhu, W., & Yang, Z. (2015). Lentivirus-Mediated Knockdown of Myosin VI Inhibits Cell Proliferation of Breast Cancer Cell. *Cancer Biotherapy and Radiopharmaceuticals*, *30*(8), 330–335. <https://doi.org/10.1089/cbr.2014.1759>
- Wang, T., Shigdar, S., Shamaileh, H. Al, Gantier, M. P., Yin, W., Xiang, D., Wang, L., Zhou, S. F., Hou, Y., Wang, P., Zhang, W., Pu, C., & Duan, W. (2017). Challenges and opportunities for siRNA-based cancer treatment. In *Cancer Letters* (Vol. 387, pp. 77–83). Elsevier Ireland Ltd. <https://doi.org/10.1016/j.canlet.2016.03.045>
- Wang, Y., Wu, R., Cho, K. R., Thomas, D. G., Gossner, G., Liu, J. R., Giordano, T. J., Shedden, K. A., Misek, D. E., & Lubman, D. M. (2009). Differential protein mapping of ovarian serous adenocarcinomas: identification of potential markers

- for distinct tumor stage. *Journal of Proteome Research*, 8(3), 1452–1463. <https://doi.org/10.1021/pr800820z>
- Weaver, B. A. (2014). How Taxol/paclitaxel kills cancer cells. *Molecular Biology of the Cell*, 25(18), 2677–2681.
- Weil, M. K., & Chen, A. P. (2011). PARP Inhibitor Treatment in Ovarian and Breast Cancer. *Current Problems in Cancer*, 35(1), 7–50. <https://doi.org/10.1016/j.currprobcancer.2010.12.002>
- Welch, H. G., & Black, W. C. (2010). Overdiagnosis in Cancer. *JNCI: Journal of the National Cancer Institute*, 102(9), 605–613. <https://doi.org/10.1093/jnci/djq099>
- Wells, A. L., Lin, A. W., Chen, L.-Q., Safer, D., Cain, S. M., Hasson, T., Carragher, B. O., Milligan, R. A., & Sweeney, H. L. (1999). Myosin VI is an actin-based motor that moves backwards. *Nature*, 401(6752), 505–508. <https://doi.org/10.1038/46835>
- Wiech, T., Stein, S., Lachenmaier, V., Schmitt, E., Schwarz-Finsterle, J., Wiech, E., Hildenbrand, G., Werner, M., & Hausmann, M. (2009). Spatial allelic imbalance of BCL2 genes and chromosome 18 territories in nonneoplastic and neoplastic cervical squamous epithelium. *European Biophysics Journal*, 38(6), 793–806. <https://doi.org/10.1007/s00249-009-0474-5>
- Williams, R. R. E., Broad, S., Sheer, D., & Ragoussis, J. (2002). Subchromosomal Positioning of the Epidermal Differentiation Complex (EDC) in Keratinocyte and Lymphoblast Interphase Nuclei. *Experimental Cell Research*, 272(2), 163–175. <https://doi.org/https://doi.org/10.1006/excr.2001.5400>
- Winham, S. J., Larson, N. B., Armasu, S. M., Fogarty, Z. C., Larson, M. C., McCauley, B. M., Wang, C., Lawrenson, K., Gayther, S., Cunningham, J. M., Fridley, B. L., & Goode, E. L. (2018). Molecular signatures of X chromosome inactivation and associations with clinical outcomes in epithelial ovarian cancer. *Human Molecular Genetics*, 28(8), 1331–1342. <https://doi.org/10.1093/hmg/ddy444>
- Wolf, C. R., Hayward, I. P., Lawrie, S. S., Buckton, K., McIntyre, M. A., Adams, D. J., Lewis, A. D., Scott, A. R. R., & Smyth, J. F. (1987). Cellular heterogeneity and drug resistance in two ovarian adenocarcinoma cell lines derived from a single patient. *International Journal of Cancer*, 39(6), 695–702. <https://doi.org/10.1002/ijc.2910390607>
- Wu, S., Fatkhutdinov, N., Rosin, L., Luppino, J. M., Iwasaki, O., Tanizawa, H., Tang, H.-Y., Kossenkov, A. V., Gardini, A., Noma, K.-I., Speicher, D. W., Joyce, E. F., & Zhang, R. (2019). ARID1A spatially partitions interphase chromosomes. *Science Advances*, 5(5), eaaw5294–eaaw5294. <https://doi.org/10.1126/sciadv.aaw5294>
- Xue, T., Wang, L., Li, Y., Song, H., Chu, H., Yang, H., Guo, A., & Jiao, J. (2019). SiRNA-Mediated RRM2 Gene Silencing Combined with Cisplatin in the Treatment of Epithelial Ovarian Cancer In Vivo: An Experimental Study of Nude Mice. *International Journal of Medical Sciences*, 16(11), 1510–1516. <https://doi.org/10.7150/ijms.33979>
- Yanaihara, N., Nishioka, M., Kohno, T., Otsuka, A., Okamoto, A., Ochiai, K., Tanaka, T., & Yokota, J. (2004). Reduced expression of MYO18B, a candidate tumor-suppressor gene on chromosome ARM 22Q, in ovarian cancer. *International Journal of Cancer*, 112(1), 150–154. <https://doi.org/10.1002/ijc.20339>
- Yang-Hartwich, Y., Soteras, M. G., Lin, Z. P., Holmberg, J., Sumi, N., Craveiro, V., Liang, M., Romanoff, E., Bingham, J., Garofalo, F., Alvero, A., & Mor, G. (2015). p53 protein aggregation promotes platinum resistance in ovarian cancer. *Oncogene*, 34(27), 3605–3616. <https://doi.org/10.1038/onc.2014.296>
- Yang, S. H., Chang, S. Y., Yin, L., Tu, Y., Hu, Y., Yoshinaga, Y., de Jong, P. J., Fong, L. G., & Young, S. G. (2011). An absence of both lamin B1 and lamin B2 in keratinocytes has no effect on cell proliferation or the development of skin and hair. *Human Molecular Genetics*, 20(18), 3537–3544. <https://doi.org/10.1093/hmg/ddr266>
- Yang, S. H., Jung, H.-J., Coffinier, C., Fong, L. G., & Young, S. G. (2011). Are B-type lamins essential in all mammalian cells? *Nucleus (Austin, Tex.)*, 2(6), 562–569. <https://doi.org/10.4161/nucl.2.6.18085>
- Yang, X., Iyer, A. K., Singh, A., Milane, L., Choy, E., Hornicek, F. J., Amiji, M. M., & Duan, Z. (2015). Cluster of Differentiation 44 Targeted Hyaluronic Acid Based Nanoparticles for MDR1 siRNA Delivery to Overcome Drug Resistance in Ovarian Cancer. *Pharmaceutical Research*, 32(6), 2097–2109. <https://doi.org/10.1007/s11095-014-1602-1>
- Yoshida, H., Cheng, W., Hung, J., Montell, D., Geisbrecht, E., Rosen, D., Liu, J., & Naora, H. (2004). Lessons from border cell migration in the Drosophila ovary: A role for myosin VI in dissemination of human ovarian cancer. *Proceedings of the National Academy of Sciences of the United States of America*, 101(21), 8144–8149. <https://doi.org/10.1073/pnas.0400400101>
- Yusufzai, T. M., Tagami, H., Nakatani, Y., & Felsenfeld, G. (2004). CTCF Tethers an Insulator to Subnuclear Sites, Suggesting Shared Insulator Mechanisms across Species. *Molecular Cell*, 13(2), 291–298. [https://doi.org/https://doi.org/10.1016/S1097-2765\(04\)00029-2](https://doi.org/https://doi.org/10.1016/S1097-2765(04)00029-2)
- Zeitz, M. J., Ay, F., Heidmann, J. D., Lerner, P. L., Noble, W. S., Steelman, B. N., & Hoffman, A. R. (2013). Genomic Interaction Profiles in Breast Cancer Reveal Altered Chromatin Architecture. *PLoS ONE*, 8(9), 73974. <https://doi.org/10.1371/journal.pone.0073974>
- Zink, D., Fischer, A. H., & Nickerson, J. A. (2004). Nuclear structure in cancer cells. *Nature Reviews Cancer*, 4(9), 677–687. <https://doi.org/10.1038/nrc1430>



## References

---

- Zorca, C. E., Kim, L. K., Kim, Y. J., Krause, M. R., Zenklusen, D., Spilianakis, C. G., & Flavell, R. A. (2015). Myosin VI regulates gene pairing and transcriptional pause release in T cells. *Proceedings of the National Academy of Sciences*, *112*(13), E1587 LP-E1593. <https://doi.org/10.1073/pnas.1502461112>

## 7 APPENDIX

**Figure 7.1 Overview of OC cell lines characteristics (Next Page):** Morphology: E-Epithelial, R-Round, S-Spindle. Histology: S-serous, HGS-high-grade serous, LGS-low-grade serous, E-endometrioid, C-clear cell, Mx-mixed, M-mucinous. Origin: A-ascites, T-tumour tissue, TM-tissue from metastasis, TO-ovarian tumour tissue, P-pleural effusion. Time: P-primary disease, R-relapsed disease, CR-clinical resistance. Platinum treated: U-untreated, P-platinum-based treatment, O-other chemotherapy, R-radiotherapy. Protein markers: bright red-no expression, light red-low expression, light green-expression, bright green-high expression, grey-not determined. Therapy response: green to red - sensitive to resistant. Doubling time: green-less than one day, yellow-1-2days, orange >2days. Mutations: dark blue-identified by at least two methods, light blue-identified by one method, light red-identified with one method BUT not with second method. Amplification: orange-amplified, red-highly amplified. The homologous recombination repair (HRR) and WNT/bCatenin pathway (WNT/bCAT) columns show the number of mutated genes in these pathways. MSI-microsatellite instability (Beaufort *et al.*, 2014).



